

IN THE UNITED STATES PATENT AND TRADEMARK OFFICE

In re Patent Application of

Date: May 15, 2008

Applicants: Bednorz et al.

Docket: YO987-074BZ

Serial No.: 08/479,810

Group Art Unit: 1751

Filed: June 7, 1995

Examiner: M. Kopec

For: NEW SUPERCONDUCTIVE COMPOUNDS HAVING HIGH TRANSITION
TEMPERATURE, METHODS FOR THEIR USE AND PREPARATION

Commissioner for Patents
United States Patent and Trademark Office
P.O. Box 1450
Alexandria, VA 22313-1450

APPEAL BRIEF

PART IX

CFR 37 § 41.37(c) (1) (*ix*)

SECTION 1

VOLUME 4

Part 1

BRIEF ATTACHMENTS A TO C

Respectfully submitted,

/Daniel P Morris/

Dr. Daniel P. Morris, Esq.

Reg. No. 32,053

(914) 945-3217

IBM CORPORATION
Intellectual Property Law Dept.
P.O. Box 218
Yorktown Heights, New York 10598

BRIEF ATTACHMENT A



IN THE UNITED STATES PATENT AND TRADEMARK OFFICE

In re Patent Application of

Applicants: Bednorz et al.

Serial No.: 08/479,810

Filed: June 7, 1995

Date: March 1, 2005

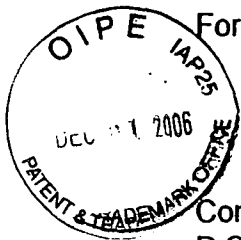
Docket: YO987-074BZ

Group Art Unit: 1751

Examiner: M. Kopec

For: **NEW SUPERCONDUCTIVE COMPOUNDS HAVING HIGH TRANSITION
TEMPERATURE, METHODS FOR THEIR USE AND PREPARATION**

Commissioner for Patents
P.O. Box 1450
Alexandria, VA 22313-1450



FIRST SUPPLEMENTAL AMENDMENT

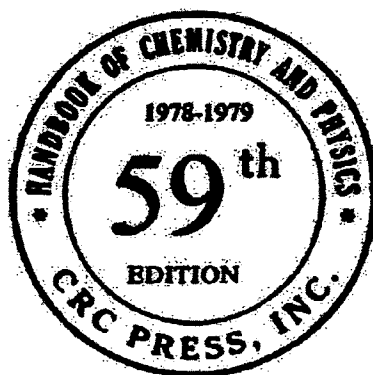
Sir:

In response to the Office Action dated July 28, 2004, please consider the
following:

ATTACHMENT A

CRC Handbook OF Chemistry and Physics

A Ready-Reference Book of Chemical and Physical Data



EDITOR

ROBERT C. WEAST, Ph.D.

*Vice President, Research, Consolidated Natural Gas Service Company, Inc.
Formerly Professor of Chemistry at Case Institute of Technology*

ASSOCIATE EDITOR

MELVIN J. ASTLE, Ph.D.

*Formerly Professor of Organic Chemistry at Case Institute of Technology
and
Manager of Research at Glidden-Durkee Division of SCM Corporation*

In collaboration with a large number of professional chemists and physicists
whose assistance is acknowledged in the list of general collaborators and in
connection with the particular tables or sections involved.



CRC PRESS, Inc.
2255 Palm Beach Lakes Blvd., West Palm Beach, Florida 33409

BEST AVAILABLE COPY

PROPERTIES OF RARE EARTH METALS

PROPERTIES OF RARE EARTH METALS

F. H. Spedding

Symbol	Crystal Structure at Room Temperature 25°C	Alloy Form Transition Temperatures Expressed in °C
Sc	Hex. (to 1335°)	bcc (above 1335°)
Y	Hex. (to 1478°)	bcc (above 1478°)
La	Hex. (to 310°) (usually contains fcc alloy)	fcc (310°-865°) bcc (above 865°)
Ce	fcc (~ 0° to 726°)	fcc (below 157° on cooling) (up to 24° on heating) Hex. (below 23° on cooling) (up to 168° on heating)
Pr	Hex. (to 795°)	a=3.6721A, c=11.832A
Nd	Hex. (to 863°)	a=3.6583A, c=11.7966A
Sm	* Rhomb. (to 926°)	a=8.9834A, c=23° 49.5
Eu	bcc	a=4.5827A
Gd	Hex. (to 1235°)	a=3.6336A, c=5.7810A
Tb	Hex. (to 1289°)	a=3.6055A, c=5.6966A
Dy	Hex. (to 1381°)	a=3.5915A, c=5.6501A
Ho	Hex.	a=3.5778A, c=5.6178A
Er	Hex.	a=3.5592A, c=5.5850A
Tm	Hex.	a=3.5375A, c=5.5540A
Yb	Hex. (to 795°)	a=5.4848A
Lu	Hex.	a=3.5052A, c=5.5494A
		a=4.08A
		a=4.26A
		a=4.85A
		a=3.68A
		a=11.92A
		a=4.13A
		a=4.07A
		a=4.05A†
		a=4.02A†
		a=3.98A†
		a=4.44A

† Extrapolated from magnesium alloy studies. Hex. refers to close packed hexagonal. La, Ce, Pr, and Nd have a stacking order ABAC, the other rare earths ABAB. fcc refers to close packed face centered cubic with a stacking order ABC, ABC, bcc refers to body centered cubic. These high temperature forms are very soft and deform very easily.

* The rhombic Sm cell can be expressed as hexagonal with a=3.6290A, c=26.207 and possess a stacking order ABABCBAC.

PERIODIC TABLE OF THE ELEMENTS

1a	2a	3a	4a	5a	6a	7a	0	Orbit
1 H 1.0079							2 He 4.00260	K
3 Li 6.94	4 Be 9.01218							
11 Na 22.98977	12 Mg 24.305							
19 K 39.0983	20 Ca 40.08							
37 Rb 85.467	38 Sr 87.62							
55 Cs 132.9054	56 Ba 137.33							
87 Fr (223)	88 Ra 226.0254							
107 Bohrium	108 Hassium							
111 Roentgenium	112 Copernicium							
115 Moscovium	116 Livermorium							
117 Tennessine	118 Oganesson							

	58	59	60	61	62	63	64	65	66	67	68	69	70	71
•Lanthanides	Ce ⁺⁴	Pr	Nd	Pm	Sm	Eu	Gd	Tb	Dy	Ho	Er	Tm	Yb	Lu
	140.12	140.9077	144.24	(145)	150.4	151.96	157.25	158.9254	162.50	164.9304	167.26	168.9342	173.04	174.967 ± 0.003
	-20-8-2	-21-8-2	-22-8-2	-23-8-2	-24-8-2	-25-8-2	-25-9-2	-27-8-2	-28-8-2	-29-8-2	-30-8-2	-31-8-2	-32-8-2	-32-9-2
••Actinides	Th	Pa	U	Np ⁺⁵	Pu ⁺⁵	Am ⁺⁴	Cm ⁺⁵	Bk ⁺⁴	Cf	Es	Fm	Md ⁺³	No	Lr
	232.0381	231.0359	238.029	237.0482	(244)	(243)	(247)	(247)	(251)	(254)	(257)	(258)	(259)	(260)
	-18-10-2	-20-4-2	-21-9-2	-22-9-2	-24-8-2	-25-8-2	-25-9-2	-27-8-2	-28-8-2	-29-8-2	-30-8-2	-31-8-2	-32-8-2	-32-9-2

BRIEF ATTACHMENT B

IN THE UNITED STATES PATENT AND TRADEMARK OFFICE

In re Patent Application of

Applicants: Bednorz et al.

Serial No.: 08/479,810

Filed: June 7, 1995

For: **NEW SUPERCONDUCTIVE COMPOUNDS HAVING HIGH TRANSITION
TEMPERATURE, METHODS FOR THEIR USE AND PREPARATION**

Date: March 1, 2005

Docket: YO987-074BZ

Group Art Unit: 1751

Examiner: M. Kopec

Commissioner for Patents
P.O. Box 1450
Alexandria, VA 22313-1450

FIRST SUPPLEMENTAL AMENDMENT

Sir:

In response to the Office Action dated July 28, 2004, please consider the
following:

ATTACHMENT B

Introduction to Ceramics

Second Edition

W. D. Kingery

PROFESSOR OF CERAMICS
MASSACHUSETTS INSTITUTE OF TECHNOLOGY

H. K. Bowen

ASSOCIATE PROFESSOR OF CERAMICS
MASSACHUSETTS INSTITUTE OF TECHNOLOGY

D. R. Uhlmann

PROFESSOR OF CERAMICS AND POLYMERS
MASSACHUSETTS INSTITUTE OF TECHNOLOGY

A Wiley-Interscience Publication

JOHN WILEY & SONS, New York • Chichester • Brisbane • Toronto

Copyright © 1960, 1976 by John Wiley & Sons, Inc.

All rights reserved. Published simultaneously in Canada.

Reproduction or translation of any part of this work beyond that permitted by Sections 107 or 108 of the 1976 United States Copyright Act without the permission of the copyright owner is unlawful. Requests for permission or further information should be addressed to the Permissions Department, John Wiley & Sons, Inc.

Library of Congress Cataloging in Publication Data:

Kingery, W. D.

Introduction to ceramics.

(Wiley series on the science and technology of materials)

"A Wiley-Interscience publication."

Includes bibliographical references and index.

1. Ceramics. I. Bowen, Harvey Kent, joint author.
- II. Uhlmann, Donald Robert, joint author. III. Title.

TP807.K52 1975 666 75-22248
ISBN 0-471-47860-1

Printed in the United States of America

10 9 8 7 6 5

During the fifteen years since it was first published, the book has been widely cited. However, the rapid development of new materials and the need for new modifications in the processing of new material.

In particular, the book provides a new insight into the spinodal decomposition of glass-ceramics, the recognition of the sintering phenomenon, the transmission electron microscopy, and a myriad of other magnetic ceramic materials. These advances are a testament to the competence of the author.

The necessary background for the recent availability of new processing methods (1970); F. H. Norton, *Elementary Ceramics* (1974); F. V. T. Ogden Publ. Co.

or prepare fine particles, shape them, and then stick them back together by heating. The second basic process is to melt the material to form a liquid and then shape it during cooling and solidification; this is most widely practiced in forming glasses. For completeness, we should also mention forming shapes in a mold or by dipping a form with a slurry containing a ceramic binder such as portland cement or ethyl silicate.

Raw Materials. The types of minerals found in nature are controlled mainly by the abundance of the elements and their geochemical characteristics. Since oxygen, silicon, and aluminum together account for 90% of the elements in the earth's crust, as shown in Fig. 1.1, it is not surprising that the dominant minerals are silicates and aluminum silicates. These, together with other mineral compounds of oxygen, constitute the great bulk of naturally occurring ceramic raw materials.

The mineral raw materials used in the ceramic industry are mainly

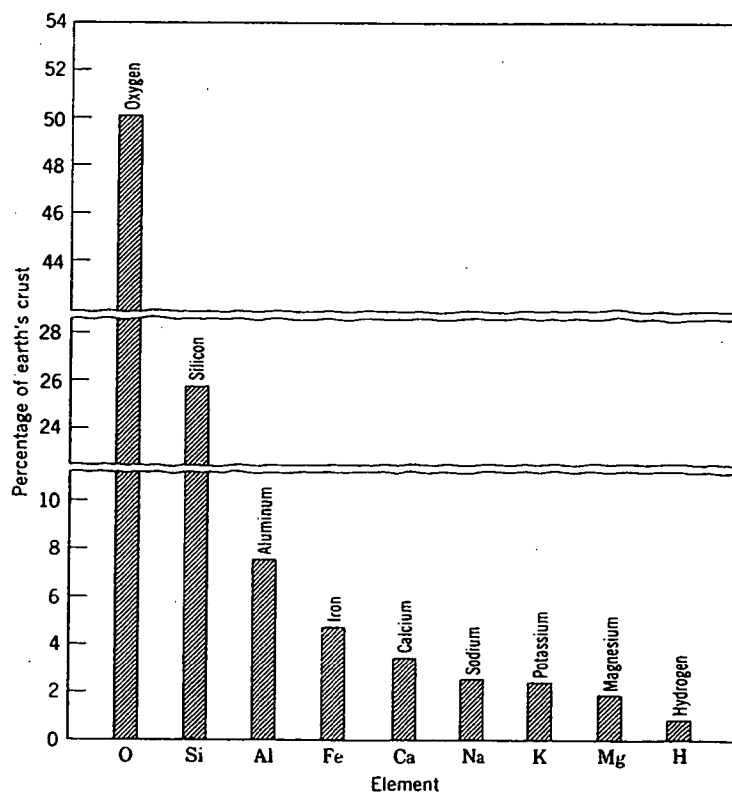


Fig. 1.1 Abundance of common elements in the earth's crust.

inorganic nonmetallic crystalline solids formed by complex geologic processes. Their ceramic properties are largely determined by the crystal structure and the chemical composition of their essential constituents and the nature and amounts of accessory minerals present. The mineralogic characteristics of such materials and therefore their ceramic properties are subject to wide variation among different occurrences or even within the same occurrence, depending on the geological environment in which the mineral deposit was formed as well as the physical and chemical modifications that have taken place during subsequent geological history.

Since silicate and aluminum silicate materials are widely distributed, they are also inexpensive and thus provide the backbone of high-tonnage products of the ceramic industry and determine to a considerable extent its form. Low-grade clays are available almost everywhere; as a result, the manufacture of building brick and tile not requiring exceptional properties is a localized industry for which extensive beneficiation of the raw material is not appropriate. In contrast, for fine ceramics requiring the use of better-controlled raw materials, the raw materials are normally beneficiated by mechanical concentration, froth floatation, and other relatively inexpensive processes. For materials in which the value added during manufacture is high, such as magnetic ceramics, nuclear-fuel materials, electronic ceramics, and specialized refractories, chemical purification and even chemical preparation of raw materials may be necessary and appropriate.

The raw materials of widest application are the clay minerals—fine-particle hydrous aluminum silicates which develop plasticity when mixed with water. They vary over wide limits in chemical, mineralogical, and physical characteristics, but a common characteristic is their crystalline layer structure, consisting of electrically neutral aluminosilicate layers, which leads to a fine particle size and platelike morphology and allows the particles to move readily over one another, giving rise to physical properties such as softness, soapy feel, and easy cleavage. Clays perform two important functions in ceramic bodies. First, their characteristic plasticity is basic to many of the forming processes commonly used; the ability of clay-water compositions to be formed and to maintain their shape and strength during drying and firing is unique. Second, they fuse over a temperature range, depending on composition, in such a way as to become dense and strong without losing their shape at temperatures which can be economically attained.

The most common clay minerals and those of primary interest to ceramists, since they are the major component of high-grade clays, are based on the kaolinite structure, $\text{Al}_2(\text{Si}_2\text{O}_5)(\text{OH})_4$. Other compositions often encountered are shown in Table 1.1.

st
M
of
m
st

an
in
ab
in
ab
oc
as
ma
bo
br
th
by

sti
(o
ca
gl
fel
Na
ma
ro
we
gr
ref

Table 1.1. Ideal Chemical Formulas of the Clay Minerals

Kaolinite	$\text{Al}_2(\text{Si}_2\text{O}_5)(\text{OH})_4$
Halloysite	$\text{Al}_2(\text{Si}_2\text{O}_5)(\text{OH})_4 \cdot 2\text{H}_2\text{O}$
Pyrophyllite	$\text{Al}_2(\text{Si}_2\text{O}_5)_2(\text{OH})_2$
Montmorillonite	$\left(\text{Al}_{1.67} \text{Na}_{0.33} \text{Mg}_{0.33} \right) (\text{Si}_2\text{O}_5)_2 (\text{OH})_2$
Mica	$\text{Al}_2\text{K}(\text{Si}_{1.5}\text{Al}_{0.5}\text{O}_5)_2(\text{OH})_2$
Illite	$\text{Al}_{2-x}\text{Mg}_x\text{K}_{1-y}(\text{Si}_{1.5-y}\text{Al}_{0.5+y}\text{O}_5)_2(\text{OH})_2$

A related material is talc, a hydrous magnesium silicate with a layer structure similar to the clay minerals and having the ideal formula $\text{Mg}_3(\text{Si}_2\text{O}_5)_2(\text{OH})_2$. Talc is an important raw material for the manufacture of electrical and electronic components and for making tile. Asbestos minerals are a group of hydrous magnesium silicates which have a fibrous structure. The principal variety is chrysotile, $\text{Mg}_3\text{Si}_2\text{O}_5(\text{OH})_4$.

In addition to the hydrous silicates already discussed, anhydrous silica and silicate materials are basic raw materials for much of the ceramic industry. SiO_2 is a major ingredient in glass, glazes, enamels, refractories, abrasives, and whiteware compositions. It is widely used because it is inexpensive, hard, chemically stable, and relatively infusible and has the ability to form glasses. There is a variety of mineral forms in which silica occurs, but by far the most important as a raw material is quartz. It is used as quartzite rock, as quartz sand, and as finely ground *potter's flint*. The major source of this material is sandstone, which consists of lightly bonded quartz grains. A denser quartzite, *gannister*, is used for refractory brick. Quartz is also used in the form of large, nearly perfect crystals, but these have been mostly supplanted by synthetic crystals, manufactured by a hydrothermal process.

Together with quartz, which serves as a refractory backbone constituent, and clay, which provides plasticity, traditional triaxial porcelains (originally invented in China) include feldspar, an anhydrous aluminosilicate containing K^+ , Na^+ , or Ca^{2+} as a flux which aids in the formation of a glass phase. The major materials of commercial interest are potash feldspar (microcline or orthoclase), $\text{K}(\text{AlSi}_3)\text{O}_8$, soda feldspar (albite), $\text{Na}(\text{AlSi}_3)\text{O}_8$, and lime feldspar (anorthite), $\text{Ca}(\text{Al}_2\text{Si}_2)\text{O}_8$. Other related materials sometimes used are nepheline syenite, a quartzfree igneous rock composed of nephelite, $\text{Na}_2(\text{Al}_2\text{Si}_2)\text{O}_8$, albite, and microcline; also wollastonite, CaSiO_3 . One group of silicate minerals, the sillimanite group, having the composition Al_2SiO_5 , is used for the manufacture of refractories.

Most of the naturally occurring nonsilicate materials are used primarily as refractories. Aluminum oxide is mostly prepared from the mineral bauxite by the Bayer process, which involves the selective leaching of the alumina by caustic soda, followed by the precipitation of aluminum hydroxide. Some bauxite is used directly in the electric-furnace production of alumina, but most is first purified. Magnesium oxide is produced both from natural magnesite, MgCO_3 , and from magnesium hydroxide, Mg(OH)_2 , obtained from seawater or brines. Dolomite, a solid solution of calcium and magnesium carbonates with the formula $\text{CaMg(CO}_3)_2$, is used to make basic brick for use in the steel industry. Another refractory widely used for metallurgical purposes is chrome ore, which consists primarily of a complex solid solution of spinels, $(\text{Mg,Fe})(\text{Al,Cr})_2\text{O}_4$, which make up most of the material; the remainder consists of various magnesium silicates.

Other mineral-based materials which are widely used include soda ash, Na_2CO_3 , mostly manufactured from sodium chloride; borate materials including kernite, $\text{Na}_2\text{B}_4\text{O}_7 \cdot 4\text{H}_2\text{O}$, and borax, $\text{Na}_2\text{B}_4\text{O}_7 \cdot 10\text{H}_2\text{O}$, used as fluxing agents; fluorspar, CaF_2 , used as a powerful flux for some glazes and glasses; and phosphate materials mostly derived from apatite, $\text{Ca}_5(\text{OH,F})(\text{PO}_4)_3$.

Although most traditional ceramic formulations are based on the use of natural mineral materials which are inexpensive and readily available, an increasing fraction of specialized ceramic ware depends on the availability of chemically processed materials which may or may not start directly from mined products and in which the particle-size characteristics and chemical purity are closely controlled. Silicon carbide for abrasives is manufactured by electrically heating mixtures of sand and coke to a temperature of about 2200°C where they react to form SiC and carbon monoxide. Already mentioned, seawater magnesia, Bayer alumina, and soda ash are widely used chemical products. In the manufacture of barium titanate capacitors, chemically purified titania and barium carbonate are used as raw materials. A wide range of magnetic ceramics is manufactured from chemically precipitated iron oxide. Nuclear-fuel elements are manufactured from chemically prepared UO_2 . Single crystals of sapphire and ruby and also porefree polycrystalline aluminum oxide are prepared from aluminum oxide made by precipitating and carefully calcining alum in order to maintain good control of both chemistry and particle size. Special techniques of material preparation such as freeze-drying droplets of solution to form homogeneous particles of small size and high purity are receiving increasing attention, as is the vapor deposition of thin-film materials in a carefully controlled chemical and physical form. In general, raw-material preparation is clearly headed

towa
tion
partic
on m

For
firing
conce
the ra
which
prepa
have
micro
beles
suspe
depen
stable
propo
coher
of the
partic
size, i
Mixer
the co
achiev
partic
result
numb
with a
during

In a
intima
within
firing
usual
ball m
improv
tion of
either
which
mainta
gates,
formin

toward the increasing use of mechanical, physical, and chemical purification and upgrading of raw materials together with special control of particle size and particle-size distribution and away from the sole reliance on materials in the form found in nature.

Forming and Firing. The most critical factors affecting forming and firing processes are the raw materials and their preparation. We have to be concerned with both the particle size and the particle-size distribution of the raw materials. Typical clay materials have a particle-size distribution which ranges from 0.1 to 50 microns for the individual particles. For the preparation of porcelain compositions the flint and feldspar constituents have a substantially larger particle size ranging between 10 and 200 microns. The fine-particle constituents, which for special ceramics may be less than 1 micron, are essential for the forming process, since colloidal suspensions, plastic mixes with a liquid-phase binder, and dry pressing all depend on very small particles flowing over one another or remaining in a stable suspension. For suspensions, the settling tendency is directly proportional to the density and particle size. For plastic forming the coherence of the mass and its yield point are determined by the capillarity of the liquid between particles; this force is inversely proportional to the particle size. However, if all the material were of a uniformly fine particle size, it would not be feasible to form a high concentration of solids. Mixing in a coarser material allows the fines to fill the interstices between the coarse particles such that a maximum particle-packing density is achieved at a ratio of about 70% coarse and 30% fine material when two particle sizes are used. In addition, during the drying process, shrinkage results from the removal of water films between particles. Since the number of films increases as the particle size decreases, bodies prepared with a liquid binder and all fine-particle materials have a high shrinkage during drying and the resultant problems of warping and distortion.

In addition to a desired particle size and particle-size distribution, intimate mixing of material is necessary for uniformity of properties within a body and for the reaction of individual constituents during the firing process. For preparing slurries or a fine-grain plastic mass, it is the usual practice to use wet mixing, with the raw materials placed together in ball mills or a blunger. Shearing stresses developed in the mixing process improve the properties of a plastic mix and ensure the uniform distribution of the fine-grain constituent. For dewatering the wet-milled mix, either a filter press may be used, or more commonly spray-drying, in which droplets of the slurry are dried with a countercurrent of warm air to maintain their uniform composition during drying. The resulting aggregates, normally 1 mm or so in size, flow and deform readily in subsequent forming.

Since the firing process also depends on the capillary forces resulting from surface energy to consolidate and densify the material and since these forces are inversely proportional to particle size, a substantial percentage of fine-particle material is necessary for successful firing. The clay minerals are unique in that their fine particle size provides both the capability for plastic forming and also sufficiently large capillary forces for successful firing. Other raw materials have to be prepared by chemical precipitation or by milling into the micron particle range for equivalent results to be obtained.

Perhaps the simplest method of compacting a ceramic shape consists of forming a dry or slightly damp powder, usually with an organic binder, in a metal die at sufficiently high pressures to form a dense, strong piece. This method is used extensively for refractories, tiles, special electrical and magnetic ceramics, spark-plug insulators and other technical ceramics, nuclear-fuel pellets, and a variety of products for which large numbers of simple shapes are required. It is relatively inexpensive and can form shapes to close tolerances. Pressures in the range of 3000 to 30,000 psi are commonly used, the higher pressures for the harder materials such as pure oxides and carbides. Automatic dry pressing at high rates of speed has been developed to a high state of effectiveness. One limitation is that for a shape with a high length-to-diameter ratio the frictional forces of the powder, particularly against the die wall, lead to pressure gradients and a resulting variation of density within the piece. During firing these density variations are eliminated by material flow during sintering; it necessarily follows that there is a variation in shrinkage and a loss of the original tolerances. One modification of the dry-pressing method which leads to a more uniform density is to enclose the sample in a rubber mold inserted in a hydrostatic chamber to make pieces by hydrostatic molding, in which the pressure is more uniformly applied. Variations in sample density and shrinkage are less objectionable. This method is widely used for the manufacture of spark-plug insulators and for special electrical components in which a high degree of uniformity and high level of product quality are required.

A quite different method of forming is to extrude a stiff plastic mix through a die orifice, a method commonly used for brick, sewer pipe, hollow tile, technical ceramics, electrical insulators, and other materials having an axis normal to a fixed cross section. The most widely practiced method is to use a vacuum auger to eliminate air bubbles, thoroughly mix the body with 12 to 20% water, and force it through a hardened steel or carbide die. Hydraulic piston extruders are also widely used.

The earliest method of forming clay ware, one still widely used, is to add enough water so that the ware can readily be formed at low pressures.

This may be done under hand pressure such as building ware with coils, free-forming ware, or hand throwing on a potter's wheel. The process can be mechanized by soft-plastic pressing between porous plaster molds and also by automatic *jigging*, which consists of placing a lump of soft plastic clay on the surface of a plaster-of-paris mold and rotating it at about 400 rpm while pulling a profile tool down on the surface to spread the clay and form the upper surface.

When a larger amount of water is added, the clay remains sticky plastic until a substantial amount has been added. Under a microscope it is seen that individual clay particles are gathered in aggregates or flocs. However, if a small quantity of sodium silicate is added to the system, there is a remarkable change, with a substantial increase in fluidity resulting from the individual particles being separated or *deflocculated*. With proper controls a fluid suspension can be formed with as little as 20% liquid, and a small change in the liquid content markedly affects the fluidity. When a suspension such as this is cast into a porous plaster-of-paris mold, the mold sucks liquid from the contact area, and a hard layer is built on the surface. This process can be continued until the entire interior of the mold is filled (solid casting) or the mold can be inverted and the excess liquid poured out after a suitable wall thickness is built up (drain casting).

In each of the processes which require the addition of some water content, the drying step in which the liquid is removed must be carefully controlled for satisfactory results, more so for the methods using a higher liquid content. During drying, the initial drying rate is independent of the water content, since in this period there is a continuous film of water at the surface. As the liquid evaporates, the particles become pressed more closely together and shrinkage occurs until they are in contact in a solid structure free from water film. During the shrinkage period, stresses, warping, and possibly cracks may develop because of local variations in the liquid content; during this period rates must be carefully controlled. Once the particles are in contact, drying can be continued at a more rapid rate without difficulty. For the dry-pressing or hydrostatic molding process, the difficulties associated with drying are avoided, an advantage for these methods.

After drying, ceramic ware is normally fired to temperatures ranging from 700 to 1800°C, depending on the composition and properties desired. Ware which is to be glazed or decorated may be fired in different ways. The most common procedure is to fire the ware without a glaze to a sufficiently high temperature to mature the body; then a glaze is applied and fired at a low temperature. Another method is to fire the ware initially to a low temperature, a *bisque* fire; then apply the glaze and mature the body and glaze together at a higher temperature. A third method is to

apply the glaze to the unfired ware and heat them together in a one-fire process.

During the firing process, either a viscous liquid or sufficient atomic mobility in the solid is developed to permit chemical reactions, grain growth, and sintering; the last consists of allowing the forces of surface tension to consolidate the ware and reduce the porosity. The volume shrinkage which occurs is just equal to the porosity decrease and varies from a few to 30 or 40 vol%, depending on the forming process and the ultimate density of the fired ware. For some special applications, complete density and freedom from all porosity are required, but for other applications some residual porosity is desirable. If shrinkage proceeds at an uneven rate during firing or if part of the ware is restrained from shrinking by friction with the material on which it is set, stresses, warping, and cracking can develop. Consequently, care is required in setting the ware to avoid friction. The rate of temperature rise and the temperature uniformity must be controlled to avoid variations in porosity and shrinkage. The nature of the processes taking place is discussed in detail in Chapters 11 and 12.

Several different types of kilns are used for firing ware. The simplest is a skove kiln in which a benchwork of brick is set up inside a surface coating with combustion chambers under the material to be fired. Chamber kilns of either the up-draft or down-draft type are widely used for batch firing in which temperature control and uniformity need not be too precise. In order to achieve uniform temperatures and maximum use of fuel, chamber kilns in which the air for combustion is preheated by the cooling ware in an adjacent chamber, the method used in ancient China, is employed. The general availability of more precise temperature controls for gas, oil, and electric heating and the demands for ware uniformity have led to the increased use of tunnel kilns in which a temperature profile is maintained constant and the ware is pushed through the kiln to provide a precise firing schedule under conditions such that effective control can be obtained.

Melting and Solidification. For most ceramic materials the high volume change occurring during solidification, the low thermal conductivity, and the brittle nature of the solid phase have made melting and solidification processes comparable with metal casting and foundry practice inappropriate. Recently, techniques have been developed for unidirectional solidification in which many of these difficulties can be substantially avoided. This process has mainly been applied to forming controlled structures of metal alloys which are particularly attractive for applications such as turbine blades for high-temperature gas turbines. So far as we are aware, there is no large scale manufacture of ceramics in this way,

but we anticipate that the development of techniques for the unidirectional solidification of ceramics will be an area of active research during the next decade.

Another case in which these limitations do not apply is that of glass-forming materials in which the viscosity increases over a broad temperature range so that there is no sharp volume discontinuity during solidification and the forming processes can be adjusted to the fluidity of the glass. Glass products are formed in a high-temperature viscous state by five general methods: (1) blowing, (2) pressing, (3) drawing, (4) rolling, and (5) casting. The ability to use these processes depends to a large extent on the viscous flow characteristics of the glass and its dependence on temperature. Often surface chilling permits the formation of a stable shape while the interior remains sufficiently fluid to avoid the buildup of dangerous stresses. Stresses generated during cooling are relieved by annealing at temperatures at which the force of gravity is insufficient to cause deformation. This is usually done in an annealing oven or lehr which, for many silicate glasses, operates at temperatures in the range of 400 to 500°C.

The characteristics most impressive about commercial glass-forming operations are the rapidity of forming and the wide extent of automation. Indeed, this development is typical of the way in which technical progress affects an industry. Before the advent of glass-forming machinery, a major part of the container industry was based on ceramic stoneware. Large numbers of relatively small stoneware potters existed solely for the manufacture of containers. The development of automatic glass-forming machinery allowing the rapid and effective production of containers on a continuous basis has eliminated stoneware containers from common use.

Special Processes. In addition to the broadly applicable and widely used processes discussed thus far, there is a variety of special processes which augment, modify, extend, or replace these forming methods. These include the application of glazes, enamels, and coatings, hot-pressing materials with the combined application of pressure and temperature, methods of joining metals to ceramics, glass crystallization, finishing and machining operations, preparation of single crystals, and vapor-deposition processes.

Much ceramic ware is coated with a glaze, and porcelain enamels are commonly applied on a base of sheet steel or cast iron as well as for special jewelry applications. Glazes and enamels are normally prepared in a wet process by milling together the ingredients and then applying the coating by brushing, spraying, or dipping. For continuous operation, spray coating is most frequently used, but for some applications more satisfactory coverage can be obtained by dipping or painting. For

porcelain enamels on cast iron, large castings heated in a furnace are coated with a dry enamel powder which must be distributed uniformly over the surface, where it fuses and sticks. In addition to these widely used processes, special coatings for technical ware have been applied by flame spraying to obtain a refractory dense layer; vacuum-deposited coatings have been formed by evaporation or cathodic sputtering; coatings have been applied by chemical vapor deposition; electrophoretic deposition has been applied; and other specialized techniques have had some limited applications.

To obtain a high density together with fine particle size, particularly for materials such as carbides and borides, the combination of pressure with high temperature is an effective technique mostly used for small samples of a simple configuration. At lower temperatures, glass-bonded mica is formed in this way for use as an inexpensive insulation. One of the main advantages of the hot-pressing method is that material preparation is less critical than for the sintering processes, which require a high degree of material uniformity for successful applications of the highest-quality products. The main difficulties with hot-pressing techniques are applying the method to large shapes and the time required for heating the mold and sample, which makes the method slow and expensive.

For many applications, joining processes are necessary to form fabricated units. In manufacturing teacups, for example, the handle is normally molded separately, dipped in a slip, and stuck on the body of the cup. Sanitary fixtures of complex design are similarly built up from separately formed parts. For many electronic applications requiring pressure-tight seals, it is necessary to form a bond between metals and ceramics. For glass-metal seals, the main problem is matching the expansion coefficient of the glass to that of the metal and designing the seal so that large stresses do not develop in use; special metal alloys and sealing glasses have been designed for this purpose. For crystalline ceramics, the most widely applied method has been to use a molybdenum-manganese layer which, when fired under partially oxidizing conditions, forms an oxide that reacts with the ceramic to give an adhesive bonding layer. In some cases, reactive metal brazes containing titanium or zirconium have been used.

One of the most important developments in ceramic forming has been to use a composition which can be formed as a glass and then transformed subsequent to forming into a product containing crystals of controlled size and amount. Classic examples of this are the striking gold-ruby glasses, in which the color results from the formation of colloidal gold particles. During rapid initial cooling, nucleation of the metal particles

occurs; subsequent reheating into the growth region develops proper crystallite sizes for the colloidal ruby color. In the past 10 years there has been extensive development of glasses in which the volume of crystals formed is much larger than the volume of the residual glass. By controlled nucleation and growth, glass-ceramics are made in which the advantage of automatic glass-forming processes is combined with some of the desirable properties of a highly crystalline body.

For most forming operations, some degree of finishing or machining is required which may range from fettling the mold lines from a slip-cast shape to diamond-grinding the final contour of a hard ceramic. For hard materials such as aluminum oxide, as much machining as feasible is done in the unfired state or the presintered state, with final finishing only done on the hard, dense ceramic where required.

A number of processes have been developed for the formation of ceramics directly from the vapor phase. Silica is formed by the oxidation of silicon tetrachloride. Boron and silicon carbide fibers are made by introducing a volatile chloride with a reducing agent into a hot zone, where deposition occurs on a fine tungsten filament. Pyrolytic graphite is prepared by the high-temperature deposition of graphite layers on a substrate surface by the pyrolytic decomposition of a carbon-containing gas. Many carbides, nitrides, and oxides have been formed by similar processes. For electronic applications, the development of single-crystal films by these techniques appears to have many potential applications.

Thin-wafer substrates are formed by several techniques, mostly from alumina. A widely used development is the technique in which a fluid body is prepared with an organic binder and uniformly spread on a moving nonporous belt by a doctor blade to form thin, tough films which can subsequently be cut to shape; holes can be introduced in a high-speed punch press.

There is an increasing number of applications in which it is necessary or desirable to have single-crystal ceramics because of special optical, electrical, magnetic, or strength requirements. The most widespread method of forming these is the Czochralski process, in which the crystal is slowly pulled from a molten melt, a process used for aluminum oxide, ruby, garnet, and other materials. In the Verneuil process a liquid cap is maintained on a growing boule by the constant-rate addition of powdered material at the liquid surface. For magnetic and optical applications thin single-crystal films are desirable which have been prepared by epitaxial growth from the vapor phase. Hydrothermal growth from solution is widely used for the preparation of quartz crystals, largely replacing the use of natural mineral crystals for device applications.

1.3 Ceramic Products

The diversity of ceramic products, which range from microscopic single-crystal whiskers, tiny magnets, and substrate chips to multiton refractory furnace blocks, from single-phase closely controlled compositions to multiphase multicomponent brick, and from porefree transparent crystals and glasses to lightweight insulating foams is such that no simple classification is appropriate. From the point of view of historical development and tonnage produced, it is convenient to consider the mineral-raw-material products, mostly silicates, separately from newer nonsilicate formulations.

Traditional Ceramics. We can define traditional ceramics as those comprising the silicate industries—primarily clay products, cement, and silicate glasses.

The art of making pottery by forming and burning clay has been practiced from the earliest civilizations. Indeed, the examination of pottery fragments has been one of the best tools of the archeologist. Burnt clayware has been found dating from about 6500 B.C. and was well developed as a commercial product by about 4000 B.C.

Similarly, the manufacture of silicate glasses is an ancient art. Naturally occurring glasses (obsidian) were used during the Stone Age, and there was a stable industry in Egypt by about 1500 B.C.

In contrast, the manufacture of portland cement has only been practiced for about 100 years. The Romans combined burned lime with volcanic ash to make a natural hydraulic cement; the art seems then to have disappeared, but the hydraulic properties of lightly burned clayey limes were rediscovered in England about 1750, and in the next 100 years the manufacturing process, essentially the same as that used now, was developed.

By far the largest segment of the silicate ceramic industry is the manufacture of various glass products. These are manufactured mostly as sodium-calcium-silicate glasses. The next largest segment of the ceramic industry is lime and cement products. In this category the largest group of materials is hydraulic cements such as those used for building construction. A much more diverse group of products is included in the classification of whitewares. This group includes pottery, porcelain, and similar fine-grained porcelainlike compositions which comprise a wide variety of specific products and uses. The next classification of traditional ceramics is porcelain enamels, which are mainly silicate glasslike coatings on metals. Another distinct group is the structural clay products, which consist mainly of brick and tile but include a variety of similar products such as sewer pipe. A particularly important group of the traditional

ceramics industry is refractories. About 40% of the refractory industry consists of fired-clay products, and another 40% consists of heavy nonclay refractories such as magnesite, chromite, and similar compositions. In addition there is a sizable demand for various special refractory compositions. The abrasives industry produce mainly silicon carbide and aluminum oxide abrasives. Finally, a segment of the ceramic industry which does not produce ceramic products as such is concerned with the mineral preparation of ceramic and related raw materials.

Most of these traditional ceramics could be adequately defined as the silicate industries, which indeed was the description originally proposed for the American Ceramic Society in 1899. The silicate industries still compose by far the largest part of the whole ceramic industry, and from this point of view they can be considered the backbone of the field.

New Ceramics. In spite of its antiquity, the ceramic industry is not stagnant. Although traditional ceramics, or silicate ceramics, account for the large bulk of material produced, both in tonnage and in dollar volume, a variety of new ceramics has been developed in the last 20 years. These are of particular interest because they have either unique or outstanding properties. Either they have been developed in order to fulfill a particular need in greater temperature resistance, superior mechanical properties, special electrical properties, and greater chemical resistivity, or they have been discovered more or less accidentally and have become an important part of the industry. In order to indicate the active state of development, it may be helpful to describe briefly a few of these new ceramics.

Pure oxide ceramics have been developed to a high state of uniformity and with outstanding properties for use as special electrical and refractory components. The oxides most often used are alumina (Al_2O_3), zirconia (ZrO_2), thorium (ThO_2), beryllia (BeO), magnesia (MgO), spinel (MgAl_2O_4), and forsterite (Mg_2SiO_4).

Nuclear fuels based on uranium dioxide (UO_2) are widely used. This material has the unique ability to maintain its good properties after long use as a fuel material in nuclear reactors.

Electrooptic ceramics such as lithium niobate (LiNbO_3) and lanthanum-modified lead zirconate titanate (PLZT) provide a medium by which electrical information can be transformed to optical information or by which optical functions can be performed on command of an electrical signal.

Magnetic ceramics with a variety of compositions and uses have been developed. They form the basis of magnetic memory units in large computers. Their unique electrical properties are particularly useful in high-frequency microwave electronic applications.

Single crystals of a variety of materials are now being manufactured,

either to replace natural crystals which are unavailable or for their own unique properties. Ruby and garnet laser crystals and sapphire tubes and substrates are grown from a melt; large quartz crystals are grown by a hydrothermal process.

Ceramic nitrides with unusually good properties for special applications have been developed. These include aluminum nitride, a laboratory refractory for melting aluminum; silicon nitrides and SiAlON, commercially important new refractories and potential gas turbine components; and boron nitride, which is useful as a refractory.

Enamels for aluminum have been developed and have become an important part of the architectural industry.

Metal-ceramic composites have been developed and are now an important part of the machine-tool industry and have important uses as refractories. The most important members of this group are various carbides bonded with metals and mixtures of a chromium alloy with aluminum oxide.

Ceramic carbides with unique properties have been developed. Silicon carbide and boron carbide in particular are important as abrasive materials.

Ceramic borides have been developed which have unique properties of high-temperature strength and oxidation resistance.

Ferroelectric ceramics such as barium titanate have been developed which have extremely high dielectric constants and are particularly important as electronic components.

Nonsilicate glasses have been developed and are particularly useful for infrared transmission, special optical properties, and semiconducting devices.

Molecular sieves which are similar to, but are more controlled than, natural zeolite compositions are being made with controlled structures so that the lattice spacing, which is quite large in these compounds, can be used as a means of separating compounds of different molecular sizes.

Glass-ceramics are a whole new family of materials based on fabricating ceramics by forming as a glass and then nucleating and crystallizing to form a highly crystalline ceramic material. Since the original introduction of Pyroceram by the Corning Glass Works the concept has been extended to dozens of compositions and applications.

Porefree polycrystalline oxides have been made based on alumina, yttria, spinel, magnesia, ferrites, and other compositions.

Literally dozens of other new ceramic materials, unknown 10 or 20 years ago are now being manufactured and used. From this point of view the ceramic industry is one of our most rapidly changing industries, with new products having new and useful properties constantly being de-

veloped. These ceramics are being developed because there is a real need for new materials to transform presently available designs into practical, serviceable products. By far the major hindrance to the development of many new technologically feasible structures and systems is the lack of satisfactory materials. New ceramics are constantly filling this need.

New Uses for Ceramics. In the same way that the demand for new and better properties has led to the development of new materials, the availability of new materials had led to new uses based on their unique properties. This cycle of new ceramics—new uses—new ceramics has accelerated with the attainment of a better understanding of ceramics and their properties.

One example of the development of new uses for ceramics has occurred in the field of magnetic ceramic materials. These materials have hysteresis loops which are typical for ferromagnetic materials. Some have very nearly the square loop that is most desirable for electronic computer memory circuits. This new use for ceramics has led to extensive studies and development of materials and processes.

Another example is the development of nuclear power, which requires uranium-containing fuels having large fractions of uranium (or sometimes thorium), stability against corrosion, and the ability to withstand the fissioning of a large part of the uranium atoms without deterioration. For many applications UO_2 is an outstanding material for this fuel. Urania ceramics have become an important part of reactor technology.

In rocketry and missile development two critical parts which must withstand extreme temperatures and have good erosion resistance are the nose cone and the rocket throat. Ceramic materials are used for both.

For machining metals at high speeds it has long been known that oxide ceramics are superior in many respects as cutting tools. However, their relatively low and irregular strength makes their regular use impossible. The development of alumina ceramics with high and uniform strength levels has made them practicable for machining metals and has opened up a new field for ceramics.

In 1946 it was discovered that barium titanate had a dielectric constant 100 times larger than that of other insulators. A whole new group of these ferroelectric materials has since been discovered. They allow the manufacture of capacitors which are smaller in size but have a larger capacity than other constructions, thus improving electronic circuitry and developing a new use for ceramic materials.

In jet aircraft and other applications metal parts have had to be formed from expensive, and in wartime unobtainable, alloys to withstand the moderately high temperatures encountered. When a protective ceramic coating is applied, the temperature limit is increased, and either higher

temperatures can be reached or less expensive and less critical alloys can be substituted.

Many further applications of ceramics which did not even exist a few years ago can be cited, and we may expect new uses to develop that we cannot now anticipate.

Suggested Reading

1. F. H. Norton, *Elements of Ceramics*, 2d ed., Addison Wesley Publishing Company, Inc., Reading, Mass., 1974.
2. F. H. Norton, *Fine Ceramics*, McGraw-Hill Book Company, New York, 1970.
3. F. H. Norton, *Refractories*, 4th ed., McGraw-Hill Book Company, New York, 1968.
4. Institute of Ceramics Textbook Series:
 - (a) W. E. Worrall, *Raw Materials*, Maclaren & Sons, Ltd., London, 1964.
 - (b) F. Moore, *Rheology of Ceramic Systems*, Maclaren & Sons, Ltd., London, 1965.
 - (c) R. W. Ford, *Drying*, Maclaren & Sons, Ltd., London, 1964.
 - (d) W. F. Ford, *The Effect of Heat on Ceramics*, Maclaren & Sons, Ltd., London, 1967.
5. "Fabrication Science," *Proc. Brit. Ceram. Soc.*, No. 3 (September, 1965).
6. "Fabrication Science: 2," *Proc. Brit. Ceram. Soc.*, No. 12 (March, 1969).
7. J. E. Burke, Ed., *Progress in Ceramic Science*, Vols. 1-4, Pergamon Press, Inc., New York, 1962-1966.
8. W. D. Kingery, Ed., *Ceramic Fabrication Processes*, John Wiley & Sons, Inc., New York, 1958.
9. F. V. Tooley, Ed., *Handbook of Glass Manufacture*, 2 Vols., Ogden Publishing Company, New York, 1961.
10. A. Davidson, Ed., *Fabrication of Non-metals: Handbook of Precision Engineering*, Vol. 3, McGraw-Hill Book Company, New York, 1971.

Ceramic Phase-Equilibrium Diagrams

At equilibrium a system is in its lowest free energy state for the composition, temperature, pressure, and other imposed conditions. When a given set of system parameters is fixed, there is only one mixture of phases that can be present, and the composition of each of these phases is determined. Phase-equilibrium diagrams provide a clear and concise method of graphically representing this equilibrium situation and are an invaluable tool for characterizing ceramic systems. They record the composition of each phase present, the number of phases present, and the amounts of each phase present at equilibrium.

The time that it takes to reach this equilibrium state from any arbitrary starting point is highly variable and depends on factors other than the final equilibrium state. Particularly for systems rich in silica the high viscosity of the liquid phase leads to slow reaction rates and very long times before equilibrium is established; equilibrium is rarely achieved. For these systems and for others, metastable equilibrium, in which the system tends to a lower but not the lowest free energy state, becomes particularly important.

It is obvious that the phases present and their composition are an essential element in analysing, controlling, improving, and developing ceramic materials. Phase diagrams are used for determining phase and composition change occurring when the partial pressure of oxygen or other gases is changed, for evaluating the effects of heat treatments on crystallization and precipitation processes, for planning new compositions, and for many other purposes. We have already seen the importance of thermodynamic equilibrium in our discussions of single-phase systems: crystalline solid solutions (Chapter 2), crystalline imperfections (Chapter 4), structure of glasses (Chapter 3), and surfaces and interfaces (Chapter 5). In this chapter we concentrate our attention on equilibria involving two or more phases.

7.1 Gibbs's Phase Rule

When a system is in equilibrium, it is necessary that the temperature and pressure be uniform throughout and that the chemical potential or vapor pressure of each constituent be the same in every phase. Otherwise there would be a tendency for heat or material to be transferred from one part of the system to some other part. In 1874 J. Willard Gibbs* showed that these equilibrium conditions can occur only if the relationship

$$P + V = C + 2 \quad (7.1)$$

is satisfied. This is known as the *phase rule*, with P being the number of phases present at equilibrium, V the variance or number of degrees of freedom, and C the number of components. This relationship is the basis for preparing and using phase-equilibrium diagrams.

A phase is defined as any part of the system which is physically homogeneous and bounded by a surface so that it is mechanically separable from other parts of the system. It need not be continuous; that is, two ice cubes in a drink are one phase. The number of degrees of freedom or the variance is the number of intensive variables (pressure, temperature, composition) that can be altered independently and arbitrarily without bringing about the disappearance of a phase or the appearance of a new phase. The number of components is the smallest number of independently variable chemical constituents necessary and sufficient to express the composition of each phase present. The meaning of these terms will become clearer as they are applied to specific systems in the following sections.

Deduction of the phase rule follows directly from the requirement that the chemical potential μ_i of each constituent i be the same in every phase present at equilibrium. The chemical potential is equal to the partial molar free energy \bar{G}_i ,

$$\bar{G}_i = \left(\frac{\partial G}{\partial n_i} \right)_{T, P, n_1, n_2, \dots}$$

which is the change in free energy of a system at constant temperature and pressure resulting from the addition of one mole of constituent i to such a large quantity of the system that there is no appreciable change in the concentration. In a system with C components we have an independent equation for each component representing the equality of chemical potentials. For a system containing P phases, we have

$$\mu_1^a = \mu_1^b = \mu_1^c = \dots = \mu_1^P \quad (7.2)$$

*Collected Works, Vol. 1, Longmans, Green & Co., Ltd., London, 1928.

which
C(P -
C - 1)
phases
impose

V

which i
The
equilibr
and het
equilibr
that equ
conform

7.2 Or

In a
liquid,
differen
graphic
reviewe
The ind
phases:
it boils;
water v
changes
present
Since
and diff
practice
usually
7.2d. Al
one as
pressure

381-518

CERAMIC PHASE-EQUILIBRIUM DIAGRAMS

271

$$\mu_2^a = \mu_2^b = \mu_2^c = \dots = \mu_2^P \quad (7.3)$$

etc.

which constitute $C(P - 1)$ independent equations which serve to fix $C(P - 1)$ variables. Since the composition of each phase is defined by $C - 1$ concentration terms, completely defining the composition of P phases requires $P(C - 1)$ concentration terms, which together with the imposed conditions of temperature and pressure give

$$\text{Total number of variables} = P(C - 1) + 2 \quad (7.4)$$

$$\text{Variables fixed by equality of chemical potentials} = C(P - 1) \quad (7.5)$$

$$\text{Variables remaining to be fixed} = P(C - 1) + 2 - C(P - 1) \quad (7.6)$$

$$V = C - P + 2 \quad (7.7)$$

which is Gibbs's phase rule (Eq. 7.1).

The main limitation on the phase rule is that it applies only to equilibrium states, requiring homogeneous equilibrium within each phase and heterogeneous equilibrium between phases. Although a system in equilibrium always obeys the phase rule (and nonconformance proves that equilibrium does not exist), the reverse is not always true. That is, conformance with the phase rule is not a demonstration of equilibrium.

7.2 One-Component Phase Diagrams

In a single-component system the phases that can occur are vapor, liquid, and various polymorphic forms of the solid. (The energy of different polymorphic forms as related to temperature and crystallographic structure has been discussed in Section 2.10, and might well be reviewed by the reader, since it is closely related to the present section.) The independent variables that cause appearance or disappearance of phases are temperature and pressure. For example, when we heat water, it boils; if we cool it, it freezes. If we put it in an evacuated chamber, the water vapor pressure quickly reaches some equilibrium value. These changes can be diagrammatically represented by showing the phases present at different temperatures and pressures (Fig. 7.1).

Since this is a one-component system, even the air phase is eliminated, and different phase distributions correspond to Fig. 7.2a to c. In actual practice measurements in which the vapor phase is unimportant are usually made at constant atmospheric pressure in a way similar to Fig. 7.2d. Although this is not an ideal closed system, it closely approximates one as long as the vapor pressure is low compared with atmospheric pressure (so that we can ignore the insignificant vapor phase which would

erature
ntial or
erwise
om one
howed
ip

(7.1)

iber of
rees of
e basis

sically
nically
s; that
ees of
ssure,
bitrar-
ance
ber of
ient to
these
in the

nt that
phase
molar

erature
it i to
nge in
lepen-
mical

(7.2)

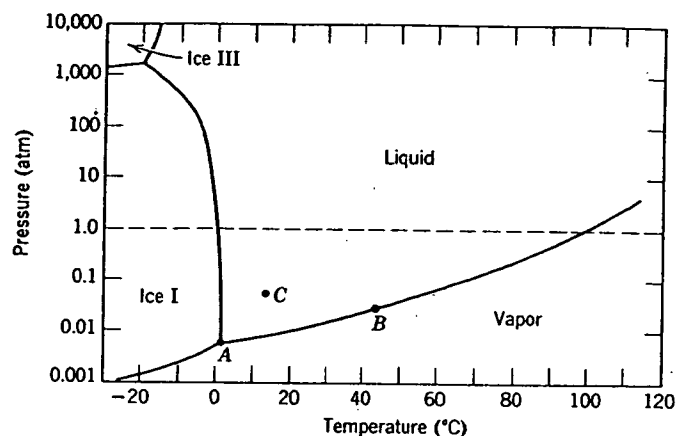
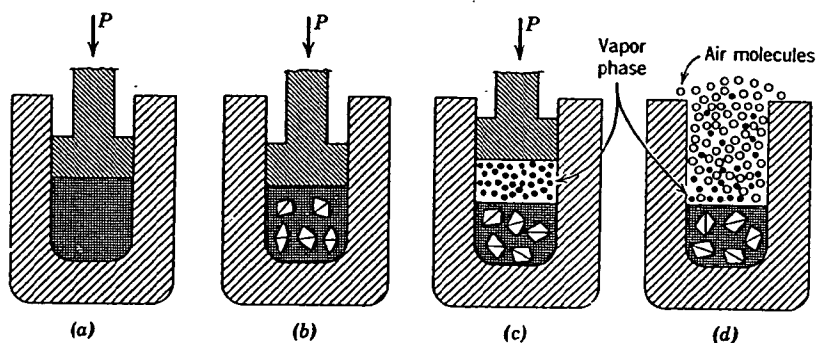
Fig. 7.1. Pressure-temperature diagram for H_2O .

Fig. 7.2. Experimental conditions for a single-component system with (a) one phase, (b) two phases, (c) three phases, and (d) common conditions, with the condensed phase exposed to a gas atmosphere.

not exist at all in a closed system) or is equal to or greater than atmospheric pressure (so that the vapor phase has the partial pressure predicted by the phase diagram). For many condensed systems of interest, the first criterion is satisfied.

In a one-component system the largest number of phases that can occur at equilibrium is given when the variance is zero: $P + V = C + 2$, $P + 0 = 1 + 2$, $P = 3$. When three phases are present at equilibrium (ice, water, vapor), as at point A in Fig. 7.1, any change in pressure or temperature causes the disappearance of a phase. The lines on the diagram represent conditions for two phases to exist together at equilibrium; for example, when liquid and vapor are present, as at point B, $P + V = C + 2$,

381-515

$2 + V = 1 + 2$, $V = 1$, and the variance is one. This means that either pressure or temperature, but not both, can be changed arbitrarily without the disappearance of a phase. If we change T_1 to T_2 , P_1 must also change to P_2 if both phases are to remain present. If only one phase is present, as at C,

$$P + V = C + 2, 1 + V = 1 + 2, V = 2,$$

and both pressure and temperature can be arbitrarily changed without the appearance of a new phase.

At 1 atm pressure, as shown in Fig. 7.1, equilibrium between the solid and liquid occurs at 0°C , the freezing point. Equilibrium coexistence of liquid and vapor occurs at 100°C , the boiling point. The slope of these phase-boundary curves is at any point determined by the Clausius-Clapeyron equation

$$\frac{dp}{dT} = \frac{\Delta H}{T \Delta V} \quad (7.8)$$

where ΔH is the molar heat of fusion, vaporization, or transformation, ΔV is the molar volume change, and T is the temperature. Since ΔH is always positive and ΔV is usually positive on going from a low-temperature to a high-temperature form, the slopes of these curves are usually positive. Since ΔV is usually small for condensed-phase transformations, lines between solid phases are often almost vertical.

There are a number of applications of one-component phase diagrams in ceramics. Perhaps the most spectacular of these is the development of the commercial production of synthetic diamonds from graphite. High temperatures and high pressures are necessary, as shown in Fig. 7.3. In addition, the presence of a liquid metal catalyst or mineralizer such as nickel is required for the reaction to proceed at a useful rate. Another system which has been extensively studied at high pressure and temperature is SiO_2 . At pressures above 30 to 40 kilobars a new phase, *coesite*, appears which has been found to occur in nature as a result of meteorite impacts. At even higher pressures, above 100 kilobars, another new phase, *stishovite*, has been found.

Of greater interest for ceramic applications are the low-pressure phases of silica, still subject to some dispute as to the role of minor impurities, but illustrated schematically in Fig. 7.4. There are five condensed phases which occur at equilibrium— α -quartz, β -quartz, β_2 -tridymite, β -cristobalite, and liquid silica. At 1 atm pressure the transition temperatures are as shown. As discussed in Section 2.10, the α -quartz- β -quartz transition at 573° is rapid and reversible. The other transformations shown are sluggish, so that long periods of time are required to reach equilib-

ecules

phase,
d phasethan
ssure
ns ofoccur
+ 0 =
water,
ature
esent
mple,
C + 2,

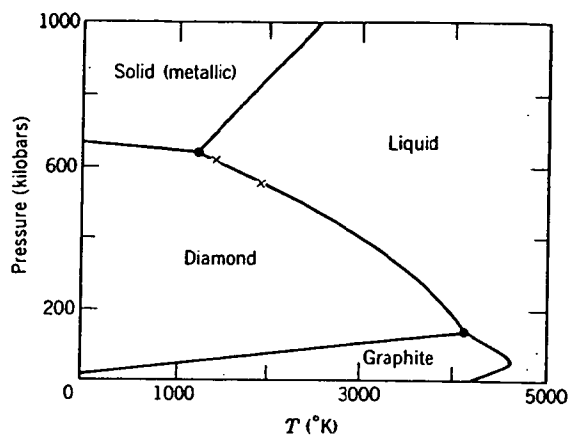


Fig. 7.3. High-pressure, high-temperature phase equilibrium diagram for carbon. From C. G. Suits, *Am. Sci.*, 52, 395 (1964).

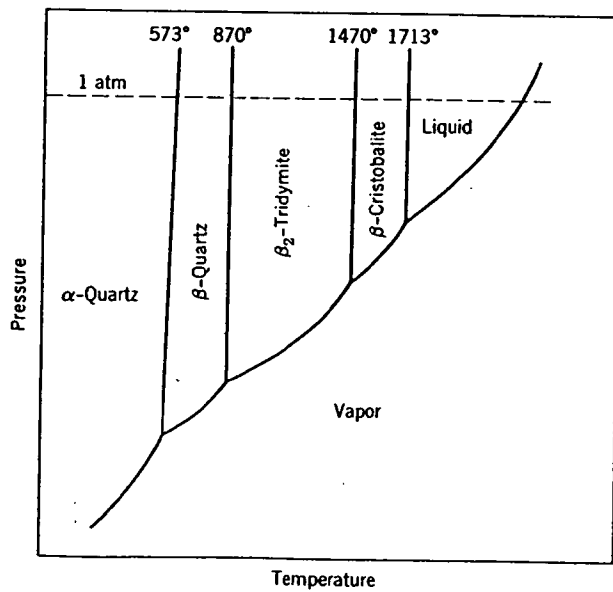


Fig. 7.4. Equilibrium diagram for SiO_2 .

rium. The chemical diagram may occur lines in the phase. For quartz is into α -c and β -tr the form when cooled to this state.

At any into another reverse transition, however, at 1100° β -tr-tridymite.

381-513

rium. The vapor pressure shown in the diagram is a measure of the chemical potential of silica in the different phases, and this same kind of diagram can be extended to include the metastable forms of silica which may occur (Fig. 7.5). The phase with the lowest vapor pressure (the heavy lines in the diagram) is the most stable at any temperature, the equilibrium phase. However, once formed, the transition between cristobalite and quartz is so sluggish that β -cristobalite commonly transforms on cooling into α -cristobalite. Similarly, β_2 -tridymite commonly transforms into α - and β -tridymite rather than into the equilibrium quartz forms. These are the forms present in the refractory silica brick, for example. Similarly, when cooled, the liquid forms silica glass, which can remain indefinitely in this state at room temperature.

At any constant temperature there is always a tendency to transform into another phase of lower free energy (lower vapor pressure), and the reverse transition is thermodynamically impossible. It is not necessary, however, to transform into the lowest energy form shown. For example, at 1100° silica glass could transform into β -cristobalite, β -quartz, or β_2 -tridymite. Which of these transformations actually takes place is

on. From C.

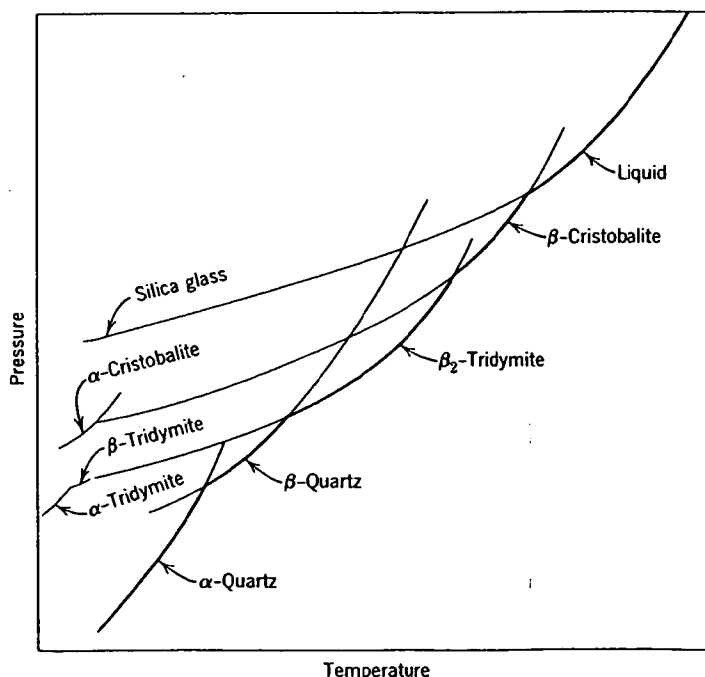


Fig. 7.5. Diagram including metastable phases occurring in the system SiO₂.

determined by the kinetics of these changes. In practice, when silica glass is heated for a long time at this temperature, it crystallizes, or devitrifies, to form cristobalite, which is not the lowest energy form but is structurally the most similar to silica glass. On cooling, β -cristobalite transforms into α -cristobalite.

The silica system illustrates that the phase-equilibrium diagram graphically represents the conditions for minimum free energy in a system; extension to include metastable forms also allows certain deductions about possible nonequilibrium behavior. Almost always, however, a number of alternative nonequilibrium courses are possible, but there is only one equilibrium possibility.

7.3 Techniques for Determining Phase-Equilibrium Diagrams

The phase-equilibrium diagrams discussed in the last section and in the rest of this chapter are the product of experimental studies of the phases present under various conditions of temperature and pressure. In using phase-equilibrium diagrams it is important to remember this experimental basis. In critical cases, for example, diagrams should not be used without referring directly to the original experimenter's description of exactly how the diagram was determined and with what detail the measurements were made. As additional measurements are carried out, diagrams are subject to constant revision.

There is a large body of literature describing methods of determining phase equilibrium. In general, any physical or chemical difference between phases or effect occurring on the appearance or disappearance of a phase can be used in determining phase equilibrium. Two general methods are used: dynamic methods use the change in properties of a system when phases appear or disappear, and static methods use a sample held under constant conditions until equilibrium is reached, when the number and composition of the phases present are determined.

Dynamic Methods. The most common dynamic method is thermal analysis, in which the temperature of a phase change is determined from changes in the rate of cooling or heating brought about by the heat of reaction. Other properties such as electrical conductivity, thermal expansion, and viscosity have also been used. Under the experimental conditions used, the phase change must take place rapidly and reversibly at the equilibrium temperature without undercooling, segregation, or other nonequilibrium effects. In silicate systems the rate of approach toward equilibrium is slow; as a result thermal-analysis methods are less useful for silicates than they are for metals, for example.

381-518

Dynamic methods are suitable for determining the temperature of phase changes but give no information about the exact reactions taking place. In addition to the measurements of temperature changes then, phase identification before and after any phase change is required. This analysis is usually carried out by chemical determination of composition, determination of optical characteristics, X-ray determination of crystal structure, and microscopic examination of phase amounts and phase distribution.

Static Methods. In contrast to dynamic measurements, static measurements often consist of three steps. Equilibrium conditions are held at elevated temperatures or pressures, the sample is quenched to room temperature sufficiently rapidly to prevent phase changes during cooling, and then the specimen is examined to determine the phases present. By carrying out these steps at a number of different temperatures, pressures, and compositions, the entire phase diagram can be determined. Sometimes high-temperature X-ray and high-temperature microscopic examinations can determine the phases present at high temperatures, making quenching unnecessary.

For silicate systems the major problem encountered in determining phase-equilibrium diagrams is the slow approach toward equilibrium and the difficulty in ensuring that equilibrium has actually been reached. For most systems this means that static measurements are necessary. A common technique is to mix together carefully constituents in the correct ratio to give the final composition desired. These are held at a constant temperature in platinum foil; after rapid cooling, the mixture is reground in a mortar and pestle and then heated for a second time and quenched. The phases present are examined, the sample mixture remixed, reheated, and quenched again. The resulting material is then reexamined to ensure that the phase composition has not changed.

This process requires much time and effort; since several thousand individual experiments, such as those just described, may be necessary for one ternary diagram, we can understand why only a few systems have been completely and exhaustively studied.

Reliability of Individual Diagrams. In general, the original experimenter investigating a particular phase diagram is usually concerned with some limited region of composition, temperature, and pressure. His effort is concentrated in that area, and the other parts of the phase diagram are determined with much less precision and detail. As reported in summarizing descriptions (such as those given in this chapter), the diagram is not evaluated as to which parts are most reliable. As a result, although the general configuration of diagrams given can be relied on, the exact temperatures and compositions of individual lines or points on the

diagram should only be accepted with caution. They represent the results of difficult experimental techniques and analysis.

These cautions are particularly applicable to regions of limited crystalline solution at high temperatures, since for many systems exsolution occurs rapidly on cooling and for many systems this was not a feature of the experimenters' interest. Similarly, phase separation at moderate and low temperatures often results in submicroscopic phases which are not recognized without the use of electron microscopy and electron diffraction, which have not as yet been widely applied to crystalline solid solutions.

7.4 Two-Component Systems

In two-component systems one additional variable, the composition, is introduced so that if only one phase is present, the variance is three: $P + V = C + 2$, $1 + V = 2 + 2$, $V = 3$. In order to represent the pressure, temperature, and composition region of the stability of a single phase, a three-dimensional diagram must be used. However, the effect of pressure is small for many condensed-phase systems, and we are most often concerned with the systems at or near atmospheric pressure. Consequently, diagrams at constant pressure can be drawn with temperature and composition as variables. A diagram of this kind is shown in Fig. 7.6.

If one phase is present, both temperature and composition can be arbitrarily varied, as illustrated for point A. In the areas in which two phases are present at equilibrium, the composition of each phase is

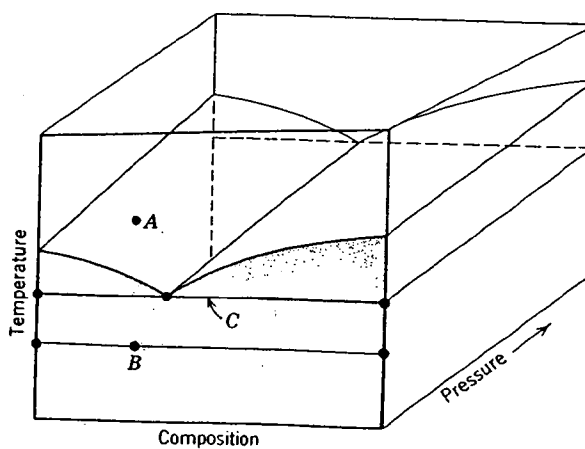


Fig. 7.6. Simple binary diagram.

381-513

indicated by lines on the diagram. (In binary diagrams two-phase regions will often be shaded, single-phase regions not.) The intersection of a constant-temperature "tie line" with the phase boundaries gives the compositions of the phases in equilibrium at temperature T . With two phases present, $P + V = C + 2$, $2 + V = 2 + 2$, $V = 2$. At an arbitrarily fixed pressure, any arbitrary change in either temperature or composition of one of the phases present requires a corresponding change in the other variable. The maximum number of phases that can be present where pressure is arbitrarily fixed ($V = 1$) is

$$P + V = C + 2, P + 1 = 2 + 2, P = 3.$$

When three phases are present, the composition of each phase and the temperature are fixed, as indicated by the solid horizontal line at C .

Systems in Which a Gas Phase Is Not Important. Systems containing only stable oxides in which the valence of the cations is fixed comprise a large fraction of the systems of interest for ceramics and can adequately be represented at a constant total pressure of 1 atm. At equilibrium the chemical potential of each constituent must be equal in each phase present. As a result the variation of chemical potential with composition is the underlying thermodynamic consideration which determines phase stability. If we consider a simple mechanical mixture of two pure components, the free energy of the mixture G^M is

$$G^M = X_A G_A + X_B G_B \quad (7.9)$$

For the simplest case, an ideal solution in which the heat of mixing and changes in vibrational entropy terms are zero, random mixing gives rise to a configurational entropy of mixing ΔS_m which has been derived in Eq. 4.14; the free energy of the solution is

$$G^{id,s} = G^M - T \Delta S_m \quad (7.10)$$

and under all conditions the free energy of the solution is less than that of a mechanical mixture; the free energy curves for the solid and liquid solutions and the resulting phase-equilibrium diagram are similar to those already illustrated in Fig. 4.2. Since very dilute solutions approach ideal behavior, Eq. 7.10 requires that there is always at least some minute solubility on the addition of any solute to any pure substance.

Most concentrated solutions are not ideal, but many can be well represented as *regular* solutions in which the excess entropy of the solution is negligible, but the excess enthalpy or heat of mixing ΔH^{ss} is significant. In this case the free energy of the regular solution is

$$G^{r,s} = G^M + \Delta H^{ss} - T \Delta S_m \quad (7.11)$$

The resulting forms of typical free-energy-composition curves for an ideal solution and for regular solutions with positive or negative excess enthalpies are shown in Fig. 7.7. In Fig. 7.7c the minimum free energy for the system at compositions intermediate between α and β consists of a mixture of α and β in which these two solution compositions have the same chemical potential for each component and a lower free energy than intermediate single-phase compositions; that is, phase separation occurs. When differences of crystal structure occur (as discussed in Chapter 2), a complete series of solid solutions between two components is not possible, and the free energy of the solution increases sharply after an initial decrease required by the configurational entropy of mixing. This

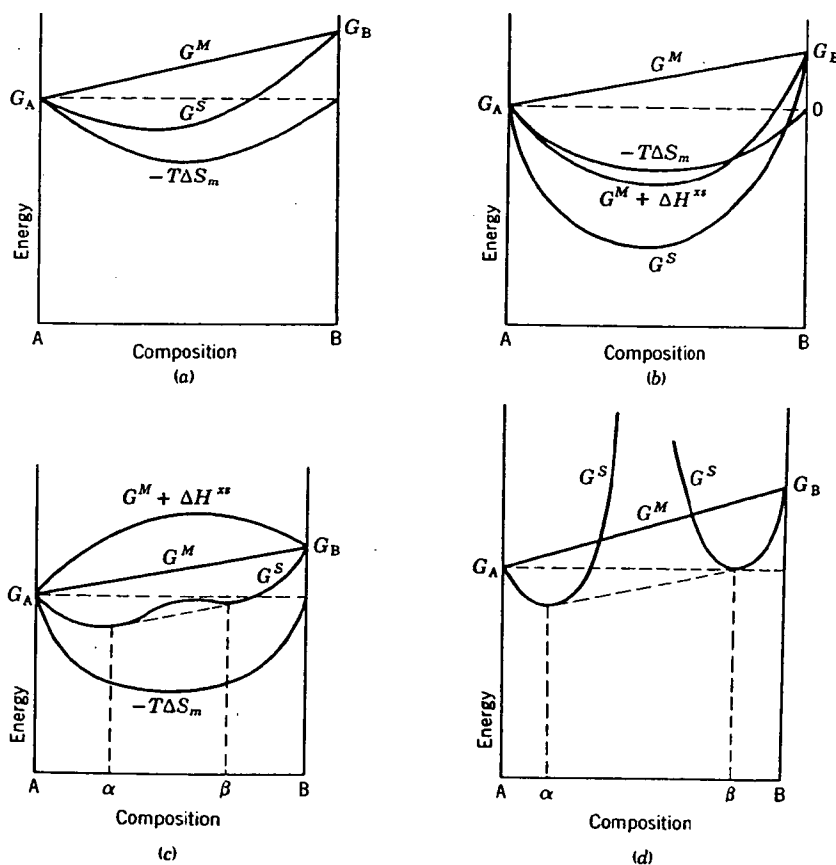


Fig. 7.7. Free-energy-composition diagrams for (a) ideal solution, (b) and (c) regular solutions, and (d) incomplete solid solution.

381-515

situation is illustrated in Fig. 7.7d, in which the minimum system free energy again consists of a mixture of the two solutions α and β .

When, for any temperature and composition, free-energy curves such as shown in Fig. 7.7 are known for each phase which may exist, these phases actually occur at equilibrium which give the lowest system free energy consistent with equal chemical potentials for the components in each phase. This has been illustrated for an ideal solution in Fig. 4.2, compound formation in Fig. 4.3, and phase separation in Fig. 3.10 and is illustrated for a series of temperatures in a eutectic system in Fig. 7.8.

Systems in Which a Gas Phase Is Important. In adjusting the oxygen pressure in an experimental system, it is often convenient to use the equilibria



In this case, with no condensed phase present, $P + V = C + 2$, $1 + V = 2 + 2$, $V = 3$, and it is necessary to fix the temperature, system total pressure, and the gas composition, that is, CO_2/CO or $\text{H}_2/\text{H}_2\text{O}$ ratio, in order to fix the oxygen partial pressure. If a condensed phase, that is, graphite, is in equilibrium with an oxygen-containing vapor phase, $P + V = C + 2$, $2 + V = 2 + 2$, $V = 2$, and fixing any two independent variables completely defines the system.

The most extensive experimental data available for a two-component system in which the gas phase is important is the Fe-O system, in which a number of condensed phases may be in equilibrium with the vapor phase. A useful diagram is shown in Fig. 7.9, in which the heavy lines are boundary curves separating the stability regions of the condensed phases and the dash-dot curves are oxygen isobars. In a single condensed-phase region (such as wüstite) $P + V = C + 2$, $2 + V = 2 + 2$, $V = 2$, and both the temperature and oxygen pressure have to be fixed in order to define the composition of the condensed phase. In a region of two condensed phases (such as wüstite plus magnetite) $P + V = C + 2$, $3 + V = 2 + 2$, $V = 1$, and fixing either the temperature or oxygen pressure fully defines the system. For this reason, the oxygen partial-pressure isobars are horizontal, that is, isothermal, in these regions, whereas they run diagonally across single condensed-phase regions.

An alternative method of representing the phases present at particular oxygen pressures is shown in Fig. 7.9b. In this representation we do not show the O/Fe ratio, that is, the composition of the condensed phases, but only the pressure-temperature ranges for each stable phase.

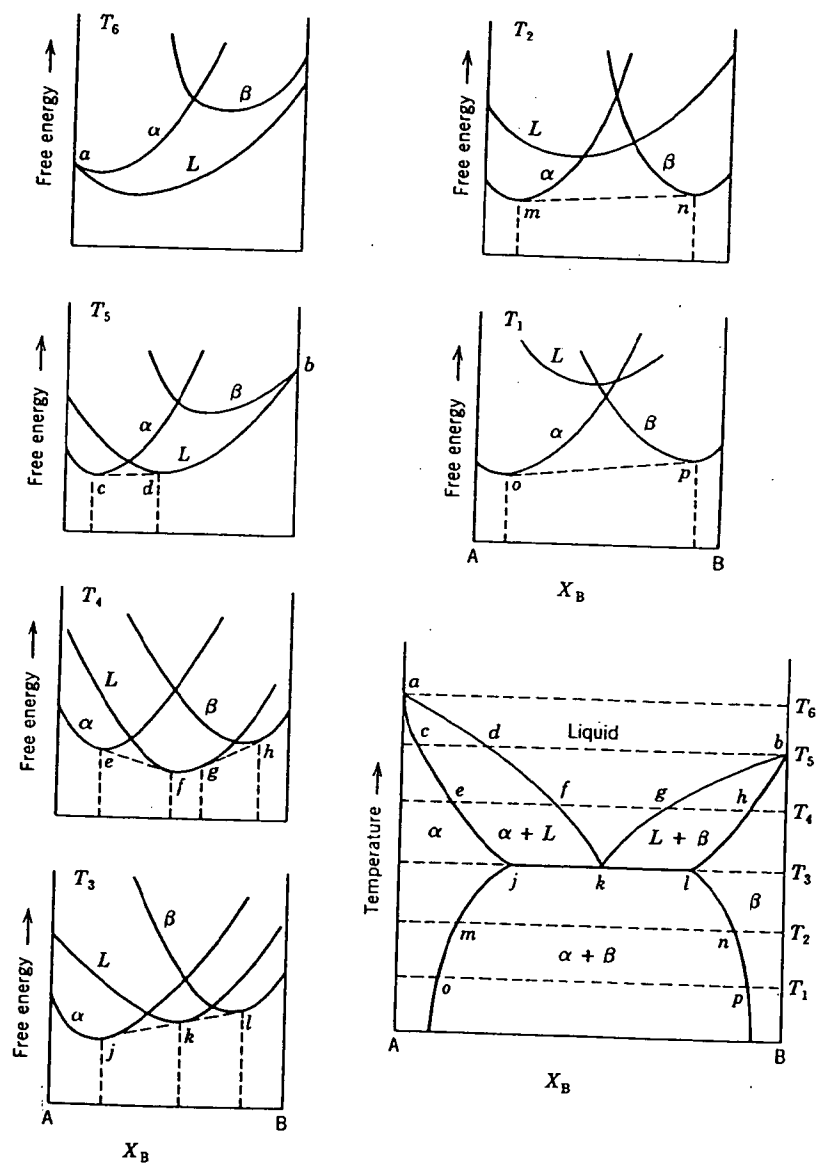


Fig. 7.8. Free-energy-composition curves and the temperature-composition equilibrium diagram for a eutectic system. From P. Gordon, *Principles of Phase Diagrams in Materials Systems*, McGraw-Hill Book Company, New York, 1968.

381-513

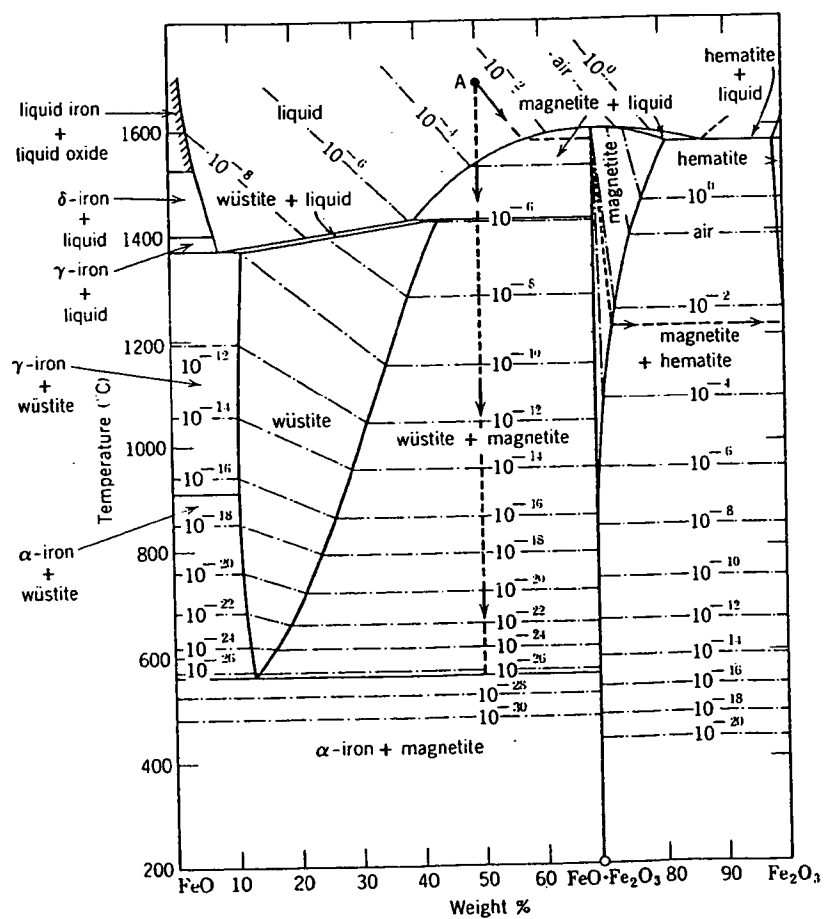


Fig. 7.9. (a) Phase relations in the FeO-Fe₂O₃ system. Dash-dot lines are oxygen isobars. Alternate solidification paths for composition A are discussed in text. From A. Muan and E. F. Osborn, *Phase Equilibria among Oxides in Steelmaking*, Addison-Wesley Publishing Company, Inc., Reading, Mass., 1965.

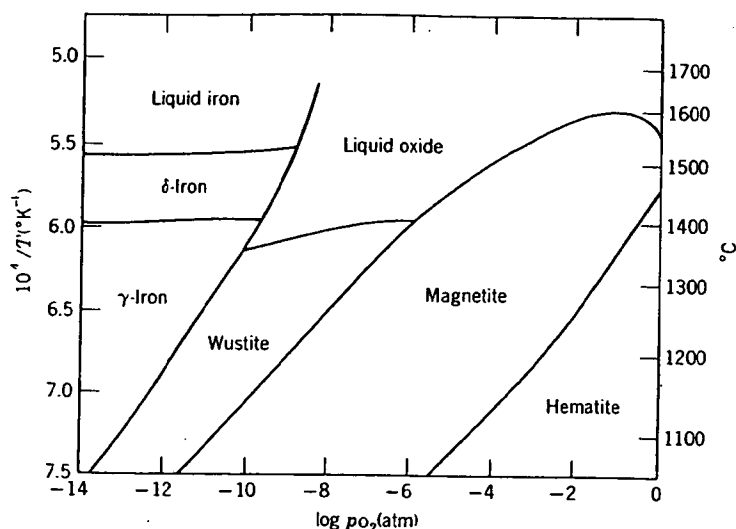


Fig. 7.9 (continued). (b) Temperature-oxygen pressure diagram for the Fe-Fe₂O₃ system. From J. B. Wagner, *Bull. Am. Cer. Soc.*, 53, 224 (1974).

7.5 Two-Component Phase Diagrams

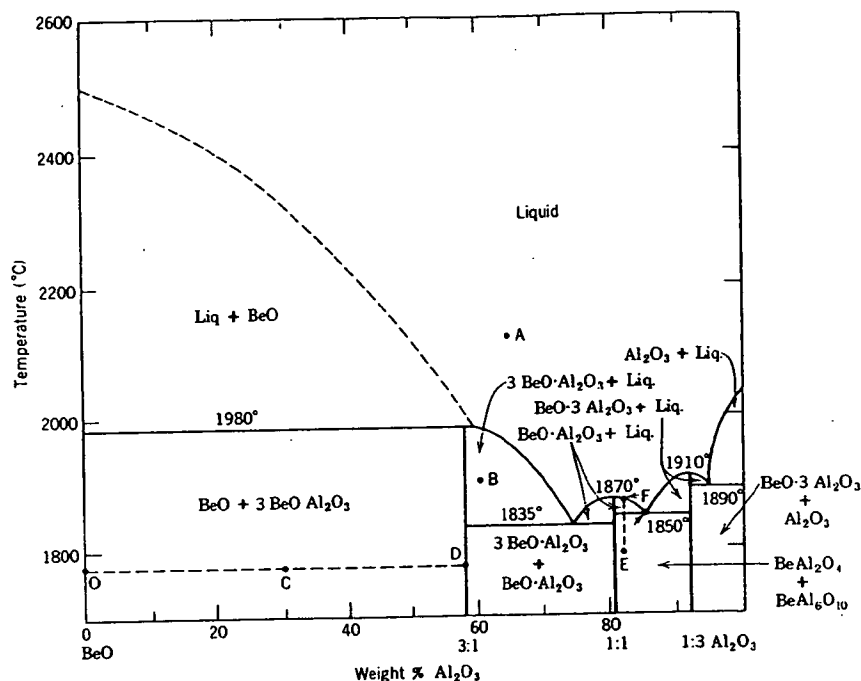
Phase-equilibrium diagrams are graphical representations of experimental observations. The most extensive collection of diagrams useful in ceramics is that published by the American Ceramic Society in two large volumes, which are an important working tool of every ceramist.* Phase diagrams can be classified into several general types.

Eutectic Diagrams. When a second component is added to a pure material, the freezing point is often lowered. A complete binary system consists of lowered liquidus curves for both end members, as illustrated in Fig. 7.8. The *eutectic temperature* is the temperature at which the liquidus curves intersect and is the lowest temperature at which liquid occurs. The eutectic composition is the composition of the liquid at this temperature, the liquid coexisting with two solid phases. At the eutectic temperature three phases are present, so the variance is one. Since pressure is fixed, the temperature cannot change unless one phase disappears.

In the binary system BeO-Al₂O₃ (Fig. 7.10) the regions of solid solution that are necessarily present have not been determined and are presumed

*E. M. Levin, C. R. Robbins, and H. F. McMurdie, *Phase Diagrams for Ceramists*, American Ceramic Society, Columbus, 1964; *Supplement*, 1969.

381-518

Fig. 7.10. The binary system BeO-Al₂O₃.

to be of limited extent, although this is uncertain, and are not shown in the diagram. The system can be divided into three simpler two-component systems (BeO-BeAl₂O₄, BeAl₂O₄-BeAl₆O₁₀, and BeAl₆O₁₀-Al₂O₃) in each of which the freezing point of the pure material is lowered by addition of the second component. The BeO-BeAl₂O₄ subsystem contains a compound, Be₃Al₂O₆, which melts incongruently, as discussed in the next section. In the single-phase regions there is only one phase present, its composition is obviously that of the entire system, and it comprises 100% of the system (point A in Fig. 7.10). In two-phase regions the phases present are indicated in the diagram (point B in Fig. 7.10); the composition of each phase is represented by the intersection of a constant temperature tie line and the phase-boundary lines. The amounts of each phase can also be determined from the fact that the sum of the composition times the amount of each phase present must equal the composition of the entire system. For example, at point C in Fig. 7.10 the entire system is composed of 29% Al₂O₃ and consists of two phases, BeO (containing no Al₂O₃) and 3BeO·Al₂O₃ (which contains 58% Al₂O₃). There

must be 50% of each phase present for a mass balance to give the correct overall composition. This can be represented graphically in the diagram by the *lever principle*, in which the distance from one phase boundary to the overall system composition, divided by the distance from that boundary to the second phase boundary, is the fraction of the second phase present. That is, in Fig. 7.10,

$$\frac{OC}{OD} (100) = \text{Per cent } 3\text{BeO} \cdot \text{Al}_2\text{O}_3$$

A little consideration indicates that the ratio of phases is given as

$$\frac{DC}{OC} = \frac{\text{BeO}}{3\text{BeO} \cdot \text{Al}_2\text{O}_3}$$

This same method can be used for determining the amounts of phases present at any point in the diagram.

Consider the changes that occur in the phases present on heating a composition such as *E*, which is a mixture of BeAl_2O_4 and $\text{BeAl}_6\text{O}_{10}$. These phases remain the only ones present until a temperature of 1850°C is reached; at this eutectic temperature there is a reaction, $\text{BeAl}_2\text{O}_4 + \text{BeAl}_6\text{O}_{10} = \text{Liquid (85\% Al}_2\text{O}_3)$, which continues at constant temperature to form the eutectic liquid until all the $\text{BeAl}_6\text{O}_{10}$ is consumed. On further heating more of the BeAl_2O_4 dissolves in the liquid, so that the liquid composition changes along *GF* until at about 1875°C all the BeAl_2O_4 has disappeared and the system is entirely liquid. On cooling this liquid, exactly the reverse occurs during equilibrium solidification.

As an exercise students should calculate the fraction of each phase present for different temperatures and different system compositions.

One of the main features of eutectic systems is the lowering of the temperature at which liquid is formed. In the $\text{BeO}-\text{Al}_2\text{O}_3$ system, for example, the pure end members melt at temperatures of 2500°C and 2040°C , respectively. In contrast, in the two-component system a liquid is formed at temperatures as low as 1835°C . This may be an advantage or disadvantage for different applications. For maximum temperature use as a refractory we want no liquid to be formed. Addition of even a small amount of BeO to Al_2O_3 results in the formation of a substantial amount of a fluid liquid at 1890°C and makes it useless as a refractory above this temperature. However, if high-temperature applications are not of major importance, it may be desirable to form the liquid as an aid to firing at lower temperatures, since liquid increases the ease of densification. This is true, for example, in the system TiO_2-UO_2 , in which addition of 1% TiO_2 forms a eutectic liquid, which is a great aid in obtaining high densities at low temperatures. The structure of this system, shown in Fig.

381-515

7.11, consists of large grains of UO_2 surrounded by the eutectic composition.

The effectiveness of eutectic systems in lowering the melting point is made use of in the $\text{Na}_2\text{O}-\text{SiO}_2$ system, in which glass compositions can be melted at low temperatures (Fig. 7.12). The liquidus is lowered from 1710°C in pure SiO_2 to about 790° for the eutectic composition at approximately 75% SiO_2 -25% Na_2O .

Formation of low-melting eutectics also leads to some severe limitations on the use of refractories. In the system $\text{CaO}-\text{Al}_2\text{O}_3$ the liquidus is strongly lowered by a series of eutectics. In general, strongly basic oxides such as CaO form low-melting eutectics with amphoteric or basic oxides, and these classes of materials cannot be used adjacent to each other, even though they are individually highly refractive.

Incongruent Melting. Sometimes a solid compound does not melt to form a liquid of its own composition but instead dissociates to form a new solid phase and a liquid. This is true of enstatite (MgSiO_3) at 1557°C (Fig. 7.13); this compound forms solid Mg_2SiO_4 plus a liquid containing about 61% SiO_2 . At this *incongruent melting point* or *peritectic temperature* there

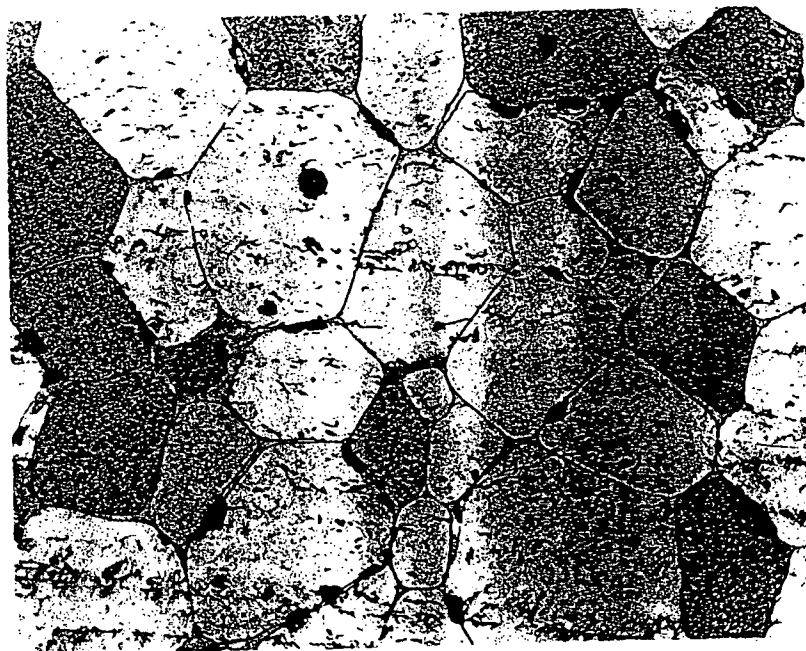


Fig. 7.11. Structure of 99% UO_2 -1% TiO_2 ceramic (228X, HNO_3 etch). UO_2 is the primary phase, bonded by eutectic composition. Courtesy G. Ploetz.

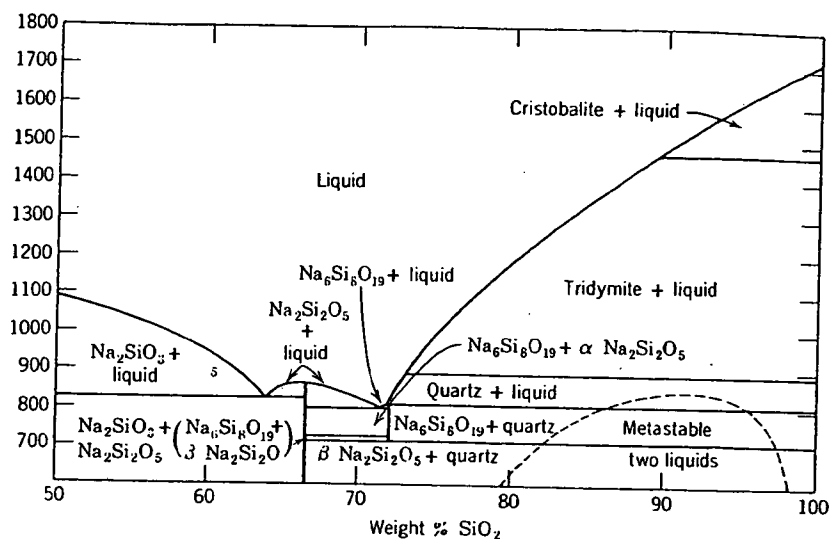


Fig. 7.12. The binary system $\text{Na}_2\text{SiO}_3\text{-SiO}_2$. The dashed line shows metastable liquid-liquid phase separation.

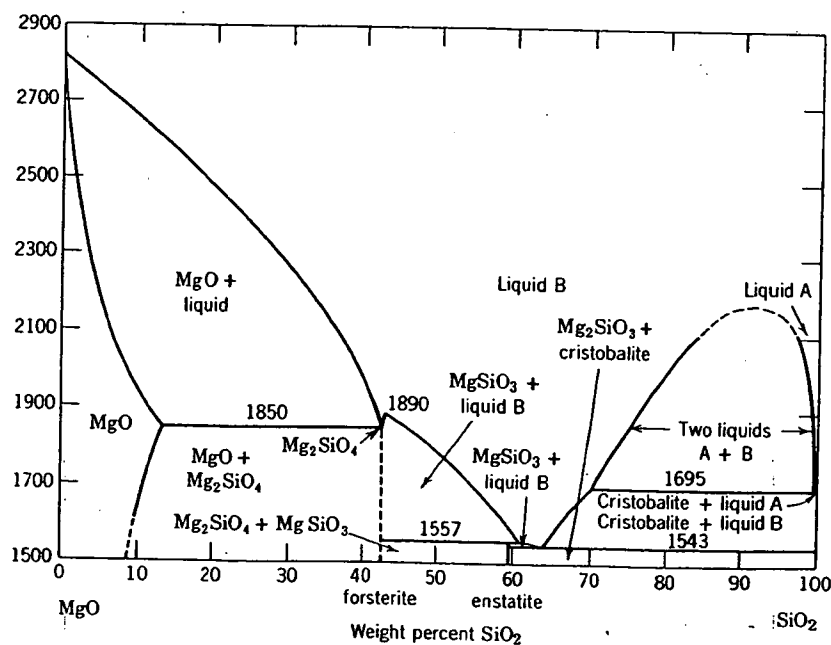


Fig. 7.13. The binary system MgO-SiO_2 .

381-518

are three phases present (two solids and a liquid), so that the temperature remains fixed until the reaction is completed. Potash feldspar (Fig. 7.14) also melts in this way.

Phase Separation. When a liquid or crystalline solution is cooled, it separates into two separate phases at the *consolute temperature* as long as the excess enthalpy is positive (see Fig. 7.7). This phenomenon is particularly important relative to the development of substructure in glasses, as discussed in Chapter 3 (Figs. 3.11, 3.12, 3.14 to 3.19). Although it has been less fully investigated for crystalline oxide solid solutions, it is probably equally important for these systems when they are exposed to moderate temperatures for long periods of time. The system CoO-NiO is shown in Fig. 7.15.

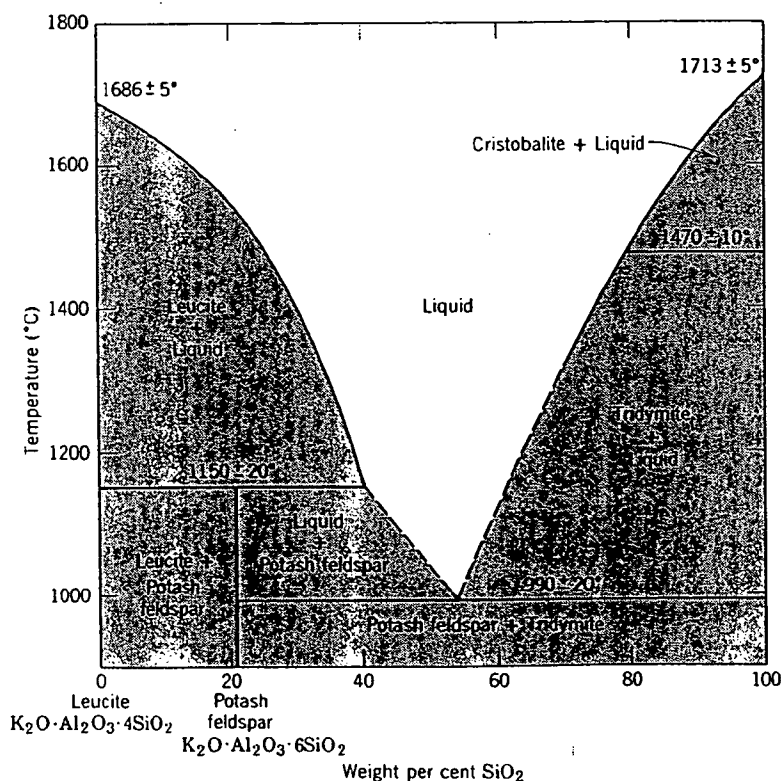


Fig. 7.14. The binary system $K_2O \cdot Al_2O_3 \cdot 4SiO_2$ (leucite)- SiO_2 . From J. F. Schairer and N. L. Bowen, *Bull. Soc. Geol. Finl.*, 20, 74 (1947). Two-phase regions are shown shaded in this diagram.

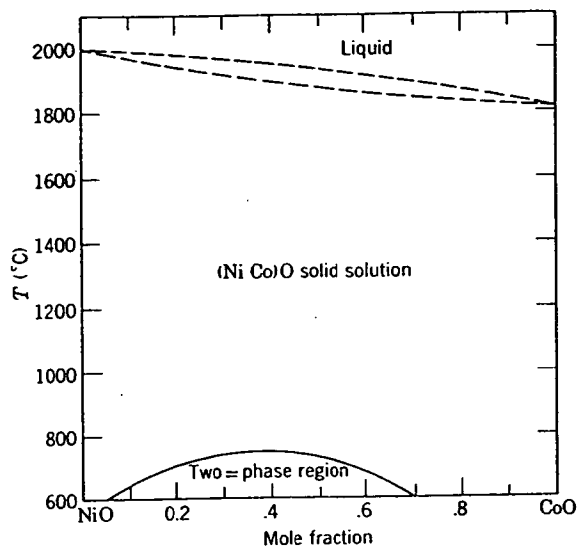


Fig. 7.15. The binary system NiO-CoO.

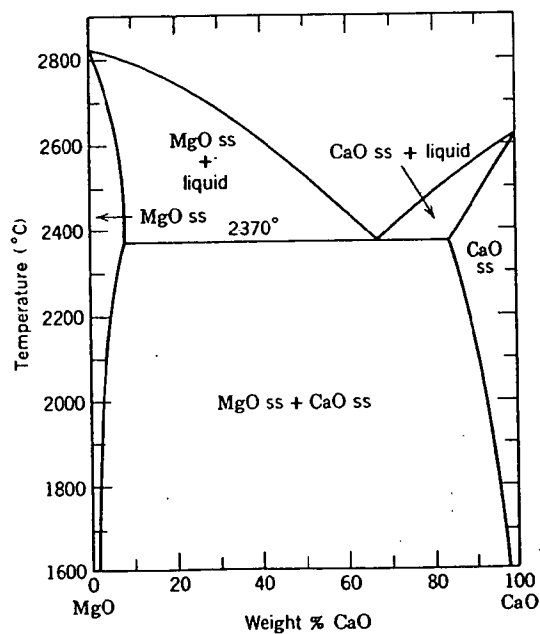


Fig. 7.16. The binary system MgO-CaO.

381-518

Solid Solutions. As discussed in Chapter 4 and in Section 7.4, a complete series of solid solutions occurs for some systems such as illustrated in Fig. 4.2 and Fig. 7.15, and some minute or significant limited solid solution occurs for all systems, as shown in Figs. 4.3, 7.13, and 7.15.

It has only been in the last decade or so that careful experimentation has revealed the wide extent of solid solubility, reaching several percent at high temperatures in many systems, as shown in Figs. 4.3, 7.13, and 7.15 and for the MgO–CaO system in Fig. 7.16 and the MgO–Cr₂O₃ system in Fig. 7.17. For steel-plant refractories directly bonded magnesia–chromite brick is formed when these materials are heated together at temperatures above 1600°C as a result of the partial solubility of the constituents; exsolution occurs on cooling. Almost all open-hearth roofs are formed of either direct-bonded, rebonded fine-grain, or fusion-cast magnesia–chromite refractories. In the basic oxygen-furnace process for steel making MgO–CaO refractories bonded with pitch are widely used, and the solid solubility at high temperatures forms a high-temperature bond. In magnesia refractories the lower solid solubility of SiO₂ as compared

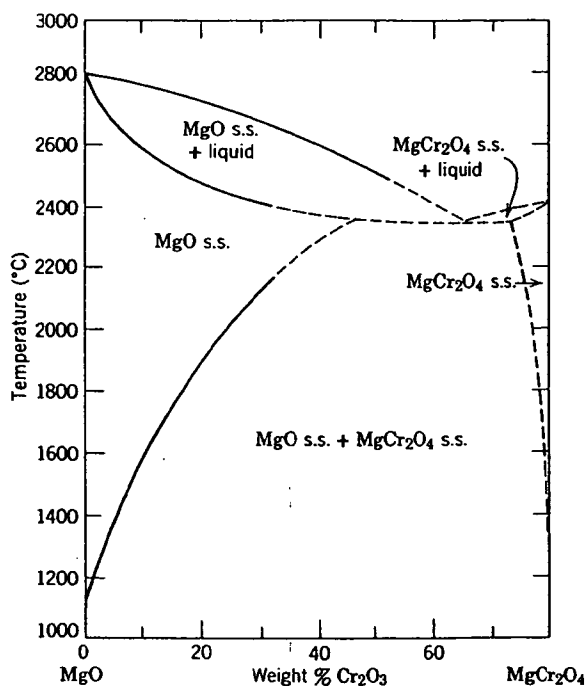


Fig. 7.17. The binary system MgO–MgCr₂O₄.

with CaO in MgO requires that excess CaO be added to prevent the formation of low-melting intergranular silicates.

In the MgO-Al₂O₃ system (Fig. 4.3) there is extensive solubility of MgO and of Al₂O₃ in spinel. As spinel in this composition range is cooled, the solubility decreases, and corundum precipitates as a separate solid phase (Fig. 7.18).

This same sort of limited solid solution is observed in the CaO-ZrO₂ system (Fig. 7.19); in this system there are three different fields of solid solution, the tetragonal form, the cubic form, and the monoclinic form. Pure ZrO₂ exhibits a monoclinic tetragonal phase transition at 1000°C, which involves a large volume change and makes the use of pure zirconia impossible as a ceramic material. Addition of lime to form the cubic solid solution, which has no phase transition, is one basis for *stabilized zirconia*, a valuable refractory.

Complex Diagrams. All the basic parts of binary phase-equilibrium diagrams have been illustrated; readers should be able to identify the number of phases, composition of phases, and amounts of phases present at any composition and temperature from any of these diagrams with ease and confidence. If they cannot, they should consult one of the more extensive treatments listed in the references.



Fig. 7.18. Precipitation of Al₂O₃ from spinel solid solution on cooling (400× H₂SO₄ etch). Courtesy R. L. Coble.

Fig. 7.1
J. Am.

Co:
fright
inter
find t
form:
alrea
Ge:
with
inter
partia

381-513

CERAMIC PHASE-EQUILIBRIUM DIAGRAMS

293

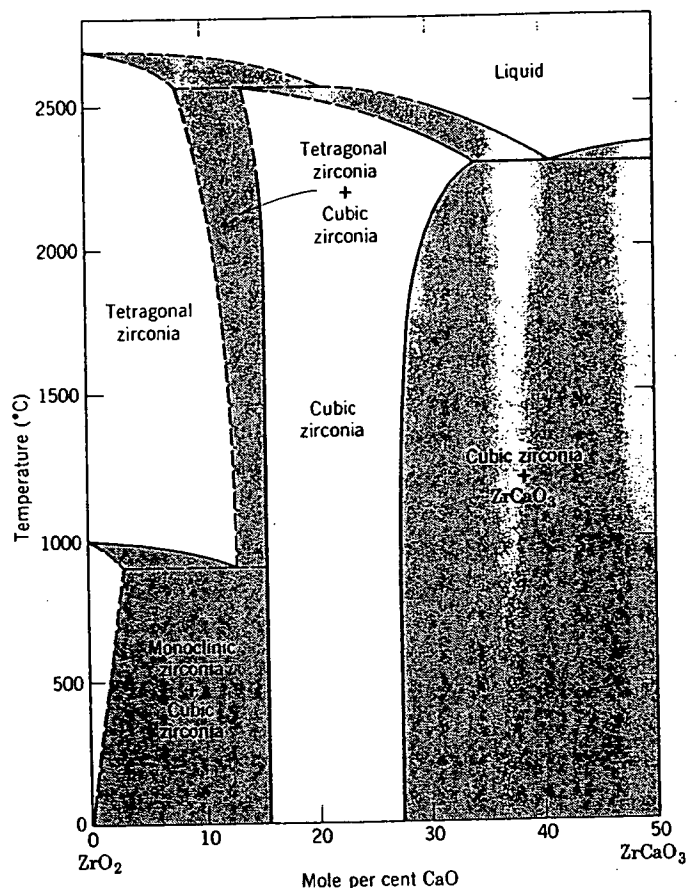


Fig. 7.19. The binary system CaO-ZrO₂. From P. Duwez, F. Odell, and F. H. Brown, Jr., *J. Am. Ceram. Soc.*, 35, 109 (1952). Two-phase regions are shown shaded in this figure.

Combinations of simple elements in one system sometimes appear frightening in their complexity but actually offer no new problems in interpretation. In the system Ba₂TiO₄-TiO₂ (Fig. 7.20), for example, we find two eutectics, three incongruently melting compounds, polymorphic forms of BaTiO₃, and an area of limited solid solution. All of these have already been discussed.

Generally phase diagrams are constructed at a total pressure of 1 atm with temperature and composition as independent variables. Since the interesting equilibrium conditions for many ceramics involve low oxygen partial pressures, phase diagrams at a fixed temperature but with oxygen

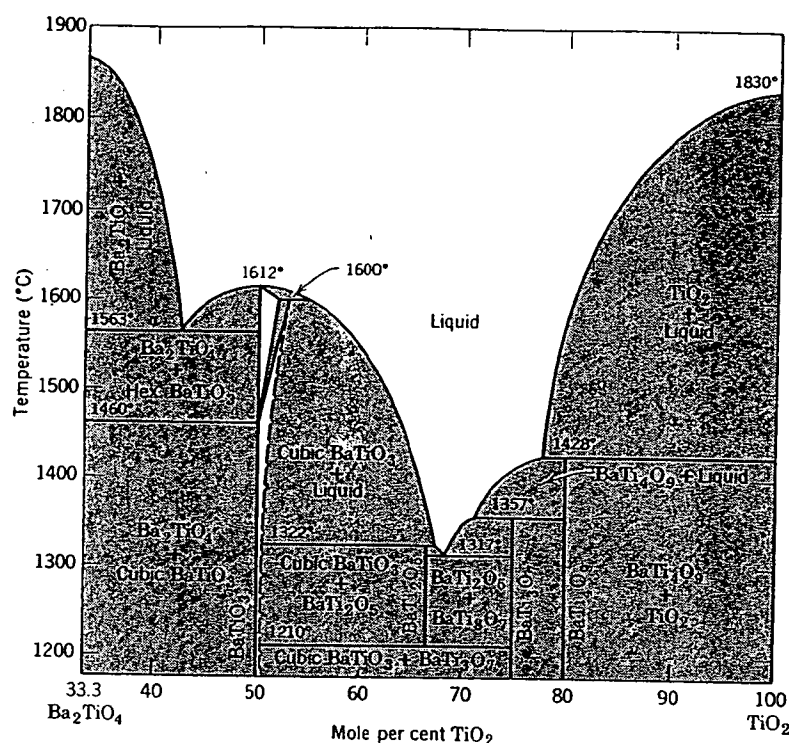


Fig. 7.20. The binary system $\text{Ba}_2\text{TiO}_4\text{-TiO}_2$. From D. E. Rase and R. Roy, *J. Am. Ceram. Soc.* 38, 111 (1955). Two-phase regions are shown shaded in this figure.

pressure and composition as variables become a useful alternative for describing phase equilibria, for example, Fig. 7.9b. Figure 7.21(a-1) shows such a diagram for Co-Ni-O at 1600°K. The lens-shaped two-phase region between (Co,Ni)O and the NiCo alloy is similar to that between the liquid oxides and (Co,Ni)O in a temperature-composition plot (Fig. 7.15). Figure 7.21(a-2) shows the oxygen isobar tie lines between the metal alloy and the oxide solid solution; for example, the dotted line represents the equilibrium at $P_{\text{O}_2} = 1.5 \times 10^{-7}$ atm between $\text{Ni}_{0.62}\text{Co}_{0.38}\text{O}$ and $\text{Ni}_{0.9}\text{Co}_{0.1}$. (A tie line connects phases in equilibrium and designates the composition of each phase. For example, a constant temperature tie line in Fig. 7.17 at 2600°C specifies the composition of the solid solution, 10 w/o Cr_2O_3 , in equilibrium with the liquid, which contains 40 w/o Cr_2O_3 .) A plot of the nickel activity as a function of P_{O_2} is shown in Fig. 7.21(a-3). In systems which form intermediate compounds, such as spinels, the diagrams become more complex. The Fe-Cr-O ternary

syst
 P_{O_2}
 (Fe,
 chro
 betw

7.6

TI
 com
 pres
 fix t
 give
 tern
 tion:
 a v
 two-
 equi

Fig. 7
 (2) o
 nicke

381-515

system at 1573°K is shown in Fig. 7.21b. At an oxygen pressure of $P_{O_2} = 10^{-10}$ atm, the stable phases may be FeO, FeO + (Fe,Cr)₂O₃, (Fe,Cr)₂O₃ + (Fe,Cr)₂O₃, or (Fe,Cr)₂O₃, depending on the concentration of chromium. The oxygen isobars shown in Fig. 7.21(b-2) are tie lines between the compositions in equilibrium at 1573°K.

7.6 Three-Component Phase Diagrams

Three-component systems are fundamentally no different from two-component systems, except that there are four independent variables—pressure, temperature, and the concentrations of two components (which fix the third). If pressure is arbitrarily fixed, the presence of four phases gives rise to an invariant system. A complete graphical representation of ternary systems is difficult, but if the pressure is held constant, compositions can be represented on an equilateral triangle and the temperature on a vertical ordinate to give a phase diagram such as Fig. 7.22. For two-dimensional representation the temperatures can be projected on an equilateral triangle, with the liquidus temperatures represented by



100
TiO₂

Am. Ceram.

ative for
7.21(a-1)
ped two-
r to that
mposition
tie lines
mple, the
between
rium and
constant
ion of the
contains
shown in
s, such as
ternary

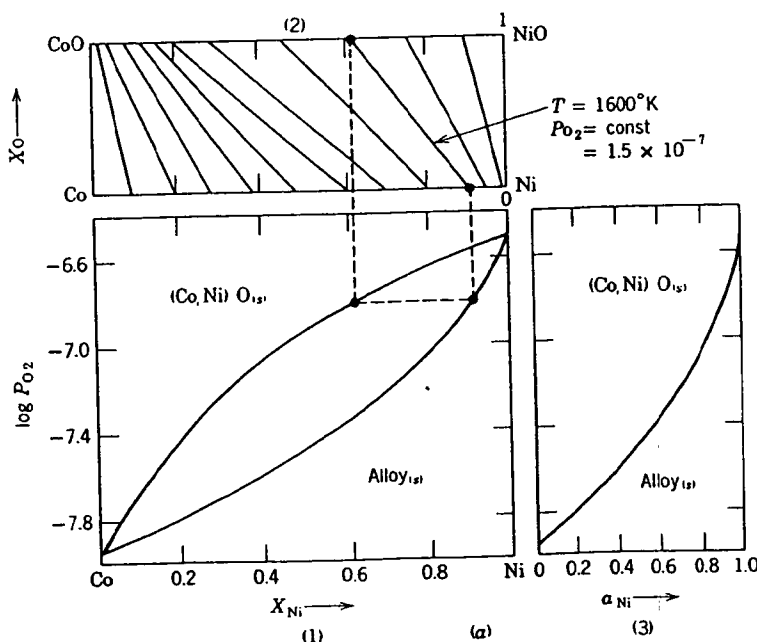


Fig. 7.21. (a) Co-Ni-O system. (1) Composition of condensed phases as a function of P_{O_2} ; (2) oxygen isobars for equilibrium between the oxide solid solution and the alloy solution; (3) nickel activity as a function of P_{O_2} .

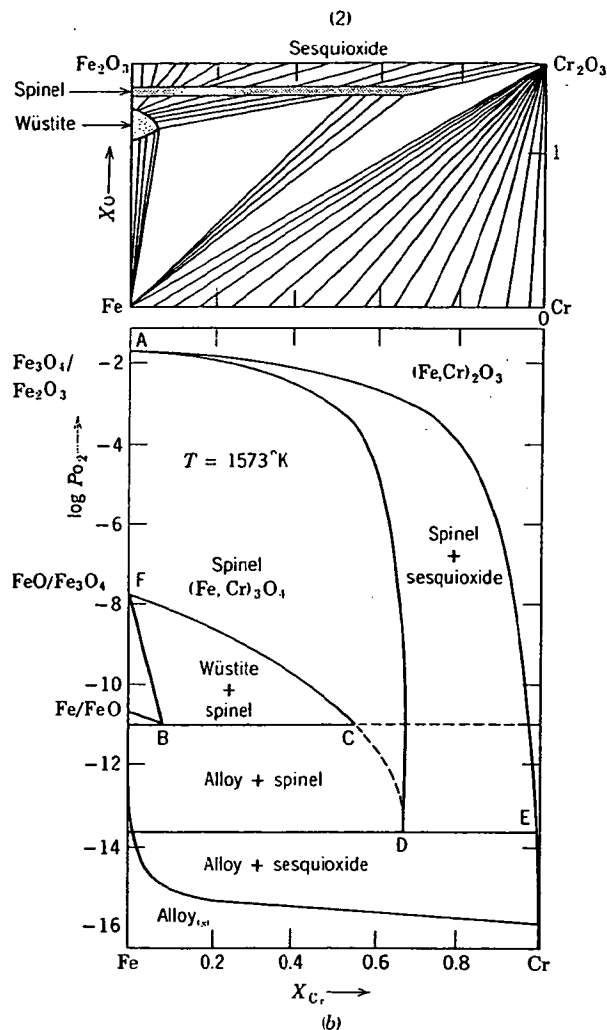


Fig. 7.21 (continued). (b) Fe-Cr-O system. (1) Composition- P_{O_2} diagram and (2) oxygen isobars for equilibrium between two phases. From A. Pelton and H. Schmalzried, *Met. Trans.*, 4, 1395 (1973).

isotherms. The diagram is divided into areas representing equilibrium between the liquid and a solid phase. Boundary curves represent equilibrium between two solids and the liquid, and intersections of three boundary curves represent points of four phases in equilibrium (invariant points in the constant-pressure system). Another method of two-

Fig. 7.22.

dimensional diagram.

Interpretation of the composition- P_{O_2} diagram. The diagram is divided into areas representing equilibrium between the liquid and a solid phase. Boundary curves represent equilibrium between two solids and the liquid, and intersections of three boundary curves represent points of four phases in equilibrium (invariant points in the constant-pressure system). Another method of two-

381-513

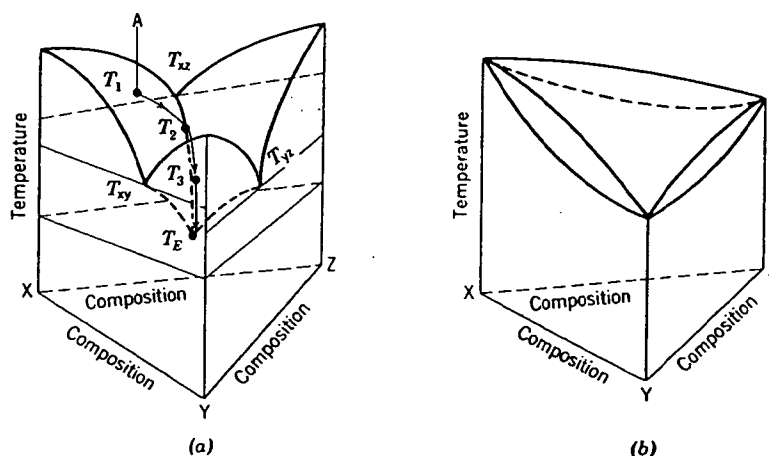


Fig. 7.22. Space diagram of (a) ternary eutectic and (b) complete series of solid solutions.

dimensional representation is to take a constant-temperature cut through the diagram, indicating the phases at equilibrium at some fixed temperature.

Interpretation of ternary diagrams is not fundamentally different from that of binary diagrams. The phases in equilibrium at any temperature and composition are shown; the composition of each phase is given by the phase-boundary surfaces or intersections; the relative amounts of each phase are determined by the principle that the sum of the individual phase compositions must equal the total composition of the entire system. In Fig. 7.22 and Fig. 7.23, for example, the composition A falls in the primary field of X. If we cool the liquid A, X begins to crystallize from the melt when the temperature reaches T_1 . The composition of the liquid changes along AB because of the loss of X. Along this line the lever principle applies, so that at any point the percentage of X present is given by $100(BA/XB)$. When the temperature reaches T_2 and the crystallization path reaches the boundary representing equilibrium between the liquid and two solid phases X and Z, Z begins to crystallize also, and the liquid changes in composition along the path CD. At L, the phases in equilibrium are a liquid of composition L and the solids X and Z, whereas the overall composition of the entire system is A. As shown in Fig. 7.23b, the only mixture of L, X, and Z that gives a total corresponding to A is $x A/x X (100) = \text{Per cent X}$, $z A/z Z (100) = \text{Per cent Z}$, $l A/l L (100) = \text{Per cent L}$. That is, the smaller triangle XZL is a ternary system in which the composition of A can be represented in terms of its three constituents.

gen
ns.,

im
ib-
ee
nt
o-

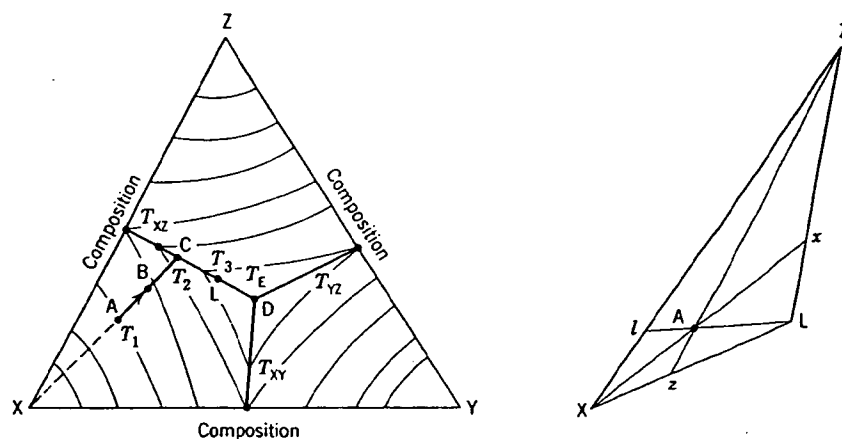


Fig. 7.23. (a) Crystallization path illustrated in Fig. 7.22a and (b) application of center of gravity principle to a ternary system.

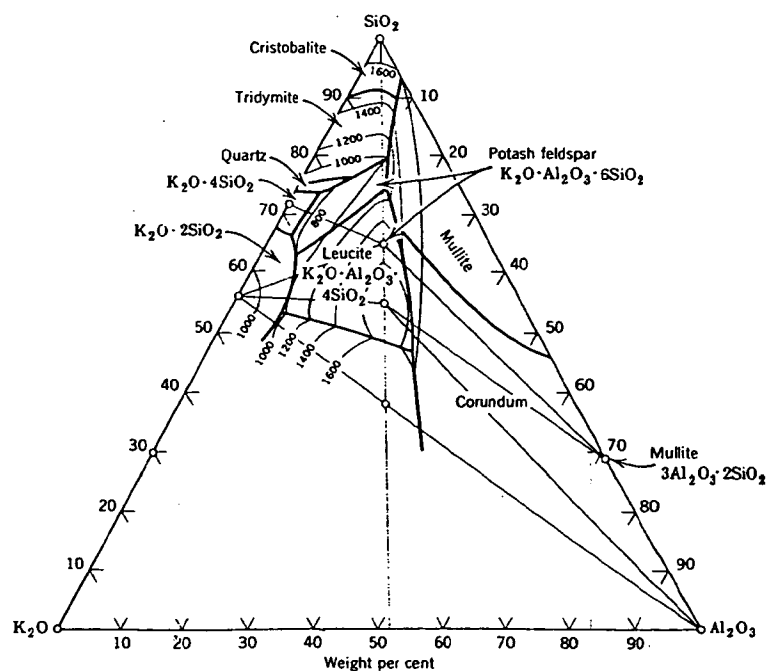


Fig. 7.24. The ternary system $K_2O-Al_2O_3-SiO_2$. From J. F. Schairer and N. L. Bowen, *Am. J. Sci.*, 245, 199 (1947).

Many t
ogy. Two
system, a
the MgC
 $K_2O-Al_2O_3$
compositi
silica-mu
discussed
the basis
systems
provides
 SiO_2 syst
tions fall
 $Na_2O \cdot 3C$

2N:
 $2Na_2O$
N
To Na

Fig. 7.25
Glass T

381-518

CERAMIC PHASE-EQUILIBRIUM DIAGRAMS

299

Many ternary systems are of interest in ceramic science and technology. Two of these, the $K_2O-Al_2O_3-SiO_2$ system and the $Na_2O-CaO-SiO_2$ system, are illustrated in Figs. 7.24 and 7.25. Another important system, the $MgO-Al_2O_3-SiO_2$ system, is discussed in Section 7.8. The $K_2O-Al_2O_3-SiO_2$ system is important as the basis for many porcelain compositions. The eutectic in the subsystem potash-feldspar-silica-mullite determines the firing behavior in many compositions. As discussed in Chapter 10, porcelain compositions are adjusted mainly on the basis of (a) ease in forming and (b) firing behavior. Although real systems are usually somewhat more complex, this ternary diagram provides a good description of the compositions used. The $Na_2O-CaO-SiO_2$ system forms the basis for much glass technology. Most compositions fall along the border between the primary phase of devitrite, $Na_2O \cdot 3CaO \cdot 6SiO_2$, and silica; the liquidus temperature is 900 to 1050°C.

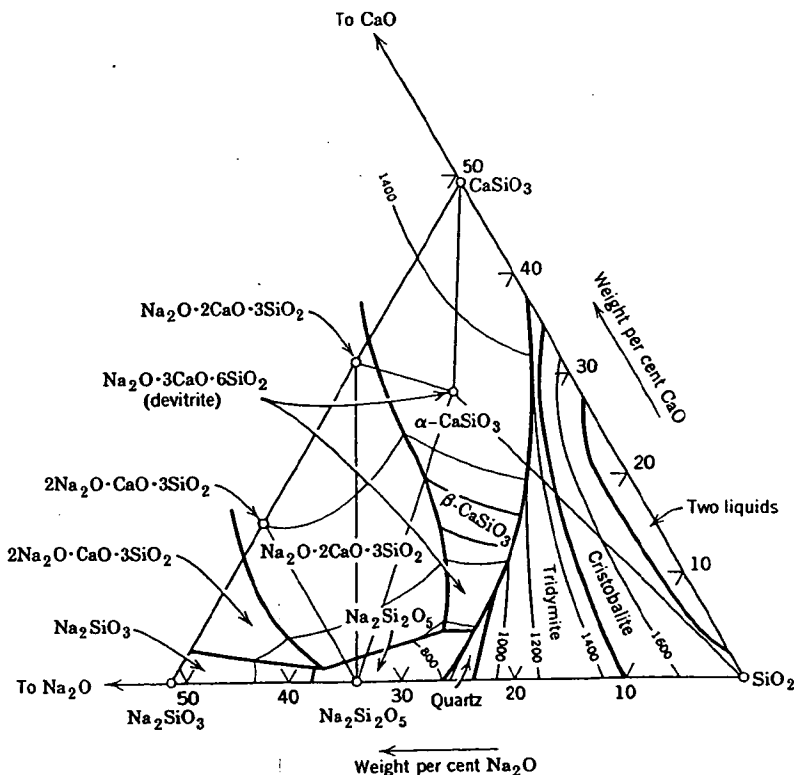


Fig. 7.25. The $Na_2O-O-CaO-SiO_2$ system. From G. W. Morey and N. L. Bowen, *J. Soc. Glass Technol.*, 9, 232 (1925).

This is a compositional area of low melting temperature, but the glasses formed contain sufficient calcium oxide for reasonable resistance to chemical attack. When glasses are heated for extended times above the transition range, devitrite or cristobalite is the crystalline phase formed as the devitrification product.

Very often constant-temperature diagrams are useful. These are illustrated for subsolidus temperatures in Figs. 7.24 and 7.25 by lines between the forms that exist at equilibrium. These lines form composition triangles in which three phases are present at equilibrium, sometimes called compatibility triangles. Constant-temperature diagrams at higher temperatures are useful, as illustrated in Fig. 7.26, in which the 1200° isothermal

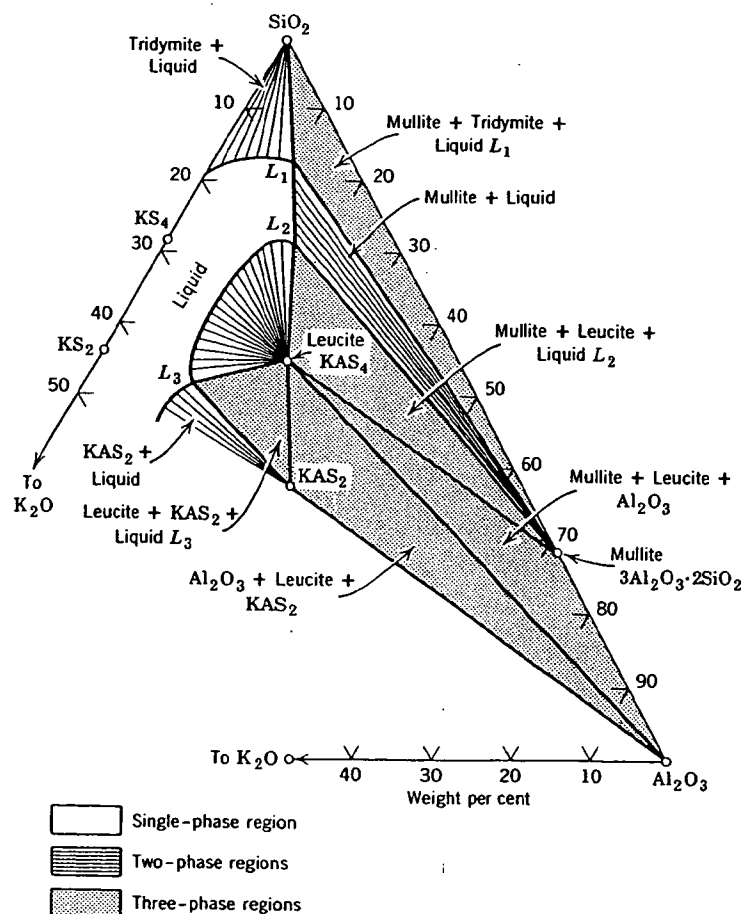


Fig. 7.26. Isothermal cut in the $K_2O-Al_2O_3-SiO_2$ diagram at 1200°C.

plane is shown this system are amount of liquid isothermal diagram different compositions selected. Frequently rather than an

Although our and we do not component system familiar with the

7.7 Phase Con

One of the ceramic systems at high temperatures. The amount of

Consider, for instance, a composition of 50 wt% forsterite and 50 wt% silica. Upon heating the amount of liquid at some temperature is a function of composition. The phase diagram shows that at 1557°C, the eutectic composition, the composition becomes eutectic compositions and

Several things are noted: the large difference in the small change in composition, the temperatures, the liquid is formed, chromite refractory, 3MgO·2SiO₂·2H₂O, sufficient MgO has a deleterious effect on the temperatures.

Another app

381-518

asses
e to
e the
ed as

illus-
ween
ngles
alled
nper-
ermal

plane is shown for the $K_2O-Al_2O_3-SiO_2$ diagram. The liquids formed in this system are viscous; in order to obtain vitrification, a substantial amount of liquid must be present at the firing temperature. From isothermal diagrams the composition of liquid and amount of liquid for different compositions can be easily determined at the temperature selected. Frequently it is sufficient to determine an isothermal plane rather than an entire diagram, and obviously it is much easier.

Although our discussion of three-component diagrams has been brief and we do not discuss phase-equilibrium behavior for four or more component systems at all, students would be well advised to become familiar with these as an extra project.

7.7 Phase Composition versus Temperature

One of the useful applications for phase equilibrium diagrams in ceramic systems is the determination of the phases present at different temperatures. This information is most readily used in the form of plots of the amount of phases present versus temperature.

Consider, for example, the system $MgO-SiO_2$ (Fig. 7.13). For a composition of 50 wt% MgO -50 wt% SiO_2 , the solid phases present at equilibrium are forsterite and enstatite. As they are heated, no new phases are formed until 1557°C. At this temperature the enstatite disappears and a composition of about 40% liquid containing 61% SiO_2 is formed. On further heating the amount of liquid present increases until the liquidus is reached at some temperature near 1800°C. In contrast, for a 60% MgO -40% SiO_2 composition the solid phases present are forsterite, Mg_2SiO_4 , and periclase, MgO . No new phase is found on heating until 1850°C, when the composition becomes nearly all liquid, since this temperature is near the eutectic composition. The changes in phase occurring for these two compositions are illustrated in Fig. 7.27.

Several things are apparent from this graphical representation. One is the large difference in liquid content versus temperature for a relatively small change in composition. For compositions containing greater than 42% silica, the forsterite composition, liquids are formed at relatively low temperatures. For compositions with silica contents less than 42% no liquid is formed until 1850°C. This fact is used in the treatment of chromite refractories. The most common impurity present is serpentine, $3MgO \cdot 2SiO_2 \cdot 2H_2O$, having a composition of about 50 wt% SiO_2 . If sufficient MgO is added to put this in the MgO -forsterite field, it no longer has a deleterious effect. Without this addition a liquid is formed at low temperatures.

Another application of this diagram is in the selection of compositions

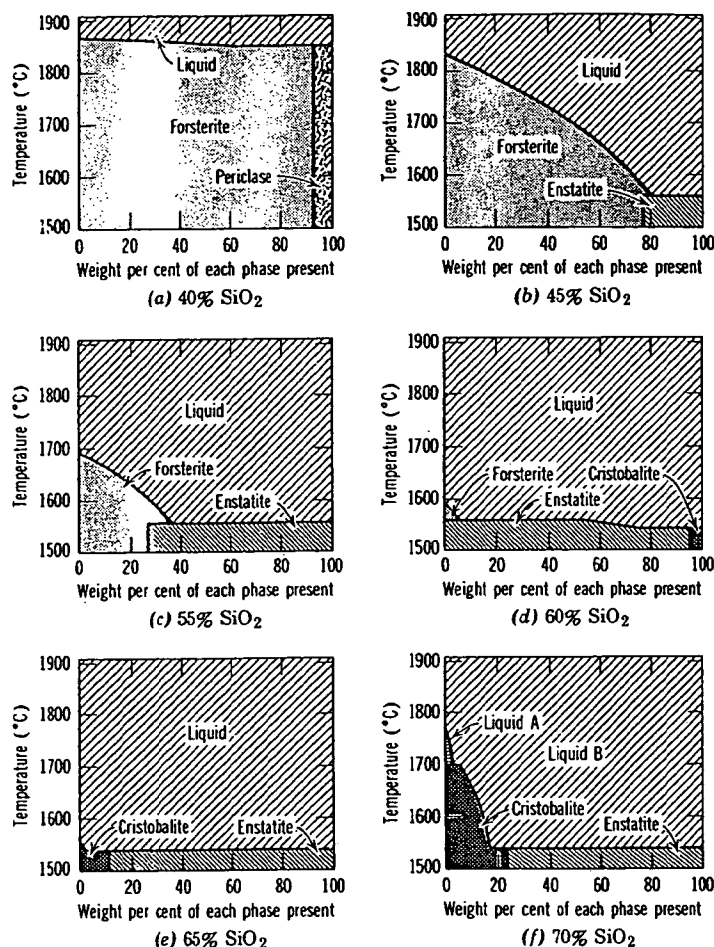


Fig. 7.27. Phase composition versus temperature for samples in the MgO-SiO₂ system.

that have desirable firing characteristics. It is necessary to form a sufficient amount of liquid for vitrification, but not so much that ware slumps or warps during firing. The limits of liquid required vary with the properties of the liquid but are in the range of 20 to 50 wt%. To have a sufficient range of firing temperature, it is desirable that the liquid content not change much with temperature. Forsterite compositions cannot be fired until very high temperatures if the composition is exactly 42% SiO₂, since no liquid is formed below 1850°C. Compositions in the forsterite-enstatite field which are mainly forsterite form a liquid at 1557°C, and

381-515

since the liquidus curve is steep, the amount of liquid present changes but slightly with temperature, as shown in Fig. 7.27. Consequently, these compositions have a good firing range and are easy to vitrify. In contrast, compositions that are mostly enstatite (55, 60, 65% SiO_2) form large amounts of liquid at low temperature, and the amount of liquid present changes rapidly with temperature. These materials have a limited firing range and pose difficult control problems for economic production.

For systems in which the gas phase is important the way in which condensed phases appear and their compositional changes on cooling depend on the conditions imposed. Referring back to the Fe-O system illustrated in Fig. 7.9, if the total condensed-phase composition remains constant, as occurs in a closed nonreactive container with only a negligible amount of gas phase present, the composition A solidifies along the dotted line with a corresponding decrease in the system oxygen pressure. In contrast, if the system is cooled at constant oxygen pressure, the solidification path is along the dashed line. In one case the resulting product at room temperature is a mixture of iron and magnetite; in the second case the resulting product is hematite. Obviously in such systems the control of oxygen pressure during cooling is essential for the control of the products formed.

For detailed discussions of crystallization paths in ternary systems the references should be consulted. The following summary* can serve as a review.

1. When a liquid is cooled, the first phase to appear is the primary phase for that part of the system in which the composition of the melt is represented.
2. The crystallization curve follows to the nearest boundary the extension of the straight line connecting the composition of the original liquid with that of the primary phase of that field. The composition of the liquid within the primary fields is represented by points on the crystallization curve. This curve is the intersection of a plane (perpendicular to the base triangle and passing through the compositions of original melt and the primary phase) with the liquidus surface.
3. At the boundary line a new phase appears which is the primary phase of the adjacent field. The two phases separate together along this boundary as the temperature is lowered.
4. The ratio of the two solids crystallizing is given by the intersection of the tangent to the boundary curve with a line connecting the composi-

*After E. M. Levin, H. F. McMurdie, and F. P. Hall, *Phase Diagrams for Ceramists*, American Ceramic Society, Cleveland, Ohio, 1956.

stem.

rm a
ware
h the
ave a
ntent
ot be
 SiO_2 ,
erite-
, and

tions of the two solid phases. Two things can occur. If this tangent line runs between the compositions of the two solid phases, the amount of each of these phases present increases. If the tangent line intersects an extension of the line between solid compositions, the first phase decreases in amount (is resorbed; Reaction $A + \text{Liquid} = B$) as crystallization proceeds. In some systems the crystallization curve leaves the boundary curve if the first phase is completely resorbed, leaving only the second phase. Systems in which this occurs may be inferred from a study of the mean composition of the solid separating between successive points on the crystallization path.

5. The crystallization curve always ends at the invariant point which represents equilibrium of liquid with the three solid phases of the three components within whose composition triangle the original liquid composition was found.

6. The mean composition of the solid which is crystallizing at any point on a boundary line is shown by the intersection at that point of the tangent with a line joining the composition of the two solid phases which are crystallizing.

7. The mean composition of the total solid that has crystallized up to any point on the crystallization curve is found by extending the line connecting the given point with the original liquid composition to the line connecting the compositions of the phases that have been separating.

8. The mean composition of the solid that has separated between two points on a boundary is found at the intersection of a line passing through these two points with a line connecting the compositions of the two solid phases separating along this boundary.

7.8 The System $\text{Al}_2\text{O}_3\text{-SiO}_2$

As an example of the usefulness of phase diagrams for considering high-temperature phenomena in ceramic systems, the $\text{Al}_2\text{O}_3\text{-SiO}_2$ system illustrates many of the features and problems encountered. In this system (Fig. 7.28), there is one compound present, mullite, which is shown as melting incongruently. (The melting behavior of mullite has been controversial; we show the metastable extensions of the phase boundaries in Fig. 7.28. For our purposes this is most important as indicative of the fact that experimental techniques are difficult and time consuming; the diagrams included here and in standard references are summaries of experimental data. They usually include many interpolations and extrapolations and have been compiled with greater or lesser care, depending on the needs of the original investigator.) The eutectic between mullite and

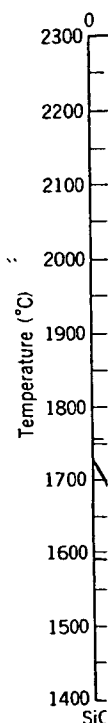


Fig. 7.28.

cristob
 SiO_2 . T

Fact
 can be
 1.0 wt%
 to 90 %
 sintere

At c
 furnac
 tempe
 furnac
 this te
 develo
 alumin

381-513

CERAMIC PHASE-EQUILIBRIUM DIAGRAMS

305

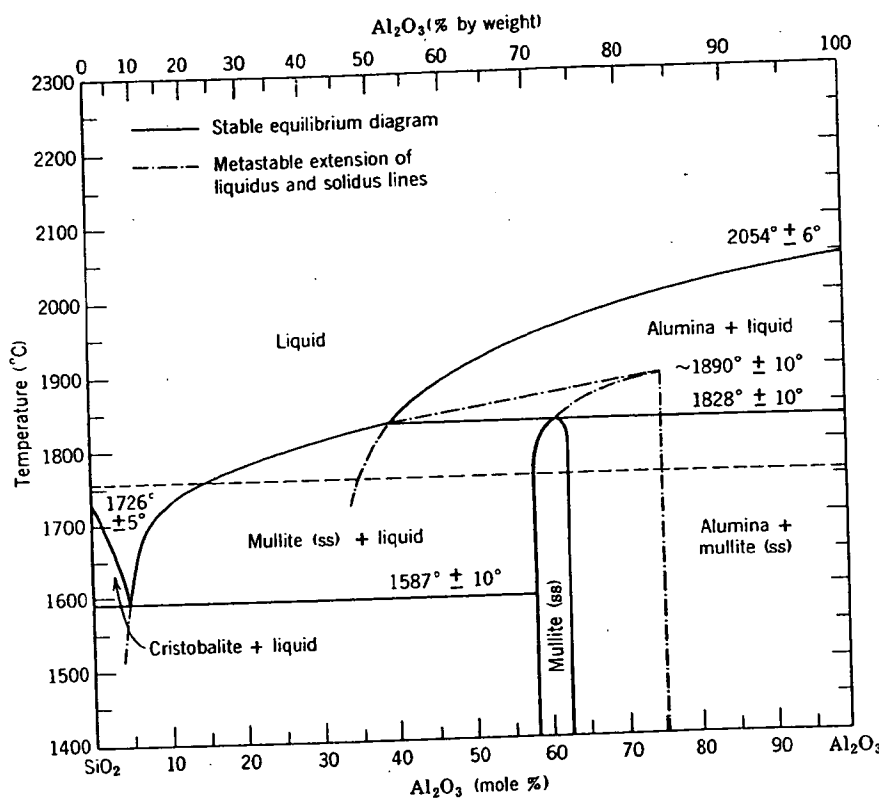


Fig. 7.28. The binary system Al_2O_3 - SiO_2 . From Aksay and Pask, *Science*, 183, 69 (1974).

cristobalite occurs at 1587°C to form a liquid containing about 95 mole% SiO_2 . The solidus temperature between mullite and alumina is at 1828°C .

Factors affecting the fabrication and use of several refractory products can be related to this diagram. They include refractory silica brick (0.2 to 1.0 wt% Al_2O_3), clay products (35 to 50 wt% Al_2O_3), high-alumina brick (60 to 90 wt% Al_2O_3), pure fused mullite (72 wt% Al_2O_3), and pure fused or sintered alumina (>90 wt% Al_2O_3).

At one end of the composition range are silica bricks widely used for furnace roofs and similar structures requiring high strength at high temperatures. A major application was as roof brick for open-hearth furnaces in which temperatures of 1625 to 1650°C are commonly used. At this temperature a part of the brick is actually in the liquid state. In the development of silica brick it has been found that small amounts of aluminum oxide are particularly deleterious to brick properties because

the eutectic composition is close to the silica end of the diagram. Consequently, even small additions of aluminum oxide mean that substantial amounts of liquid phase are present at temperatures above 1600°C. For this reason *supersilica* brick, which has a lower alumina content through special raw-material selection or treatment, is used in structures that will be heated to high temperatures.

Fire-clay bricks have a composition ranging from 35 to 55% aluminum oxide. For compositions without impurities the equilibrium phases present at temperatures below 1587°C are mullite and silica (Fig. 7.29). The relative amounts of these phases present change with composition, and there are corresponding changes in the properties of the brick. At temperatures above 1600°C the amount of liquid phase present is sensitive to the alumina-silica ratio, and for these high-temperature applications the higher-alumina brick is preferred.

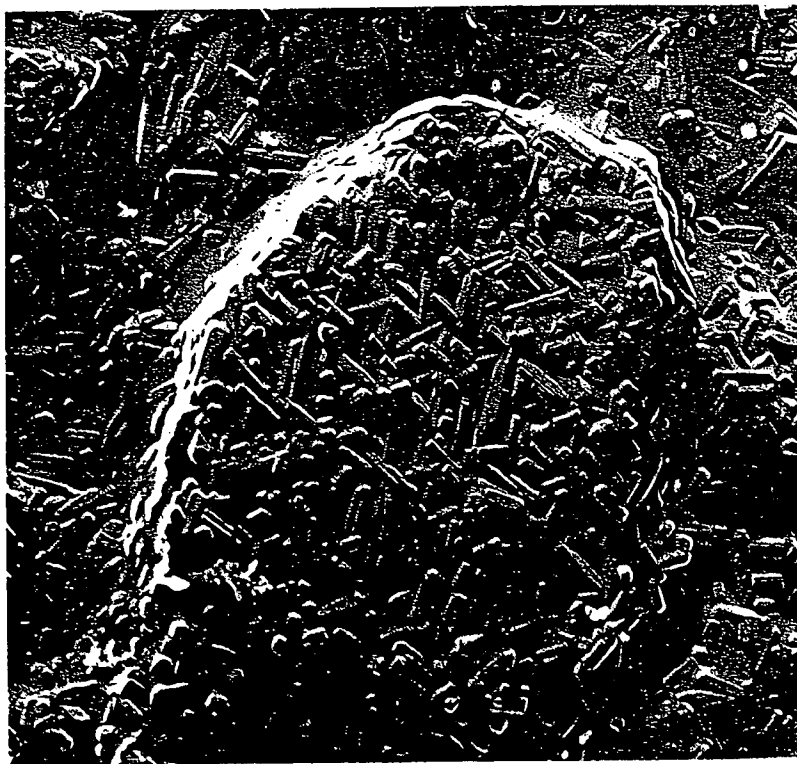


Fig. 7.29. Mullite crystals in silica matrix formed by heating kaolinite (37,000 \times). Courtesy J. J. Comer.

Refr.
cient a
greater
mullite
temper
mullite
deform
with p
fusion-

7.9 T

A te
of cera
Fig. 7.

d
Mg
2800

Fig. 7.3
Geol., 6

381-518

Refractory properties of brick can be substantially improved if sufficient alumina is added to increase the fraction of mullite present until at greater than 72 wt% alumina the brick is entirely mullite or a mixture of mullite plus alumina. Under these conditions no liquid is present until temperatures above 1828°C are reached. For some applications fused mullite brick is used; it has superior ability to resist corrosion and deformation at high temperatures. The highest refractoriness is obtained with pure alumina. Sintered Al_2O_3 is used for laboratory ware, and fusion-cast Al_2O_3 is used as a glass tank refractory.

7.9 The System $\text{MgO}-\text{Al}_2\text{O}_3-\text{SiO}_2$

A ternary system important in understanding the behavior of a number of ceramic compositions is the $\text{MgO}-\text{Al}_2\text{O}_3-\text{SiO}_2$ system, illustrated in Fig. 7.30. This system is composed of several binary compounds which

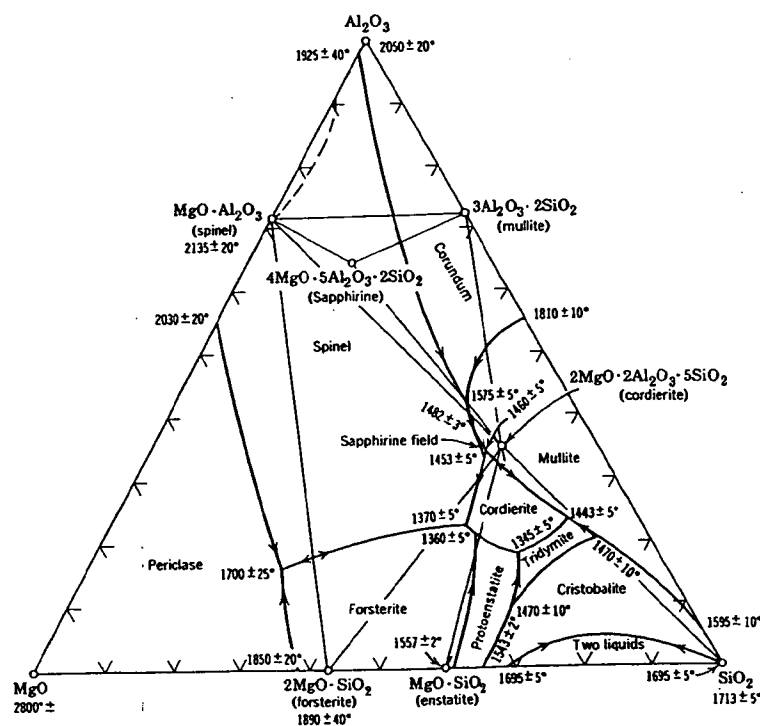


Fig. 7.30. The ternary system $\text{MgO}-\text{Al}_2\text{O}_3-\text{SiO}_2$. From M. L. Keith and J. F. Schairer, *J. Geol.*, 60, 182 (1952). Regions of solid solution are not shown; see Figs. 4.3 and 7.13.

firing process
clay decomposition
Talc decomposition
protoenstatite
heating of
crystallization
eutectic liquid
growth of talc
At this temperature
SiO₂, 33.4%
MgO-SiO₂

The main
ite, steatite
firing range
fusion. In g
to 35% of a
indicated in
compositio
clay mixtu
which is 90
tions. At t
liquidus ter
with tempe
necessary,

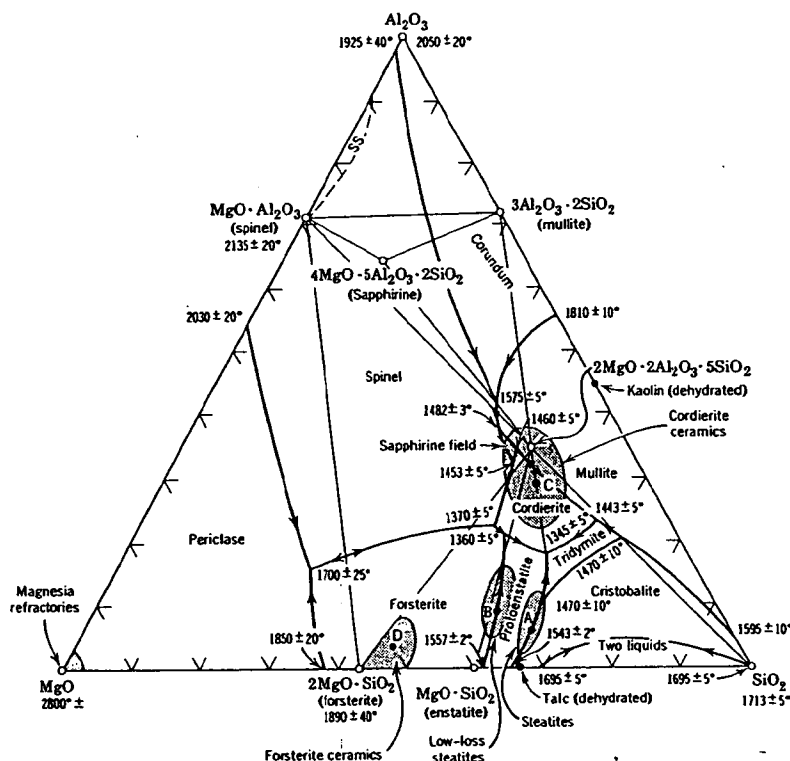


Fig. 7.31. Common compositions in the ternary system $\text{MgO}-\text{Al}_2\text{O}_3-\text{SiO}_2$. See text for other additives.

Fig. 7.32. A
in Fig. 7.31.

381-518

firing process, which is described in more detail in Chapter 12. On heating, clay decomposes at 980°C to form fine-grained mullite in a silica matrix. Talc decomposes and gives rise to a similar mixture of fine-grained protoenstatite crystals, MgSiO_3 , in a silica matrix at about 1000°C. Further heating of clay gives rise to increased growth of mullite crystals, crystallization of the silica matrix as cristobalite, and formation of a eutectic liquid at 1595°C. Further heating of pure talc leads to crystal growth of the enstatite, and liquid is formed at a temperature of 1547°C. At this temperature almost all the composition melts, since talc (66.6% SiO_2 , 33.4% MgO) is not far from the eutectic composition in the MgO-SiO_2 system (Fig. 7.13).

The main feature which characterizes the melting behavior of cordierite, steatite porcelain, and low-loss steatite compositions is the limited firing range which results when pure materials are carried to partial fusion. In general, for firing to form a vitreous densified ceramic about 20 to 35% of a viscous silicate liquid is required. For pure talc, however, as indicated in Fig. 7.32, no liquid is formed until 1547°C, when the entire composition liquifies. This can be substantially improved by using talc-clay mixtures. For example, consider the composition A in Fig. 7.31 which is 90% talc-10% clay, similar to many commercial steatite compositions. At this composition about 30% liquid is formed abruptly at the liquidus temperature, 1345°C; the amount of liquid increases quite rapidly with temperature (Fig. 7.32), making close control of firing temperature necessary, since the firing range is short for obtaining a dense vitreous

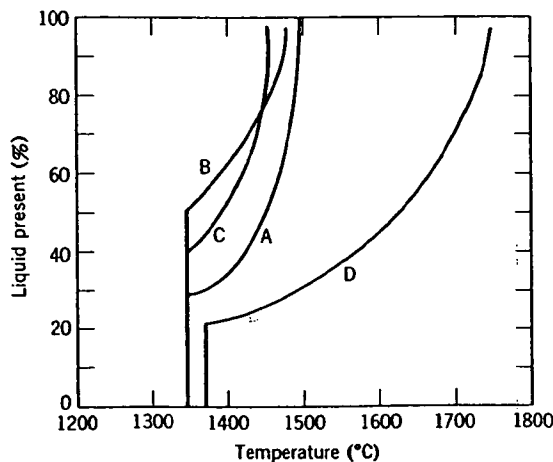


Fig. 7.32. Amount of liquid present at different temperatures for compositions illustrated in Fig. 7.31.

body (this composition would be fired at 1350 to 1370°C). In actual fact, however, the raw materials used contain Na_2O , K_2O , CaO , BaO , Fe_2O_3 , and TiO_2 as minor impurities which both lower and widen the fusion range. Additions of more than 10% clay again so shorten the firing range that they are not feasible, and only limited compositions are practicable. The addition of feldspar greatly increases the firing range and the ease of firing and has been used in the past for compositions intended as low-temperature insulators. However, the electrical properties are not good.

For low-loss steatites, additional magnesia is added to combine with the free silica to bring the composition nearer the composition triangle for forsterite-cordierite-enstatite. This changes the melting behavior so that a composition such as B in Fig. 7.31 forms about 50% liquid over a temperature range of a few degrees, and control in firing is very difficult (Fig. 7.32). In order to fire these compositions in practice to form vitreous bodies, added flux is essential. Barium oxide, added as the carbonate, is the most widely used.

Cordierite ceramics are particularly useful, since they have a very low coefficient of thermal expansion and consequently good resistance to thermal shock. As far as firing behavior is concerned, compositions show a short firing range corresponding to a flat liquidus surface which leads to the development of large amounts of liquid over a short temperature interval. If a mixture consisting of talc and clay, with alumina added to bring it closer to the cordierite composition, is heated, an initial liquidus is formed at 1345°C, as for composition C in Fig. 7.31. The amount of liquid rapidly increases; because of this it is difficult to form vitreous bodies. Frequently when these compositions are not intended for electrical applications, feldspar (3 to 10%) is added as a fluxing medium to increase the firing range.

Magnesia and forsterite compositions are different in that a eutectic liquid is formed of a composition widely different from the major phase with a steep liquidus curve so that a broad firing range is easy to obtain. This is illustrated for the forsterite composition D in Fig. 7.31 and the corresponding curve in Fig. 7.32. The initial liquid is formed at the 1360°C eutectic, and the amount of liquid depends mainly on composition and does not change markedly with temperature. Consequently, in contrast to the steatite and cordierite bodies, forsterite ceramics present few problems in firing.

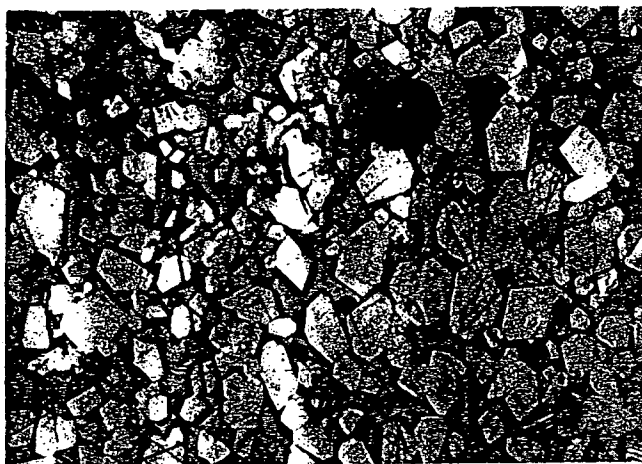
In all these compositions there is normally present at the firing temperature an equilibrium mixture of crystalline and liquid phases. This is illustrated for a forsterite composition in Fig. 7.33. Forsterite crystals are present in a matrix of liquid silicate corresponding to the liquidus

composi
phase at
and the
liquid ph
(or a part
for fixin
deduced

7.10 No

The ki
in the ne
in Chapt
lowest e
systems.
free ene
illustrate
phases t
equilibri
solution
liquid an
phases in
the com
slowness

381-518

Fig. 7.33. Crystal-liquid structure of a forsterite composition (150 \times).

composition at the firing temperature. For other systems the crystalline phase at the firing temperature is protoenstatite, periclase, or cordierite, and the crystal size and morphology are usually different as well. The liquid phase frequently does not crystallize on cooling but forms a glass (or a partly glass mixture) so that the compatibility triangle cannot be used for fixing the phases present at room temperature, but they must be deduced instead from the firing conditions and subsequent heat treatment.

7.10 Nonequilibrium Phases

The kinetics of phase transitions and solid-state reactions is considered in the next two chapters; however, from our discussion of glass structure in Chapter 3 and atom mobility in Chapter 6 it is already apparent that the lowest energy state of phase equilibria is not achieved in many practical systems. For any change to take place in a system it is necessary that the free energy be lowered. As a result the sort of free-energy curves illustrated in Figs. 3.10, 4.2, 4.3, 7.7, and 7.8 for each of the possible phases that might be present remain an important guide to metastable equilibrium. In Fig. 7.8, for example, if at temperature T_2 the solid solution α were absent for any reason, the common tangent between the liquid and solid solution β would determine the composition of those phases in which the constituents have the same chemical potential. One of the common types of nonequilibrium behavior in silicate systems is the slowness of crystallization such that the liquid is supercooled. When this

happens, metastable phase separation of the liquid is quite common, discussed in Chapter 3.

Glasses. One of the most common departures from equilibrium behavior in ceramic systems is the ease with which many silicates are cooled from the liquid state to form noncrystalline products. This requires that the driving force for the liquid-crystal transformation be low and that the activation energy for the process be high. Both of these conditions are fulfilled for many silicate systems.

The rate of nucleation for a crystalline phase forming from the liquid is proportional to the product of the energy difference between the crystal and liquid and the mobility of the constituents that form a crystal, as discussed in Chapter 8. In silicate systems, both of these factors change so as to favor the formation of glasses as the silica content increases. Although data for the diffusion coefficient are not generally available, the limiting mobility is that of the large network-forming anions and is inversely proportional to the viscosity. Thus, the product of $\Delta H_f/T_{mp}$ and $1/\eta$ can be used as one index for the tendency to form glasses on cooling, as shown in Table 7.1.

Table 7.1. Factors Affecting Glass-Forming Ability

Compo- sition	$T_{mp}(^{\circ}\text{C})$	$\Delta H_f/T_{mp}$ (cal/mole/ $^{\circ}\text{K}$)	$(1/\eta)_{mp}$ (poise $^{-1}$)	$(\Delta H_f/T_{mp}) \times$ $(1/\eta)_{mp}$	Comments
B_2O_3	450	7.3	2×10^{-5}	1.5×10^{-4}	Good glass former
SiO_2	1713	1.1	1×10^{-6}	1.1×10^{-6}	Good glass former
$\text{Na}_2\text{Si}_2\text{O}_5$	874	7.4	5×10^{-4}	3.7×10^{-3}	Good glass former
Na_2SiO_3	1088	9.2	5×10^{-3}	4.5×10^{-2}	Poor glass former
CaSiO_3	1544	7.4	10^{-1}	0.74	Very difficult to form as glass
NaCl	800.5	6.9	50	345	Not a glass former

Metastable Crystalline Phases. Frequently in ceramic systems crystalline phases are present that are not the equilibrium phases for the conditions of temperature, pressure, and composition of the system. These remain present in a metastable state because the high activation

energ
rate
same
one
more
energ

Th
Fig.
energ
been
whic
into
into
preci
exam
phas
prese

Th
going
porc
of 12
quar
raw
trans
The
elim

Fig

381-513

ite common,

uililibrium be-
es are cooled
requires that
' and that the
onditions are

i the liquid is
n the crystal
a crystal, as
ctors change
nt increases.
available, the
ions and is
 $\Delta H_f/T_{mp}$ and
s on cooling,

Comments

Good glass
former
Good glass
former
Good glass
former
Poor glass
former
Very diffi-
cult to
form as
glass
Not a glass
former

ms crystal-
ses for the
he system.
i activation

energies required for their conversion into more stable phases cause a low rate of transition. The energy relationships among three phases of the same composition might be represented as given in Fig. 7.34. Once any one of these phases is formed, its rate of transformation into another more stable phase is slow. In particular, the rate of transition to the lowest energy state is specially slow for this system.

The kinetics of transformation in systems such as those illustrated in Fig. 7.34 are discussed in Chapter 9 in terms of the driving force and energy barrier. Structural aspects of transformations of this kind have been discussed in Chapter 2. In general, there are two common ways in which metastable crystals are formed. First, if a stable crystal is brought into a new temperature or pressure range in which it does not transform into the more stable form, metastable crystals are formed. Second, a precipitate or transformation may form a new metastable phase. For example, if phase 1 in Fig. 7.34 is cooled into the region of stability of phase 3, it may transform into the intermediate phase 2, which remains present as a metastable crystal.

The most commonly observed metastable crystalline phases not undergoing transformation are the various forms of silica (Fig. 7.5). When a porcelain body containing quartz as an ingredient is fired at a temperature of 1200 to 1400°C, tridymite is the stable form but it never is observed; the quartz always remains as such. In refractory silica brick, quartz used as a raw material must have about 2% calcium oxide added to it in order to be transformed into the tridymite and cristobalite forms which are desirable. The lime provides a solution-precipitation mechanism which essentially eliminates the activation energy barrier, shown in Fig. 7.34, and allows

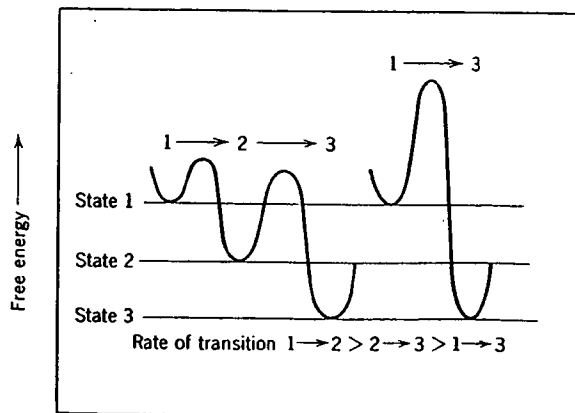


Fig. 7.34. Illustration of energy barriers between three different states of a system.

the stable phase to be formed. This is, in general, the effect of mineralizers such as fluorides, water, and alkalis in silicate systems. They provide a fluid phase through which reactions can proceed without the activation energy barrier present for the solid-state process.

Frequently, when high-temperature crystalline forms develop during firing of a ceramic body, they do not revert to the more stable forms on cooling. This is particularly true for tridymite and cristobalite, which never revert to the more stable quartz form. Similarly, in steatite bodies the main crystalline phase at the firing temperature is the protoenstatite form of MgSiO_3 . In fine-grained samples this phase remains as a metastable phase dispersed in a glassy matrix after cooling. In large-grain samples or on grinding at low temperature, protoenstatite reverts to the equilibrium form, clinoenstatite.

A common type of nonequilibrium behavior is the formation of a metastable phase which has a lower energy than the mother phase but is not the lowest-energy equilibrium phase. This corresponds to the situation illustrated in Fig. 7.34 in which the transition from the highest-energy phase to an intermediate energy state occurs with a much lower activation energy than the transition to the most stable state. It is exemplified by the devitrification of silica glass, which occurs in the temperature range of 1200 to 1400°C, to form cristobalite as the crystalline product instead of the more stable form, tridymite. The reasons for this are usually found in the structural relationships between the starting material and the final product. In general, high-temperature forms have a more open structure than low-temperature crystalline forms and consequently are more nearly like the structure of a glassy starting material. These factors tend to favor crystallization of the high-temperature form from a supercooled liquid or glass, even in the temperature range of stability of a lower-temperature modification.

This phenomenon has been observed in a number of systems. For example, J. B. Ferguson and H. E. Merwin* observed that when calcium-silicate glasses are cooled to temperatures below 1125°C, at which wollastonite (CaSiO_3) is the stable crystalline form, the high-temperature modification, pseudowollastonite, is found to crystallize first and then slowly transform into the more stable wollastonite. Similarly, on cooling compositions corresponding to $\text{Na}_2\text{O} \cdot \text{Al}_2\text{O}_3 \cdot 2\text{SiO}_2$, the high-temperature crystalline form (carnegieite) is observed to form as the reaction product, even in the range in which nephelite is the stable phase; transformation of carnegieite into nephelite occurs slowly.

In order for any new phase to form, it must be lower in free energy than the starting material but need not be the lowest of all possible new phases.

* *Am. J. Science, Series 4*, 48, 165 (1919).

This requires the phase diagram to show other phase precipitates. Fig. 7.35. difficulty frequently potassium eutectic temperature which both the liquid and this system cristobalite equilibrium quartz by the double

Extension

Temperature (°C)

Fig. 7.35. E system.

381-518

This requirement means that when a phase does not form as indicated on the phase equilibrium diagram, the liquidus curves of other phases on the diagram must be extended to determine the conditions under which some other phase becomes more stable than the starting solution and a possible precipitate. This is illustrated for the potassium disilicate-silica system in Fig. 7.35. Here, the compound $K_2O \cdot 4SiO_2$ crystallizes only with great difficulty so that the eutectic corresponding to this precipitation is frequently not observed. Instead, the liquidus curves for silica and for potassium disilicate intersect at a temperature about 200° below the true eutectic temperature. This nonequilibrium eutectic is the temperature at which both potassium disilicate and silica have a lower free energy than the liquid composition corresponding to the false eutectic. Actually, for this system the situation is complicated somewhat more by the fact that cristobalite commonly crystallizes from the melt in place of the equilibrium quartz phase. This gives additional possible behaviors, as indicated by the dotted line in Fig. 7.35.

Extension of equilibrium curves on phase diagrams, such as has been

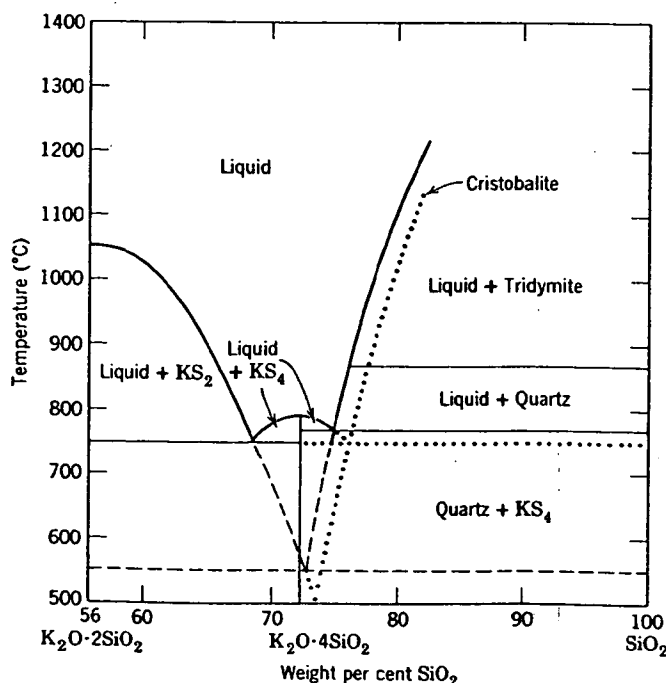


Fig. 7.35. Equilibrium and nonequilibrium liquidus curves in the potassium disilicate-silica system.

shown in Fig. 7.35 and also in Fig. 7.5, provides a general method of using equilibrium data to determine possible nonequilibrium behavior. It provides a highly useful guide to experimental observations. The actual behavior in any system may follow any one of several possible courses, so that an analysis of the kinetics of these processes (or more commonly experimental observations) is also required.

Incomplete Reactions. Probably the most common source of nonequilibrium phases in ceramic systems are reactions that are not completed in the time available during firing or heat treatment. Reaction rates in condensed phases are discussed in Chapter 9. The main kinds of incomplete reactions observed are incomplete solution, incomplete solid-state reactions, and incomplete resorption or solid-liquid reactions. All of these arise from the presence of reaction products which act as barrier layers and prevent further reaction. Perhaps the most striking example of incomplete reactions is the entire metallurgical industry, since almost all metals are thermodynamically unstable in the atmosphere but oxidize and corrode only slowly.

A particular example of incomplete solution is the existence of quartz grains which are undissolved in a porcelain body, even after firing at temperatures of 1200 to 1400°C. For the highly siliceous liquid in contact with the quartz grain, the diffusion coefficient is low, and there is no fluid flow to remove the boundary layer mechanically. The situation is similar to diffusion into an infinite medium, illustrated in Fig. 6.5. To a first approximation, the diffusion coefficient for SiO_2 at the highly siliceous boundary may be of the order of 10^{-8} to 10^{-9} cm^2/sec at 1400°C. With these data it is left as an exercise to estimate the thickness of the diffusion layer after 1 hr of firing at this temperature.

The way in which incomplete solid reactions can lead to residual starting material being present as nonequilibrium phases will be clear from the discussion in Chapter 9. However, new products that are not the final equilibrium composition can also be formed. For example, in heating equimolar mixtures of CaCO_3 and SiO_2 to form CaSiO_3 , the first product formed and the one that remains the major phase through most of the reaction is the orthosilicate, Ca_2SiO_4 . Similarly, when BaCO_3 and TiO_2 are reacted to form BaTiO_3 , substantial amounts of Ba_2TiO_4 , BaTi_3O_7 , and BaTi_4O_9 are formed during the reaction process, as might be expected from the phase-equilibrium diagram (Fig. 7.20). When a series of intermediate compounds is formed in a solid reaction, the rate at which each grows depends on the effective diffusion coefficient through it. Those layers for which the diffusion rate is high form most rapidly. For the CaO-SiO_2 system this is the orthosilicate. For the BaO-TiO_2 system the most rapidly forming compound is again the orthotitanate, Ba_2TiO_4 .

381-515

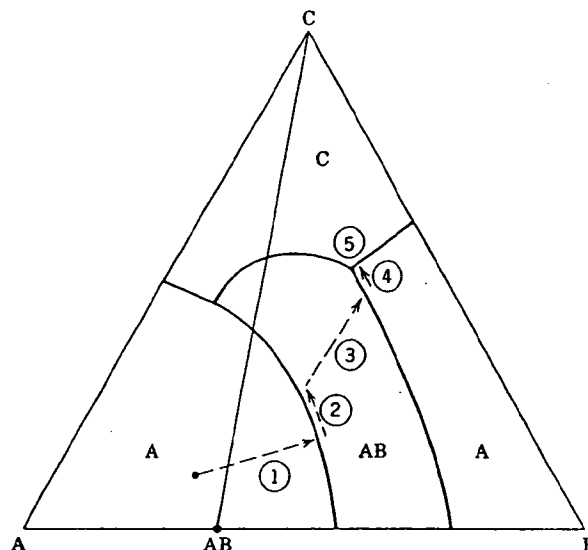


Fig. 7.36. Nonequilibrium crystallization path with (1) Liquid \rightarrow A, (2) A + liquid \rightarrow AB, (3) Liquid \rightarrow AB, (4) Liquid \rightarrow AB + B, (5) Liquid \rightarrow AB + B + C.

A final example of nonequilibrium conditions important in interpreting phase-equilibrium diagrams is the incomplete resorption that may occur whenever a reaction, $A + \text{Liquid} = AB$, takes place during crystallization. This is the case, for example, when a primary phase reacts with a liquid to form a new compound during cooling. A layer tends to build up on the surface of the original particle, forming a barrier to further reaction. As the temperature is lowered, the final products are not those anticipated from the equilibrium diagram. A nonequilibrium crystallization path for incomplete resorption is schematically illustrated in Fig. 7.36.

Suggested Reading

1. E. M. Levin, C. R. Robbins, and H. F. McMurdie, *Phase Diagrams for Ceramists*, American Ceramic Society, Columbus, Ohio, 1964.
2. E. M. Levin, C. R. Robbins, H. F. McMurdie, *Phase Diagrams for Ceramists, 1969 Supplement*, American Ceramic Society, Columbus, Ohio, 1969.
3. A. M. Alper, Ed., *Phase Diagrams: Materials Science and Technology*, Vol. I, "Theory, Principles, and Techniques of Phase Diagrams," Academic Press, Inc., New York, 1970; Vol. II, "The Use of Phase Diagrams in Metal, Refractory, Ceramic, and Cement Technology," Academic Press, Inc., New

thod of using
avior. It pro-
The actual
sible courses,
re commonly

urce of non-
are not com-
eaction rates
ain kinds of
mplete solid-
ctions. All of
act as barrier
g example of
ice almost all
it oxidize and

nce of quartz
after firing at
rid in contact
ere is no fluid
ion is similar
5. To a first
hly siliceous
C. With these
diffusion layer

l to residual
will be clear
at are not the
le, in heating
first product
most of the
and TiO_2 are
 BaTi_3O_7 , and
be expected
ries of inter-
t which each
gh it. Those
idly. For the
 O_2 -system the
 Ba_2TiO_4 .

- York, 1970; Vol. III, "The Use of Phase Diagrams in Electronic Materials and Glass Technology," Academic Press, Inc., New York, 1970.
4. A. Muan and E. F. Osborn, *Phase Equilibria among Oxides in Steelmaking*, Addison-Wesley, Publishing Company, Inc., Reading, Mass., 1965.
 5. A. Reisman, *Phase Equilibria*, Academic Press, Inc., New York, 1970.
 6. P. Gordon, *Principles of Phase Diagrams in Materials Systems*, McGraw Hill Book Company, New York, 1968.
 7. A. M. Alper, Ed., *High Temperature Oxides*, Part I, "Magnesia, Lime and Chrome Refractories," Academic Press, Inc., New York, 1970; Part II, "Oxides of Rare Earth, Titanium, Zirconium, Hafnium, Niobium, and Tantalum," Academic Press, Inc., New York, 1970; Part III, "Magnesia, Alumina, and Beryllia Ceramics: Fabrication, Characterization and Properties," Academic Press, Inc., New York; Part IV, "Refractory Glasses, Glass-Ceramics, Ceramics," Academic Press, New York, Inc., 1971.
 8. J. E. Ricci, *The Phase Rule and Heterogeneous Equilibrium*, Dover Books, New York, 1966.

Problems

- 7.1. A power failure allowed a furnace used by a graduate student working in the K_2O - CaO - SiO_2 system to cool down over night. For the fun of it, the student analyzed the composition he was studying by X-ray diffraction. To his horror, he found β - $CaSiO_3$, $2K_2O \cdot CaO \cdot 3SiO_2$, $2K_2O \cdot CaO \cdot 6SiO_2$, $K_2O \cdot 3CaO \cdot 6SiO_2$, and $K_2O \cdot 2CaO \cdot 6SiO_2$ in his sample.
 - (a) How could he get more than three phases?
 - (b) Can you tell him in which composition triangle his original composition was?
 - (c) Can you predict the minimum temperature above which his furnace was operating before power failure?
 - (d) He thought at first he also had some questionable X-ray diffraction evidence for $K_2O \cdot CaO \cdot SiO_2$, but after thinking it over he decided $K_2O \cdot CaO \cdot SiO_2$ should not crystallize out of his sample. Why did he reach this conclusion?
- 7.2. According to Alper, McNally, Ribbe, and Doman,* the maximum solubility of Al_2O_3 in MgO is 18 wt% at 1995°C and of MgO in $MgAl_2O_4$ is 39% MgO , 51% Al_2O_3 . Assuming the NiO - Al_2O_3 binary is similar to the MgO - Al_2O_3 binary, construct a ternary. Make isothermal plots of this ternary at 2200°C, 1900°C, and 1700°C.
- 7.3. You have been assigned to study the electrical properties of calcium metasilicate by the director of the laboratory in which you work. If you were to make the material synthetically, give a batch composition of materials commonly obtainable in high purity. From a production standpoint, 10% liquid would increase the rate of sintering and reaction. Adjust your composition accordingly. What would be the expected firing temperature? Should the boss ask you to explore the possibility of lowering the firing temperature and maintain a white body, suggest the direction to procede. What polymorphic transformations would you be conscious of in working with the above systems?

*J. Am. Ceram. Soc. 45(6), 263-268 (1962).

7.4. Di
rel
on
an
im
7.5. A
ox

Al
7.6. Tr
ter
(m
ar
fo
ph
7.7. Fe
in
fo
tic
rit
sti
7.8. If
to
th
7.9. Ti
Al
ter
th
fo

381-518

CERAMIC PHASE-EQUILIBRIUM DIAGRAMS

319

- 7.4. Discuss the importance of liquid-phase formation in the production and utilization of refractory bodies. Considering the phase diagram for the MgO-SiO_2 system, comment on the relative desirability in use of compositions containing 50MgO-50SiO₂ by weight and 60MgO-40SiO₂ by weight. What other characteristics of refractory bodies are important in their use?
- 7.5. A binary silicate of specified composition is melted from powders of the separate oxides and cooled in different ways, and the following observations are made:

Condition	Observations
(a) Cooled rapidly	Single phase, no evidence of crystallization
(b) Melted for 1 hr, held 80°C below liquidus for 2 hr	Crystallized from surface with primary phases SiO ₂ plus glass
(c) Melted for 3 hr, held 80°C below liquidus for 2 hr	Crystallized from surface with primary phases compound $\text{AO} \cdot \text{SiO}_2$ plus glass
(d) Melted for 2 hr, cooled rapidly to 200°C below liquidus, held for 1 hr, and then cooled rapidly	No evidence of crystallization but resulting glass is cloudy

Are all these observations self consistent? How do you explain them?

- 7.6. Triaxial porcelains (flint-feldspar-clay) in which the equilibrium phases at the firing temperature are mullite and a silicate liquid have a long firing range; steatite porcelains (mixtures of talc plus kaolin) in which the equilibrium phases at the firing temperature are enstatite and a silicate liquid have a short firing range. Give plausible explanations for this difference in terms of phases present, properties of phases, and changes in phase composition and properties with temperature.
- 7.7. For the composition 40MgO-55SiO₂-5Al₂O₃, trace the equilibrium crystallization path in Fig. 7.30. Also, determine the crystallization path if incomplete resorption of forsterite occurs along the forsterite-protoenstatite boundary. How do the compositions and temperatures of the eutectics compare for the equilibrium and nonequilibrium crystallization paths? What are the compositions and amounts of each constituent in the final product for the two cases?
- 7.8. If a homogeneous glass having the composition 13Na₂O-13CaO-74SiO₂ were heated to 1050°C, 1000°C, 900°C, and 800°C, what would be the possible crystalline products that might form? Explain.
- 7.9. The clay mineral kaolinite, $\text{Al}_2\text{Si}_2\text{O}_5(\text{OH})_4$, when heated above 600°C decomposes to $\text{Al}_2\text{Si}_2\text{O}_7$ and water vapor. If this composition is heated to 1600°C and left at that temperature until equilibrium is established, what phase(s) will be present. If more than one is present, what will be their weight percentages. Make the same calculations for 1585°C.

Reactions with and between Solids

In heterogeneous reactions there is a reaction interface between the reacting phases, such as nucleus and matrix or crystal and melt. In order for the reaction to proceed, three steps must take place in series—material transport to the interface, reaction at the phase boundary, and sometimes transport of reaction products away from the interface. In addition, reactions at the phase boundary liberate or absorb heat, changing the boundary temperature and limiting the rate of the process. Any of these steps may determine the overall rate at which a heterogeneous reaction takes place, since the overall reaction rate is determined by the slowest of these series steps.

In this chapter we consider these rate-determining steps as applied to changes taking place in ceramic systems. Decomposition of hydrates and carbonates, solid-state reactions, oxidation, corrosion, and many other phenomena must be considered on the basis of limitations imposed by the rates of phase-boundary reactions, material transport, and heat flow.

9.1 Kinetics of Heterogeneous Reactions

Reaction Order. Classical chemical-reaction kinetics has been mainly concerned with homogeneous reactions and cannot be directly applied to many phenomena of particular interest in ceramics, but it provides the basis for understanding rate phenomena. Reaction rates are frequently classified as to molecularity—the number of molecules or atoms formally taking part in the reaction. Overall reactions are also commonly classified as to reaction order—the sum of the powers to which concentrations c_1 , c_2 , and so on, must be raised to give empirical agreement with a rate equation of the form

$$-\frac{dc}{dt} = Kc_1^{\alpha}c_2^{\beta}c_3^{\gamma} \dots \quad (9.1)$$

In a first-order reaction, for example,

$$\frac{-dc}{dt} = Kc \quad (9.2)$$

On integration this gives

$$\ln \frac{c}{c_0} = K(t - t_0) \quad (9.3)$$

where K is a constant and c_0 is the initial concentration at time t_0 . For the simplest overall reactions which involve but one elementary step, the order and molecularity are the same. For more complex reactions which consist of several consecutive elementary steps involving different species and for heterogeneous reactions in general, the molecularity and order are quite different, and characterization by reaction order is a purely formal empirical method. In fact, zero and fractional reaction orders are sometimes found. Although the reaction-order concept is useful as a means of representing data for heterogeneous reactions, these cannot usually be interpreted simply in terms of molecular interactions.

Activation Energy and Reaction Rate. The effect of temperature on the rate of processes taking place is frequently great. The historical basis for its understanding is the Arrhenius equation, in which it was found that for many processes the specific reaction-rate constant could be related to temperature by the relation $\log K \sim 1/T$ or, alternatively, $K = A \exp(-Q/RT)$, where Q is the experimental activation energy. The basis of this relationship in a general theory of rate processes has been discussed in Chapter 6 in connection with diffusion as an activated process. In general, an activation energy is required for each of the steps involved in an overall rate process (Fig. 9.1).

Two general considerations are the basis for interpreting most kinetic data. The first of these is that each individual step in a rate process must be relatively simple and that the reaction path of each step, such as an individual atom jump in diffusion, a molecular decomposition, or a new chemical bond being formed, involves an *activated complex* or *transition state* of maximum energy along the reaction path. Of all possible parallel paths of reaction, the one with the lowest energy barrier is the most rapid and the major contributor to the overall process. This activated-complex theory has provided a general form of equation for rate processes and a model that allows semiempirical calculations for simple processes. The second general consideration has been that the overall rate of a complex process involving a series of consecutive steps is fixed by the rate of the slowest individual step.

If we plot energy along a distance coordinate corresponding to the

Fig. 9.1. Several steps each step has

(9.2)

(9.3)

For the ep, the which different ity and er is a eaction cept is , these ons.

on the isis for hat for ited to $K =$ y. The s been tivated e steps

kinetic s must as an a new nsition arallel t rapid mplex and a s. The mplex of the

to the

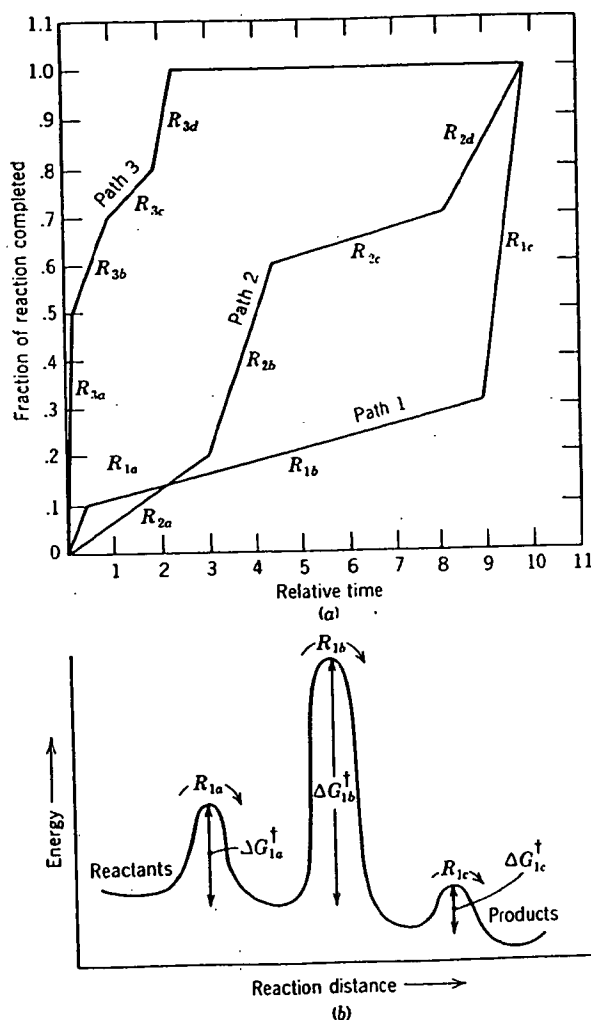


Fig. 9.1. Schematic representation of (a) multipath process in which each path contains several steps; the process is dominated by the fastest path (path 3). (b) Multistep path in which each step has an activation energy; the overall rate along this path is determined by the slowest step.

reaction path of lowest energy between the reactant and product, there is an energy maximum, actually a saddle point, corresponding to the activated complex or transition state, such as discussed for diffusion in Chapter 6. This concept of an activated complex has been generally accepted as the basis for reaction-rate studies and, as discussed in Chapter 6, leads to a specific reaction-rate constant given by

$$k = \frac{kT}{h} \exp\left(-\frac{\Delta H^\ddagger}{RT}\right) \exp \frac{\Delta S^\ddagger}{R} \quad (9.4)$$

where k is the Boltzmann constant, h the Planck constant, and ΔH^\ddagger and ΔS^\ddagger the enthalpy and entropy of activation, respectively. Individual reaction steps in an overall reaction process are usually simple and may be designated as monomolecular or bimolecular. Semiempirical treatments of the unit steps on the basis of activated-complex theory allow a rational theoretical approach to reaction processes.

Complex Processes. Overall processes are frequently complex and require a series of individual separate unit steps. In such a sequence the rate of any individual step depends on the specific reaction-rate constant and the concentration of the reactants for this step. For a series of consecutive steps,

$$A_1 = A_2 = \dots A_i = A_{i+1} = \dots A_n \quad (9.5)$$

We can define a *virtual maximum rate* for each step as the rate that would be found if equilibria were established for all previous and following steps. Under these conditions the reaction with the lowest virtual maximum rate controls the overall rate if it is much lower than the rates of other steps. Under these conditions equilibrium will have been virtually established for all previous steps but will not necessarily be established for the following steps. As shown schematically in Fig. 9.1, the reaction rate for path 1 is determined by step 1b of the process; it has the slowest rate and the largest activation energy barrier and accounts for 85% of the reaction time; steps 1a and 1c occur more rapidly. Reaction step R_{1a} will be slowed to a rate giving a virtual equilibrium concentration of products; reaction R_{1c} will be slowed because R_{1b} is producing few reactants for step R_{1c} .

We have already noted that most condensed-phase processes of interest in ceramics involve heterogeneous systems; changes take place at a phase boundary. The overall process involves (1) transport of reactants to the phase boundary, (2) reaction at the phase boundary, (3) transport of products away from the phase boundary. This series of reaction steps has relatively simple kinetics, provided the virtual maximum rate of one step is much slower than that of any of the other steps. If we assume this to be

the case, we have two general classes of heterogeneous reactions: (1) those controlled by transport rate and (2) those controlled by phase-boundary reaction rate. In general, both the transport process and the phase-boundary process involve a number of individual steps, one of which has the lowest virtual maximum rate. In going from reactants to products, there may be several possible reaction paths for transport processes and for phase-boundary reactions. There are three different possible reaction paths shown in Fig. 9-1a.

9.2 Reactant Transport through a Planar Boundary Layer

Slip Casting. As an example of the usefulness of determining the rate-limiting step for deriving kinetic equations, we begin with the ceramic processing technique of slip casting, in which a slurry containing clay particles dispersed in water is poured into a plaster of paris (gypsum) mold which contains fine capillaries (see Fig. 11.36) that absorb water from the slip. This causes a compact layer of clay particles to form at the mold-slip interface (Fig. 9.2). The rate of the process is determined by the

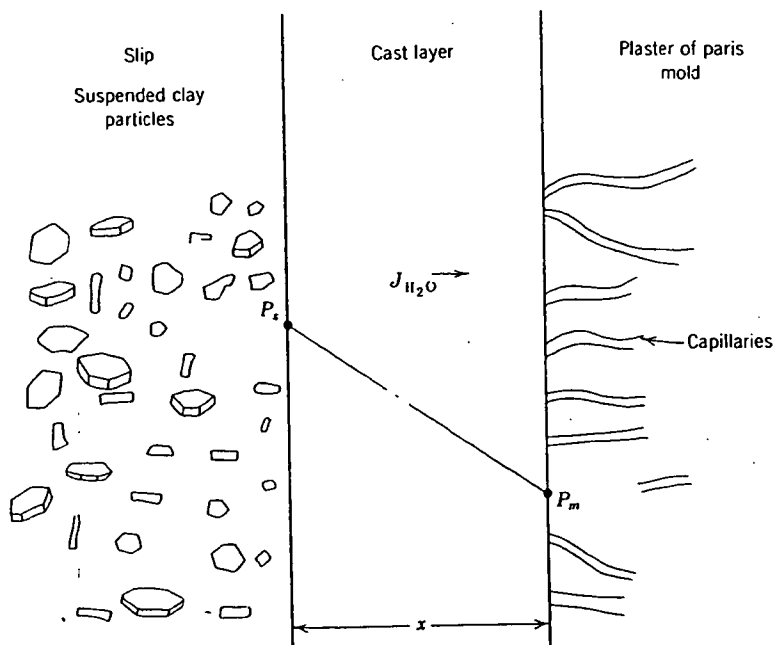


Fig. 9.2. Schematic representation of the formation of a slip-cast layer formed by the extraction of water by capillary action of a plaster of paris mold.

transport of water out of the slip and into the capillaries; the rate-limiting step is the flow of water through the compact clay layer. As the layer thickness increases, the overall rate of material transport decreases because of the increased permeation distance (similar to gas permeation through glasses, discussed in Chapter 6).

We begin by writing the flux equation for water,

$$J = -K \frac{dP}{dx} \quad (9.6)$$

where we assume a planar deposit (unidirectional flow) and that the water flux J_{H_2O} is proportional to the pressure gradient resulting from the capillaries of the plaster mold. The permeation coefficient K depends on the clay particle size, particle packing, and the viscosity of water and is temperature-sensitive. The water pressure in the slip, P_s , is 1 atm; in the mold, P_m , it is determined by capillarity, $\Delta P = P_s - P_m \approx 2\gamma/r$ (Chapter 5). The surface tension is a function of the deflocculating agents used. Until the capillaries become filled with water, ΔP is approximately constant, and the flux can be related to the change of the layer thickness dx/dt ,

$$J = \left(\frac{1}{\kappa\rho} \right) \frac{dx}{dt} = -K \frac{dP}{dx} = -K \frac{\Delta P}{x} \approx -K \frac{2\gamma}{rx} \quad (9.7)$$

where ρ is the density of the cast layer and κ is a factor for converting the volume of water removed to the volume of clay particles deposited. Integration of Eq. 9.7 gives

$$x = \left(2K\rho\kappa \frac{2\gamma}{r} \right)^{1/2} t^{1/2}$$

or in the general parabolic form

$$x = (K' t)^{1/2} \quad (9.8)$$

That is, the wall thickness of a planar casting should increase with the square root of time (Fig. 9.3).

This parabolic rate law is commonly observed for kinetic processes in which the limiting step is mass transport through a reaction layer.

Interdiffusion between Solids. In Section 6.3, we discussed the chemical diffusion coefficient and its formulation in terms of the tracer diffusion coefficients for the case of interdiffusion. If we measure the rate at which two ceramics interdiffuse, this too can be considered the formation of a reaction product which is a solid solution rather than a distinct or separate phase. Let us consider the interdiffusion between crystals of NiO and CoO at a high temperature. The solid solution that forms is nearly ideal;

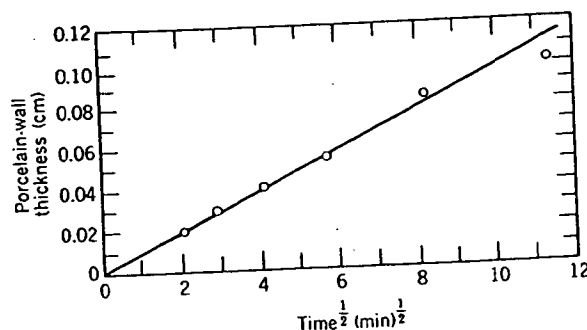


Fig. 9.3. Parabolic dependence of the slip-casting rate of a porcelain slip in a plaster of paris mold.

thus the chemical potential is related directly to the composition (concentration) by $\mu_i = \mu_i^\circ + RT \ln \gamma_i$ where the activity coefficient γ is equal to one. Thus Eq. 6.41 becomes

$$\bar{D} = [D_1^* X_2 + D_2^* X_1] \left(1 + \frac{d \ln \gamma_1}{d \ln X_1} \right) = D_{Co}^* X_{Co} + D_{Ni}^* (1 - X_{Co}) \quad (9.9)$$

This is the familiar Darken equation and assumes local equilibrium everywhere in the interdiffusion zone and is not strictly valid in ceramics. As will be seen later, ambipolar coupling will decrease the value of \bar{D} through electrochemical fields which arise if one charged specie moves faster than another.

The measured interdiffusion data for the CoO-NiO system are shown in Fig. 9.4a. The curves on the plot were calculated from the tracer diffusivities (Fig. 9.4b) and Eq. 9.9, assuming ideal solution behavior. In the case of interdiffusion of NiO-MgO, Eq. 9.9 is not directly applicable because the tracer diffusivities are a function of the nickel concentration. The experimental interdiffusion coefficient (Fig. 9.5a) has an exponential dependence on the concentration of nickel. Trivalent nickel ions and cation vacancies become associated (see Sections 4.7 and 6.4) and increase the transport rate of nickel into MgO. The measurements were made in air, so that there is sufficient trivalent nickel to dominate the cation vacancy formation process. That is, most of the vacancies arise from the presence of Ni_{Ni}^{3+} . As discussed in Sections 4.7 and 6.4, a significant fraction of the trivalent nickel ions and cation vacancies are coupled by association. Data for some other systems are shown in Fig. 9.5b.

Next let us consider a reaction in which a compound is formed as the reaction layer, for example, the formation of nickel aluminate spinel ($NiAl_2O_4$) from NiO and Al_2O_3 . There are many possible reaction paths; five are shown schematically in Fig. 9.6. The rate of spinel formation

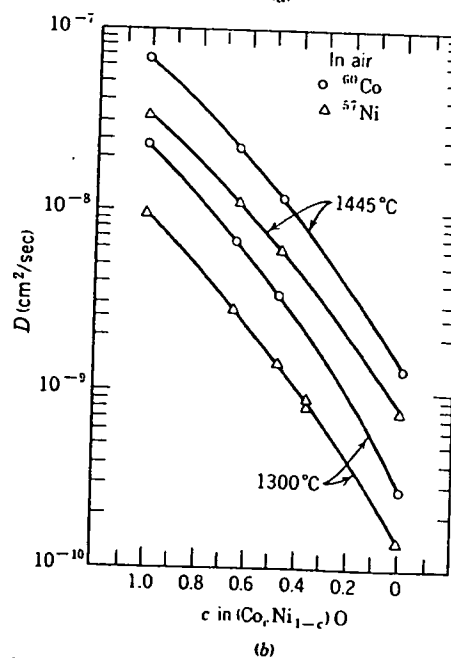
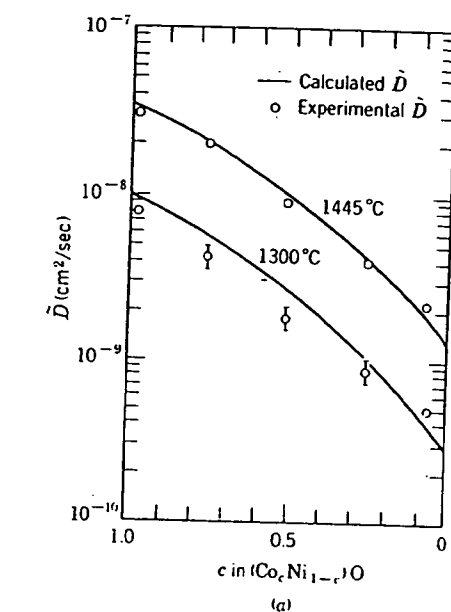
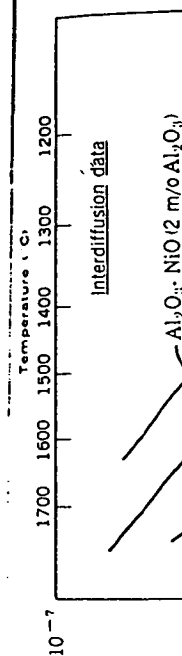


Fig. 9.4. (a) Comparison of the calculated interdiffusion coefficients \bar{D} and experimental values at 1445 and 1300°C in air. (b) Tracer diffusion coefficients of ^{60}Co and ^{57}Ni in $(\text{Co}_x\text{Ni}_{1-x})\text{O}$ crystals at 1445 and 1300°C in air. Plotted as $\log D$ versus c . From W. K. Chen and N. L. Petersen, *J. Phys. Chem. Soc.*, **34**, 1093 (1973).



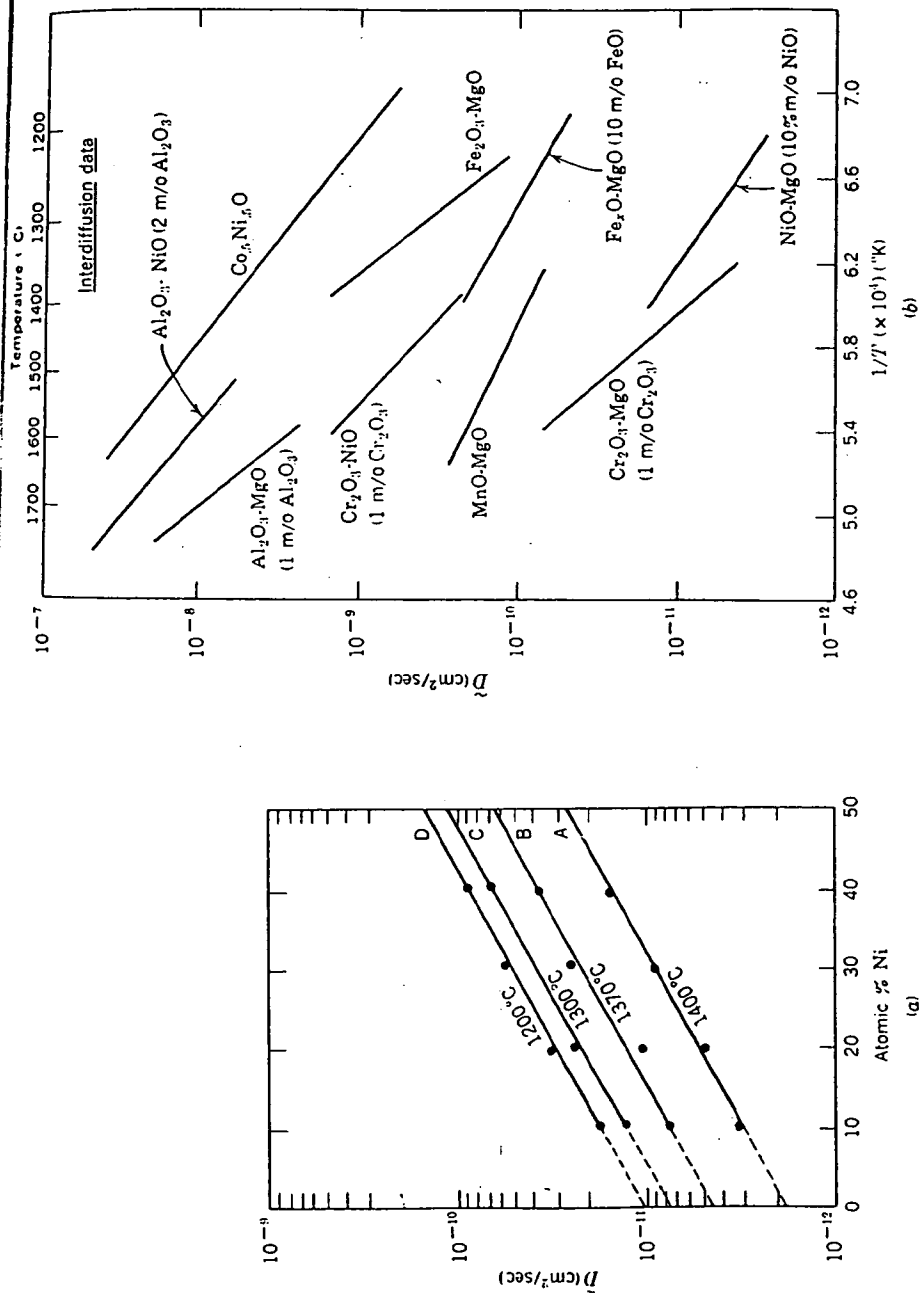
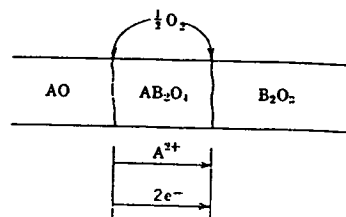
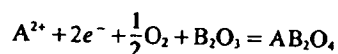
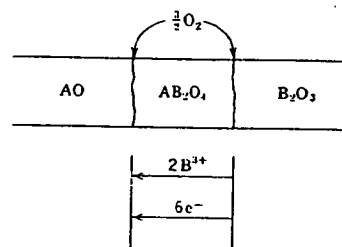
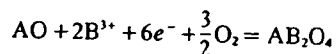


Fig. 9.5. (a) Diffusivity versus nickel concentration at several temperatures in the NiO-MgO system in air. From S. L. Blank and J. A. Pask, *J. Am. Ceram. Soc.*, 52, 669 (1969). (b) Interdiffusion coefficients in several oxides for specific compositions.

Reaction occurs at $AB_2O_4-B_2O_3$ interface:
oxygen gas phase transport with A^{2+} ion and
electron transport through AB_2O_4 :



Reaction occurs at $AO-AB_2O_4$ interface:
oxygen gas phase transport with B^{3+} ion and
electron transport through AB_2O_4 :

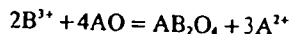


Oxygen and cation transport through AB_2O_4 :

- (1) Both cations diffuse ($J_{B^{3+}} = \frac{2}{3}J_{A^{2+}}$).

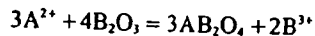
Reactions occur at

$AO-AB_2O_4$ interface



and at

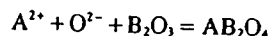
$AB_2O_4-B_2O_3$ interface



- (2) A^{2+} and O^{2-} diffuse.

Reaction at

$AB_2O_4-B_2O_3$ interface



- (3) B^{3+} and O^{2-} diffuse.

Reaction at

$AO-AB_2O_4$ interface

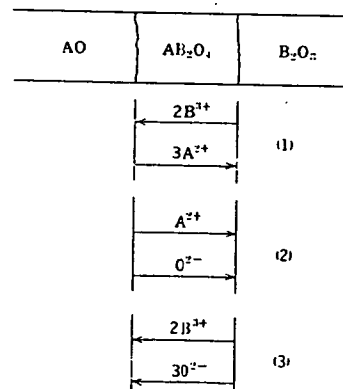
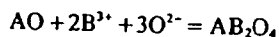


Fig. 9.6. Schematic representation of several mechanisms which may control the rate of AB_2O_4 (e.g., spinel) formation. From Ref. 1.

might
the tr
interf
Wh
throu
9.8), i
Figur
two c
plana
when
sed i

might be controlled by the diffusion of A^{2+} ions; B^{3+} ions or O^{2-} ions, by the transport of electrons (holes), by the transport of O_2 gas, or by the interface reactions at $AO-AB_2O_4$ or $AB_2O_4-B_2O_3$.

When the rate of reaction-product formation is controlled by diffusion through the planar product layer, the parabolic rate law is observed (Eq. 9.8), in which the diffusion coefficient is that for the rate-limiting process. Figure 9.7 shows the parabolic time dependence for $NiAl_2O_4$ formation at two different temperatures, and Fig. 9.8 is a photomicrograph of the planar spinel reaction product on Al_2O_3 . (More complex situations arise when several phases are formed as reaction products. These are discussed in reference 1 and by C. Wagner.*)

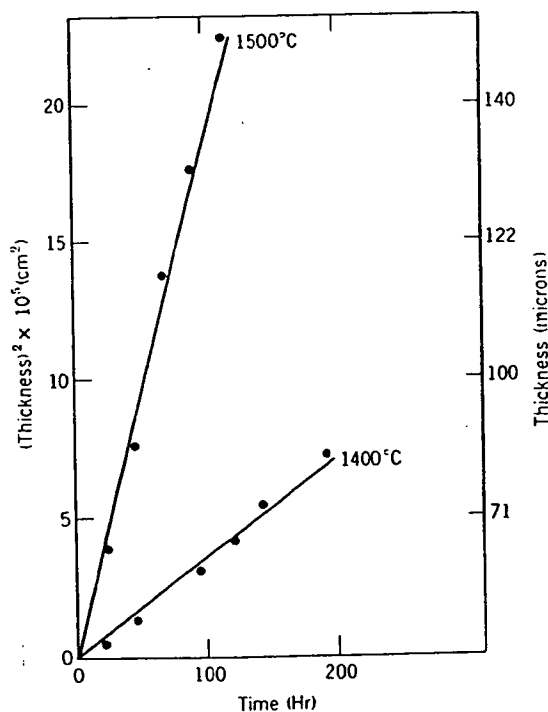


Fig. 9.7. Thickness of $NiAl_2O_4$ formed in $NiO-Al_2O_3$ couples as a function of time for couples heated in argon at 1400 and 1500°C. From F. S. Pettit et al., *J. Am. Ceram. Soc.*, **49**, 199 (1966).

The Electrochemical Potential in Ionic Solids. When considering point defects (Chapter 4) and atom mobility (Chapter 6), we noted that a

Acta Met.*, **17, 99 (1969).

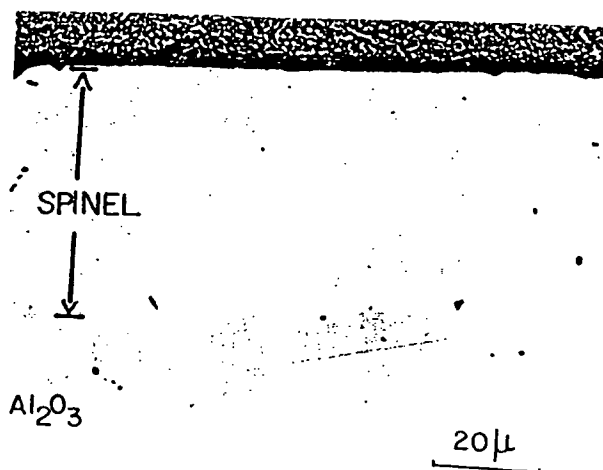


Fig. 9.8. Cross-sectional view of a typical NiAl_2O_4 layer formed in an $\text{NiO}-\text{Al}_2\text{O}_3$ couple after 73 hr at 1400°C . From F. S. Pettit, et al., *J. Am. Ceram. Soc.*, 49, 199 (1966).

distinguishing feature of ionic crystals is the effective charge that an atomic specie may have within the crystal lattice. When there is mass transport in a ceramic, the transport of one charged specie is usually coupled to the transport of an ion or defect of the opposite charge. We must therefore consider the electrochemical potential as the motivating force for mass transport rather than just the chemical potential or concentration gradient. The electrochemical potential of the i th specie η_i is the sum of the chemical potential μ_i and the electrical potential ϕ acting on it:

$$\eta_i = \mu_i + Z_i F \phi \quad (9.10)$$

where Z_i is the effective charge and F is the Faraday constant. We have already noted in Table 6.1 the interrelationship between the mobilities expressed in terms of electrical and chemical driving forces. The flux due to an electrochemical potential gradient is thus given by

$$j_i = c_i v_i = -c_i B_i \frac{\partial \eta_i}{\partial x} = -c_i B_i \left[\frac{\partial \mu_i}{\partial x} + Z_i F \frac{\partial \phi}{\partial x} \right] \quad (9.11)$$

Examination of the two gradient terms in this equation shows the importance of the ionic nature of ceramics. For example, a concentration gradient (chemical-potential gradient) in one direction may be offset by an electrical-field gradient that motivates the ion in the opposite direction. Another kind of effect results from the local electrical field between oppositely charged species. For example, the cations in most close-

packed oxide
NiO-CoO
case in which
coefficients
ions in aluminum
motion of
(9.11) are

Oxidation
law in which
reaction products
metals. They
begin with
results extremely
coherent or
 P_{O_2} and then
determined
of the oxide

The oxygen
layer (Fig.
the metal-oxide
metal ion is
the oxygen
also a net
determines
cations and
and then
determining

The flux
changed to

packed oxides diffuse more rapidly than oxygen, as for the NiO-MgO and NiO-CoO interdiffusion already discussed. If this begins to happen in the case in which there is a net mass flow (not for the case of diffusion coefficient measurements using radioactive tracers), for example, Al^{3+} ions in alumina, a net electrical field results and thereby couples the motion of Al^{3+} ions and O^{2-} ions. Several solid reactions based on Eq. (9.11) are now considered.

Oxidation of a Metal. The most extensive studies of the parabolic rate law in which the process is controlled by diffusive transport through the reaction product are investigations into the formation of oxide layers on metals. The analysis techniques were developed by Carl Wagner which begin with Eq. (9.11). They are described here in some detail because the results extend to many ceramic problems. Consider the formation of a coherent oxide layer on a metal where the ambient oxygen pressure is $P_{\text{O}_2}^*$ and the effective oxygen pressure at the oxide-metal interface $P_{\text{O}_2}^i$ is determined by the temperature and the standard free energy of formation of the oxidation reaction (see Fig. 9.9):



The oxygen concentration gradient (chemical potential) across the oxide layer (Fig. 9.10) provides the driving force for oxygen diffusion towards the metal-oxide interface. A gradient of the chemical potential of the metal ion in the opposite direction produces metal-ion diffusion toward the oxygen atmosphere. If one atomic flux is larger than the other, there is also a net flux of electrons or electron holes. The net transport, which determines the rate of oxide growth, is the sum of flux of anions and cations and electrons or holes. First we must consider each of these fluxes and then we shall look for circumstances when one specie is rate-determining and the complex relationships reduce to more simple forms.

The flux of the atomic and electronic species given by Eq. 9.11 can be changed to the flux of charged particles by multiplying by the valence:

$$J_{\text{O}} = -|Z_{\text{O}}|c_{\text{O}}B_{\text{O}}\frac{\partial\eta_{\text{O}}}{\partial x} = |Z_{\text{O}}|j_{\text{O}}$$

$$J_{\text{Me}} = -|Z_{\text{Me}}|c_{\text{Me}}B_{\text{Me}}\frac{\partial\eta_{\text{Me}}}{\partial x} = |Z_{\text{Me}}|j_{\text{Me}} \quad (9.13)$$

$$J_{\text{e}} = -nB_{\text{e}}\frac{\partial\eta_{\text{e}}}{\partial x} = |-1|j_{\text{e}}$$

$$J_{\text{h}} = -pB_{\text{h}}\frac{\partial\eta_{\text{h}}}{\partial x} = |+1|j_{\text{h}}$$

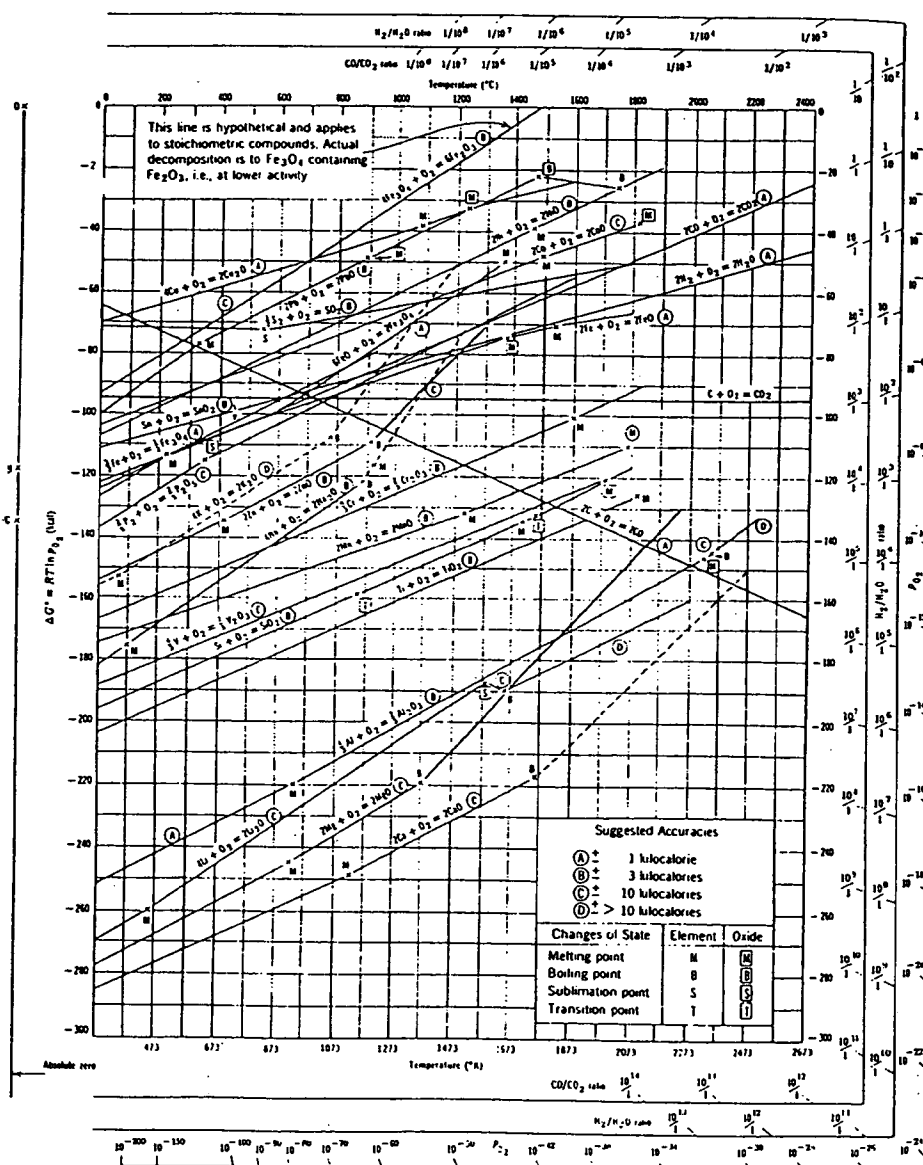


Fig. 9.9. Standard free energy of formation of oxides as a function of temperature. From F. D. Richardson and J. H. E. Jeffes, *J. Iron Steel Inst.*, 160, 261 (1948); modified by L. S. Darken and R. W. Gurry, *Physical Chemistry of Metals*, McGraw-Hill Book Company, New York, 1953.

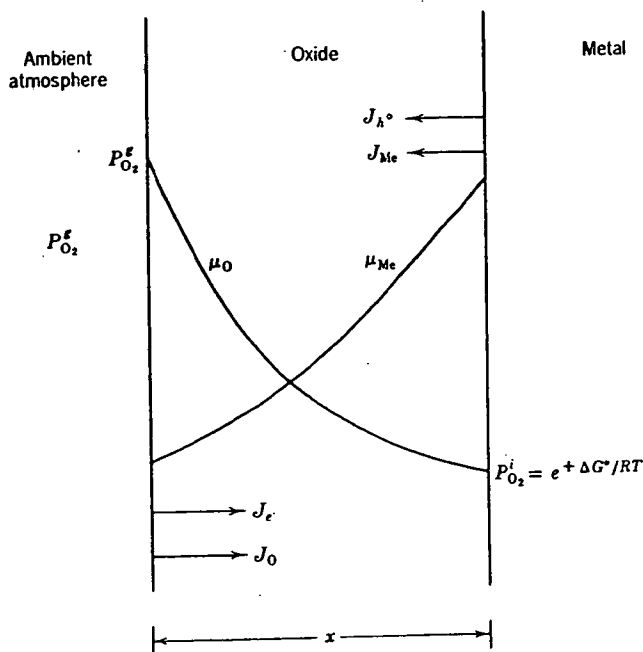


Fig. 9.10. Chemical-potential gradients across an oxide layer on a metal.

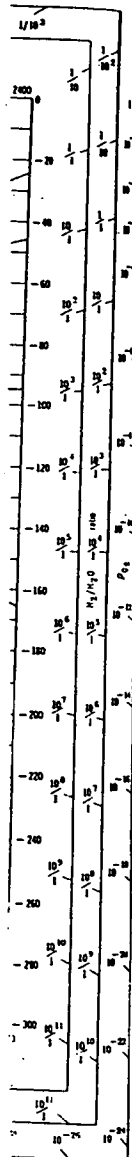
For a given oxide layer, either electrons or holes are predominant, so that only one of the last two equations is necessary. The constraint on the net flux is electrical neutrality. If we assume electrons to be the important electronic defect, this constraint requires that

$$J_O + J_{e^-} = J_{Me} \quad (9.14)$$

The net flux and therefore the rate of oxidation is the sum $J_{ox} = |J_O| + |J_{Me}|$. The general result can be expressed in terms of the conductivity σ and the transference number t_i (see also Chapter 17), which represents the fraction of the total charge flux carried by a particular specie;

$$\begin{aligned} J_{ox} &= \frac{\sigma t_{e^-}}{|Z_{Me}|F^2} (t_O + t_{Me}) \left| \frac{\partial \mu_{Me}}{\partial x} \right| \\ &= \frac{\sigma t_{e^-}}{|Z_O|F^2} (t_O + t_{Me}) \left| \frac{\partial \mu_O}{\partial x} \right| \end{aligned} \quad (9.15)$$

Although the composition varies through the layer, average values can be assumed for t_i and σ to simplify the result, which yields a form of the



from F.
Darken
New York,

parabolic rate law;

$$\frac{dx}{dt} = \frac{1}{x} \left[\frac{\bar{\sigma} \bar{t}_e}{|Z_{Mc}| F^2} (\bar{t}_0 + \bar{t}_{Mc}) |\Delta \mu_{Mc}| \right] = \frac{K}{x} \quad (9.16)$$

Recalling that,

$$t_i \sigma = \sigma_i = e Z_i c_i \mu_i = \frac{c_i Z_i^2 e^2 F^2}{RT} D_i \quad (9.17)$$

we can see that the oxidation rate is governed by the atomic mobilities or diffusivities. Let us now consider specific rate limiting cases:

1. The electrical current is carried primarily by electronic defects, $t_e \approx 1$ or $t_h \approx 1$:

a. If $D_0 \gg D_{Mc}$, then

$$K = \frac{\bar{\sigma} \bar{t}_0}{|Z_{Mc}| F^2} |\Delta \mu_{Mc}| \quad (9.18)$$

which for an oxide for predominant $V_o^{\cdot\cdot}$ defects reduces to the approximation

$$K \approx \frac{c_0}{2|Z_{Mc}|} \int_{\mu_0}^{\mu_0^*} D_0 d\mu_0 \quad (9.19)$$

since $\mu_0 = 1/2 \mu_{O_2} = 1/2 (\mu_{O_2}^0 + RT \ln P_{O_2})$. If we assume that $[V_o^{\cdot\cdot}] \propto P_{O_2}^{-1/6}$, as discussed in Chapter 6, and that the diffusion coefficient varies similarly;

$$D_0 = [V_o^{\cdot\cdot}] D_{V_o^{\cdot\cdot}} = \frac{(K_{V_o^{\cdot\cdot}})^{1/3}}{4^{1/3}} D_{V_o^{\cdot\cdot}} P_{O_2}^{-1/6} \quad (9.20)$$

and the rate constant becomes

$$K \approx \frac{3c_0}{4^{1/3}|Z_{Mc}|} (K_{V_o^{\cdot\cdot}})^{1/3} D_{V_o^{\cdot\cdot}} \{ (P_{O_2}^*)^{-1/6} - (P_{O_2}^i)^{-1/6} \} \quad (9.21)$$

b. If $D_{Mc} \gg D_0$ and we assume singly charged metal vacancies V'_{Mc} , the rate constant is

$$K \approx 2(K_{V'_{Mc}})^{1/2} D_{V'_{Mc}} \{ (P_{O_2}^*)^{1/4} - (P_{O_2}^i)^{1/4} \} c_{Mc} \quad (9.22)$$

note that $D_{V'_{Mc}} [V'_{Mc}] = D_{Mc}$.

2. If the electrical current is carried primarily by the ions, $(t_0 + t_{Mc}) \approx 1$, the rate constant from Eq. 9.16 becomes

$$K \approx \frac{kT}{8|Z_{Mc}| e^2} \int_{P_{O_2}^i}^{P_{O_2}^*} \sigma_{e,i} d \ln P_{O_2} \quad (9.23)$$

where $\sigma_{e,i}$ is the conduction due to electrons and holes which have mobilities μ_e and μ_h , respectively (see Table 6.1 $\mu_i = B''$).

$$\sigma_{e1} = en\mu_e + ep\mu_h \quad (9.24)$$

If we assume that the defect concentration does not have a large variation over the oxide layer

$$K \approx \frac{\sigma_{e1} kT}{8|Z_{Mc}|e^2} [\ln P_{O_2}^s - \ln P_{O_2}^i] \quad (9.25)$$

An example of the applicability of this relationship is the diffusive transport of oxygen through calcia-stabilized zirconia. The oxygen diffusion coefficient plotted in Fig. 6.11 is very large and accounts for $t_0 \approx 1$. Thus, the slower-moving specie, the electron hole, becomes rate-limiting for oxygen permeation (Eq. 9.25), as shown in Fig. 9.11.

3. If the metal undergoing oxidation has an impurity with a different oxidation state, for example, Li in Ni, the defect concentration in the oxide may be determined by the impurity concentration. As an example, consider the analogous case to Eq. 9.22 for which $D_{Mc} \gg D_0$ but where $[V'_{Mc}] = [F'_{Mc}]$. The thickness of this extrinsic layer is again determined by the parabolic rate law, Eq. 9.16, but with the reaction constant,

$$K_{ex} = 2D_{V'_{Mc}} [V'_{Mc}] [\ln P_{O_2}^s - \ln P_{O_2}^i] c_{Mc} \quad (9.26)$$

If the impurity concentration and oxygen pressure are such that the defect concentrations are in an intermediate range, an intrinsic layer may

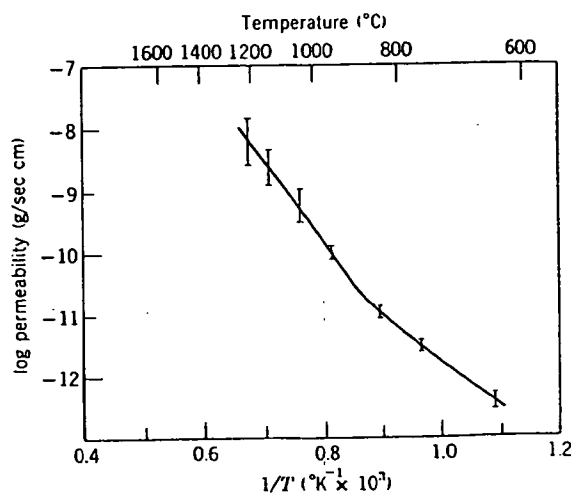


Fig. 9.11. Oxygen permeation through calcia-stabilized zirconia as a function of temperature. The oxygen transport is controlled by the concentration and mobility of electron holes, Eq. 9.25. From K. Kitazawa, Ph.D. thesis, MIT, 1972.

form on the oxygen-rich side (external) and an extrinsic oxide layer on the metal-rich side (at the oxide-metal interface).

Short-Circuit Diffusion Paths. In each of the examples of metal oxidation, lattice diffusion D_l was assumed to be the rate-determining transport process. In Section 6.6 the importance of other more rapid diffusion paths was discussed. The effects of short-circuit paths can be incorporated into the parabolic rate equations. For example, an apparent diffusivity D_a from Eq. 6.67 can be used in Eq. 9.16 to include the contributions from lattice D_l and boundary diffusion D_b ;

$$D_a = D_l(1 - f) + fD_b$$

$$\frac{dx}{dt} = \frac{K' D_a}{x} \quad (9.27)$$

where the diffusion coefficient has been extracted from the rate constant to give another constant K' . Low-temperature oxidation and oxide layers with fine grain sizes are expected to form by boundary diffusion.

Chemical Diffusion in Nonstoichiometric Oxides. The chemical diffusion coefficient for the counter diffusion of cations and anions can also be determined from the Wagner analysis. If we assume that electrical conduction is mainly electronic ($t_{el} \approx 1$) that is, movement of electrical charge is not the rate-limiting step for mass transport (ions), the chemical diffusion coefficient \bar{D} can be determined. In terms of diffusion coefficients rather than transference numbers Eq. 9.15 becomes

$$J_{ox} = \frac{c_o}{[Z_{Mc}]} (|Z_{Mc}|D_o + |Z_o|D_{Mc}) \frac{1}{kT} \frac{d\mu_o}{dx} \quad (9.28)$$

In terms of Fick's first law this can be rewritten

$$J_{ox} = \left[(|Z_{Mc}|D_o + |Z_o|D_{Mc}) \frac{c_o}{[Z_{Mc}]} \left(\frac{1}{kT} \frac{d\mu_o}{d\bar{c}} \right) \right] \frac{d\bar{c}}{dx} = \bar{D} \frac{d\bar{c}}{dx} \quad (9.29)$$

where \bar{c} represents the excess (or deficit) of the metal or oxygen in the nonstoichiometric compound. The chemical diffusion coefficient is the bracketed term. Consider, for example, the transition metal monoxides ($\text{Fe}_{1-\delta}\text{O}$, $\text{Ni}_{1-\delta}\text{O}$, $\text{Co}_{1-\delta}\text{O}$...) for which $\bar{c} \propto [V_{Mc}^{\alpha\cdot}]$, where α is the effective charge on the vacancy and where $D_{Mc} \gg D_o$. The chemical diffusion coefficient can be written from Eq. 9.29 in the form

$$\bar{D} = \frac{1}{2} \frac{c_{Mc}}{[V_{Mc}^{\alpha\cdot}]} D_{Mc} \frac{d \ln P_{O_2}}{d \ln [V_{Mc}^{\alpha\cdot}]} \quad (9.30)$$

for which the substitution $d\mu_o = 1/2 kT d \ln P_{O_2}$ has been made. From the defect equilibrium reaction, the mass action law gives

$$[h^{\cdot}]^{\alpha} [V_{Mc}^{\alpha\cdot}] = K_{V_{Mc}} \cdot P_{O_2}^{1/2} \quad (9.31)$$

The

Sub:
cherThu
vac:If
O/M
oxic
type
the
in F
conFig
sev
(19)

The derivative in Eq. 9.30 can now be determined;

$$\frac{d \ln P_{O_2}}{d \ln [V_{Me}^{\alpha}]} = 2(\alpha + 1) \quad (9.32)$$

Substituting this into Eq. 9.30 and recalling that $c_{Me}D_{Me} = c_V D_V$, the chemical diffusion coefficient is given by

$$\tilde{D} = (\alpha + 1)D_{V_{Me}} \quad (9.33)$$

Thus for singly charged vacancies, $\tilde{D} = 2D_{V_{Me}}$, and for doubly charged vacancies, $\tilde{D} = D_{V_{Me}}$.

If the oxygen pressure is changed from one value to another, a new O/Me value is established in a nonstoichiometric oxide, and the oxidation-reduction rate is determined by a diffusion coefficient of the type in Eq. 9.33. This value is larger than the diffusivity of the cation or the anion. Figure 9.12 shows the chemical diffusion coefficient determined in $Fe_{1-x}O$ by step changes in the oxygen pressure which cause diffusion-controlled changes in the composition. The value of the chemical diffu-

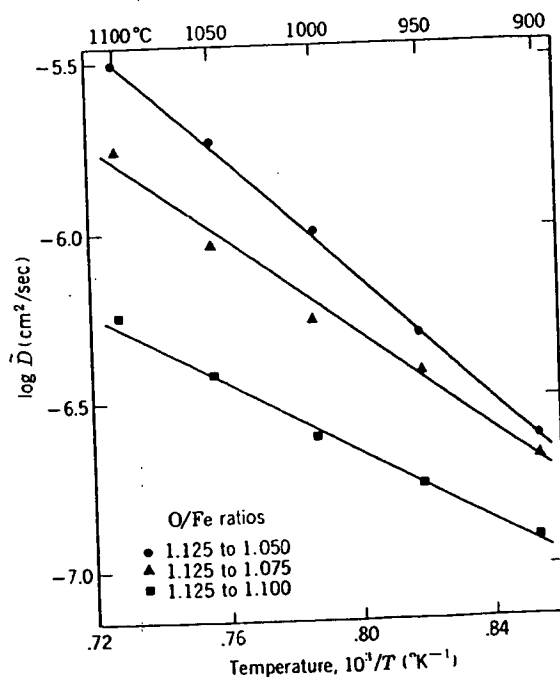


Fig. 9.12. Temperature dependence of the chemical-diffusion coefficient of wustite for several composition increments. From R. L. Levin and J. B. Wagner, *Trans. AIME*, 233, 159 (1965).

sion coefficient correlates with the tracer value (Eq. 9.30) when the defect equilibrium relationships are known.

Ambipolar Diffusion. The formality used to derive Eqs. 9.11 and 9.13 also allows us to determine the effective diffusion constants when cations and anions are flowing in the same direction. Referred to as ambipolar diffusion, a description of the atomistic process must again consider the coupling between the oppositely charged species when the transport of electrons and holes is slower than ion transport. If the flux of cations becomes excessive, a local internal electric field builds up to "drag" along the anions. This behavior is important in processes involving reactions which cause product formation, in processes which are in response to an applied electric field, and in processes which result in a shape change due to mechanical or surface tension forces such as sintering and creep.

As an example, consider a pure oxide for which $t_{el} \approx 0$. Equation 9.11 can be written for anion and cation transport as in Eq. 9.13. Since the transport of each ion is in the same direction, electrical neutrality is maintained when

$$J_T = \frac{J_0}{|Z_{Mc}|} = \frac{J_{Mc}}{|Z_0|} \quad (9.34)$$

where J_T refers to the total molecular flux. Equating the anion and cation charge flux allows for the solution of the internal electric field, $\partial\phi/\partial x$,

$$|Z_0|c_0B_0 \left[\frac{\partial\mu_0}{\partial x} + Z_0F \frac{\partial\phi}{\partial x} \right] = |Z_{Mc}|c_{Mc}B_{Mc} \left[\frac{\partial\mu_{Mc}}{\partial x} + Z_{Mc}F \frac{\partial\phi}{\partial x} \right] \quad (9.35)$$

in terms of the chemical potential of the oxide, $\mu(\text{Me}_{Z_0}\text{O}_{Z_{Mc}})$. The chemical potential of the oxide is the sum of the chemical potentials of cations and anions,

$$d\mu(\text{Me}_{Z_0}\text{O}_{Z_{Mc}}) = Z_{Mc} d\mu_0 + Z_0 d\mu_{Mc} \quad (9.36)$$

which yields the coupling field in terms of mobilities, concentrations, and the chemical potential,

$$\frac{\partial\phi}{\partial x} = \frac{[|Z_0|c_0B_0 - |Z_{Mc}|c_{Mc}B_{Mc}]}{F[|Z_{Mc}|Z_{Mc}|c_{Mc}B_{Mc} - |Z_0|Z_0|c_0B_0]} \frac{\partial\mu_{Mc}}{\partial x} \quad (9.37)$$

where we have assumed local equilibrium, $|Z_{Mc}| dc_{Mc} = |Z_0| dc_0$. Substitution of Eq. 9.37 into Eqs. 9.34 and 9.13 yields

$$J_T = \frac{-c_{Mc}B_{Mc}c_0B_0}{Z_{Mc}|Z_{Mc}|c_{Mc}B_{Mc} - |Z_0|Z_0|c_0B_0} \frac{\partial\mu(\text{Me}_{Z_0}\text{O}_{Z_{Mc}})}{\partial x} \quad (9.38)$$

This term is the correction due to ambipolar effects to the diffusion transport resulting from a chemical potential gradient. Consider as an

example of the applicability of Eq. 9.38 to sintering of pure MgO for which the values of $Z_{Mg} = |Z_0| = 2$ and $c_{Mg} = c_0 = c$:

$$J_T = -\frac{cB_{Mg}B_0}{[B_{Mg} + B_0]} \frac{\partial \mu_{MgO}}{\partial x} \quad (9.39)$$

Since $\mu_{Mg} = \mu_{Mg}^0 + RT \ln a \approx \mu_{Mg}^0 + RT \ln c$, Eq. (9.39) can be expressed as

$$J_T = -\frac{c_{MgO}B_{Mg}B_0RT}{[B_{Mg} + B_0]} \frac{d \ln c_{MgO}}{dx} = -\frac{B_{Mg}B_0RT}{[B_{Mg} + B_0]} \frac{dc_{MgO}}{dx} \quad (9.40)$$

where $\frac{dc_{MgO}}{dx}$ is the concentration gradient due to curvature (Chapter 10).

Recalling that the tracer diffusion coefficient and mobility are related by Eq. (6.11),

$$J_T \approx -\frac{D_{Mg}^T D_0^T}{[D_{Mg}^T + D_0^T]} \frac{dc_{MgO}}{dx} \quad (9.41)$$

Thus the total molecular transport may be governed by the slowest-moving specie if there is a large difference in diffusivities (e.g., $D_{Mg} \gg D_0$; $J_T \propto D_0$) or by an intermediate value when they are not too dissimilar (e.g., $D_{Mg} = 3D_0$; $J_T \propto D_{Mg}/4$).

Since some ions transport more rapidly in boundaries or along dislocations, a relationship for ambipolar diffusion can be derived when paths other than the lattice are assumed. A simple case has been derived for steady-state grain boundary and lattice transport.* The effective area of transport in the lattice A^l and boundary A^b must be incorporated in the equation for total mass flow. For the case of a pure material MO the effective diffusion coefficient is similar in form to Eq. 9.41 and given by

$$D_{\text{effective}} \approx \frac{(A^l D_{Mc}^l + A^b D_{Mc}^b)(A^l D_0^l + A^b D_0^b)}{(A^l D_{Mc}^l + A^b D_{Mc}^b) + (A^l D_0^l + A^b D_0^b)} \quad (9.42)$$

where D^l refers to lattice diffusion and D^b refers to boundary diffusion. In many oxides, it has been observed that $A^b D_0^b \gg A^l D_0^l$ and that $A^l D_{Mc}^l > A^b D_{Mc}^b$; thus Eq. 9.42 reduces to

$$D_{\text{effective}} \approx \frac{A^l D_{Mc}^l A^b D_0^b}{A^l D_{Mc}^l + A^b D_0^b} \quad (9.43)$$

Diffusive transport in real materials is more complex, owing to impurities and imperfections, but relationships like these can be derived to include more complex situations.†

*R. S. Gordon, *J. Am. Ceram. Soc.*, 56, 147 (1973).

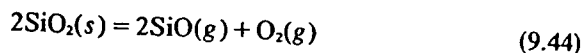
†D. W. Readey, *J. Am. Ceram. Soc.*, 49, 366 (1966).

9.3 Reactant Transport through a Fluid Phase

As discussed in Section 9.1, heterogeneous reactions at high temperatures require, first, material transfer to the reaction interface, second, reaction at the phase boundary, and in some cases diffusion of products away from the reaction site. Any of these steps can have the lowest virtual reaction rate and be rate-controlling for the overall process. Generally, once a reaction is initiated, material-transfer phenomena determine the overall rate in the high-temperature systems of importance in ceramics. As discussed in the previous section, the diffusion of ions and electrons through a stable oxide film on the surface of a metal determines the reaction rate. If, however, the film forms with cracks and fissures, the rate may be determined by gaseous diffusion through these channels. In this section we wish to consider several important examples of the way ceramic materials interact with gases and liquids and to determine the rate-limiting kinetic equations.

Gas-Solid Reactions: Vaporization. The simplest kind of solid-gas reactions are those related to vaporization or thermal decomposition of the solid. Section 9.4 contains a discussion of the decomposition of a solid to a gas and another solid; in this section we are primarily concerned with reactions in which the solid forms only gaseous products. The rate of decomposition is dependent on the thermodynamic driving forces, on the surface-reaction kinetics, on the condition of the reaction surface, and on the ambient atmosphere; for example, at high temperatures oxides volatilize much more rapidly in a vacuum than in air.

The loss of silica from glass and refractories in reducing atmospheres is an important factor which limits the usefulness of these ceramic products. Consider the following reaction which can cause the volatilization of SiO_2 :



At 1320°C , the equilibrium constant is

$$K_{eq} = \frac{P_{\text{SiO}}^2 P_{\text{O}_2}}{a_{\text{SiO}_2}^2} = 10^{-25} \quad (9.45)$$

Assuming unit activity for the silica, it is apparent that the ambient oxygen partial pressure controls the pressure of $\text{SiO}(g)$ and therefore the rate of vaporization. Under reducing conditions (inert atmosphere, H_2 or CO atmosphere) of $P_{\text{O}_2} = 10^{-18}$ atm, the SiO pressure is 3×10^{-4} atm (0.23 torr).

The rate of evaporation near equilibrium is given by the Knudsen

equation:*

where $\frac{dn_i}{dt}$ is sample area, weight of i , a gas flow rate sample is no evaporation, be in equilib, total pressure

where A is
When the
mixtures P_{O_2}

where P_{O_2} is
tion reaction

For the va
rate of abou
actual SiO_2 k
in hydrogen.

The effect of
from Fig. 9.
decreased by

Chemical
active transp
vapor-phase
film electron
controlling tl
rate of depos
the temperat

*M. Knudsen

equation:*

$$\frac{dn_i}{dt} = \frac{AP_i\alpha_i}{\sqrt{2\pi M_i RT}} \quad (9.46)$$

where $\frac{dn_i}{dt}$ is the loss of component i in moles per unit time, A is the sample area, α_i is the evaporation coefficient ($\alpha_i \leq 1$), M_i is the molecular weight of i , and P_i is the pressure of i above the sample. If there is a high gas flow rate over the sample or if the evaporation is into a vacuum, the sample is not able to maintain its equilibrium vapor pressure P_i , and the evaporation rate is controlled by the interface reaction rate. For the gas to be in equilibrium with the solid, the gas flow rate S (moles/sec) and the total pressure P^T (atm) must satisfy the inequality

$$\frac{A\alpha_i P^T}{S(M_i T)^{1/2}} \gg 2.3 \times 10^{-9} \quad (9.47)$$

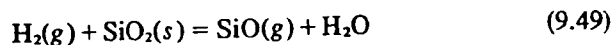
where A is in square centimeters and T in degrees Kelvin.

When the oxygen partial pressure in the gas phase is controlled by gas mixtures $P_{O_2}^{ext}$, the equation (9.46) becomes

$$J_{O_2} = \frac{(P_{O_2} - P_{O_2}^{ext})\alpha_{O_2}}{(2\pi M_{O_2} RT)^{1/2}} \quad (9.48)$$

where P_{O_2} is calculated from the standard free energy of the decomposition reaction (e.g. Eq. 9.45).

For the vaporization of SiO_2 by reaction (9.44), Eq. 9.46 predicts a loss rate of about 5×10^{-5} moles SiO_2/cm^2 sec at $1320^\circ C$. Figure 9.13 shows actual SiO_2 loss rates from various silica-containing refractories annealed in hydrogen. The overall decomposition reaction in this case is



The effect of a few mole percent water vapor in the gas stream is evident from Fig. 9.14. As predicted from Eq. 9.49, the $SiO(g)$ pressure is decreased by an increase in the $H_2O(g)$ pressure.

Chemical Vapor Transport. Next let us consider the reaction of an active transport gas with a ceramic. The net effect is to increase the vapor-phase transport. Some high-temperature ceramics and many thin-film electronic devices are prepared by chemical vapor deposition. By controlling the chemical potential (concentration) of reaction gases, the rate of deposition can be controlled. Generally the rate of deposition and the temperature of deposition determine the reaction kinetics and rates at

*M. Knudsen, *Ann. Phys.*, 47, 697 (1915).

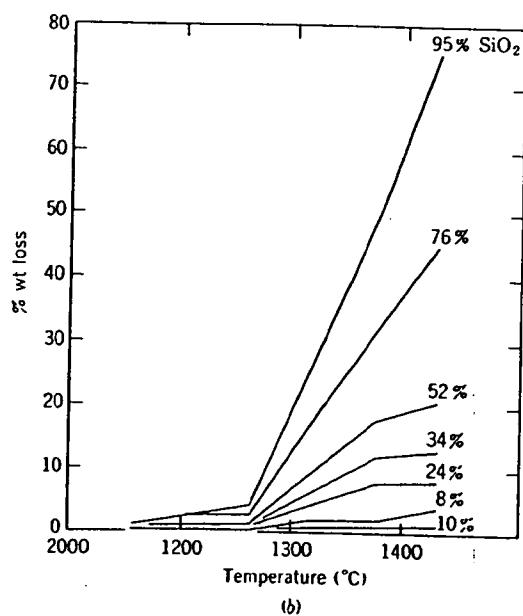
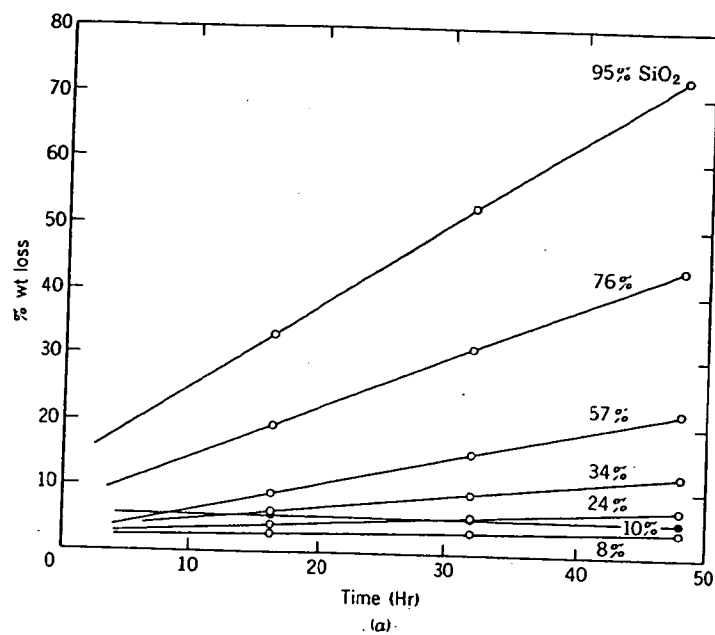


Fig. 9.13. (a) Weight loss of brick at 1425°C in 100% hydrogen. (b) Weight loss of brick after 50 hr in 100% hydrogen. From M. S. Crowley, *Bull. Am. Ceram. Soc.*, 46, 679 (1967).

Fig. 9.14
vapor wa

which
surface
tion oc
supers
a poly
porosit
material
temper
single-c
epitaxi
orienta

To u
a know
respect
reactan
nations
of the s
system
Consider
held at
chambe

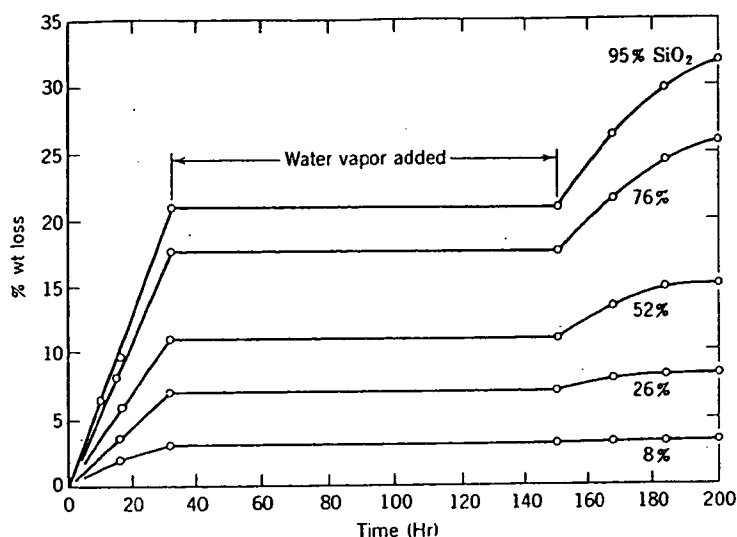


Fig. 9.14. Weight loss of brick at 1370°C in 75% H₂-25% N₂ atmosphere. After 32 hr water vapor was added for 150 hr. From M. S. Crowley, *Bull. Am. Ceram. Soc.*, 46, 679 (1967).

which the decomposition products can "crystallize" on the reaction surface. If the supersaturation is large, homogeneous gas-phase nucleation occurs; that is, a heterogeneous surface is not needed. As the supersaturation is reduced, the gases react in the vicinity of a surface, and a polycrystalline deposit is formed. The perfection of the deposit, porosity, preferred grain orientation, and so on, depend on the particular material and the rate of deposition; usually slower deposition and higher temperatures result in a more perfect reaction product. Finally, when a single-crystal substrate is used as the heterogeneous reaction surface, epitaxial deposition occurs. In the latter case, a single crystal with an orientation determined by the substrate is formed.

To understand the kinetics of chemical vapor deposition fully requires a knowledge of all of the thermodynamic equilibria involved and the respective kinetic processes for the generation of reactants, mixing of reactant gases, diffusion through the boundary layers, molecular combinations at the interface, exsolution of gaseous products, surface diffusion of the solid products, and so on. We have chosen, as an example, a simple system for which the rate-determining step is diffusion in the gas phase. Consider the closed system shown in Fig. 9.15 in which two chambers are held at thermal equilibrium. Assume that the chemical reactions in each chamber reach thermodynamic equilibrium such that the diffusion flux of

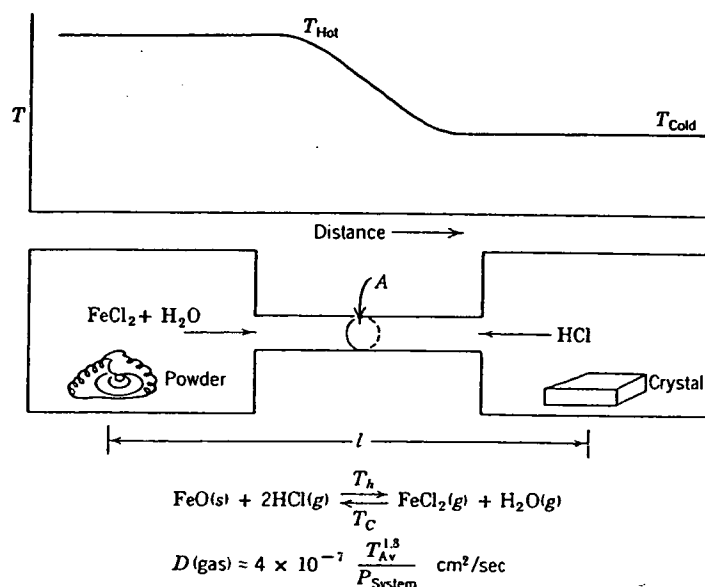


Fig. 9.15. Schematic diagram of chemical vapor transport of iron oxide in a temperature gradient.

matter is from the hot chamber to the cooler chamber because of the concentration gradient (the direction of transport is determined by the sign of the enthalpy of the reaction).

The kinetics of mass transport as determined by the diffusion of the rate-limiting specie—for example, diffusion of $\text{FeCl}_2(\text{g})$ —is given by Fick's law:

$$\frac{dn}{dt} = -AD \frac{\partial c}{\partial x} = -AD \frac{\Delta c}{l} = -AD \frac{(c_h - c_c)}{l} \quad (9.50)$$

where n is the number of moles transported, A the cross-sectional area of the connecting tube (cm^2), D the diffusion coefficient of the rate-limiting specie, and c the concentrations in the respective isothermal chambers. For an ideal gas

$$c_h = \frac{n_h}{V} = \frac{P_h}{RT_h} \quad (9.51)$$

and the composition difference is

$$(c_h - c_c) \approx \frac{(P_h - P_c)}{RT_{\text{av}}} \quad (9.52)$$

Thus, the t

The equilib
of formatic

In a clos
B atm re
formation
(9.54) redu

which car
prediction

In gener
total pres
gas-phase
line-of-sig
diffusion-l
pressures
convection
boundary

Liquid-
of the kin
in liquids,
by molter
componer
ceramic t
required f
rate of th
fixed by t
crystal gr
leads to a
away from
material
the liquid
natural c
For a s

Thus, the transport rate is determined by

$$\frac{dn}{dt} = -\frac{AD}{lRT_{av}}(P_h - P_c) \quad (9.53)$$

The equilibrium pressures can be determined by the standard free energy of formation at each temperature; for example, at the higher temperature

$$\Delta G_h^\circ = -RT_h \ln \frac{P_{\text{FeCl}_2} P_{\text{H}_2\text{O}}}{P_{\text{HCl}}^2 a_{\text{FeO}}} \quad (9.54)$$

In a closed system such as a quartz ampoule an initial HCl pressure of B atm results in the adjustment of the formation reaction by the formation of equivalent numbers of moles FeCl_2 and H_2O . The expression (9.54) reduces to

$$\Delta G_h^\circ = -RT_h \ln \frac{P_{\text{FeCl}_2}^2}{(B - 2P_{\text{FeCl}_2})^2} \quad (9.55)$$

which can be solved for each temperature and therefore leads to a prediction of the transport rate from Eq. 9.53.

In general, the rate-limiting gas-phase transport step is a function of the total pressure of the system. At very low pressures ($P_{\text{total}} < 10^{-4}$ atm) gas-phase molecular collisions are infrequent and thus transport becomes line-of-sight. At intermediate pressures ($10^{-4} < P_{\text{total}} < 10^{-1}$ atm), the diffusion-limited case discussed above becomes important. At higher pressures ($P_{\text{total}} > 10^{-1}$ atm) convective mass transport is more rapid. If convection or forced flow becomes rapid, gas-phase diffusion through the boundary layer may become the rate-determining process.

Liquid-Solid Reactions: Refractory Corrosion. An important example of the kinetics of liquid-solid reactions is the rate of dissolution of solids in liquids, particularly important in connection with refractory corrosion by molten slags and glasses, with the rate of conversion of solid batch components to glass in the glass-making process, and with the firing of a ceramic body in which a liquid phase develops. No nucleation step is required for the dissolution of a solid. One process that can determine the rate of the overall reaction is the phase-boundary reaction rate which is fixed by the movement of ions across the interface in a way equivalent to crystal growth (Section 8.4). However, reaction at the phase boundary leads to an increased concentration at the interface. Material must diffuse away from the interface in order for the reaction to continue. The rate of material transfer, the dissolution rate, is controlled by mass transport in the liquid which may fall into three regimes: (1) molecular diffusion, (2) natural convection, and (3) forced convection.

For a stationary specimen in an unstirred liquid or in a liquid with no

fluid flow produced by hydrodynamic instabilities, the rate of dissolution is governed by molecular diffusion. The kinetics are similar to those discussed in Chapter 6 on diffusion. The effective diffusion length over which mass is transported is proportional to \sqrt{Dt} , and therefore the change in thickness of the specimen, which is proportional to the mass dissolved, varies with $t^{1/2}$. Even in a system which may undergo convection due to hydrodynamic instabilities from density gradients which arise from thermal gradients or from concentration gradients (due to dissolution), the initial dissolution kinetics should be governed by molecular diffusion.

The diffusion coefficient for dissolution kinetics must be considered in the same light as in Section 9.2; the electrical and chemical effects of the various possible species must be accounted for. For example, the dissolution of Al_2O_3 in a silicate slag may be controlled by any of the cations or anions in the Al_2O_3 or slag or more probably a combination (e.g., Eq. 9.41). An example of dissolution controlled by molecular diffusion is shown in Fig. 9.16 for the dissolution of sapphire in a $\text{CaO-Al}_2\text{O}_3\text{-SiO}_2$ melt containing 21 wt% Al_2O_3 .

Natural or free convection occurs, owing to hydrodynamic instabilities in the liquid which give rise to fluid flow over the solid. This enhances the dissolution kinetics. It has often been observed in metals processing that the amount of dissolution is dependent on whether or not the ceramic is totally immersed in the liquid. Generally, a partially submerged sample undergoes more extensive dissolution near the liquid-gas interface, called

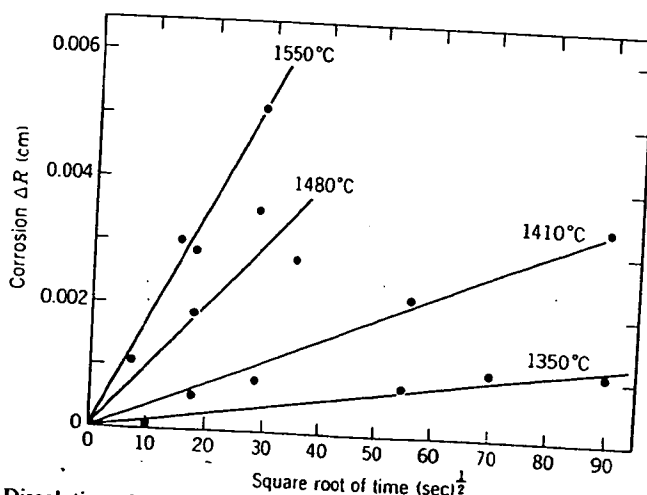


Fig. 9.16. Dissolution of sapphire cylinder in $\text{CaO-Al}_2\text{O}_3\text{-SiO}_2$ with 21 wt % Al_2O_3 , versus square root of time. From Ref. 6.

the metal lin
from free co
induction pe
of dissolutio
sion for ma

where j is
removed, c_∞
at the inter
thickness, L
layer, and \bar{V}
Fig. 9.17 an

where (dc/dx)
boundary-la
of fluid flow
slower mate
layers and p
in glasses a
combine to
boundary la
aqueous sol
ter. Also the

Fig. 9.17. Co

the metal line. Below this interface the corrosion kinetics can be analyzed from free convection principles. It is clear that after a relatively short induction period during which molecular diffusion kinetics prevail the rate of dissolution becomes nearly independent of time. The general expression for mass transport during convection is

$$j = \frac{dn/dt}{A} = \frac{D(c_i - c_\infty)}{\delta(1 - c_i \bar{V})} \quad (9.56)$$

where j is the number of moles per second per square centimeter removed, c_∞ is the concentration in the bulk liquid, c_i is the concentration at the interface (saturation concentration), δ is the boundary layer thickness, D is the effective diffusion coefficient through the boundary layer, and \bar{V} is the partial molar volume. The boundary layer is shown in Fig. 9.17 and defined by

$$\delta = \frac{c_i - c_\infty}{(dc/dy)} \quad (9.57)$$

where (dc/dy) is the concentration gradient at the interface. The boundary-layer thickness is determined by the hydrodynamic conditions of fluid flow. Viscous liquids form thicker boundary layers and cause slower material transfer. Higher liquid velocities form thinner boundary layers and permit more rapid material transfer. For refractory dissolution in glasses and silicate slags, the high viscosity and slow fluid velocity combine to give relatively thick boundary layers. The thickness of the boundary layer may be a centimeter. In comparison, for rapidly stirred aqueous solutions the boundary-layer thickness is a fraction of a millimeter. Also the diffusion rate is much slower in viscous silicate liquids than

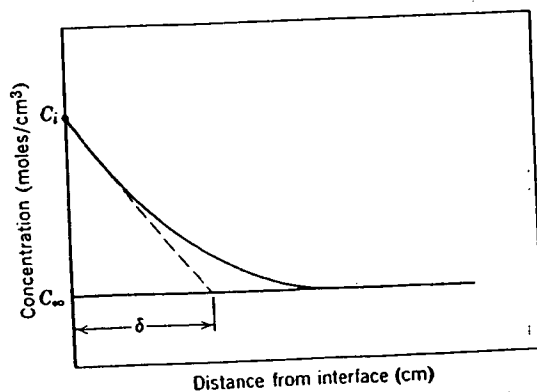


Fig. 9.17. Concentration gradient through diffusion layer at a solution interface.

in aqueous solutions, so that there is more of a tendency for the reaction process to be controlled by material-transfer phenomena rather than interface reactions.

Values for the boundary-layer thickness have been derived for special cases in fluid flow. The boundary-layer thickness for mass transport from a vertical slab with natural convection caused by density-difference driving forces is

$$\delta = 1.835 \times \left[\frac{D\nu\rho_\infty}{gx^3(\rho_i - \rho_\infty)} \right]^{1/4} \quad (9.58)$$

where x is the distance from the leading edge of the plate, ν is the kinematic viscosity η/ρ , g is the gravitational constant, ρ_∞ is the density of the bulk liquid, and ρ_i is the density of the saturated liquid (the liquid at the interface). Thus the average dissolution rate for a plate of height h is given by

$$J = \frac{dn/dt}{A} = 0.726D \left(\frac{g(\rho_i - \rho_\infty)}{\nu Dh\rho_\infty} \right)^{1/4} (c_i - c_\infty) \quad (9.59)$$

The boundary-layer thickness for mass transport from a rotating disc is

$$\delta = 1.611 \left(\frac{D}{\nu} \right)^{1/3} \left(\frac{\nu}{\omega} \right)^{1/2} \quad (9.60)$$

where ω is the angular velocity (rad/sec). The mass transfer for a rotating disc is proportional to the square root of the angular velocity:

$$j = \frac{dn/dt}{A} = 0.62D^{2/3}\nu^{-1/6}\omega^{1/2} \frac{(c_i - c_\infty)}{(1 - c_i\bar{V})} \quad (9.61)$$

Figure 9.18 shows the dissolution kinetics of sapphire into $\text{CaO-Al}_2\text{O}_3\text{-SiO}_2$ for the free convection kinetics and in Fig. 9.19 for forced flow. In each case the kinetics are time-independent, as predicted by Eqs. 9.59 and 9.61.

Comparison of the data for sapphire dissolution at 1550°C for kinetics limited by molecular diffusion, free convection, and forced convection (126 rad/sec) show the dimensional change ΔR (cm) to be related to time as

$$\begin{aligned} \Delta R \text{ (molecular diffusion)} &= (1.77 \times 10^{-4} \text{ cm/sec}^{1/2}) t^{1/2} \\ \Delta R \text{ (free convection)} &= (3.15 \times 10^{-6} \text{ cm/sec}) t \\ \Delta R \text{ (forced convection)} &= (9.2 \times 10^{-5} \text{ cm/sec}) t \end{aligned} \quad (9.62)$$

The important parameters for convective dissolution are fluid velocity, kinematic viscosity, the diffusivity, and the composition gradient.

0.06
0.05
0.04
0.03
0.02
0.01
0

Corrosion ΔR (cm)

Fig. 9.18. Dissolution kinetics of sapphire in 21 wt % Al_2O_3 ver-

It is clear from the data that the kinetics are extremely time-independent, as predicted by the free convection model in Fig. 9.20.

Fig. 9.19. (a) Dissolution kinetics of sapphire in 21 wt % Al_2O_3 ver-

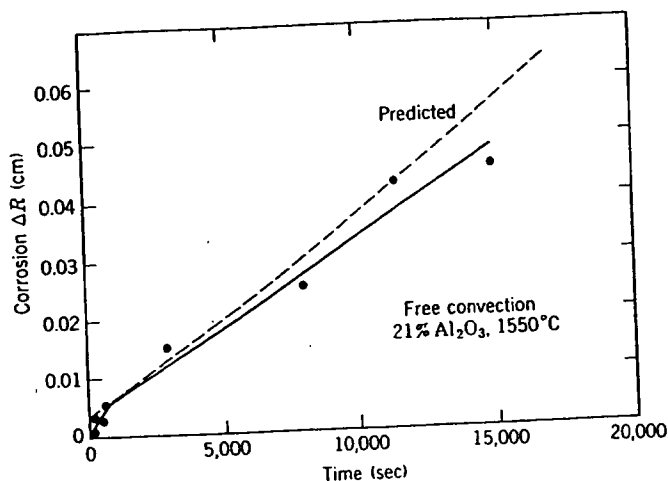


Fig. 9.18. Dissolution at relatively long times of sapphire cylinders in $\text{CaO-Al}_2\text{O}_3\text{-SiO}_2$ with 21 wt % Al_2O_3 versus time. From Ref. 6.

It is clear from the data in Figs. 9.16 and 9.19 that the dissolution rate is extremely temperature-sensitive. Since we have assumed transport-limited kinetics, the temperature dependence is largely determined by the exponential temperature dependence of diffusion (Eq. 6.39). The dependence of the corrosion rate of several ceramics on temperature is shown in Fig. 9.20.

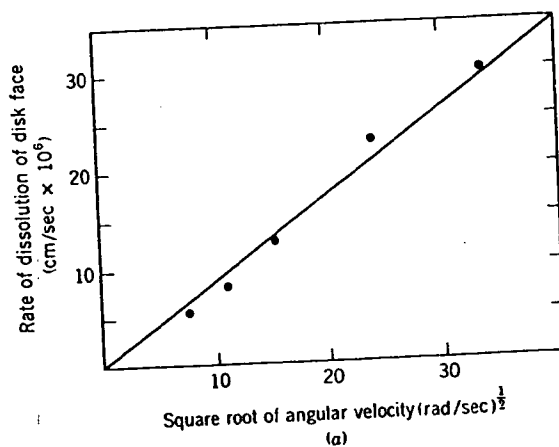


Fig. 9.19. (a) Dependence of rate of dissolution of face of sapphire disk on square root of angular velocity.

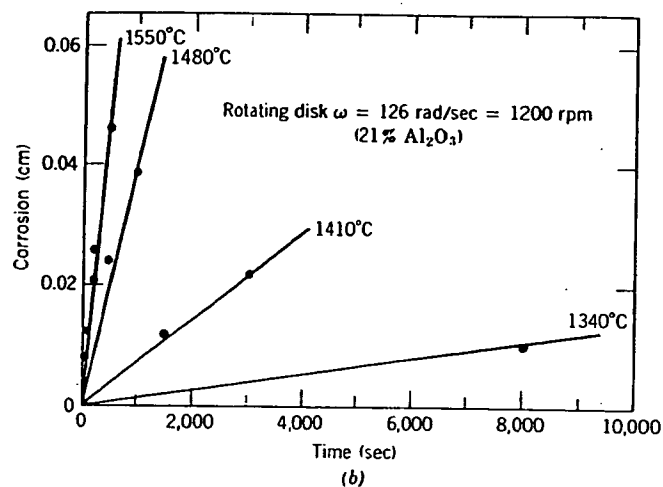


Fig. 9.19 (continued). (b) Rate of dissolution of face of sapphire disk rotating at 126 rad/sec on $\text{CaO-Al}_2\text{O}_3\text{-SiO}_2$ with 21 wt% Al_2O_3 . From Ref. 6.

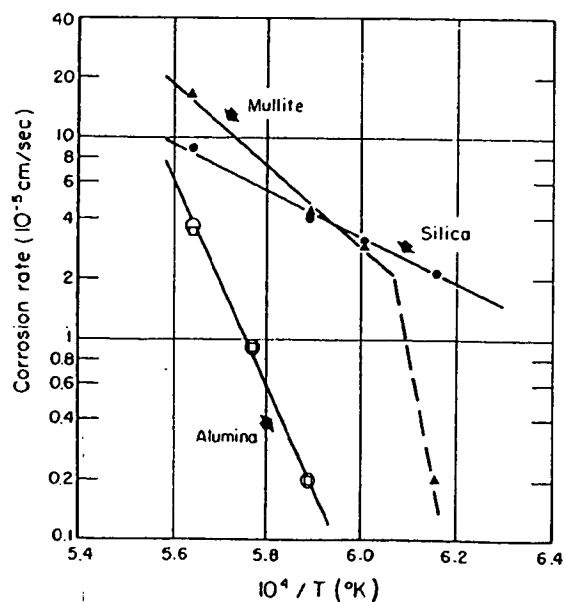


Fig. 9.20. Temperature dependence of forced convection corrosion in the $40\text{CaO-}20\text{Al}_2\text{O}_3\text{-}40\text{SiO}_2$ slag of alumina, mullite, and fused silica. From Ref. 6.

Fig. 9.21. Corrosion of indicate
From Ref. 6.

Refractor
ities in the
ideal surfac
bodies and
corrosion,
ceramics, c
from the da
is about 40

9.4 React

Of partic
tions which
the dehydr
polymorph
products in
of these re

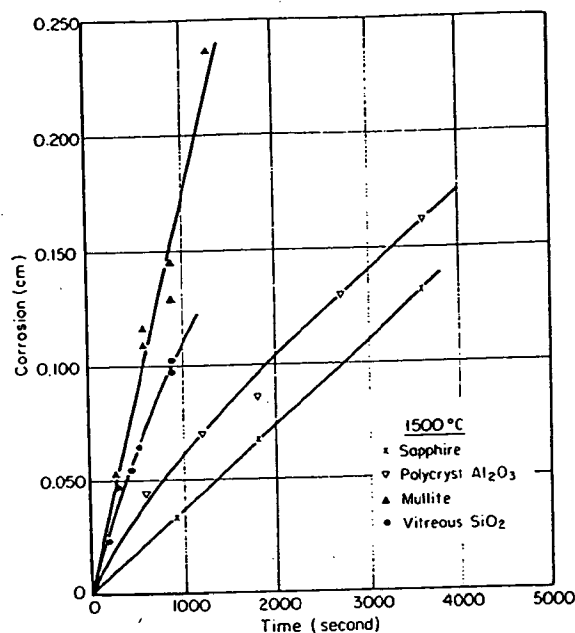


Fig. 9.21. Corrosion rate under forced convection conditions in the 40CaO-20Al₂O₃-40SiO₂ slag of indicated specimens of sapphire, polycrystalline alumina, mullite, and vitreous silica. From Ref. 6.

Refractory corrosion is often much more complex. Besides complexities in the hydrodynamics of a molten bath, refractories seldom have ideal surfaces and are usually not of uniform composition. Multiphase bodies and brick with extensive porosity provide centers for accelerated corrosion, spalling, and penetration by the liquid. In dense single-phase ceramics, corrosion may be greatest at grain boundaries. This can be seen from the data in Fig. 9.21, in which the corrosion of polycrystalline Al₂O₃ is about 40% greater than sapphire after 2500 sec.

9.4 Reactant Transport in Particulate Systems

Of particular interest to ceramists is the large number of transformations which occur with granular or powdered raw materials; for example, the dehydration of minerals, decarbonization of carbonates, and polymorphic transformations. In general, the minerals and reaction products involved are used in large volumes; thus even though the nature of these reactions is complex, study of a few examples is important and

elucidates the important kinetic parameters and illustrates the concept of the rate-limiting step.

Calcination and Dehydration Reactions. Calcination reactions are common for the production of many oxides from carbonates, hydroxides, sulfates, nitrates, acetates, oxalates, alkoxides, and so on. In general the reactions produce an oxide and a volatile reaction product (e.g., CO_2 , SO_2 , H_2O , ...). The most extensively studied reactions are the decomposition of $\text{Mg}(\text{OH})_2$, MgCO_3 , and CaCO_3 . Depending on the particular conditions of temperature, time, ambient pressure, particle size, and so on, the process may be controlled (1) by the reaction rate at the reaction surface, (2) by gas diffusion or permeation through the oxide product layer, or (3) by heat transfer. The kinetics of each of these rate-limiting steps is considered.

Let us first consider the thermodynamics of decomposition, for example, the calcination of CaCO_3 :



The standard heat of reaction is 44.3 kcal/mole, that is, strongly endothermic, which is typical for most decomposable salts of interest. This means that heat must be supplied to the decomposing salt.

The standard free energy for the decomposition of CaCO_3 , MgCO_3 , and $\text{Mg}(\text{OH})_2$ is plotted in Fig. 9.22. The equilibrium partial pressure of the gas for each of the reactions is also plotted in Fig. 9.22. Note, for example, that when ΔG° becomes zero, P_{CO_2} above MgCO_3 and CaCO_3 and $P_{\text{H}_2\text{O}}$ above $\text{Mg}(\text{OH})_2$ have become 1 atm. The temperatures at which this occurs are 1156°K (CaCO_3), 672°K (MgCO_3), and 550°K ($\text{Mg}(\text{OH})_2$). The P_{CO_2} normally in the atmosphere and the range of $P_{\text{H}_2\text{O}}$ (humidity) in air are also shown in Fig. 9.22. From these values we can determine the temperature at which the salt becomes unstable when fired in air. For example, CaCO_3 becomes unstable over 810°K, MgCO_3 above 480°K. Depending on the relative humidity, $\text{Mg}(\text{OH})_2$ becomes unstable above 445 to 465°K. Because acetates, sulfates, oxalates, and nitrates have essentially zero partial pressure of product gases in the ambient atmosphere, it is clear that they are unstable at room temperature. That they exist as salts to a decomposition temperature of about 450°K indicates that their decomposition is governed by atomistic kinetic factors and not by thermodynamics.

The kinetics, as noted above, may be limited by the reaction at the surface, the flow of heat from the furnace to the reaction surface, or the diffusion (permeation) of the product gas from the reaction surface to the ambient furnace atmosphere. This is shown schematically in Fig. 9.23, which also includes the appropriate heat and mass flow equations. The

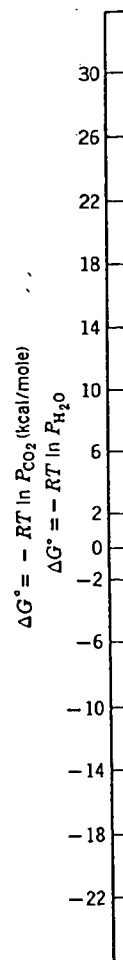


Fig. 9.22. the equilibri

rate-limit
decompo
atures th
tures su
atomistic

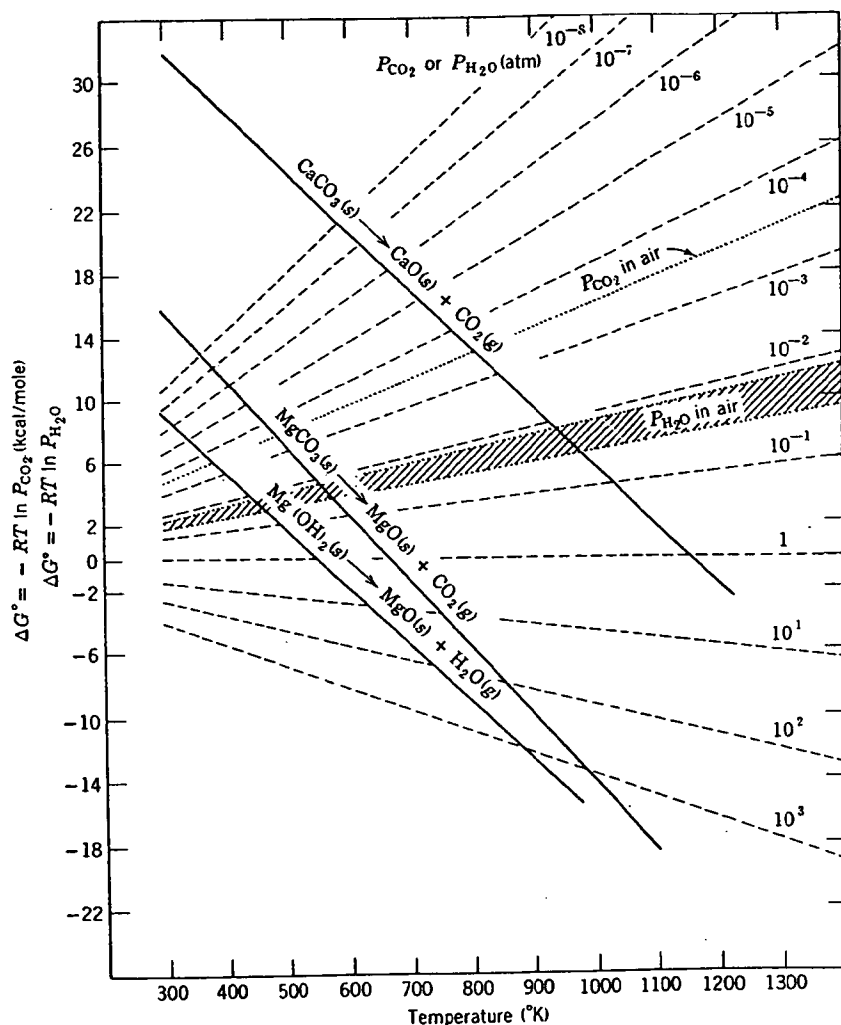
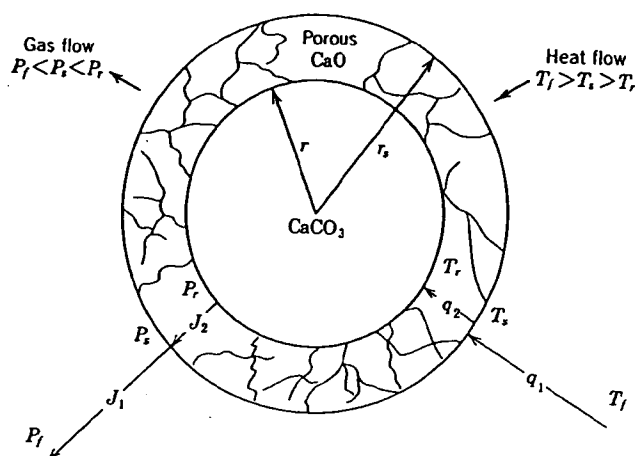


Fig. 9.22. Standard free energy of reaction as a function of temperature. The dashed lines are the equilibrium gas pressure above the oxide and carbonate (hydroxide).

rate-limiting step depends on the particular substance which is undergoing decomposition and the relative temperature. For example, at low temperatures the existence of unstable salts which decompose at higher temperatures suggests that the initial decomposition must be controlled by atomistic processes because there is no reaction-product interference in

CO₂ flow to furnace

$$J_{\text{interface}} = k, 4\pi r^2 (P_r - P_s)$$

$$J_2 = 4\pi \frac{D_{\text{CO}_2}^{\text{eff}} (P_r - P_s) r r_s}{r_s - r}$$

$$J_1 = 4\pi r_s^2 \frac{D_{\text{CO}_2}^{\text{eff}}}{\delta} (P_s - P_f)$$

$$P_r = e^{-\Delta G^\circ / RT_r}$$

 δ = boundary-layer thickness

Heat flow to reaction interface

$$q_{\text{interface}} = \frac{4\pi r^2 \rho}{M} \Delta H_r^\circ \frac{dr}{dt}$$

$$q_1 = h, 4\pi r_s^2 (T_f - T_s)$$

$$q_2 = \frac{4\pi k (T_s - T_r) r r_s}{r_s - r}$$

 ρ = density of CaCO₃ M = molecular weight h , = heat-transfer coefficient k = thermal conductivity of CaO

Fig. 9.23. Schematic representation of the decomposition of a spherical particle (e.g., CaCO₃) of a salt which yields a porous oxide product (e.g., CaO) and a gas (CO₂). The reaction is endothermic, requiring heat transfer. The driving forces for heat and mass transport for steady-state decomposition are expressed as temperatures and pressures in the furnace (T_f, P_f), at the particle surface (T_s, P_s), and at the reaction interface (T_r, P_r).

the transport of heat to the reaction interface or gaseous product away from the interface.

The reaction shown schematically in Fig. 9.23 is heterogeneous; that is, the reaction occurs at a sharply defined reaction interface. Figure 9.24 shows this interfacial area for MgCO₃, for which the reaction proceeds from nucleation sites on the surface of the MgCO₃ platelets. The

Fig. 9.24. of basic n approachin crystallite: Ceram. Sc

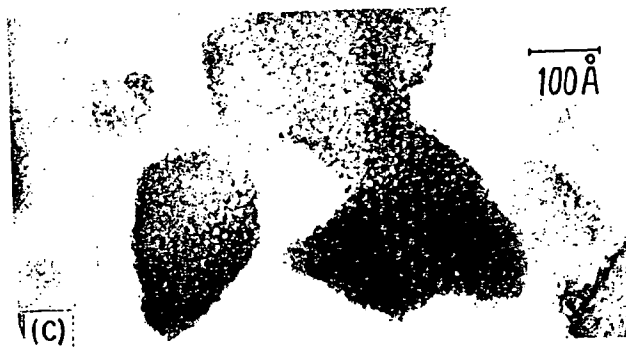
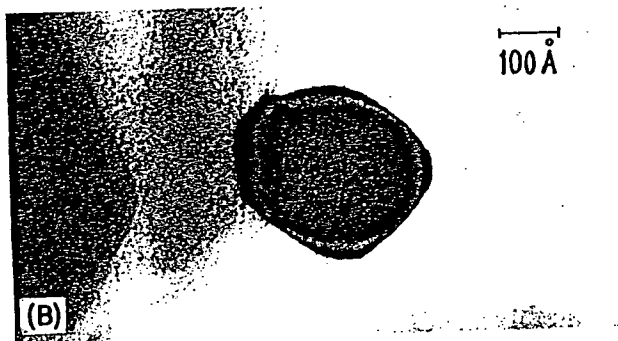
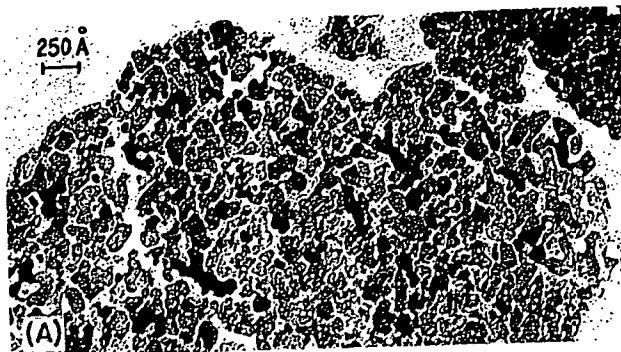


Fig. 9.24. Transmission electron micrographs of MgO prepared by thermal decomposition of basic magnesium carbonate. (a) Pseudomorphed MgO (550°C calcine); (b) crystallite approaching cube form (900°C calcine); (c) two-dimensional moiré pattern from overlapped crystallites (550°C calcine). From A. F. Moodie, C. E. Warble, and L. S. Williams, *J. Am. Ceram. Soc.*, 49, 676 (1966).

decomposition kinetics for cylindrical geometry is

$$(1 - \alpha)^{1/2} = 1 - kt/r_0 \quad (9.64)$$

where α is the fraction decomposed, k is the thermally activated kinetic constant, t is the time (assumed constant temperature), and r_0 is the initial particle radius. The first-order kinetics (Eq. 9.2) for this reaction at several temperatures is shown in Fig. 9.25 for decomposition of $\text{Mg}(\text{OH})_2$.

The importance of the surface on the decomposition rate is indicated by the time to decompose (700°C) a cleaved calcite crystal (CaCO_3), 60 hr, compared with an equivalent mass of the same material in powder form, 4 hr.

At low temperatures the crystallite size strongly affects the decomposition rate; however, at higher temperatures, as the chemical driving force increases and as the thermal energy to motivate diffusional processes and reaction kinetics increases, other steps may become rate-controlling, for example the rate of heat transfer. Figure 9.26 shows the center-line temperature of a cylindrical sample of pressed CaCO_3 powder which was thrust into a hot furnace. The sample temperature increases to a maximum, at which nucleation of CaO finally occurs. The decrease in temperature represents the endothermic heat absorbed by the reaction. The effect of varying the ambient CO_2 pressure is illustrated in Fig.

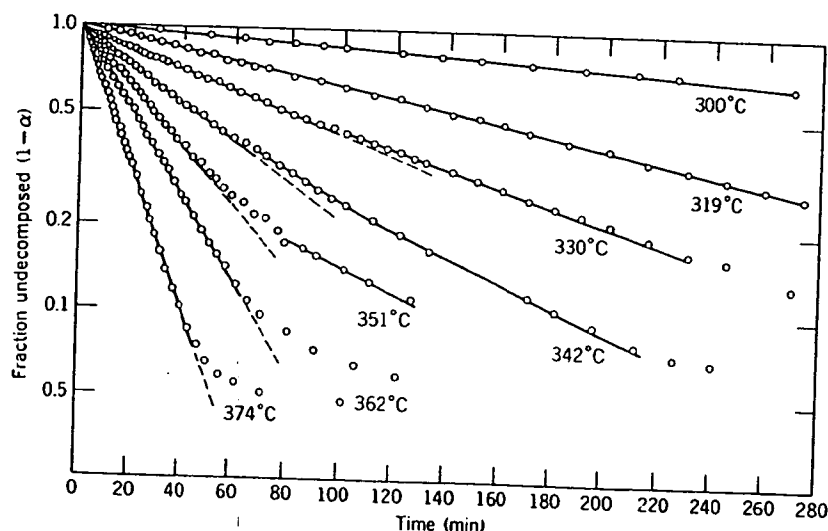


Fig. 9.25. Decomposition of $\text{Mg}(\text{OH})_2$ showing first-order kinetics. From R. S. Gordon and W. D. Kingery, *J. Am. Ceram. Soc.*, 50, 8 (1967).

Fig. 9.26.
sample of
A.I.C.H.E.J

9.27. As
decrease
Some
manner

Fig. 9.2
(1 - P_{CO_2})
 $R_0 = \text{dec}$
E. Wads

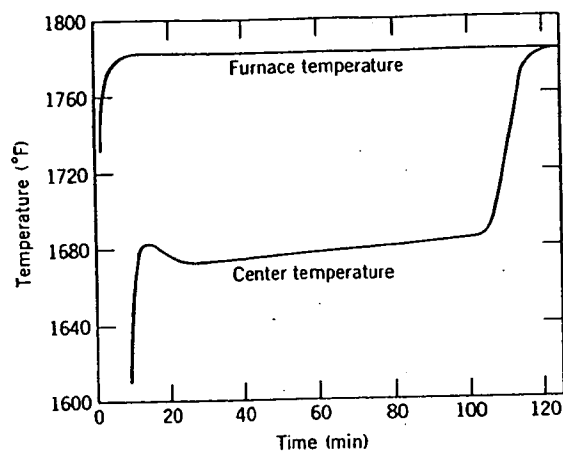


Fig. 9.26. Comparison of the furnace temperature to center-line temperature of a cylindrical sample of CaCO_3 thrust into a preheated furnace. From C. N. Satterfield and F. Feales, *A.I.C.H.E.J.*, 5, 1 (1959).

9.27. As the P_{CO_2} is increased, the driving potential for the reaction decreases, and thus the reaction rate is decreased.

Some of the clay minerals, kaolin in particular, do not decompose in the manner shown in Fig. 9.23; that is, they do not have a heterogeneous

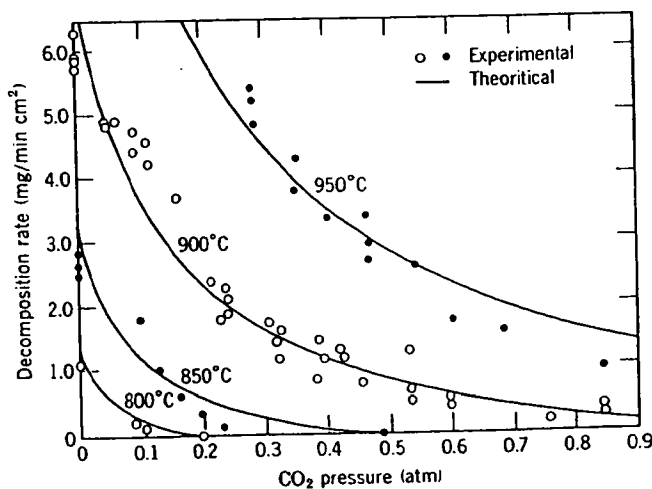


Fig. 9.27. Rate of decomposition of CaCO_3 in CO_2 atmosphere; $R_{\text{theor}} = (1 - P_{\text{CO}_2}/P_{\text{CO}_2^*})(BP_{\text{CO}_2^*} + 1/R_0)$, where $P_{\text{CO}_2^*}$ = equilibrium CO_2 pressure, B = constant, and R_0 = decomposition rate in a pure neutral atmosphere. From E. P. Hyatt, I. B. Cutler, and M. E. Wadsworth, *J. Am. Ceram. Soc.*, 41, 70 (1958).

reaction interface or a reaction product which breaks up into small crystallites. Above 500°C the water of crystallization is evolved, and a pseudomorphic structure remains until 980°C. The pseudomorph is a matrix of the original crystal structure containing large concentrations of vacant anion sites. Above 980°C the structure collapses irreversibly into crystalline mullite and silica, which releases heat (see Fig. 9.28).

The reaction kinetics is controlled by the diffusion of hydroxyl ions in the bulk rather than the heterogeneous surface decomposition illustrated in Fig. 9.23. The kinetics is thus homogeneous and controlled by diffusion in the solid, which gives a parabolic rate law. The dehydration kinetics of kaolinite is given (1) in Fig. 9.29 for size fractions. A similar situation is observed for the decomposition of $\text{Al}(\text{OH})_3$.

Powder Reactions. In most processes of interest in ceramic technology, solid-state reactions are carried out by intimately mixing fine powders. This changes the geometry from that considered in Fig. 9.6, and the actual reaction is more like that illustrated in Fig. 9.30.

If the reaction is carried out isothermally, the rate of formation of the reaction zone depends on the rate of diffusion. For the initial parts of the reaction the rate of growth of the interface layer is given to a good

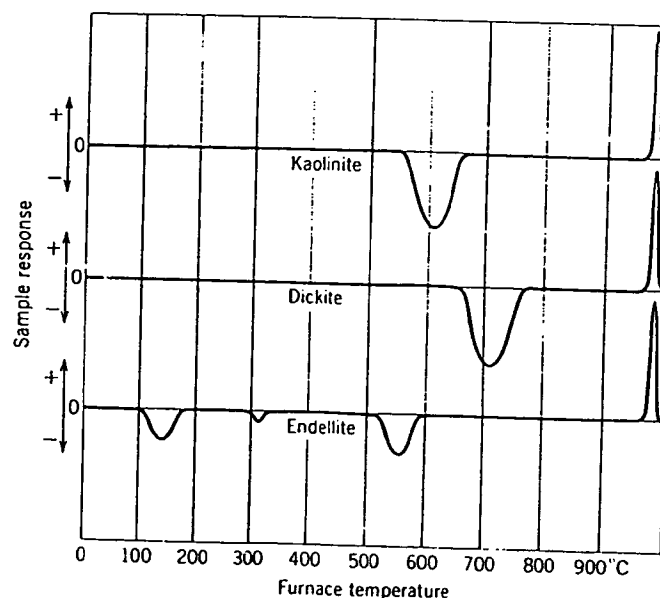


Fig. 9.28. Differential thermal analysis curves of kaolin clays. The sample temperature leads (+) or lags (-) the furnace temperature at levels at which heat is evolved or absorbed by chemical changes.

Fig. 9.2
Holt, I.

Fig. 9.
particle

small
and a
h is a
ons of
ly into

ions in
ated in
ision in
etics of
ation is

echnol-
ng fine
9.6, and

a of the
s of the
a good

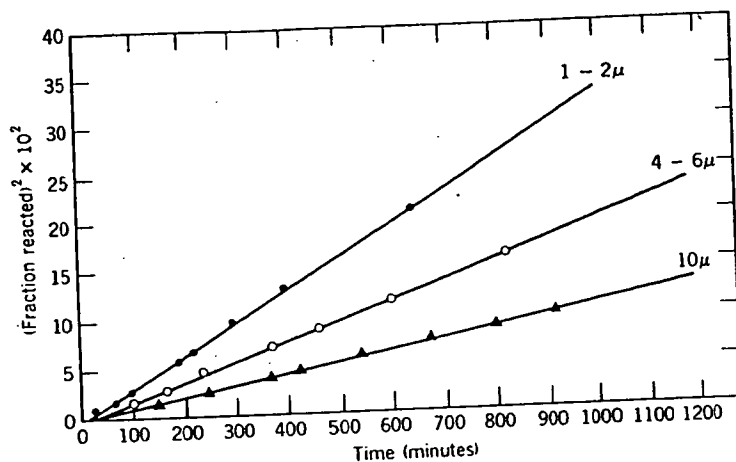


Fig. 9.29. Parabolic plots for three size fractions of kaolinite at 400°C in vacuum. From J. B. Holt, I. B. Cutler, and M. E. Wadsworth, *J. Am. Ceram. Soc.*, 45, 133 (1962).

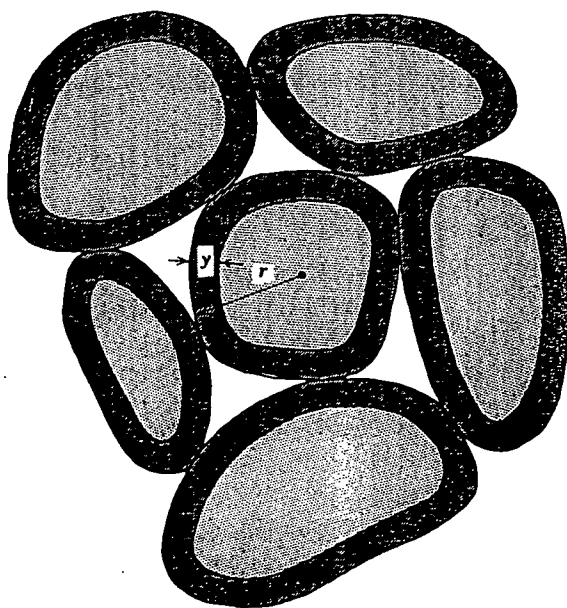


Fig. 9.30. Schematic representation of reaction-product layers forming on surface of particles in powder mixture.

approximation by the parabolic relationship in Eq. 9.8. If V is the volume of material still unreacted at time t , then

$$V = \frac{4}{3} \pi (r - y)^3 \quad (9.65)$$

The volume of unreacted material is also given by

$$V = \frac{4}{3} \pi r^3 (1 - \alpha) \quad (9.66)$$

where α is the fraction of the volume that has already reacted. Combining Eqs. 9.65 and 9.66,

$$y = r(1 - \sqrt[3]{1 - \alpha}) \quad (9.67)$$

Combining this with Eq. 9.8 gives for the rate of reaction

$$(1 - \sqrt[3]{1 - \alpha})^2 = \left(\frac{KD}{r^2} \right) t \quad (9.68)$$

Note that this is for spherical geometry where Eq. 9.64 is for cylindrical geometry. By plotting $(1 - \sqrt[3]{1 - \alpha})^2$ against time, a reaction-rate constant equivalent to KD/r^2 can be obtained which is characteristic of the reaction conditions. The constant K is determined by the chemical-potential difference for the species diffusing across the reaction layer and by details of the geometry.

The relationship given in Eq. 9.68 has been found to hold for many solid-state reactions, including silicate systems, the formation of ferrites, reactions to form titanates, and other processes of interest in ceramics. The dependence on different variables is illustrated for the reaction between silica and barium carbonate in Fig. 9.31. In Fig. 9.31a it is observed that there is a linear dependence of the function $(1 - \sqrt[3]{1 - \alpha})^2$ on time. The dependence on particle size illustrated in Fig. 9.31b shows that the rate of the reaction is directly proportional to $1/r^2$ in agreement with Eq. 9.68: in 9.31c it is shown that the temperature dependence of the reaction-rate constant follows an Arrhenius equation, $K' = K_0 \exp(-Q/RT)$, as expected from its major dependence on diffusion coefficient.

There are two oversimplifications in Eq. 9.68 which limit its applicability and the range over which it adequately predicts reaction rates. First, Eq. 9.68 is valid only for a small reaction thickness, Δy ; and second, there was no consideration of a change in molar volume between the reactants and the product layer. The time dependence of the fraction reacted

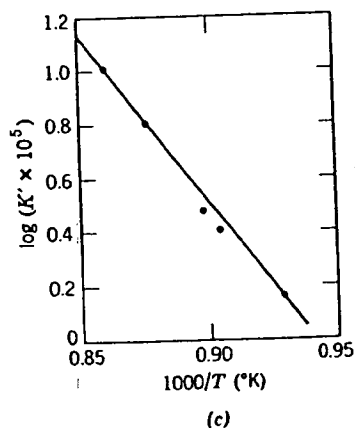
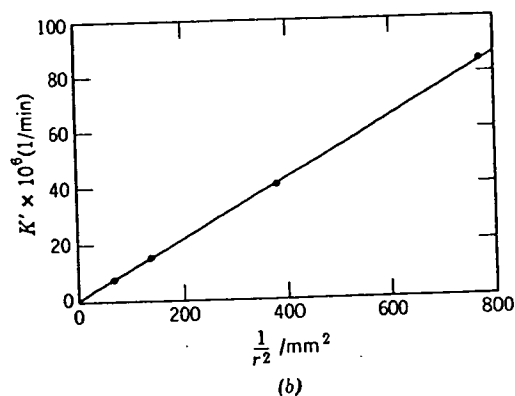
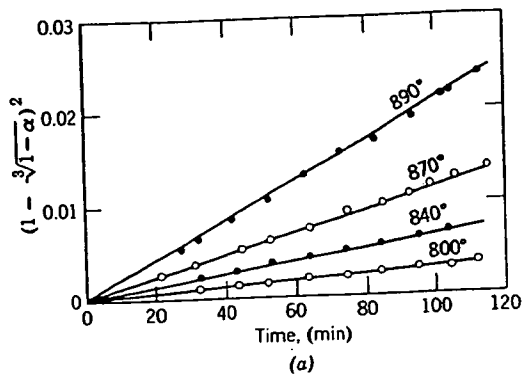


Fig. 9.31. Solid reaction between silica and barium carbonate showing (a) time dependence, (b) particle-size dependence, and (c) temperature dependence of reaction rate. From W. Jander, *Z. Anorg. Allg. Chem.*, 163, 1 (1927).

corrected for these two constraints is given as*

$$[1 + (Z - 1)\alpha]^{2/3} + (Z - 1)(1 - \alpha)^{2/3} = Z + (1 - Z) \left(\frac{KD}{r^2} \right) t \quad (9.69)$$

where Z is the volume of particle formed per unit volume of the spherical particle which is consumed, that is, the ratio of equivalent volumes. A demonstration that Eq. 9.69 is valid even to 100% reaction is shown in Fig. 9.32 for the reaction $\text{ZnO} + \text{Al}_2\text{O}_3 = \text{ZnAl}_2\text{O}_4$.

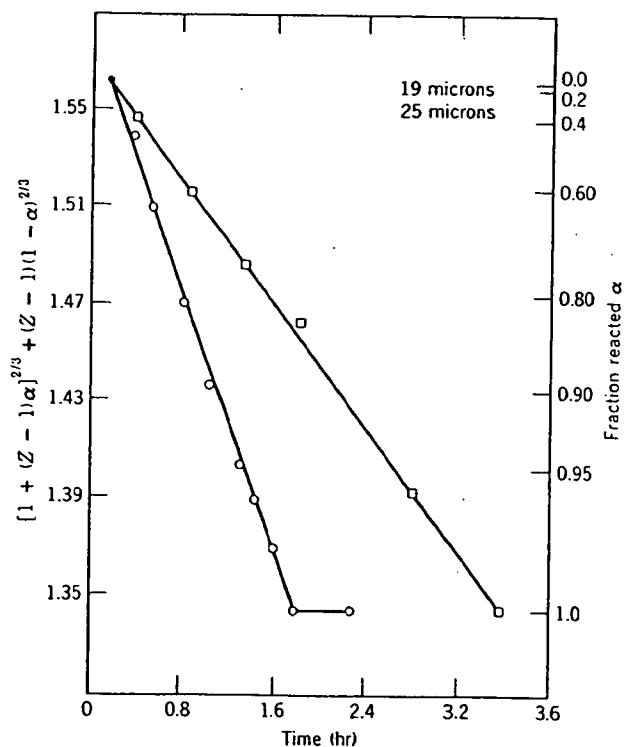


Fig. 9.32. Reaction between ZnO and Al_2O_3 to form ZnAl_2O_4 at 1400°C in air (two spherical particle sizes). See reference 1, p. 102.

Calculating the reaction rate given in Eqs. 9.68 and 9.69 on an absolute basis requires knowledge of the diffusion coefficient for all the ionic species together with a knowledge of the system's geometry and the chemical potential for each species as related to their position in the reaction-product layer. The diffusing species which control the reaction

*R. E. Carter, *J. Chem. Phys.*, **34**, 2010 (1961); **35**, 1137 (1961).

rate are the most arriving at a phase Section 9.2 must

Another difficult dependence of α in many cases the coherent with the with many defects tunity for surface indicated in Eq. through a single lower limit for rate. When new temperatures, there be some nonequilibrium structure with α and growth in nonequilibrium product. For example observed at a α This effect is α changes at the extensively in α Also, at the transformation tends to which increase transfer. At present a quantitative

Coarsening α may undergo α represents a α Generally termed dispersed in α varying size in α ones dissolve α of the interface (ter 5) relates to α a relative to α

where γ is the

rate are the most rapidly moving ions, or ions plus electrons, capable of arriving at a phase-boundary interface. All the constraints discussed in Section 9.2 must be considered.

Another difficulty in detailed quantitative calculations is the strong dependence of reaction rates on the structure of the reaction product. In many cases the reaction product is formed in such a way that it is not coherent with the reactants. Because of volume changes it may be formed with many defects and fissures. Consequently, there is extensive opportunity for surface and boundary diffusion, and the diffusion coefficient indicated in Eqs. 9.68 and 9.69 is not necessarily identical with diffusion through a single-crystal or dense polycrystalline body; these values set a lower limit for the actual diffusion coefficient and the possible reaction rate. When new phases are formed, as by carbonate decomposition at low temperatures, there is a strong tendency for the initial lattice parameter to be some nonequilibrium value corresponding to a coherent interface and structure with the reactant, as discussed in connection with nucleation and growth in Sections 8.3 and 8.4. Diffusion coefficients for this nonequilibrium lattice are normally larger than for the final equilibrium product. For example, an increase in solid-state reaction rate is frequently observed at a polymorphic transition temperature (the Hedvall effect). This effect is related to lattice strains and fissures formed by volume changes at the transition point; these lattice strains and fissures occur extensively in quartz, for example, in which the volume change is large. Also, at the transition temperature equilibrium between two polymorphic forms tends to occur with a coherent interface giving rise to lattice strains which increase the diffusion coefficients and the opportunity for material transfer. At present there are no data available for putting these effects on a quantitative basis.

Coarsening of Particles. After a solid has precipitated, the particles may undergo a coarsening effect because the variation in particle size represents a variation in the chemical activity from particle to particle. Generally termed Ostwald ripening, the principles apply to precipitates dispersed in solids or liquids. For the system of dispersed particles of varying size in a medium in which they have some solubility, the smaller ones dissolve and the larger ones grow. The driving force is the reduction of the interfacial free energy. The Thompson-Freundlich equation (Chapter 5) relates the increased solubility of the precipitate c_a to the curvature a relative to that for a planar interface $c_{p.i.}$:

$$RT \ln \frac{c_a}{c_{p.i.}} = \frac{2\gamma M}{a \rho} \quad (9.70)$$

where γ is the interfacial energy (ergs/cm²), M the molecular weight, and

.69)

ical
. A
Fig.

rical

lute
onic
the
the
tion

ρ the density of the precipitate particle. This relation also assumes that the activity is given by the concentration. If $\frac{2\gamma M}{RT\rho a_p} < 1$, the increased solubility is given by

$$c_a = c_{p.i.} \left(1 + \frac{2\gamma M}{RT\rho a_p} + \dots \right) = c_{p.i.} + \frac{2\gamma M c_{p.i.}}{RT\rho} \quad (9.71)$$

For simplicity, consider a system of two particle sizes a_1 and a_2 where $a_1 > a_2$. The a_2 particles are more soluble in the matrix and thus tend to dissolve because of the concentration driving force:

$$c_{a_1} - c_{a_2} = \frac{2\gamma M c_{p.i.}}{RT\rho} \left(\frac{1}{a_1} - \frac{1}{a_2} \right) \quad (9.72)$$

From Fick's law we can determine the rate of growth of these particles if we assume the rate is controlled by diffusion in the matrix, that is, solvent (see Fig. 9.33a). The rate of mass gain by a_1 is

$$\frac{dQ}{dt} = -D \left(\frac{A}{x} \right) (c_{a_1} - c_{a_2}) \quad (9.73)$$

where A/x is a representative area-to-length ratio for diffusion between two dissimilar particles. Substitution of Eq. 9.72 into 9.73 yields

$$\frac{dQ}{dt} = -D \left(\frac{A}{x} \right) \frac{2\gamma M c_{p.i.}}{RT\rho} \left(\frac{1}{a_1} - \frac{1}{a_2} \right) \quad (9.74a)$$

As we have assumed spherical particles and must conserve mass,

$$-\frac{dQ}{dt} = \rho 4\pi a_2^2 \frac{da_2}{dt} = -\rho 4\pi a_1^2 \frac{da_1}{dt} \quad (9.74b)$$

the growth of a_1 is

$$\rho 4\pi a_1^2 \frac{da_1}{dt} = -D \left(\frac{A}{x} \right) \frac{2\gamma M c_{p.i.}}{RT\rho} \left(\frac{1}{a_1} - \frac{1}{a_2} \right) \quad (9.75)$$

Equation 9.75 can be integrated under various approximations, however, the same solution results by considering the following approximate solution. If we assume that the small particles contribute solute to the matrix faster than the solute is precipitated onto the large particles, the growth of large particles can be treated as a diffusion-limited-growth problem. The rate-limiting step is assumed to be diffusion of matter to the large particle from the matrix. Assume a diffusion field of $r (r \gg a_1)$

Fig. 9.33. (a) C in a diffusion field

around the gr symmetry is

where

Recalling tha

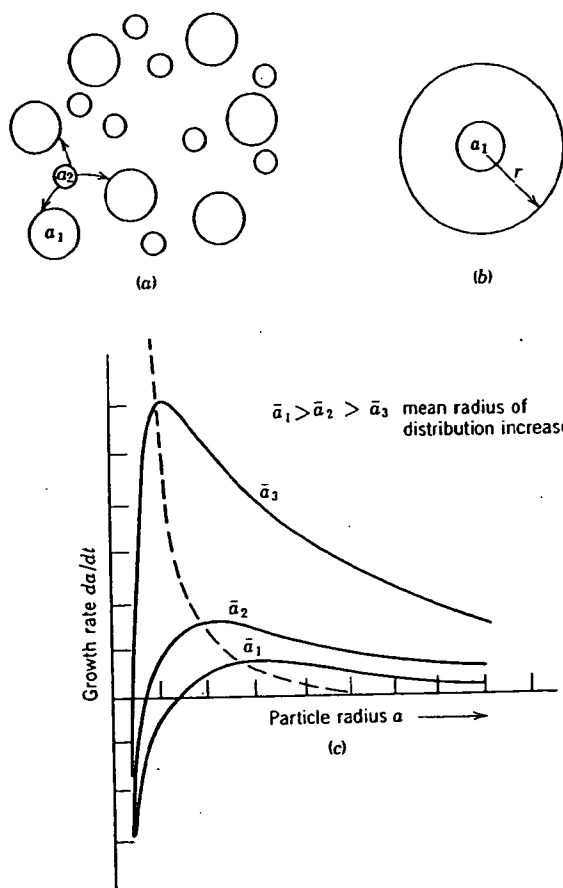


Fig. 9.33. (a) Coarsening of particles in a two-size particle system; (b) growth of particle a_1 in a diffusion field of radius r ; (c) variation in the particle growth rate with particle radius.

around the growing particle (Fig. 9.33b); thus Fick's first law of spherical symmetry is

$$J = 4\pi D \Delta c \left(\frac{a_1 r}{r - a_1} \right) \quad (9.76)$$

where

$$\Delta c = \frac{2M\gamma c_{p,i}}{RT\rho a_1}$$

Recalling that for dispersed particles $r \gg a_1$, the flux is given by

$$J = \frac{4\pi D 2M\gamma c_{p,i}}{RT\rho a_1} \left(\frac{a_1 r}{r - a_1} \right) \approx \frac{4\pi D c_{p,i} 2M\gamma}{RT\rho} = \text{const} \quad (9.77)$$

The flux is a constant, independent of the growing particle radius,

$$J = \text{constant} = \rho \frac{dV}{dt} = \rho 4\pi a_i^2 \frac{da_i}{dt} = \frac{4\pi Dc_{p,i} 2M\gamma}{\rho RT} \quad (9.78)$$

which after integration becomes

$$a_f^3 - a_i^3 = \frac{6Dc_{p,i}M\gamma}{\rho^2 RT} \quad (9.79)$$

or

$$\left(\frac{a(t)}{a_i}\right)^3 = 1 + \frac{t}{\tau}$$

where

$$\tau = \frac{6Dc_{p,i}M\gamma}{\rho^2 RTa_i^3} \quad (9.80)$$

More rigorous analyses give essentially the same result for a distribution of precipitates.* The variation in the growth rate for varying particle size and for increases in the mean radius is illustrated in Fig. 9.33c. The diffusion-limited growth of precipitates and of grains during liquid-phase sintering have been observed to have this cubic time dependence (Figs. 9.34 and 9.35).

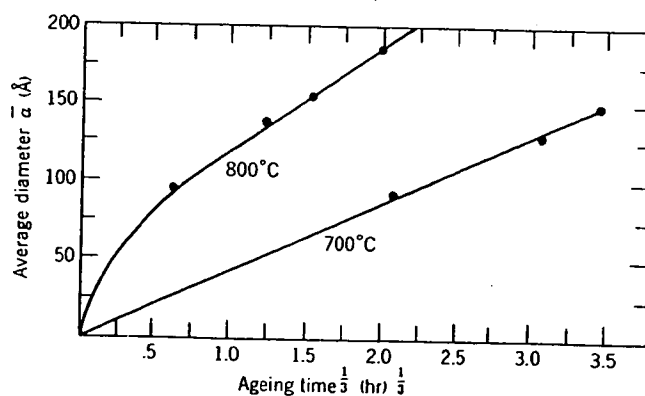


Fig. 9.34. Coarsening of $Mg_{1.2}Fe_{1.8}O_3$ precipitates in MgO. From G. P. Wirtz and M. E. Fine, *J. Am. Ceram. Soc.*, 51, 402 (1968).

The coarsening relationships discussed above assumed spherical particles. The following discussion demonstrates that faceted particles and even those with different surface energies can be included in the growth expressions by properly defining Δc , the concentration difference.

*C. Wagner, *Z. Electrochem.*, 65, 581-591 (1961); G. W. Greenwood, *Acta Met.*, 4, 243-248 (1956).

R
5.4
5.0
4.6
4.2
3.8
3.4

$\log |(\bar{G}S)^3 - (\bar{G}S_0)^3|$

Fig. 9.35. Isotherm
microns, t = time in
Publishing Corpor:

Consider a si
to-volume ratio

The chemical
the planar inte

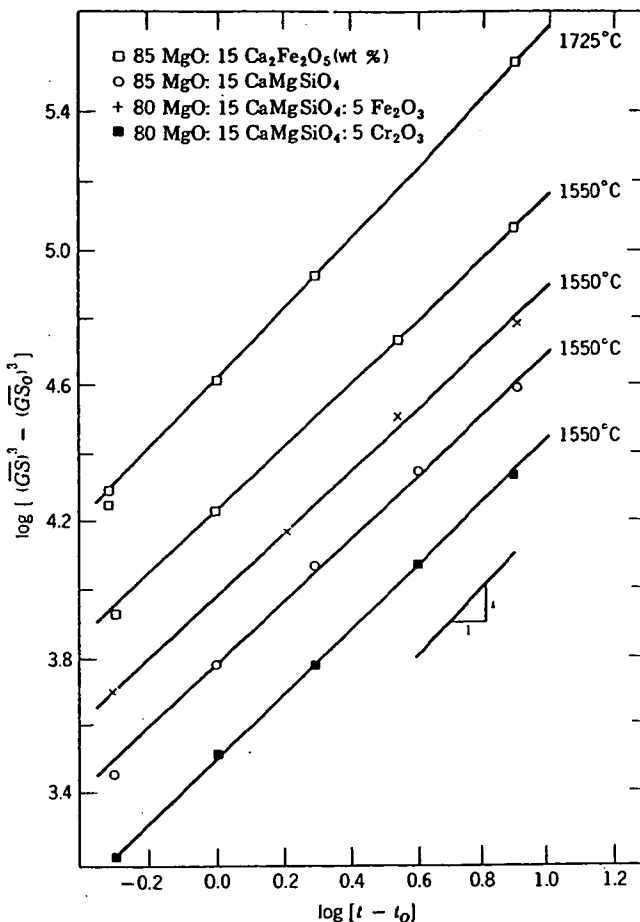


Fig. 9.35. Isothermal grain growth in systems containing MgO and liquid (GS = grain size in microns, t = time in hours) $(GS)^3$ at. From J. White in *Materials Sci. Research*, Vol. 6, Plenum Publishing Corporation, New York, 1973, p. 81.

Consider a size class of particles of constant shape but with a surface-to-volume ratio $S_v = S/V$. The surface contribution to the free energy is

$$G - G_{p.l.} = \gamma S = \gamma S_v V \quad (9.81)$$

The chemical potential difference between the faceted particle (μ) and the planar interface ($\mu_{p.l.}$) is

$$\mu - \mu_{p.l.} = \frac{d}{dn} (G - G_{p.l.}) = \gamma \bar{V} \left(\frac{dS}{dV} \right)_{S_v} \quad (9.82)$$

where \bar{V} is the molar volume for the particle phase. Let x be some linear parameter of the particle size such that $S = ax^2 = \frac{\alpha V}{x}$, where a and α are characteristic shape constants. Then

$$\left(\frac{dS}{dV}\right)_{S_v} = S_v \frac{dS/S}{dV/V} = \frac{2}{3} S_v = \frac{2\alpha}{3x} \quad (9.83)$$

and

$$\mu - \mu_{p,i} = \gamma \bar{V} \frac{2\alpha}{3x} \quad (9.84)$$

Equations 9.81 to 9.84 hold for any system of constant-shape particles, irrespective of whether they are spherical or faceted. If we assume the activity is given by the concentration,

$$\Delta c = \frac{(\mu - \mu_{p,i})c_{p,i}}{RT} = \frac{\gamma \bar{V} c_{p,i}}{RT} \left(\frac{2\alpha}{3x}\right) \quad (9.85)$$

For spheres $\alpha = 3$ and $x = r$, we have the Thompson-Freundlich equation (9.71):

$$\Delta c = \frac{2\gamma \bar{V} c_{p,i}}{rRT} = \frac{2\gamma M c_{p,i}}{RT r \rho}$$

where \bar{V} is the molar volume, M the molecular weight and ρ the density. For faceted interfaces with varying surface free energy the Wulff theorem is applicable:

$$\mu - \mu_{ref} = \frac{2}{3} \bar{V} \sum \left(\frac{\alpha_i \gamma_i}{x_i} \right) \quad (9.86)$$

where x_i is the distance from the i th facet to the particle center.

9.5 Precipitation in Crystalline Ceramics

The nucleation and growth of a new phase has been discussed in Chapter 8 and applied there to processes occurring in a liquid or glass matrix. Polymorphic phase transformations in crystalline solids are discussed in Chapter 2. Precipitation processes from a crystalline matrix in which the precipitate has a composition different from the original crystal are important in affecting the properties of many ceramic systems, and as techniques such as transmission electron microscopy capable of observing and identifying fine precipitate particles are more fully applied, the widespread occurrence and importance of precipitation is becoming more fully recognized. Initiation of the process may occur by a spinodal process or by discrete particle nucleation (Chapter 8) when a driving force

for phase separation mobility (Chapter 8).

For nucleation, the volume between free-energy maxima is replaced by

where the strain energy, and b is the strain energy can be calculated. An expression for ΔG^* , which contains the α and β structural parameters of the crystalline phase, stable nuclei at sites. The strain energy when a decomposition of precipitates occurs. The minimum increase in spherical particle is proportional to the volume change. Strain energy of the interface, which phase separates lamellae in precipitates.

The energy of the structure and composition in general kinds of planes of atoms, second coordination boundary. In planes of atoms giving rise to dislocations described in Chapter 8. Order of magnitude of formation of mother matrix commonly the formation in which

for phase separation occurs (Chapter 7); growth rates are limited by atom mobility (Chapter 6).

For nucleation in solids, strain energy resulting from differences in volume between precipitate and matrix must be included in evaluating the free-energy change on forming a nucleus. In these cases, Eq. 8.19 is replaced by

$$\Delta G_r = 4\pi r^2\gamma + \frac{4}{3}\pi r^3(\Delta G_v + \Delta G_e) \quad (9.87)$$

where the strain energy per unit volume is given by $\Delta G_e = b\epsilon^2$, ϵ is the strain, and b is a constant which depends on the shape of the nucleus and can be calculated from elasticity theory. The presence of ΔG_e in the expression for ΔG_r results in a free energy on forming the critical nucleus, ΔG^* , which corresponds to a definite crystallographic relation of the α and β structures and the boundary between them when both are crystalline phases. Inclusion of ΔG_e can affect greatly the morphology of stable nuclei and increase the tendency for nucleation at heterogeneous sites. The strain energy typically causes the formation of parallel platelets when a decomposition (precipitation) reaction occurs. The configuration of precipitates as parallel platelets allows growth to take place with the minimum increase in strain energy. In general, the formation of thick or spherical particles produces large values of strain; since the strain energy is proportional to ϵ^2 , precipitates with a platelike habit are preferred when the volume change on precipitation is appreciable, as is often the case. Strain energy also effects spinodal decomposition by increasing the energy of the inhomogeneous solution and depressing the temperature at which phase separation occurs and by causing separation to occur as lamellae in preferred crystallographic directions.

The energy for nucleation of a new phase depends on the interface structure and orientation, as discussed in Chapter 5. We can define two general kinds of precipitate. In a *coherent* precipitate, as in Fig. 9.36, planes of atoms are continuous across the interface so that only the second coordination of individual atoms is changed, similar to a twin boundary. In contrast, a *noncoherent* precipitate is one in which the planes of atoms, or some of them, are discontinuous across the interface, giving rise to dislocations or a random structure in the boundary layer, as described in Chapter 5. The interface energy of a coherent boundary is an order of magnitude less than that of an incoherent boundary, so that formation of new phases with definite structural relationships to the mother matrix is strongly preferred. In addition, the oxygen ions are commonly the more slowly moving in oxide structures, so that a transformation in which these ions must migrate to new positions is bound to be

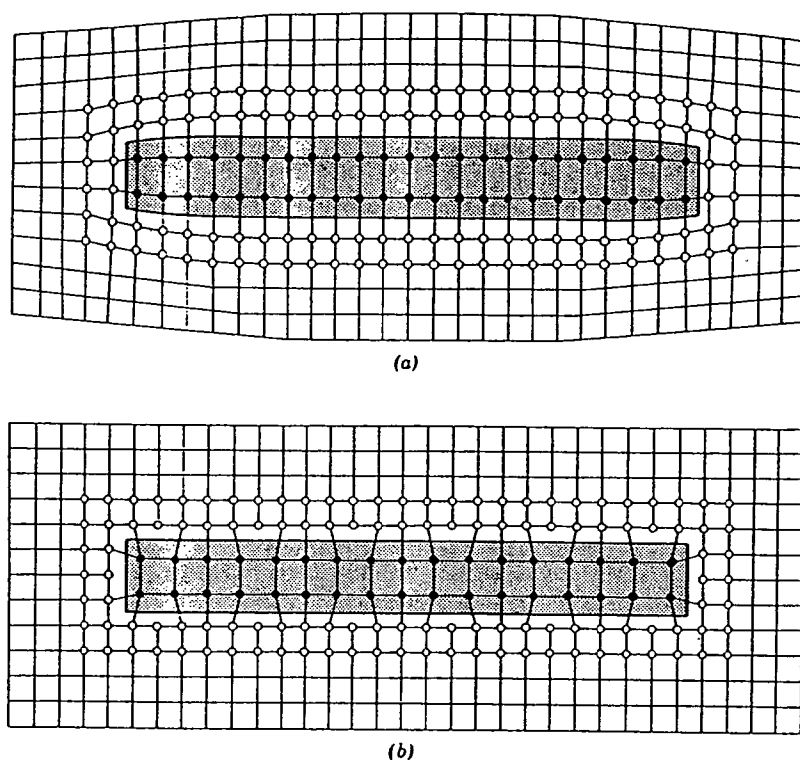


Fig. 9.36. (a) Coherent precipitate with continuous planes of atoms across the interface; (b) noncoherent precipitate with discontinuous planes of atoms across the interface.

relatively slow. Therefore, coherency of the oxygen ion lattice is favorable both for the driving force of nucleation and for the rate of nucleation and crystal growth.

Precipitation Kinetics. The kinetics of precipitation in a crystalline solid depend on both the rate of initiation or nucleation of the process and the rate of crystal growth, as discussed in Chapter 8. When the precipitation process consists of a combination of nucleation and growth, the sigmoidal curve characteristic of the Johnson-Mehl or Arrami relations (Chapter 8) results in an apparent incubation time period, as illustrated in Fig. 9.37. For precipitation processes far from an equilibrium phase boundary, which is the most usual case, both the nucleation rate and the growth rate increase with temperature, as illustrated in Fig. 9.38 such that the incubation time is decreased and the transformation time for formation of the new phase is decreased at higher temperatures, such as occurs for the process illustrated in Fig. 9.37. In many cases, however, the

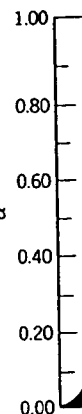


Fig. 9.37. Effect of temperature on the rate of precipitation for ZrO_2 -20 mole % B, 1075°C; B, 1075°C; Viechnicki, J. A.

nucleation rate is high, the number of nucleation sites which heterogeneously nucleate matrix crystals is small. The precipitate is nucleated by the existing nucleation sites. The precipitation of magnesium paramagnetic ions having an apparent incubation period is in accordance with the sigmoidal curve.

Precipitation Interfaces. The precipitation of many oxide ions described in Chapter 8 containing energy and

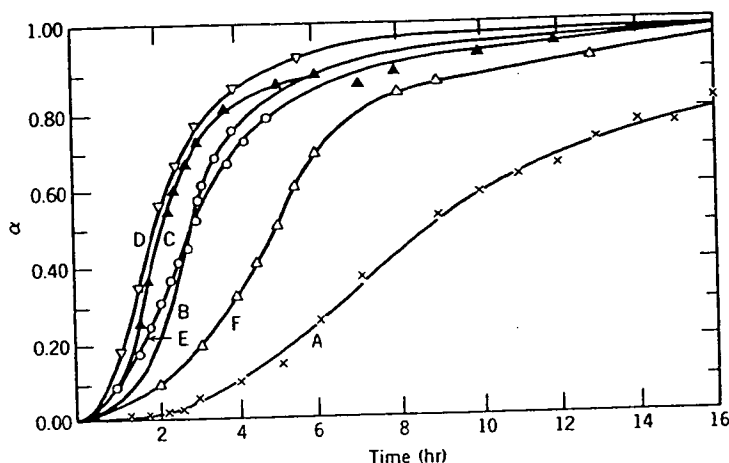


Fig. 9.37. Effect of temperature on the decomposition of solid solutions of 80 mole % ZrO_2 -20 mole % MgO . Solid solutions prepared at 1520°C for 1 hr and then decomposed at A, 1000°C ; B, 1075°C ; C, 1150°C ; D, 1250°C ; E, 1350°C ; F, 1375°C . From V. S. Stubican and D. J. Viechnicki, *J. Appl. Phys.*, 37, 2751 (1966).

nucleation process occurs rapidly during cooling, such that a large number of nuclei are available for growth. This is particularly the case in which heterogeneous nucleation sites are available in a not very perfect matrix crystal or in which the interface energy term is low for a coherent precipitate. When this occurs the overall precipitation process, as measured by the fraction of material transformed, corresponds to growth of existing nuclei and no incubation period is observed, as illustrated for precipitation of MgAl_2O_4 spinel from MgO in Fig. 9.39. For precipitation of magnesium ferrite, MgFe_2O_4 , from MgO , application of superparamagnetic measurements capable of identifying newly formed crystals having an average diameter of about 15 \AA has shown no indication of an incubation period; that is, the critical nucleus size is very very small in accordance with a low energy for the coherent interface.*

Precipitate Orientation. The influence of strain energy and coherent interfaces leads to a high degree of precipitate orientation for many oxide precipitation processes. These relationships are particularly strong for the many oxide structures based on close-packed arrangements of oxygen ions described in Chapter 2. In the case of magnesium aluminate spinel containing excess aluminum oxide in solid solution, the influence of strain energy and coherency relationships leads to precipitation of a metastable

*G. P. Wirtz and M. E. Fine, *J. Am. Ceram. Soc.*, 51, 402 (1968).

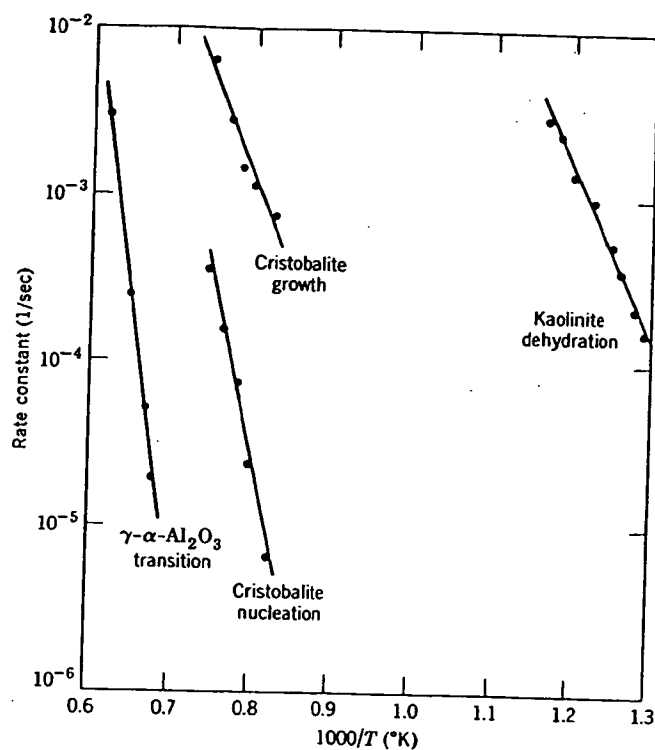


Fig. 9.38. Temperature dependence of rate of (a) nucleation, (b) growth of cristobalite from silica gel, (c) formation of α - Al_2O_3 , and (d) dehydration of kaolinite.

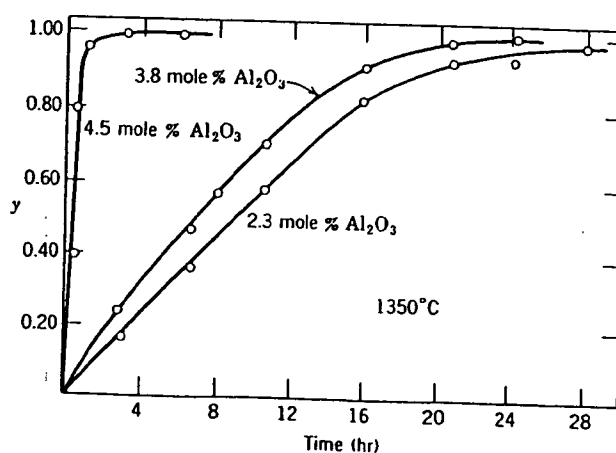


Fig. 9.39. The fractional precipitation y of spinel as a function of time at 1350°C . Specimens prepared at 1950°C . From V. S. Stubican and D. J. Viechnicki, *J. Appl. Phys.*, 37, 2751 (1966).

intermediate with product* which product, α -alumina metastable prealumina. After the expense of the

Synthetic statitaniferous pre-0.3% TiO_2 . Whence causes the times for precipitation at 1500°C . The latter as for precipitation equilibrium phase

Strong orientation believed to exhibit SnO_2 - TiO_2 system 5-min anneal at corner of Fig. 9 to the 001 direction formed by spinel Al_2O_3 - Cr_2O_3 and this manner. As spinel phase from large metal deficiency (Chapter 4) is by agglomerates in forming the spinel the resulting high in this and relative 300°C . On cooling defect clusters,

When growth change, the rate the morphology dissipated or more inverse radius of dendritic forms remaining small

* H. Jagodzinski (1962).

intermediate with a structure similar to spinel as the first precipitation product* which is more easily nucleated than the stable equilibrium product, α -alumina. In fact, as shown in Fig. 9.40, two different types of metastable precipitates initially form, plus a smaller amount of α -alumina. After long annealing at 850°C the α -alumina particles grow at the expense of the metastable intermediate precipitates.

Synthetic star sapphires are produced by precipitating an alumina-rich titaniferous precipitate from single crystals of sapphire containing 0.1 to 0.3% TiO_2 . When viewed in the direction of the c -axis stellate opalescence causes the reflected light to form a well-defined six-ray star. Aging times for precipitation range from approximately 72 hr at 1100°C to 2 hr at 1500°C. The lath-shaped precipitates formed are illustrated in Fig. 9.41. As for precipitation from spinel, the precipitate particle formed is not the equilibrium phase (Al_2TiO_5) but a metastable product.

Strong orientation effects are also observed in systems which are believed to exhibit spinodal decomposition, shown in Fig. 9.42, for the SnO_2 - TiO_2 system in which a lamellar microstructure is formed after a 5-min anneal at 1000°C. The electron diffraction pattern at the lower corner of Fig. 9.42 shows streaking of the diffraction spots perpendicular to the 001 direction, which is to be expected for the periodic structure formed by spinodal decomposition. Other crystalline systems such as Al_2O_3 - Cr_2O_3 and CoFe_2O_4 - Co_3O_4 are also believed to phase separate in this manner. A similar structure, Fig. 9.43, is found for precipitation of the spinel phase from an FeO - MnO solid solution at low temperature. The large metal deficit in this highly nonstoichiometric system (discussed in Chapter 4) is believed to result in defect association on cooling; defect agglomerates may serve as nucleation sites for the precipitation reaction forming the spinel phase. Because of the high defect concentration and the resulting high diffusivity of the cations, precipitation processes occur in this and related systems at quite low temperatures, in this case about 300°C. On cooling a sample, it is not possible to prevent the formation of defect clusters, even with the most rapid quench.

When growth is rapid or occurs at low temperatures with a composition change, the rate of flow of heat or material limits the growth rate and fixes the morphology. Under these conditions the rate at which heat is dissipated or material added to a growing precipitate is proportional to the inverse radius of curvature of the growing tip of the crystal. As a result, dendritic forms result, with the radius of curvature of the growing tip remaining small and side arms developing to form a treelike structure.

* H. Jagodzinski, *Z. Krist.*, **109**, 388 (1957), and H. Saalfeld, *Ber. Deut. Keram. Ges.*, **39**, 52 (1962).

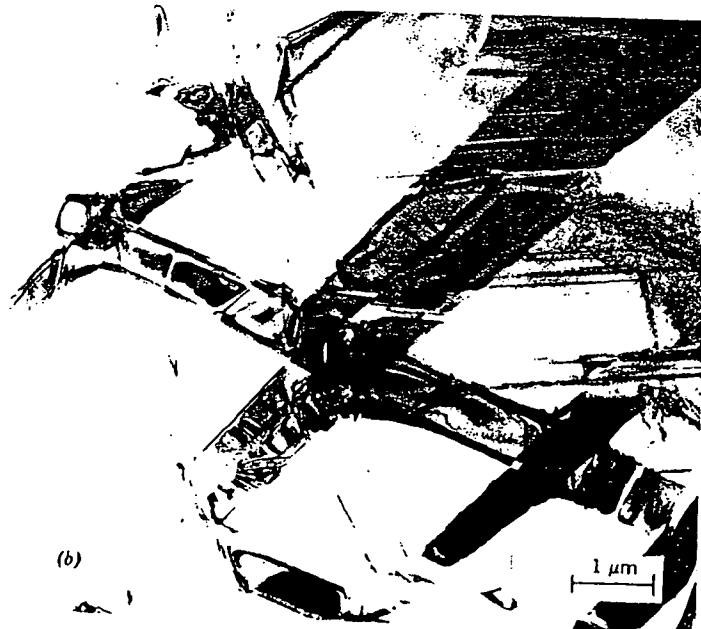


Fig. 9.40. (a) Metastable precipitates I and II first form along with $\alpha\text{-Al}_2\text{O}_3$ (A) on annealing spinel at 850°C; (b) after long times the $\alpha\text{-Al}_2\text{O}_3$ particles coarsen at the expense of the intermediate precipitates. Courtesy G. K. Bansal and A. Heuer.

Fig. 9.4
Courtes

Deper
illustr
basic
tion c
along
long p
rate-d
graph
limite
period
spher
minin
Het
that p
when
may s
precip
grain
wüsti

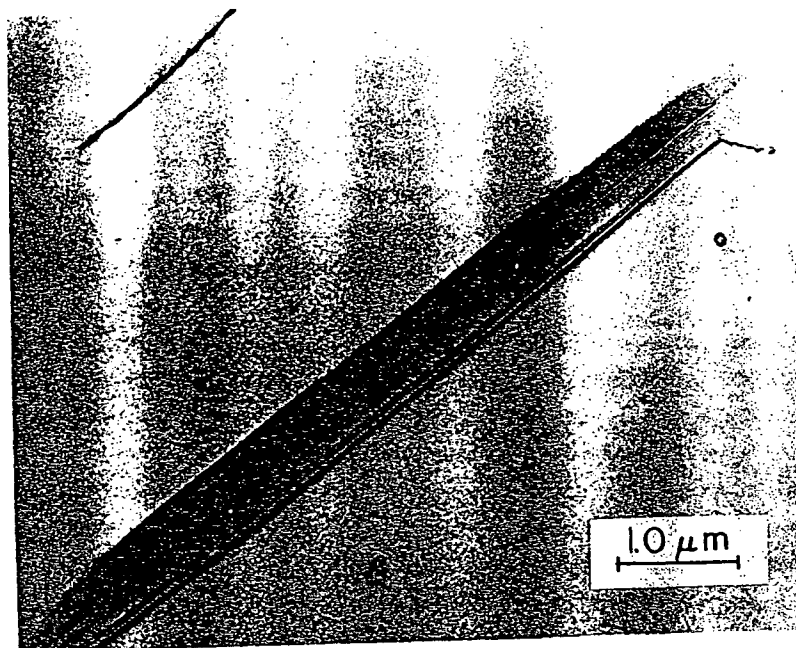


Fig. 9.41. Lath-shaped crystallographically oriented precipitate particles in star sapphire. Courtesy B. J. Pletka and A. Heuer.

Depending on the conditions of formation, different structures arise, as illustrated for the precipitation of magnesioferrite from magnesia in a basic refractory brick (Fig. 9.44). Sometimes a crystallographic orientation of the precipitate occurs in which the platelets of MgFe_2O_4 form along (100) planes in the parent magnesia phase. On precipitation during long periods of time at a lower temperature at which diffusion is probably rate-determining, dendritic precipitates form which still have crystallographic orientations with the matrix but in which the rate of growth is limited, so that starlike crystals result (Fig. 9.45b); finally, after long periods at the higher temperature levels, there is a tendency for a spheroidal precipitate to develop in which the total surface energy is a minimum and the strain energy may be relieved by plastic flow.

Heterogeneous Precipitation. It is frequently observed (Fig. 9.45a) that precipitation of a new phase occurs primarily along grain boundaries; when more extensive precipitation occurs (Fig. 9.45b) grain boundaries may show precipitates surrounded by an area of material which is nearly precipitation free. This can result from heterogeneous nucleation at the grain boundary, although in the case of precipitation of Fe_3O_4 from wüstite the microstructure observed at low magnifications results primar-

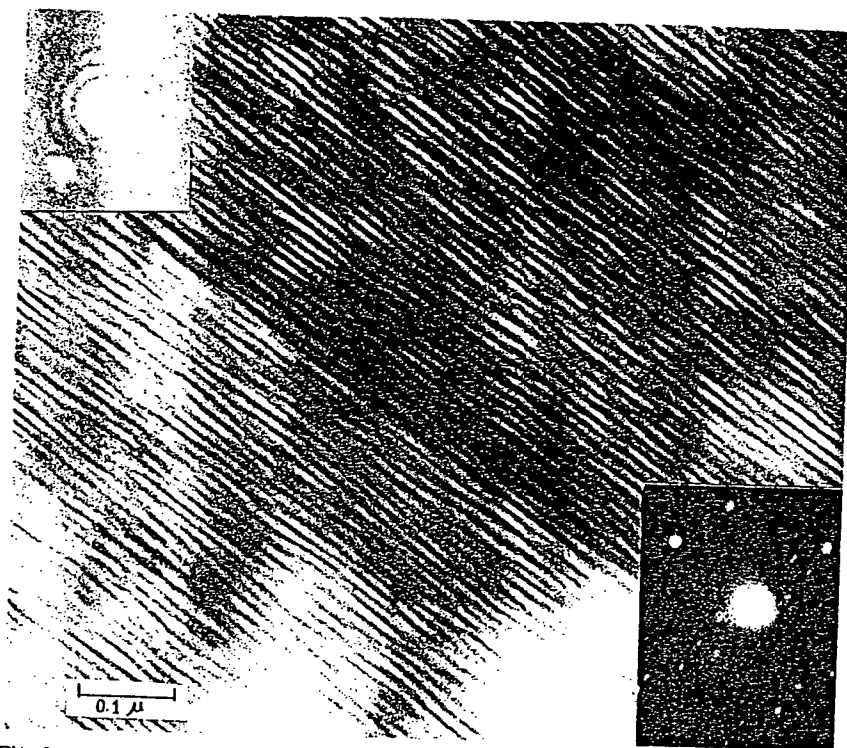


Fig. 9.42. Equimolar $\text{TiO}_2\text{-SnO}_2$ crystal homogenized at 1600°C and annealed 5 min at 1000°C . Electron diffraction pattern in lower right; optical diffraction pattern in upper left. Courtesy M. Park and A. Heuer.

ily from differences in the growth rate adjacent to grain boundaries rather than from a nucleation process. In this system the grain boundaries act as high diffusivity paths, discussed in Chapter 6, which allow nuclei at the grain boundary to grow initially at a faster rate than nuclei in the bulk, which tends to denude the area adjacent to the grain boundary of solute; at later stages in the precipitation process (Fig. 9.45b) there is an area adjacent to the grain boundaries which tends to be precipitate free. In this system, as for many of those previously described, the precipitate particles are coherent with the matrix crystal, and all have the same orientation in each grain of wüstite.

For samples in which solubility is small, direct observation of grain boundaries and dislocations indicates that second-phase precipitation at these sites is very common indeed. Particularly for many systems containing silicates as minor impurities, coherency is not to be expected;

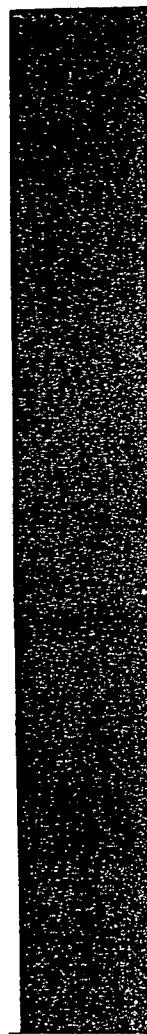


Fig. 9.43. L...
Courtesy C.1.



led 5 min at
n upper left.

ries rather
ries act as
clei at the
the bulk,
of solute;
is an area
ee. In this
recipitate
the same

1 of grain
itation at
systems
expected;



Fig. 9.43. Low-temperature precipitate of spinel phase from FeO-MnO solid solution.
Courtesy C. A. Goodwin, Ph.D. Thesis, MIT, 1973.

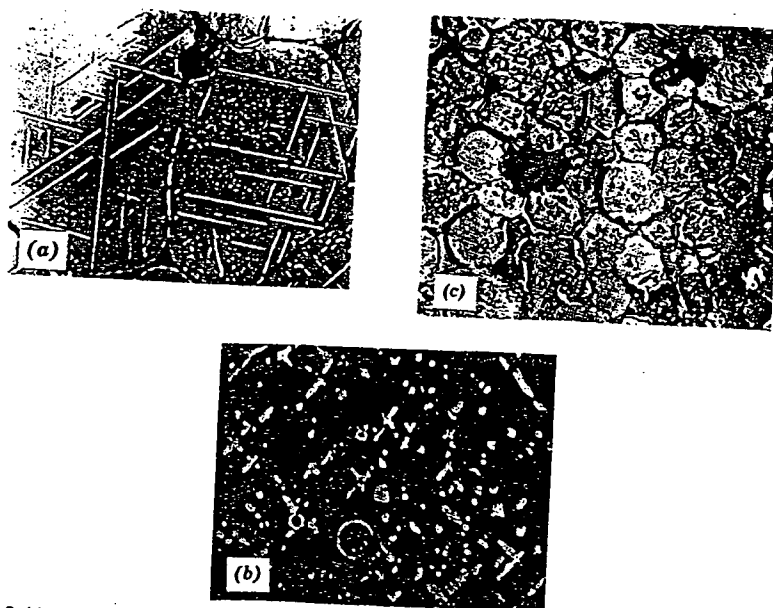


Fig. 9.44. Precipitation of MgFe_2O_4 from MgO in basic refractory brick as (a) platelets parallel to (100) planes in MgO (500 \times); (b) dendritic precipitate (975 \times); (c) spheroidal morphology (232 \times). Courtesy F. Trojer and K. Konopicky, *Radex Rdsch.*, 7, 8, 149 (1948), and B. Tavasci, *Radex Rdsch.*, 7, 245 (1949).

the smaller driving force and larger energy barrier to nucleation enhances the importance of heterogeneous nucleation and growth at dislocations and grain boundaries, as illustrated in Fig. 9.46.

9.6 Nonisothermal Processes

We have considered diffusional processes as they occur under isothermal conditions; however, many ceramic processing procedures include substantial nonisothermal periods. One important example of the effect of nonisothermal kinetic processes is the segregation and precipitation of impurities at grain boundaries while a specimen cools from a high temperature.*

If we assume that over the temperature range of interest, the diffusion coefficient is given by

$$D = D_0 e^{-Q/RT}$$

*See W. D. Kingery, *J. Am. Ceram. Soc.*, 57, 1 (1974).

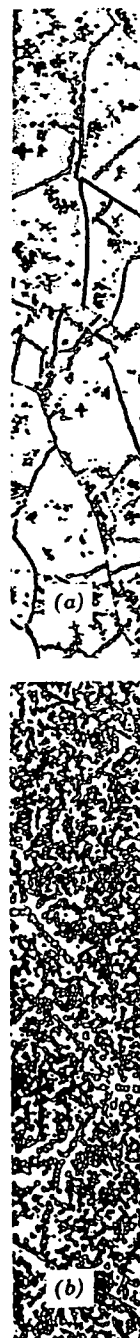


Fig. 9.45. Precipitation of MgFe_2O_4 from MgO in basic refractory brick as (a) platelets parallel to (100) planes in MgO (500 \times); (b) dendritic precipitate (975 \times).



ck as (a) platelets
×); (c) spheroidal
7, 8, 149 (1948), and

tion enhances
at dislocations

under isother-
dures include
of the effect of
ecipitation of
from a high

. the diffusion

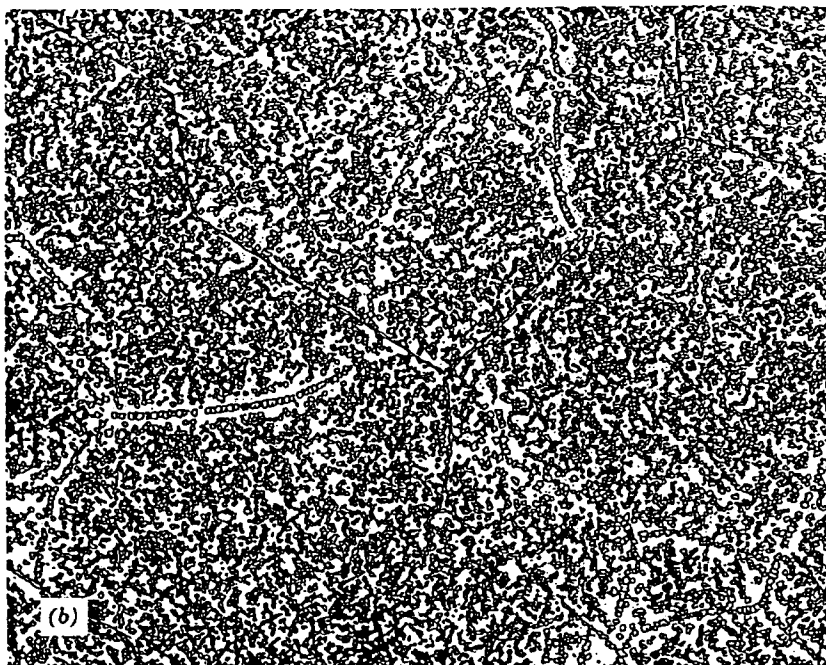


Fig. 9.45. Precipitate of Fe_3O_4 from wustite (Fe_xO) containing (a) 52.67 and (b) 53.10 atom % oxygen (95×). Courtesy L. Himmel.

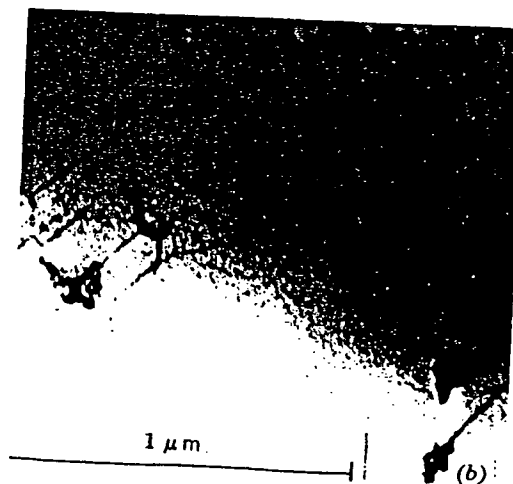
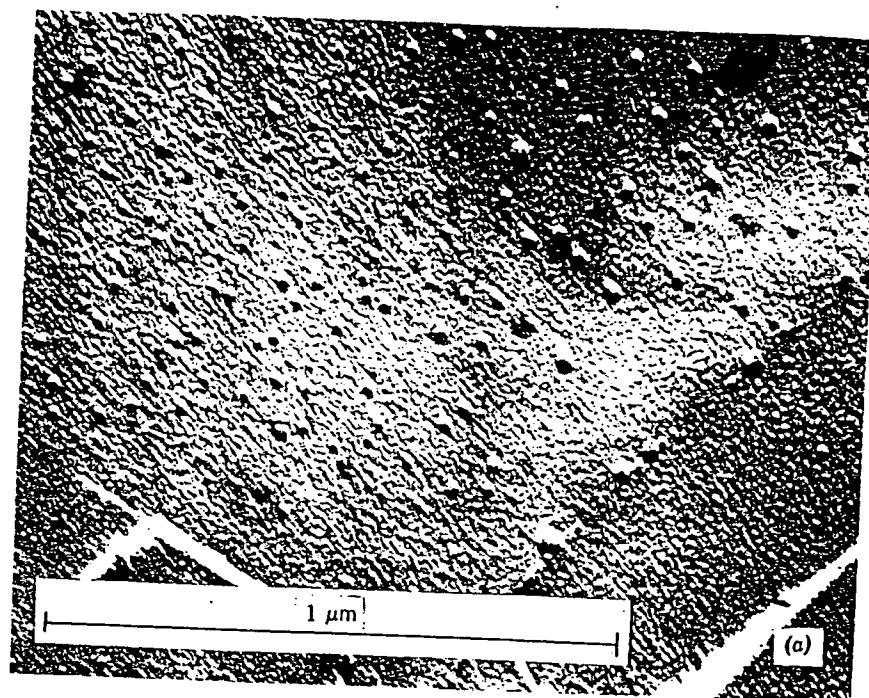


Fig. 9.46. (a) Manganese zinc ferrite containing 0.042% SiO_2 , heated 4 hr at 1200°C in $\text{N}_2 + 1\% \text{O}_2$, showing SiO_2 inclusions at grain-boundary fracture. Courtesy M. Paulus. (b) Precipitate particles at dislocations in MgO . Courtesy N. J. Tighe.

and we
the tin

An ap

Let us
 MgO .
to the g
because
6.4). Fr
to 75 l
diffusio
contain
limit at
assume
yields :
calcula
 $D \approx 5 :$

Ther
during
sed in
granula
finally
describ
tions.

First
9.63) in
determ
The re:
 CaCO_3

and we assume the temperature to vary from T_1 to T_2 at a linear rate of α , the time-dependent diffusion coefficient is

$$D = D_0 \exp \left[\frac{Q/R}{T_1 - \alpha T} \right] \quad (9.88)$$

An approximate diffusion length l may be estimated from the integral;

$$l^2 = D_0 \int_0^t \exp \left(\frac{-Q/R}{T_1 - \alpha t} \right) dt \quad (9.89)$$

$$l^2 \approx \frac{D_0 R}{\alpha Q} (T_1^2 e^{-Q/RT_1} - T_2^2 e^{-Q/RT_2}) \quad (9.90)$$

$$l^2 \approx \frac{R}{\alpha Q} [D_1 T_1^2 - D_2 T_2^2]$$

Let us consider, as an example of the use of Eq. 9.89, Al_2O_3 impurities in MgO . The diffusion of supersaturated aluminum ions from within a grain to the grain boundary is essentially that for the defect diffusion (vacancy) because of the impurity-vacancy pair which tends to form (see Section 6.4). From the data of impurity diffusion into MgO a value of 2 to 3 eV (50 to 75 kcal/mole) seems a reasonable activation energy for vacancy diffusion. Assume a sample of MgO annealed at high temperature contains 100 ppm Al_2O_3 . If the sample is cooled at $0.1^\circ\text{C}/\text{sec}$, the solubility limit at 1300°C produces the onset of grain-boundary precipitation. For an assumed diffusivity of $10^{-8} \text{ cm}^2/\text{sec}$ at 1300°C and $Q = 2 \text{ eV}$, Eq. 9.89 yields a value of 30 microns for the effective diffusion distance. A similar calculation for 100 ppm MgO in Al_2O_3 ($T_s = 1530^\circ\text{C}$, $Q \approx 3 \text{ eV}$, and $D \approx 5 \times 10^{-8} \text{ cm}^2/\text{sec}$) yields a segregation thickness of 60 microns.

There are many other examples of ceramic processes which occur during nonisothermal annealing. As porcelain or refractories are processed in production kilns, much of the densification and reaction between granular components takes place during the heating cycle. We consider finally two examples of nonisothermal kinetic processes which are described in detail in Section 9.4 and Section 10.3 for isothermal conditions.

First, let us consider the nonisothermal decomposition reaction (Eq. 9.63) in which CaCO_3 decomposes to CaO and CO_2 . The reaction rate is determined by decomposition at the surface and obeys linear kinetics. The reaction rate R is equal to the change in weight per unit area of the CaCO_3 with time, $d(\omega/a)/dt$. Thus Eq. 9.4 can be rewritten

$$\frac{d(\omega/a)}{dt} = R = \frac{kT}{h} \exp \left(\frac{\Delta S^\ddagger}{R} \right) \exp \left(-\frac{\Delta H^\ddagger}{RT} \right) = A \exp \left(-\frac{\Delta H^\ddagger}{RT} \right) \quad (9.91)$$

at 1200°C in
I. Paulus. (b)

If the temperature of the CaCO_3 is changed at a constant rate, $T = \alpha t$, the weight change as a function of temperature is obtained from

$$\frac{d(\omega/a)}{dT} = \frac{A}{\alpha} \exp\left(-\frac{\Delta H^\ddagger}{RT}\right) \quad (9.92)$$

The integration of Eq. 9.92, assuming that A is not a strong function of temperature, yields the approximate solution

$$\frac{\Delta\omega}{\omega_0} \approx \frac{ART^2}{\alpha \Delta H^\ddagger} \exp\left(-\frac{\Delta H^\ddagger}{RT}\right) \quad (9.93)$$

The form of the equation is similar to Eq. 9.89. A plot of the non-isothermal decomposition in vacuum of a single crystal of CaCO_3 is given in Fig. 9.47. For this reaction and for several other endothermic decomposition reactions the activation energy for decomposition is identical with the heat of reaction (Eq. 9.63).

As a final example of nonisothermal kinetic processes consider the sintering of glass spheres (discussed in Chapter 10). The shrinkage rate $\frac{d(\Delta L/L_0)}{dt}$, which is a function of the surface tension γ , the viscosity $\eta = B e^{Q/RT}$, and the particle radius a , can be determined from nonisother-

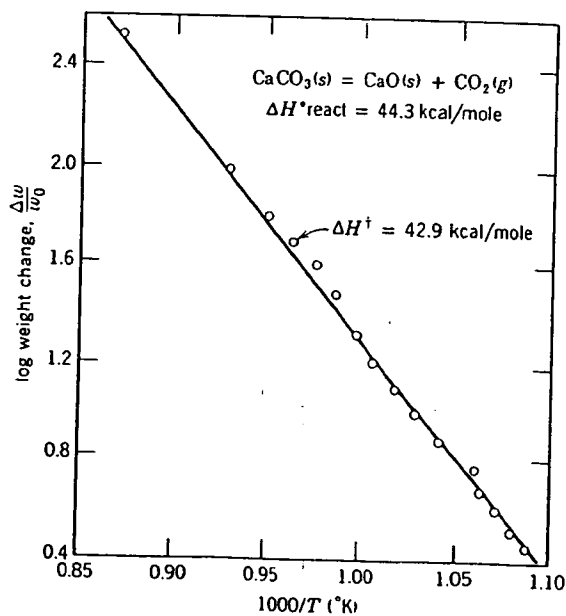


Fig. 9.47. Nonisothermal decomposition of CaCO_3 in vacuum.

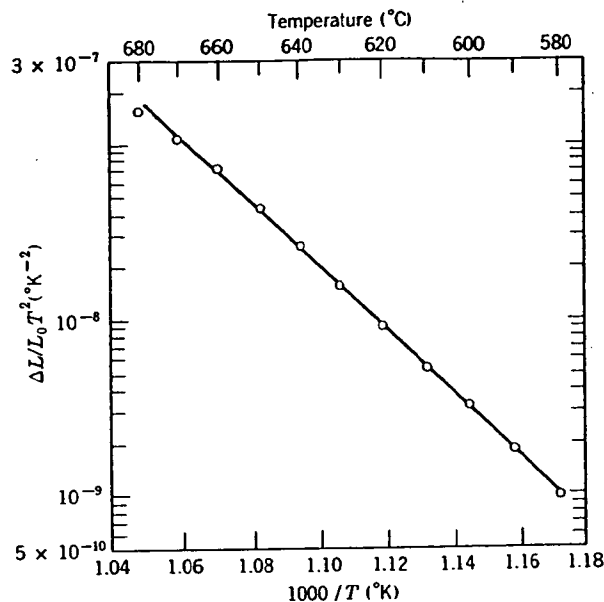
Fig.
silica

mal

Kin
25-1
wat

1.
2.
3.
4.

*



5. P. Kofstad, *Nonstoichiometry, Diffusion, and Electrical Conductivity in Binary Metal Oxides*, John Wiley & Sons, New York, 1972.
6. For a discussion of dissolution kinetics see A. R. Cooper, Jr., B. N. Samaddar, Y. Oishi, and W. D. Kingery, *J. Am. Ceram. Soc.*, **47**, 37 (1964); **47**, 249 (1964); and **48**, 88 (1965).
7. G. M. Schwab, Ed., *Reactivity of Solids*, Elsevier Publishing Company, New York, 1965.
8. W. D. Kingery, Ed., *Kinetics of High Temperature Processes*, John Wiley & Sons, New York, 1959.
9. M. E. Fine, *Introduction to Phase Transformations in Condensed Systems*, McGraw-Hill, New York, 1964; *Bull. Am. Ceram. Soc.*, **51**, 510 (1972).

Problems

- 9.1. Rates of solution can be controlled by (a) diffusion in the liquid, (b) diffusion through a reaction layer, or (c) phase-boundary reaction. How would you distinguish these?
- 9.2. While measuring the rate of decomposition of alumina monohydrate, a student finds the weight loss to increase linearly with time up to about 50% reacted during an isothermal experiment. Beyond 50%, the rate of the weight loss is less than linear. The linear isothermal rate increases exponentially with temperature. An increase of temperature from 451 to 493°C increases the rate tenfold. Compute the activation energy. Is this a diffusion-controlled reaction, a first-order reaction, or an interface-controlled reaction?
- 9.3. Consider formation of NiCr_2O_4 from spherical particles of NiO and Cr_2O_3 , when the rate is controlled by diffusion through the product layer.
 - (a) Carefully sketch an assumed geometry, and then derive a relation for the rate of formation early in the process.
 - (b) What governs the particles on which the product layer forms?
 - (c) At 1300°C, $D_{\text{Cr}} > D_{\text{Ni}} > D_{\text{O}}$ in NiCr_2O_4 . Which controls the rate of formation of NiCr_2O_4 ? Why?
- 9.4. Polymorphic transformations in solids result in polycrystalline materials of small size (fine-grained) or large size (coarse-grained), depending on the rates of nucleation and nuclei growth. How do these rates vary to produce fine-grained and coarse-grained products? Draw a time versus size for an individual grain illustrating the growth of a fine grain compared to a coarse grain. Start the time on the time axis at the moment of transformation.
- 9.5. According to Alper *et al.* [*J. Am. Ceram. Soc.*, **45**(6) 263-66 (1962)], Al_2O_3 is soluble in MgO to the extent of 3% by weight at 1700°C, 7% at 1800°C, 12% at 1900°C, and 0% at 1500°C. They observed crystallization of spinel crystals from the solid solution region on slow cooling. Fast quenching retained the solid solution as a single phase at room temperature. The exsolved spinel appeared uniformly without regard to grain boundaries within the periclase grains but on specific planes. (a) Is the nucleation of spinel homogeneous or heterogeneous within the periclase grains? (b) Account for the appearance of spinel crystals along specific planes of periclase crystals. Predict the shape of the rate of crystallization versus temperature for nucleated periclase solid solution containing 5% Al_2O_3 , over the temperature range 0°C to 1850°C.

- 9.6. In the previous problem, we described a solid solution of Al_2O_3 in MgO . Assuming a manufacturer of basic refractories uses MgO contaminated with 5 to 7% Al_2O_3 , what microstructure differences will exist in slow-cooled refractory compared to fast-cooled material? Would you predict sintering by self-diffusion (bulk), grain growth, and cation diffusion in this material would be different than in pure MgO ? Why?
- 9.7. Suppose that the formation of mullite from alumina and silica powder is a diffusion-controlled process. How would you prove it? If the activation energy is 50 kcal/mole and the reaction proceeds to 10% of completion at 1400°C in 1 hr, how far will it go in 1 hr at 1500°C ? in 4 hr at 1500°C ?
- 9.8. An amorphous SiO_2 film on SiC builds up, limiting further oxidation. The fraction of complete oxidation was determined by weight gain measurements and found to obey a parabolic oxidation law. For a particular-particle-sized SiC and pure O_2 the following data were obtained. Determine the apparent activation energy in kcal/mole. How can it be shown that this is a diffusion-controlled reaction?

Temp ($^\circ\text{C}$)	Fraction Reacted	Time (hr)
903	2.55×10^{-2}	100
1135	1.47×10^{-2}	10
	4.26×10^{-2}	100
1275	1.965×10^{-2}	10
	6.22×10^{-2}	100
1327	1.50×10^{-2}	5
	4.74×10^{-2}	50

- 9.9. The slow step in the precipitation of BaSO_4 from aqueous solution is the interface addition of the individual Ba^{++} and SO_4^{--} . Diffusion to the surface is assumed sufficiently fast that we may neglect any concentration differences in the solution. Assume that the rate of addition is first-order in both Ba^{++} and SO_4^{--} .
- Derive an expression for the approach to equilibrium in terms of the rate constants for the forward and back reaction and the surface area.
 - What is the effect of an excess of Ba^{++} ?
 - Why can you assume the surface area to be constant?
 - How would you modify your approach to include a correction for diffusion?
- 9.10. One-micron spheres of Al_2O_3 are surrounded by excess MgO powder in order to observe the formation of spinel. Twenty percent of the Al_2O_3 was reacted to form spinel during the first hour of a constant-temperature experiment. How long before all the Al_2O_3 will be reacted? Compute the time for completion on the basis of (a) no spherical geometry correction and (b) the Jander equation for correction of spherical geometry.
- 9.11. In fired chrome ore refractories, an R_2O_3 phase precipitates as platelets in the spinel phase matrix. Write the chemical equation for this reaction, and explain why it occurs. The precipitate is oriented so that the basal plane in the R_2O_3 phase is parallel to the (111) plane in the spinel. Explain why this should occur in terms of crystal structure.

Grain Growth, Sintering, and Vitrification

We have previously discussed phase changes, polymorphic transformations, and other processes independent of, or subsequent to, the fabrication of ceramic bodies. Phenomena that are of great importance are the processes taking place during heat treatment before use; these are the subject of this chapter.

During the usual processing of ceramics, crystalline or noncrystalline powders are compacted and then fired at a temperature sufficient to develop useful properties. During the firing process changes may occur initially because of decomposition or phase transformations in some of the phases present. On further heating of the fine-grained, porous compact, three major changes commonly occur. There is an increase in grain size; there is a change in pore shape; there is change in pore size and number, usually to give a decreased porosity. In many ceramics there may be solid-state reactions forming new phases, polymorphic transformations, decompositions of crystalline compounds to form new phases or gases, and a variety of other changes which are frequently of great importance in particular cases but are not essential to the main stream of events.

We shall be mainly concerned with developing an understanding of the major processes taking place. There are so many things which can happen, and so many variables that are occasionally important, that no mere cataloging of phenomena can provide a sound basis for further study. In general, we shall be concerned first with recrystallization and grain-growth phenomena, second with the densification of single-phase systems, and finally with more complex multiphase processes. There are many important practical applications for each of these cases.

10.1 Recrystallization

The terms *recrystallization* and *secondary recrystallization* have been used to describe grain growth and other phenomena. The terms are mainly confused because *recrystallization* is the generation of a new grain structure from a plastically deformed grain structure. *Secondary recrystallization* is the generation of a new grain structure from a grain structure that has grown during primary recrystallization. *Secondary recrystallization* is the growth of a grain at the expense of other grains. Although all these processes are secondary recrystallization, the term *secondary recrystallization* is used to describe the growth of a grain at the expense of other grains.

Primary Recrystallization is the growth of a grain at the expense of other grains. It is characterized by an increase in grain size and a decrease in energy stored in the material. Although this process is a change in grain size, it is not a change in energy.

If the material is deformed at a constant rate, the grain size is d ,

where U is the time period. This process is characterized by a decrease in grain size and a decrease in energy stored in the material. The nucleation process is determined by the grain size.

The nucleation process is determined by the grain size. The nucleation process is determined by the grain size. The nucleation process is determined by the grain size. The nucleation process is determined by the grain size.

10.1 Recrystallization and Grain Growth

The terms recrystallization and grain growth have had a very broad and indefinite usage in much of the ceramic literature; they have sometimes been used to include phase changes, sintering, precipitation, exsolution, and other phenomena which produce changes in the microstructure. We are mainly concerned with three quite distinct processes. *Primary recrystallization* is the process by which nucleation and growth of a new generation of strainfree grains occurs in a matrix which has been plastically deformed. *Grain growth* is the process by which the average grain size of strainfree or nearly strainfree material increases continuously during heat treatment without change in the grain-size distribution. *Secondary recrystallization*, sometimes called abnormal or discontinuous grain growth, is the process by which a few large grains are nucleated and grow at the expense of a fine-grained, but essentially strain-free, matrix. Although all these processes occur in ceramic materials, grain growth and secondary recrystallization are the ones of major interest.

Primary Recrystallization. This process has as its driving force the increased energy of a matrix which has been plastically deformed. The energy stored in the deformed matrix is of the order of 0.5 to 1 cal/g. Although this is small compared with the heat of fusion, for example (which is a 1000 or more times this value), it provides a sufficient energy change to effect grain-boundary movement and changes in grain size.

If the isothermal change in grain size of strainfree crystals in a deformed matrix is measured after an initial induction period, there is a constant rate of grain growth for the new strainfree grains. If the grain size is d ,

$$d = U(t - t_0) \quad (10.1)$$

where U is the growth rate (cm/sec), t is the time, and t_0 is the induction period. This is illustrated in Fig. 10.1 for recrystallization of a sodium chloride crystal which had been deformed at 400°C and then annealed at 470°C. The induction period corresponds to the time required for a nucleation process, so that the overall rate of recrystallization is determined by the product of a nucleation rate and a growth rate.

The nucleation process is similar to those discussed in Chapter 8. For a nucleus to be stable, its size must be larger than some critical diameter at which the lowered free energy of the new grain is equal to the increased surface free energy. The induction period corresponds to the time required for unstable embryos present to grow to the size of a stable nucleus. If an unlimited number of sites is available, the rate of nucleation increases to some constant rate after an initial induction period. In

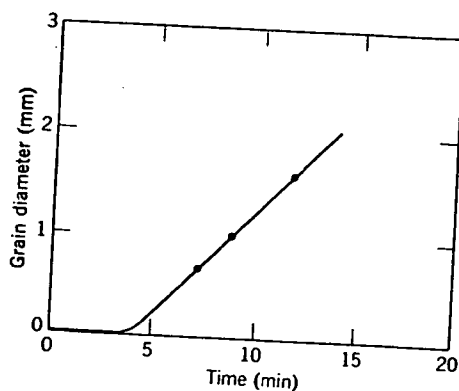


Fig. 10.1. Recrystallization of NaCl deformed at 400°C (stress = 4000 g/mm²) and recrystallized at 470°C. From H. G. Muller, *Z. Phys.*, 96, 279 (1935).

practice the number of favorable sites available is limited, and the rate of nucleation passes through a maximum as they are used up. H. G. Müller* observed that nuclei in sodium chloride tended to form first at grain corners, for example. As the temperature is increased, the rate of nucleation increases exponentially:

$$\frac{N}{dt} = N_0 \exp\left(-\frac{\Delta G_N}{RT}\right) \quad (10.2)$$

where N is the number of nuclei and ΔG_N is the experimental free energy for nucleation. Consequently, the induction period, $t_0 \sim 1/(dN/dt)$, decreases rapidly as the temperature level is raised.

As indicated in Eq. 10.1, the growth rate remains constant until the grains begin to impinge on one another. The constant in growth rate results from the constant driving force (equal to the difference in energy between the strained matrix and strainfree crystals). The final grain size is determined by the number of nuclei formed, that is, the number of grains present when they finally impinge on one another. The atomistic process necessary for grain growth is the jumping of an atom from one side of a boundary to the other and is similar to a diffusional jump in the boundary. Consequently the temperature dependence is similar to that of diffusion:

$$U = U_0 \exp\left(-\frac{E_U}{RT}\right) \quad (10.3)$$

where the activation energy E_U is normally intermediate between that for boundary and lattice diffusion. The growth-rate-temperature curve for

**Z. Phys.*, 96, 279 (1935).

recrystalliza
for diffusio

Since bot
temperature
rapidly with
different ter
recrystalliza
of cold worl
temperature
grains on on
and growth.
since the gr
However, a
rapidly, so
ments (Fig.
growth follo
creasing an
whereas the

In genera
required for
higher temp
increased at

recrystallization of sodium chloride has a knee similar to that observed for diffusion and conductivity data, as discussed in Chapter 6.

Since both the nucleation rate and the growth rate are strongly temperature-dependent, the overall rate of recrystallization changes rapidly with temperature. For a fixed holding time, experiments at different temperatures tend to show either little or nearly complete recrystallization. Consequently, it is common to plot data as the amount of cold work or the final grain size as a function of the *recrystallization temperature*. Since the final grain size is limited by impingement of the grains on one another, it is determined by the relative rates of nucleation and growth. As the temperature is raised, the final grain size is larger, since the growth rate increases more rapidly than the rate of nucleation. However, at higher temperatures recrystallization is completed more rapidly, so that the larger grain size observed in constant-time experiments (Fig. 10.2) may be partly due to the greater time available for grain growth following recrystallization. The growth rate increases with increasing amounts of plastic deformation (increased driving force), whereas the final grain size decreases with increasing deformation.

In general, it is observed that (1) some minimum deformation is required for recrystallization, (2) with a small degree of deformation a higher temperature is required for recrystallization to occur, (3) an increased annealing time lowers the temperature of recrystallization, and

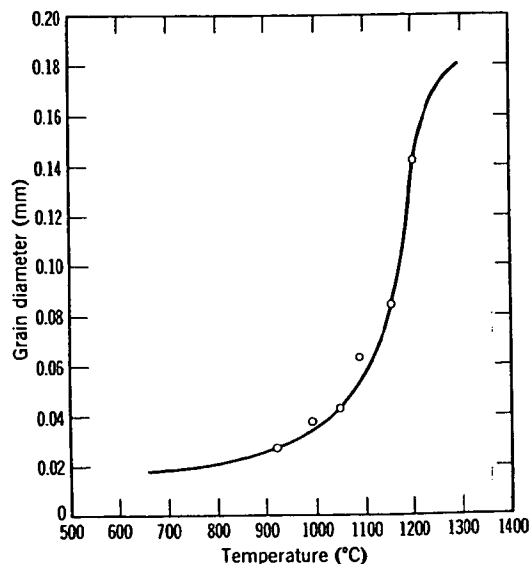


Fig. 10.2. Effect of annealing temperature on grain size of CaF_2 following compression at 80,000 psi and 10 hr at temperature. From M. J. Buerger, *Am. Mineral.*, 32, 296 (1947).

(4) the final grain size depends on the degree of deformation, the initial grain size, and the temperature of recrystallization. In addition, continued heat after recrystallization is completed leads to the continuation of grain growth.

Primary recrystallization is particularly common in metals which are extensively deformed in normal processing techniques. Ceramic materials are seldom plastically deformed during processing, so that primary recrystallization is not commonly observed. For relatively soft materials, such as sodium chloride or calcium fluoride, deformation and primary recrystallization do occur. It has also been observed directly in magnesium oxide; also, the polygonization process described in Chapter 4 (see Fig. 4.24) for aluminum oxide has many points of similarity.

Grain Growth. Whether or not primary recrystallization occurs, an aggregate of fine-grained crystals increases in average grain size when heated at elevated temperatures. As the average grain size increases, it is obvious that some grains must shrink and disappear. An equivalent way of looking at grain growth is as the rate of disappearance of grains. Then the driving force for the process is the difference in energy between the fine-grained material and the larger-grain-size product resulting from the decrease in grain-boundary area and the total boundary energy. This energy change corresponds to about 0.1 to 0.5 cal/g for the change from a 1-micron to a 1-cm grain size.

As discussed in Chapter 5, an interface energy is associated with the boundary between individual grains. In addition, there is a free-energy difference across a curved grain boundary which is given by

$$\Delta G = \gamma \bar{V} \left(\frac{1}{r_1} + \frac{1}{r_2} \right) \quad (10.4)$$

where ΔG is the change in free energy on going across the curved interface, γ is the boundary energy, \bar{V} is the molar volume, and r_1 and r_2 are the principal radii of curvature. (This relationship has been derived and discussed in Chapter 5. That part of Chapter 5 should be reviewed if its meaning is not clear.) This difference in the free energy of material on the two sides of a grain boundary is the driving force that makes the boundary move toward its center of curvature. The rate at which a boundary moves is proportional to its curvature and to the rate at which atoms can jump across the boundary.

Grain growth provides an opportunity to apply the absolute-reaction-rate theory already discussed in Chapter 6. If we consider the structure of a boundary (Fig. 10.3), the rate of the overall process is fixed by the rate at which atoms jump across the interface. The change in energy with an atom's position is shown in Fig. 10.3b, and the frequency of atomic jumps

Fig.

in the

and the

so that
jump i

and s

 $\Delta H^\ddagger -$ which
of gro
volved
energy
bound

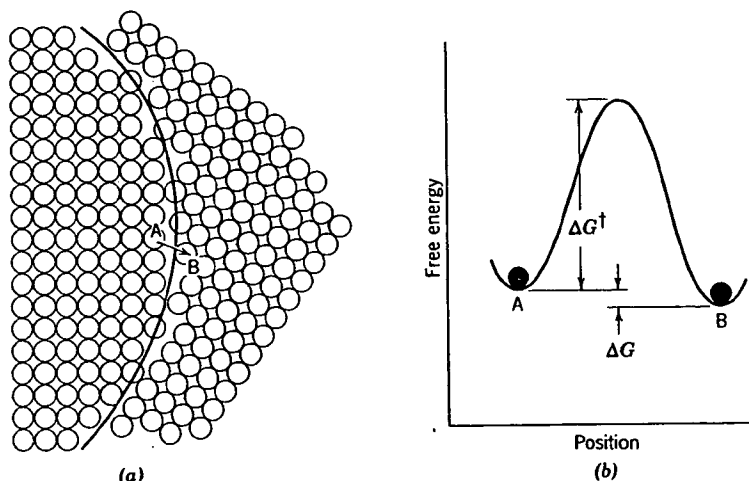


Fig. 10.3. (a) Structure of boundary and (b) energy change for atom jump.

in the forward direction is given by

$$f_{AB} = \frac{RT}{Nh} \exp\left(-\frac{\Delta G^\ddagger}{RT}\right) \quad (10.5)$$

and the frequency of reverse jumps is given by

$$f_{BA} = \frac{RT}{Nh} \exp\left(-\frac{\Delta G^\ddagger + \Delta G}{RT}\right) \quad (10.6)$$

so that the net growth process, $U = \lambda f$, where λ is the distance of each jump is given by

$$U = \lambda f = \lambda (f_{AB} - f_{BA}) = \frac{RT}{Nh} (\lambda) \exp\left(-\frac{\Delta G^\ddagger}{RT}\right) \left(1 - \exp\frac{\Delta G}{RT}\right) \quad (10.7)$$

and since $1 - \exp\frac{\Delta G}{RT} \approx \frac{\Delta G}{RT}$, where $\Delta G = \gamma \bar{V} \left(\frac{1}{r_1} + \frac{1}{r_2}\right)$ and $\Delta G^\ddagger = \Delta H^\ddagger - T \Delta S^\ddagger$,

$$U = \left(\frac{RT}{Nh}\right) (\lambda) \left[\frac{\gamma \bar{V}}{RT} \left(\frac{1}{r_1} + \frac{1}{r_2}\right)\right] \exp\frac{\Delta S^\ddagger}{R} \exp\left(-\frac{\Delta H^\ddagger}{RT}\right) \quad (10.8)$$

which is equivalent in form to Eq. 10.3 given previously. That is, the rate of growth increases exponentially with temperature. The unit step involved is the jump of an atom across the boundary, so that the activation energy should correspond approximately to the activation energy for boundary diffusion.

If all the grain boundaries are equal in energy, they meet to form angles of 120° . If we consider a two-dimensional example for illustrative purposes, angles of 120° between grains with straight sides can occur only for six-sided grains. Grains with fewer sides have boundaries that are concave when observed from the center of the grain. Shapes of grains having different numbers of sides are illustrated in Fig. 10.4; a sample with uniform grain size is shown in Fig. 10.5. Since grain boundaries migrate toward their center of curvature, grains with less than six sides tend to grow smaller, and grains with more than six sides tend to grow larger. For any one grain, the radius of curvature of a side is directly proportional to the grain diameter, so that the driving force, and therefore the rate of grain growth, is inversely proportional to grain size:

$$\dot{d} = \frac{d(d)}{dt} = \frac{k}{d} \quad (10.9)$$

and integrating,

$$d - d_0 = (2k)^{1/2} t^{1/2} \quad (10.10)$$

where d_0 is the grain diameter at time zero. Experimentally it is found that when $\log d$ is plotted versus $\log t$, a straight line is obtained (Fig. 10.6). Frequently the slope of curves plotted in this way is smaller than one-half,

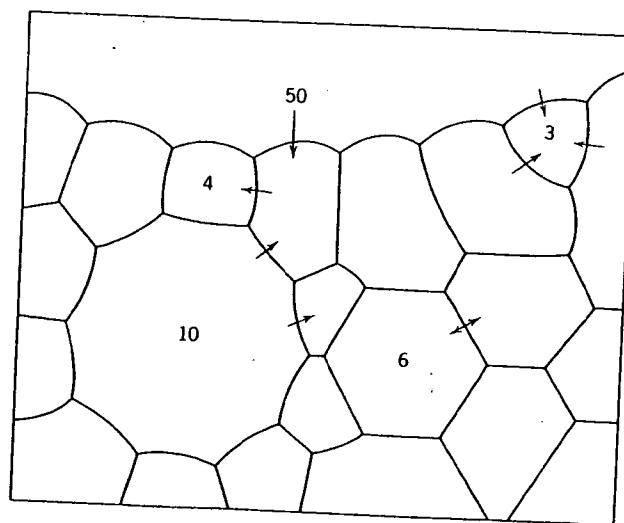


Fig. 10.4. Schematic drawing of polycrystalline specimen. The sign of curvature of the boundaries changes as the number of sides increases from less than six to more than six, and the radius of curvature is less, the more the number of sides differs from six. Arrows indicate the directions in which boundaries migrate. From J. E. Burke.



usually fall
one being
reason is th
growth.

A some
 B_i such th
force F_i re

Fig. 10.6. L
Burke.

angles
trative
r only
at are
grains
ample
daries
sides
grow
rectly
efore

(10.9)

10.10)

d that
10.6).
-half,

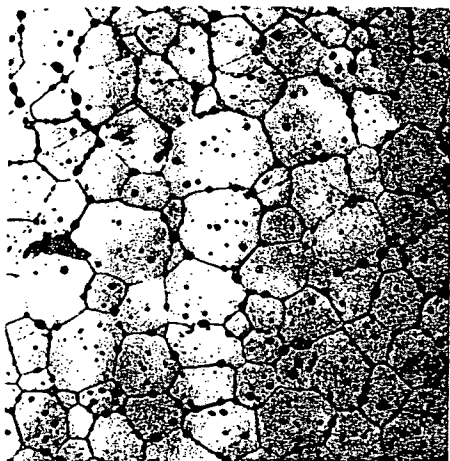


Fig. 10.5. Polycrystalline CaF_2 illustrating normal grain growth. Average angle at grain junctures is 120° .

usually falling between 0.1 and 0.5. This may occur for several reasons, one being that d_0 is not a large amount smaller than d ; another common reason is that inclusions or solute segregation or sample size inhibits grain growth.

A somewhat different approach is to define a grain-boundary mobility B_i such that the boundary velocity v is proportional to the applied driving force F_i resulting from boundary curvature:

$$v = B_i F_i \quad (10.11a)$$

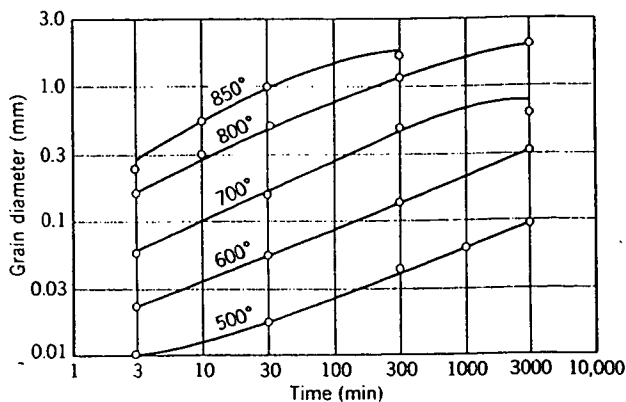


Fig. 10.6. Log grain diameter versus log time for grain growth in pure α -brass. From J. E. Burke.

of the
ix, and
idicate

For the atomic-jump mechanism illustrated in Fig. 10.3, the boundary mobility is given by the atomic mobility divided by the number of atoms involved, n_a :

$$B_i = \frac{B_a}{n_a} = \left(\frac{D_b}{kT} \right) \left(\frac{\Omega}{Sw} \right) \quad (10.11b)$$

where D_b is the grain-boundary diffusion coefficient, Ω is the atomic volume, S is the boundary area, and w is the boundary width. Since the average boundary velocity is equal to v and the driving force is inversely proportional to grain size, a grain-growth law of the form of Eqs. 10.9 and 10.10 results. However, as discussed in Chapter 5, the actual structure of a ceramic grain boundary is not quite so simple as pictured in deriving Eqs. 10.8 and 10.11b. Even for a completely pure material there is a space-charge atmosphere of lattice defects associated with the boundary and usually solute segregation as well, as shown in Figs. 5.11, 5.12, 5.17, and 5.18. The effect of this lattice defect and impurity atmosphere is to sharply reduce the grain-boundary velocity at low driving forces, as shown in Fig. 10.7 and analysed by J. Cahn* and K. Lücke and H. D. Stuwe.† The influence of this atmosphere becomes stronger as the grain

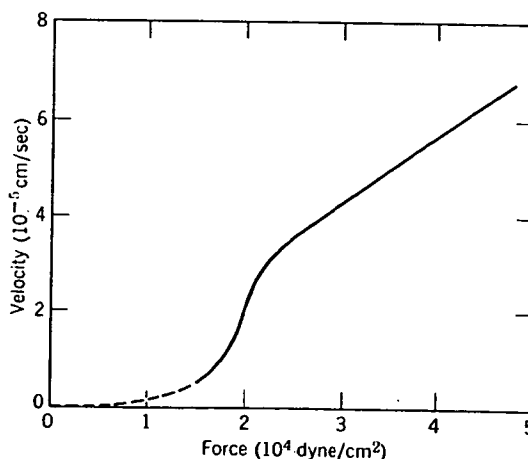


Fig. 10.7. Variation of boundary velocity v with driving force F at 750°C for a 20° tilt boundary in NaCl. From R. C. Sun and C. L. Bauer, *Acta Met.*, 18, 639 (1970).

size increases, the solute segregate concentration increases, and the average boundary curvature decreases. Additions of MgO to Al_2O_3 , $CaCl_2$

**Acta Met.*, 10, 789 (1962).

†*Acta Met.*, 19, 1087 (1971).

to KCl
proved

When
specim
when tl
to form
bounda
occurs.
movem
bounda
decreas
area of
pull it
inclusi
insuffic
It has l

where
and f_d
only a
creases
For
attache
Another

boundary
of atoms

(10.11b)

ie atomic
Since the
inversely
s. 10.9 and
ructure of
1 deriving
there is a
boundary
5.12, 5.17,
here is to
forces, as
and H. D.
the grain

to KCl and of ThO₂ to Y₂O₃ in amounts below the solubility limit have proved effective as grain-growth inhibitors.

When grains grow to such a size that they are nearly equal to the specimen size, grain growth is stopped. In a rod sample, for example, when the grain size is equal to the rod diameter, the grain boundaries tend to form flat surfaces normal to the axis so that the driving force for boundary migration is eliminated and little subsequent grain growth occurs. Similarly, inclusions increase the energy necessary for the movement of a grain boundary and inhibit grain growth. If we consider a boundary such as the one illustrated in Fig. 10.8, the boundary energy is decreased when it reaches an inclusion proportional to the cross-sectional area of the inclusion. The boundary energy must be increased again to pull it away from the inclusion. Consequently, when a number of inclusions are present on a grain boundary, its normal curvature becomes insufficient for continued grain growth after some limiting size is reached. It has been found that this size is given by

$$d_l \approx \frac{d_i}{f_{a_i}} \quad (10.12)$$

where d_l is the limiting grain size, d_i is the particle size of the inclusion, and f_{a_i} is the volume fraction of inclusions. Although this relationship is only approximate, it indicates that the effectiveness of inclusions increases as their particle size is lowered and the volume fraction increases.

For the process illustrated in Fig. 10.8, the boundary approaches, is attached to, and subsequently breaks away from a second-phase particle. Another possibility is that the grain boundary drags along the particle

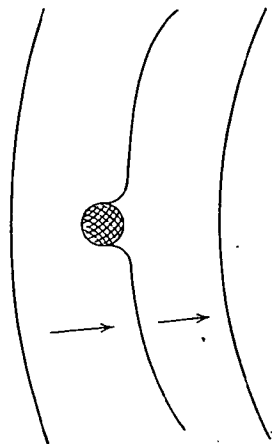


Fig. 10.8. Changing configuration of a boundary while passing an inclusion.

for a 20° tilt
(70).

s, and the
l₂O₃, CaCl₂

which remains attached to the boundary as it moves. This requires material transport across the particle, which may occur by interface or surface or volume diffusion, by viscous flow, or by solution (precipitation in a liquid or glass inclusion), or by evaporation (condensation in a gas inclusion). We can define an inclusion particle mobility B_p , relating the driving force and particle velocity $v_p = B_p F_p$ in the same way as has been done for the boundary (Eq. 10.11b) and for atomic diffusion in Chapter 6. When the inclusion is dragged by the boundary, their velocities are identical; in the case in which $B_p \ll B_b$ we can neglect the intrinsic boundary mobility, and the resulting grain-boundary velocity is controlled by the driving force on the boundary together with the mobility and number of inclusions per grain boundary, p :

$$v_b = \frac{B_p F_b}{p} \quad (10.13)$$

The inclusion particle moves along with the boundary, gradually becoming concentrated at boundary intersections and agglomerating into larger particles as grain growth proceeds. This is illustrated for the special case of pore agglomeration in Figs. 10.9 and 10.10.

Thus, second-phase inclusions can either (1) move along with boundaries, offering little impedance; (2) move along with boundaries, with the inclusion mobility controlling the boundary velocity; or (3) be so immobile that the boundary pulls away from the inclusion, depending on the relative values of the boundary driving force (inversely proportional to grain size), the boundary mobility (Fig. 10.7), and the inclusion particle mobility, which, depending on the assumed mechanism and particle shape, may be proportional to r_p^{-2} , r_p^{-3} , or r_p^{-4} .^{*} As grain growth proceeds, the driving force diminishes, and any inclusions dragged along by the boundary increase in size so that their mobility decreases. As a result, the exact way in which second-phase inclusions inhibit grain growth not only depends on the properties of the particular system but also can easily change during the grain-growth process. Sorting out these effects requires a careful evaluation of the microstructure evolution in combination with the kinetics of grain growth and a detailed knowledge of system properties. Inhibition of grain growth by solid second-phase inclusions has been observed for MgO additions to Al_2O_3 , for CaO additions to ThO_2 , and in other systems.

A second phase that is always present during ceramic sintering and in almost all ceramic products prepared by sintering is residual porosity

^{*}P. G. Shewmon, *Trans. A.I.M.E.*, 230, 1134 (1964); M. F. Ashby and R. M. A. Centamore, *Acta Met.*, 16, 1081 (1968).

Fig.
agglc

rem
com
(inte
sam
(inte
part
by 1
glon
early
forc
clus
resu
large
usua
grov

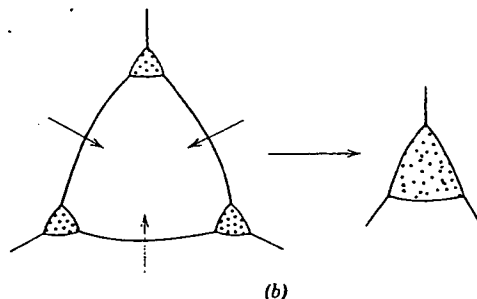
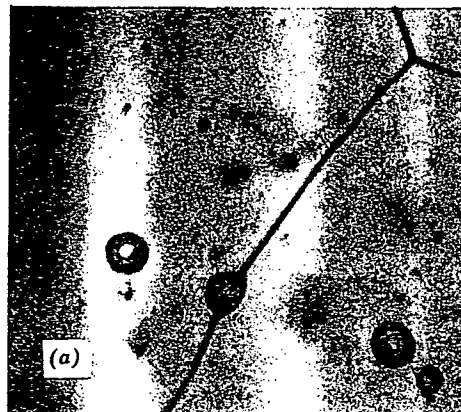


Fig. 10.9. (a) Pore shape distorted from spherical by moving boundary and (b) pore agglomeration during grain growth.

remaining from the interparticle space present in the initial powder compact. This porosity is apparent both on the grain boundaries (intergranular) and within the grains (intragranular) in the sintered CaF_2 sample shown in Fig. 10.5. It is present almost entirely at the grain corners (intergranular) in the sintered UO_2 samples shown in Fig. 10.10. As with particulate inclusions, pores on the grain boundaries may be left behind by the moving boundary or migrate with the boundary, gradually agglomerating at grain corners, as illustrated in Figs. 10.9 and 10.10. In the early stages of sintering, when the boundary curvature and the driving force for boundary migration are high, pores are often left behind, and a cluster of small pores in the center of a grain is a commonly observed result (see Fig. 10.5). In the later stages of sintering, when the grain size is larger and the driving force for boundary migration is lower, it is more usual for pores to be dragged along by the boundary, slowing grain growth.

s requires
terface or
ecipitation
n in a gas
elating the
s has been
Chapter 6.
cities are
e intrinsic
controlled
bility and

(10.13)

ly becom-
nto larger
ecial case

with boun-
s, with the
be so im-
ing on the
rtional to
n particle
d particle
proceeds,
ng by the
result, the
not only
can easily
s requires
tion with
n proper-
has been
 O_2 , and in

ng and in
porosity

Centamore,

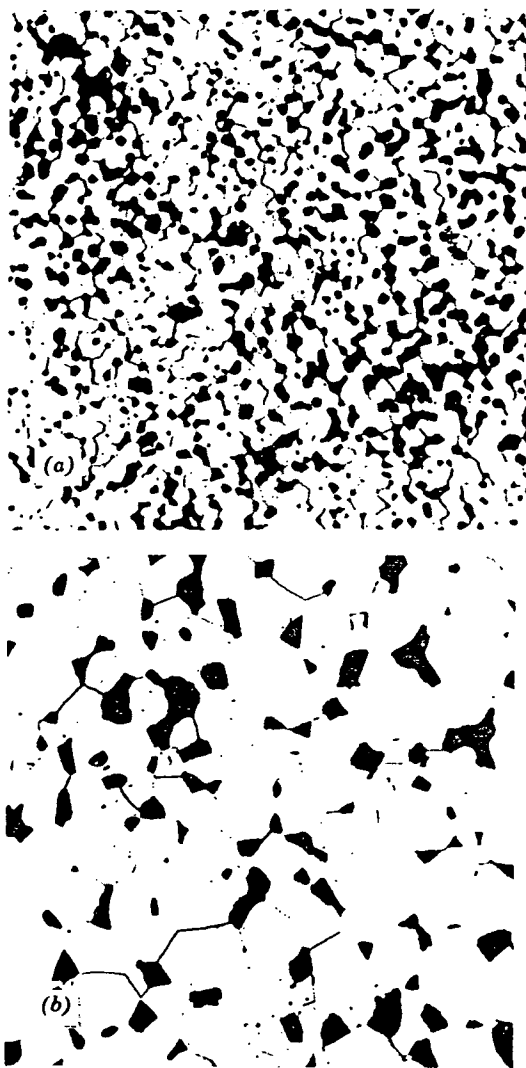


Fig. 10.10. Grain growth and pore growth in sample of UO_2 after (a) 2 min, 91.5% dense, and (b) 5 hr, 91.9% dense, at 1600°C ($400\times$). From Francois and Kingery.

Another factor that may restrain grain growth is the presence of a liquid phase. If a small amount of a boundary liquid is formed, it tends to slow grain growth, since the driving force is reduced and the diffusion path is increased. There are now two solid-liquid interfaces, and the driving force is the difference between them, that is, $(1/r_1 + 1/r_2)_A - (1/r_1 + 1/r_2)_B$, which

is smaller than the driving force for grain growth. Also, the precipitation of a second phase, even, this case, the presence of a liquid phase, as discussed in the preceding section, enhance secondary recrystallization. Large amounts of second phase, as described in the preceding section, amount of second phase, grain growth.

Secondary recrystallization, sometimes called abnormal grain growth, occurs when some grains grow much larger than the others. This happens when some grains have many more high-energy grain boundaries and it grows much faster than the others. Fig. 10.11, a uniform grain structure.

Secondary recrystallization is a grain growth process. Under these conditions, the driving force for grain growth is the curvature of the grain boundaries. With high material resistance, grain growth is much larger than normal. Grain growth is determined by the driving force, an inductive process, formation of a grain-size distribution, grain-size distribution, grain size, secondary recrystallization, even though.

Secondary recrystallization in ceramics is a process of secondary recrystallization, resultant s

is smaller than either alone; in addition, if the liquid wets the boundary, the interface energy must be lower than the pure-grain-boundary energy. Also, the process of solution, diffusion through a liquid film, and precipitation is usually slower than the jump across a boundary. However, this case is more complex in that grain growth may be enhanced by the presence of a reactive liquid phase during the densification process, as discussed in Section 10.4. In addition, a very small amount of liquid may enhance secondary recrystallization, as discussed later, whereas larger amounts of liquid phase may give rise to the grain-growth process described in Chapter 9. In practice, it is found that addition of a moderate amount of silicate liquid phase to aluminum oxide prevents the extensive grain growth which frequently occurs with purer materials.

Secondary Recrystallization. The process of secondary recrystallization, sometimes called discontinuous or exaggerated grain growth, occurs when some small fraction of the grains grow to a large size, consuming the uniform-grain-size matrix. Once a single grain grows to such a size that it has many more sides than the neighboring grains (such as the grain with fifty sides illustrated in Fig. 10.4), the curvature of each side increases, and it grows more rapidly than the smaller grains with fewer sides. The increased curvature on the edge of a large grain is particularly evident in Fig. 10.11, which shows a large alumina crystal growing at the expense of a uniform-particle-size matrix.

Secondary crystallization is particularly likely to occur when continuous grain growth is inhibited by the presence of impurities or pores. Under these conditions the only boundaries able to move are those with a curvature much larger than the average; that is, the exaggerated grains with highly curved boundaries are able to grow, whereas the matrix material remains uniform in grain size. The rate of growth of the large grains is initially dependent on the number of sides. However, after growth has reached the point at which the exaggerated grain diameter is much larger than the matrix diameter, $d_g \gg d_m$, the curvature is determined by the matrix grain size and is proportional to $1/d_m$. That is, there is an induction period corresponding to the increased growth rate and the formation of a grain large enough to grow at the expense of the constant-grain-size matrix. Therefore, the growth rate is constant as long as the grain size of the matrix remains unchanged. Consequently, the kinetics of secondary recrystallization is similar to that of primary recrystallization, even though the nature of the nucleation and driving force is different.

Secondary recrystallization is common for oxide, titanate, and ferrite ceramics in which grain growth is frequently inhibited by minor amounts of second phases or by porosity during the sintering process. A typical resultant structure is illustrated for barium titanate in Fig. 10.12, and the

11.5% dense,

of a liquid
ds to slow
ion path is
ving force
)_B, which

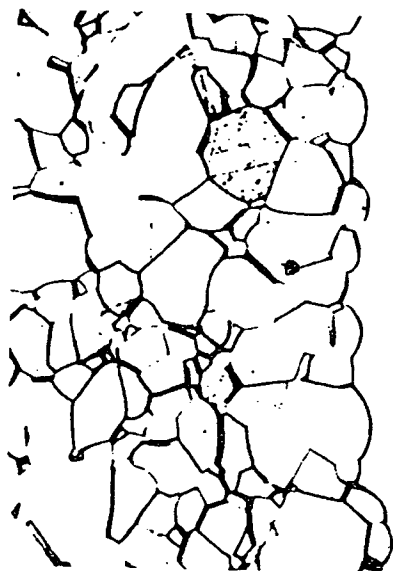


Fig. 10.11. Growth of a large Al_2O_3 crystal into a matrix of uniformly sized grains (495 \times). Compare with Fig. 10.4. Courtesy R. L. Coble.

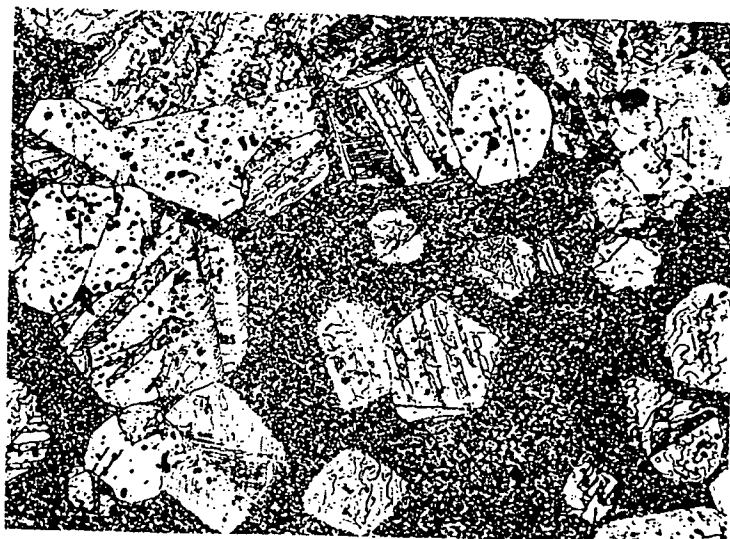
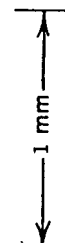
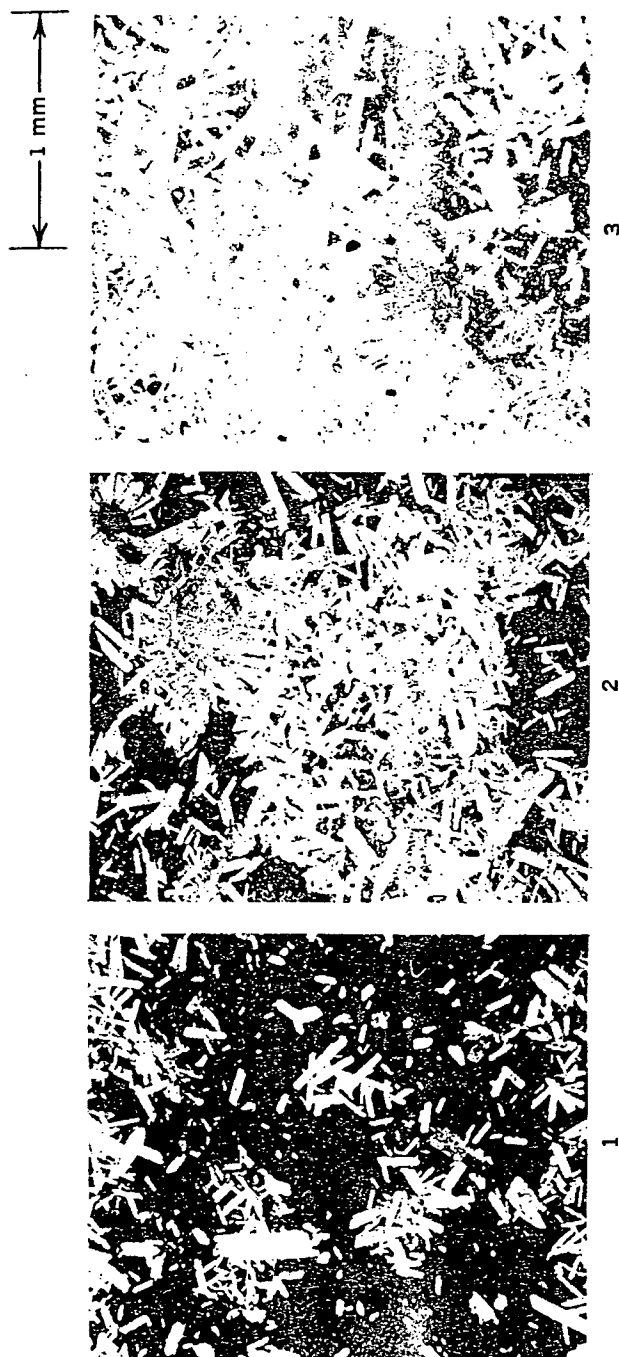


Fig. 10.12. Large grains of barium titanate growing by secondary recrystallization from a fine-grained matrix (250 \times). Courtesy R. C. DeVries.

from a

(495X).



Time at 1560°C (hr)

Fig. 10.13. Large grains of Al_2O_3 growing by secondary recrystallization from a fine-grained matrix. Courtesy I. B. Outler, in reference 5.

progressive growth of aluminum oxide crystals during secondary recrystallization is illustrated in Fig. 10.13.

When polycrystalline bodies are made from fine powder, the extent of secondary recrystallization depends on the particle size of the starting material. Coarse starting material gives a much smaller relative grain growth, as illustrated in Fig. 10.14 for beryllia. This is caused by both the rate of nucleation and the rate of growth. There are almost always present in the fine-grained matrix a few particles of substantially larger particle size than the average; these can act as embryos for secondary recrystallization, since already $d_s > d_m$, and growth proceeds to a rate proportional to $1/d_m$. In contrast, as the starting particle size increases, the chances of grains being present which are much larger in particle size than the average are much decreased, and consequently the nucleation of secondary recrystallization is much more difficult; the growth rate, proportional to $1/d_m$, is also smaller. In the data shown in Fig. 10.14, material having a starting particle size of 2 microns grows to a final particle size of about 50 microns, whereas material with an initial particle size of 10 microns shows a final grain size of only about 25 microns. This result of a much larger final grain size for a smaller initial particle size would be very puzzling if the process of secondary recrystallization was not known to occur.

Secondary recrystallization has been observed to occur with the boundaries of the large grains apparently perfectly straight (Fig. 10.15). Here the previous discussion of the surface tension and curvature of the phase boundary does not apply directly. That is, the boundary energy is

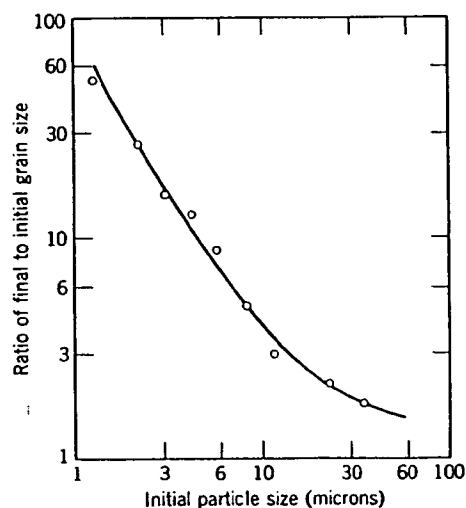


Fig. 10.14. Relative grain growth during secondary recrystallization of BeO heated $2\frac{1}{2}$ hr at 2000°C . From P. Duwez, F. Odell, and J. L. Taylor, *J. Am. Ceram. Soc.*, 32, 1 (1949).

not independent of surface energy. A small concentration of boundary plane with lower surface energy face material immediately boundaries the system, amount of 1 and this kind of previous

Secondary recrystallization produces resultant polycrystalline mechanical properties improved polycrystalline literature as this is not true oxide with texture so that has left almost

Fig. 10.15. (a) straight, when

not independent of crystal directions, and the growth planes are those of low surface energy. These structures all seem to occur in systems having a small concentration of impurity which gives rise to a small amount of a boundary phase. The driving force for secondary recrystallization is the lower surface energy of the large grain compared with the high-surface-energy faces or small radius of curvature of adjacent grains. Transfer of material under these conditions can only occur when there is an intermediate boundary phase separating the surfaces of the small and large grains. The amount of second phase present tends to increase at the boundaries of the large crystals compared with that at other boundaries in the system, and a large grain continues to grow once it is initiated. If the amount of boundary phase is increased, however, normal grain growth and this kind of secondary recrystallization are both inhibited, as discussed previously.

Secondary recrystallization affects both the sintering of ceramics and resultant properties. Excessive grain growth is frequently harmful to mechanical properties (see Sections 5.5 and 15.5). For some electrical and magnetic properties either a large or a small grain size may contribute to improved properties. Occasionally grain growth has been discussed in the literature as if it were an integral part of the densification process. That this is not true can best be seen from Fig. 10.16. A sample of aluminum oxide with an initial fine pore distribution was heated to a high temperature so that secondary recrystallization occurred. The recrystallization has left almost the same amount of porosity as was present in the initial

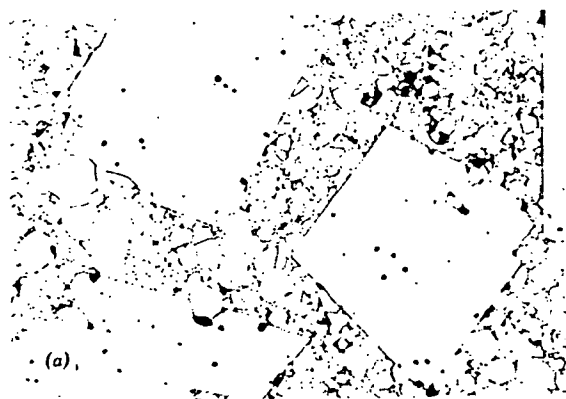


Fig. 10.15. (a) Idiomorphic grains in a polycrystalline spinel. The large grain edges appear straight, whereas the shape of the small grains is controlled by surface tension (350 \times). Courtesy R. L. Coble.

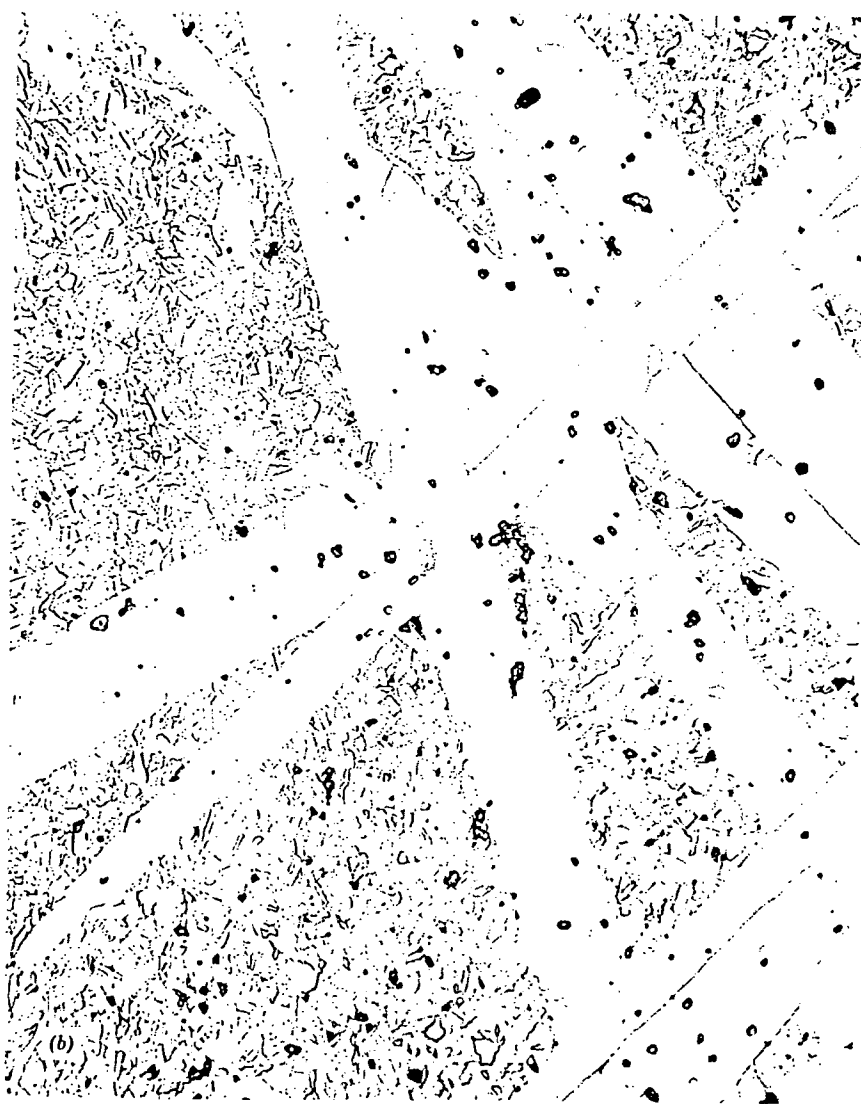


Fig. 10.15 (Continued). (b) Idiomorphic grains of α -6H SiC in a β -SiC matrix (1000 \times).

compact. Elimination of porosity is a related but separate subject and is considered in following sections. An application in which secondary recrystallization has been useful is in the development of preferred orientation on firing of the magnetically hard ferrite, $\text{BaFe}_{12}\text{O}_{19}$.^{*} For this

^{*}A. L. Stuijts, *Trans. Brit. Ceram. Soc.*, 55, 57 (1956).

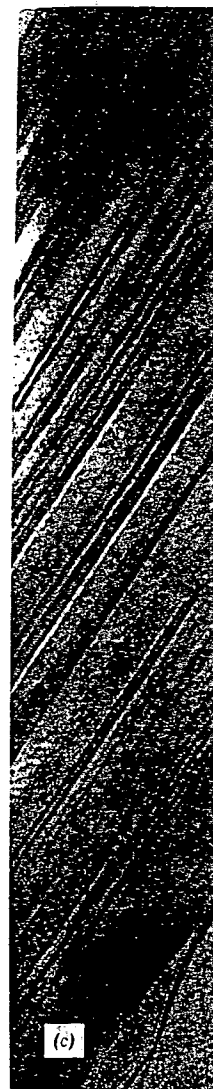


Fig. 10.15 (Continued)

magnetic material degree of preferred orientation of powdered material to a high magnetic alignment after l

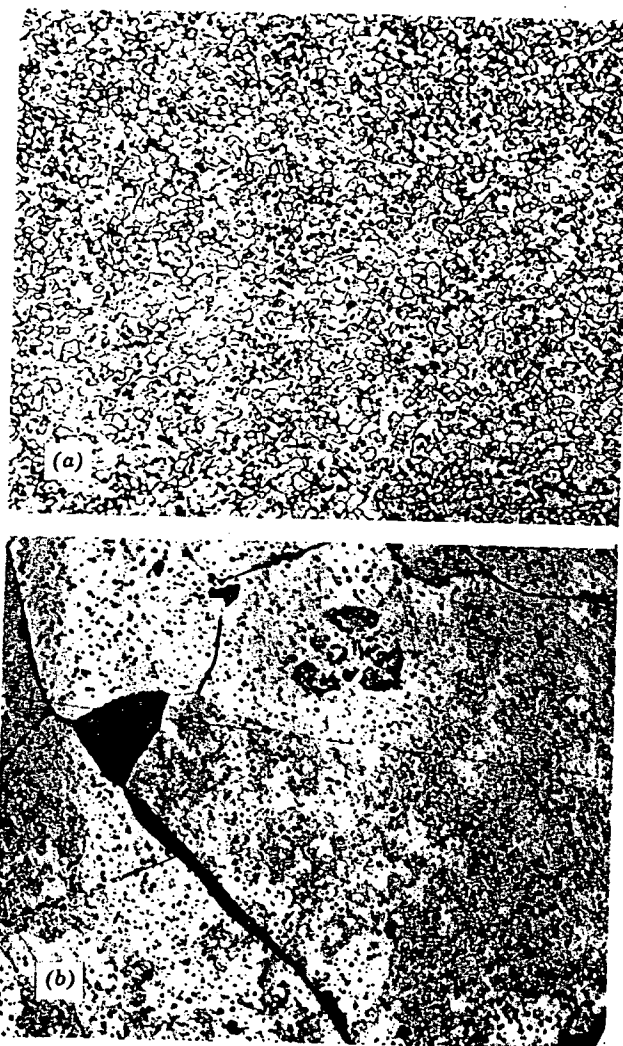


Fig. 10.15 (Continued). (c) Detail of boundary (75,000 \times). Courtesy S. Prochazka.

magnetic material it is desirable to obtain a high density as well as a high degree of preferred orientation in the sintered product. Particles of the powdered material can be oriented to a considerable extent by subjecting them to a high magnetic field while forming. On sintering there was a 57% alignment after heating at 1250°C. On further heating at 1340°C the

rix (1000 \times).

ject and is
secondary
preferred
* For this



preferred orientation increased to 93% alignment, corresponding to the structural change brought about by secondary recrystallization. It seems apparent that the few large grains in the starting material are more uniformly aligned than the fine grains in the surrounding material. These grains serve as nuclei for the secondary recrystallization process and give rise to a highly oriented final product.

Changes that occur in grain size and pore size. In Section 1 the following section that is, the change in porous compact to compact, before separated by the particular material properties such as desirable to eliminate applications it may be the gas permeability transfer of material of changes that are present can change necessarily change the shape of the pores becoming more spherical.

Driving Force for densification is the reduction of free energy by grain growth. Grain growth takes place with

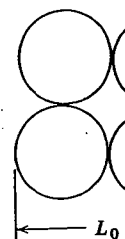


Fig. 10.17.

10.2 Solid-State Sintering

Changes that occur during the firing process are related to (1) changes in grain size and shape, (2) changes in pore shape, and (3) changes in pore size. In Section 10.1 we concentrated on changes in grain size; in this and the following section we are mainly concerned with changes in porosity, that is, the changes taking place during the transformation of an originally porous compact to a strong, dense ceramic. As formed, a powder compact, before it has been fired, is composed of individual grains separated by between 25 and 60 vol% porosity, depending on the particular material used and the processing method. For maximizing properties such as strength, translucency, and thermal conductivity, it is desirable to eliminate as much of this porosity as possible. For some other applications it may be desirable to increase this strength without decreasing the gas permeability. These results are obtained during firing by the transfer of material from one part of the structure to the other. The kind of changes that may occur are illustrated in Fig. 10.17. The pores initially present can change shape, becoming channels or isolated spheres, without necessarily changing in size. More commonly, however, both the size and shape of the pores present change during the firing process, the pores becoming more spherical in shape and smaller in size as firing continues.

Driving Force for Densification. The free-energy change that gives rise to densification is the decrease in surface area and lowering of the surface free energy by the elimination of solid-vapor interfaces. This usually takes place with the coincidental formation of new but lower-energy

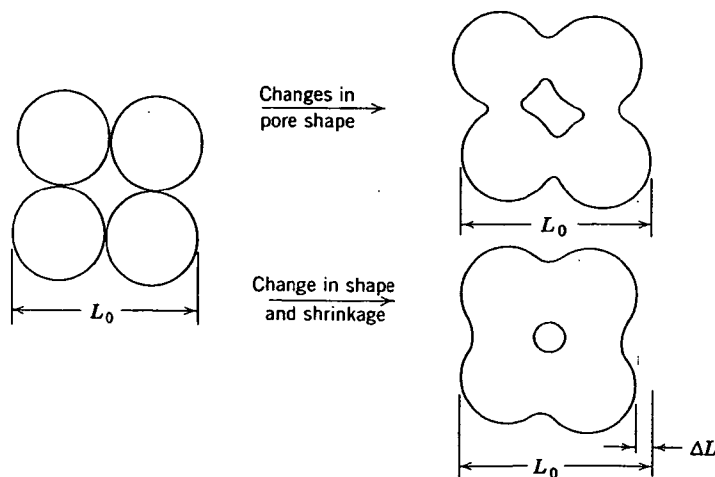


Fig. 10.17. Changes in pore shape do not necessarily require shrinkage.

1 hr at 1900°C
ed. Courtesy J.

ding to the
on. It seems
l are more
grains serve
ve rise to a

solid-solid interfaces. The net decrease in free energy occurring on sintering a 1-micron particle size material corresponds to an energy decrease of about 1 cal/g. On a microscopic scale, material transfer is affected by the pressure difference and changes in free energy across a curved surface. These changes are due to the surface energy and have been discussed in Chapter 5 and referred to in Section 10.1. If the particle size, and consequently the radius of curvature, is small, these effects may be of a substantial magnitude. As indicated in Chapter 5, they become large when the radius of curvature is less than a few microns. This is one of the major reasons why much ceramic technology is based on and depends on the use of fine-particle materials.

Most of the insight into the effect of different variables on the sintering process has come from considering simple systems and comparing experimental data with simple models. Since our major aim is to be sure we understand the importance of different variables in traditional or new systems, we use this method here. Since the driving force is the same (surface energy) in all systems, considerable differences in behavior in various types of systems must be related to different mechanisms of material transfer. Several can be imagined—evaporation and condensation, viscous flow, surface diffusion, grain-boundary or lattice diffusion, and plastic deformation are among those that occur to us. Of these, diffusion and viscous flow are important in the largest number of systems; evaporation-condensation is perhaps the easiest to visualize.

Evaporation-Condensation. During the sintering process there is a tendency for material transfer because of the differences in surface curvature and consequently the differences in vapor pressure at various parts of the system. Material transfer brought about in this way is only important in a few systems; however, it is the simplest sintering process to treat quantitatively. We derive the sintering rate in some detail, since it provides a sound basis for understanding more complex processes.

Let us consider the initial stages of the process when the powder compact is just beginning to sinter and concentrate on the interaction between two adjacent particles (Fig. 10.18). At the surface of the particle there is a positive radius of curvature so that the vapor pressure is somewhat larger than would be observed for a flat surface. However, just at the junction between particles there is a neck with a small negative radius of curvature and a vapor pressure an order of magnitude lower than that for the particle itself. The vapor-pressure difference between the neck area and the particle surface tends to transfer material into the neck area.

We can calculate the rate at which the bonding area between particles increases by equating the rate of material transfer to the surface of the

Fig. 10.18. I

lens between
pressure of
of the sur
(Kelvin) eq

where p_1 is
molecular v
radius is m
pressure di
tion, $\ln p_1/r$

where Δp
negative ra
the nearly 1
to the diffe
given by th

where α is
rate of con

From the g
at the conti

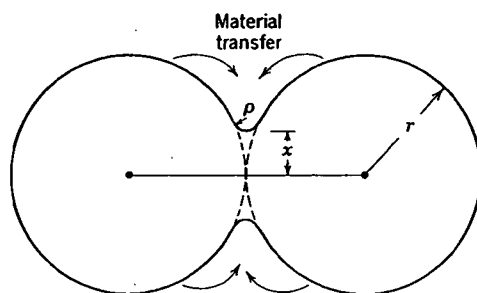


Fig. 10.18. Initial stages of sintering by evaporation-condensation.

lens between the spheres with the increase in its volume. The vapor pressure over the small negative radius of curvature is decreased because of the surface energy in accordance with the Thomson-Freundlich (Kelvin) equation discussed in Chapter 5:

$$\ln \frac{p_1}{p_0} = \frac{\gamma M}{dRT} \left(\frac{1}{\rho} + \frac{1}{x} \right) \quad (10.14)$$

where p_1 is the vapor pressure over the small radius of curvature, M is the molecular weight of the vapor, and d is the density. In this case the neck radius is much larger than the radius of curvature at the surface, ρ , and the pressure difference $p_0 - p_1$ is small. Consequently, to a good approximation, $\ln p_1/p_0$ equals $\Delta p/p_0$, and we can write

$$\Delta p = \frac{\gamma M p_0}{d \rho RT} \quad (10.15)$$

where Δp is the difference between the vapor pressure of the small negative radius of curvature and the saturated vapor in equilibrium with the nearly flat particle surfaces. The rate of condensation is proportional to the difference in equilibrium and atmospheric vapor pressure and is given by the Langmuir equation to a good approximation as

$$m = \alpha \Delta p \left(\frac{M}{2\pi RT} \right)^{1/2} \quad \text{g/cm}^2/\text{sec} \quad (10.16)$$

where α is an accommodation coefficient which is nearly unity. Then the rate of condensation should be equal to the volume increase. That is,

$$\frac{mA}{d} = \frac{dv}{dt} \quad \text{cm}^3/\text{sec} \quad (10.17)$$

From the geometry of the two spheres in contact, the radius of curvature at the contact points is approximately equal to $x^2/2r$ for x/r less than 0.3;

the area of the surface of the lens between spheres is approximately equal to $\pi^2 x^3/r$; the volume contained in the lenticular area is approximately $\pi x^4/2r$. That is,

$$\rho = \frac{x^2}{2r}; \quad A = \frac{\pi^2 x^3}{r}; \quad v = \frac{\pi x^4}{2r} \quad (10.18)$$

Substituting values for m in Eq. 10.16, A and v in Eq. 10.18 into Eq. 10.17 and integrating, we obtain a relationship for the rate of growth of the bond area between particles:

$$\frac{x}{r} = \left(\frac{3\sqrt{\pi}\gamma M^{3/2} p_0}{\sqrt{2} R^{3/2} T^{3/2} d^2} \right)^{1/3} r^{-2/3} t^{1/3} \quad (10.19)$$

This equation gives the relationship between the diameter of the contact area between particles and the variables influencing its rate of growth.

The important factor from the point of view of strength and other material properties is the bond area in relation to the individual particle size, which gives the fraction of the projected particle area which is bonded together—the main factor in fixing strength, conductivity, and related properties. As seen from Eq. 10.19, the rate at which the area between particles forms varies as the two-thirds power of time. Plotted on a linear scale, this decreasing rate curve has led to characterizations of *end point* conditions corresponding to a certain sintering time. This concept of an end point is useful, since periods of time for sintering are not widely changed; however, the same rate law is observed for the entire process (Fig. 10.19b).

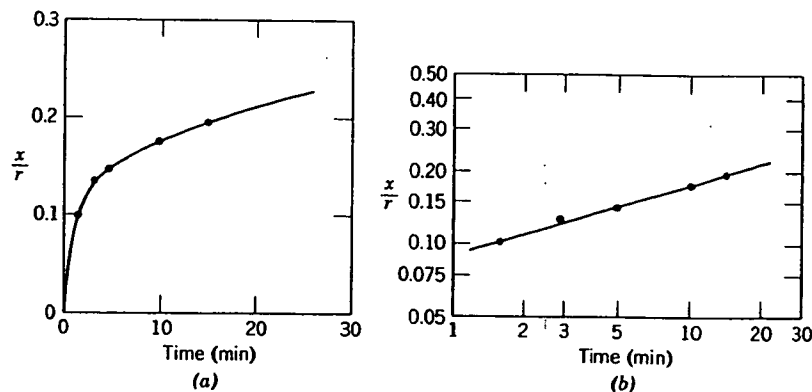


Fig. 10.19. (a) Linear and (b) log-log plots of neck growth between spherical particles of sodium chloride at 725°C.

If we c
such as
particles
particle
shrinkag
by vapo
changed.
propertie

The p
pore-sha
proportio
Since the
process
From a
control c
and the t
generally
condition

The n
fer is p
changes
particles

(a)

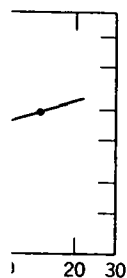
imately equal
approximately

(10.18)

into Eq. 10.17
th of the bond

(10.19)

of the contact
e of growth.
th and other
idual particle
rea which is
luctivity, and
hich the area
e. Plotted on
erizations of
g time. This
sintering are
for the entire



cal particles of

If we consider the changes in structure that take place during a process such as this, it is clear that the distance between centers of spherical particles (Fig. 10.18) is not affected by the transfer of material from the particle surface to the interparticle neck. This means that the total shrinkage of a row of particles, or of a compact of particles, is unaffected by vapor-phase-material transfer and that only the shape of pores is changed. This changing shape of pores can have an appreciable effect on properties but does not affect density.

The principal variables in addition to time that affect the rate of pore-shape change through this process are the initial particle radius (rate proportional to $1/r^{2/3}$) and the vapor pressure (rate proportional to $p_o^{1/3}$). Since the vapor pressure increases exponentially with temperature, the process of vapor-phase sintering is strongly temperature-dependent. From a processing point of view, the two main variables over which control can be exercised for any given material are the initial particle size and the temperature (which fixes the vapor pressure). Other variables are generally not easy to control, nor are they strongly dependent on conditions of use.

The negligible shrinkage corresponding to vapor-phase-material transfer is perhaps best illustrated in Fig. 10.20, which shows the shape changes that occur on heating a row of initially spherical sodium chloride particles. After long heating the interface contact area has increased; the

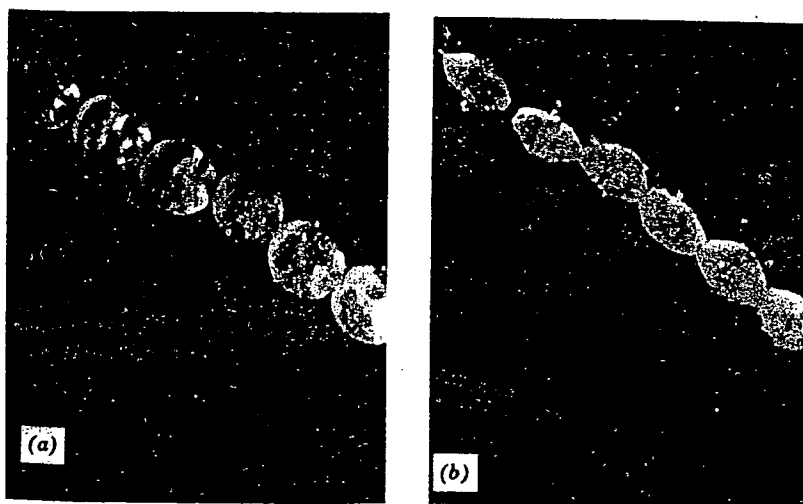


Fig. 10.20. Photomicrographs of sintering sodium chloride at 750°C: (a) 1 min; (b) 90 min.

particle diameter has been substantially decreased, but the distance between particle centers, that is, the shrinkage, has not been affected.

Vapor-phase-material transfer requires that materials be heated to a temperature sufficiently high for the vapor pressure to be appreciable. For micron-range particle sizes this requires vapor pressures in the order of 10^{-4} to 10^{-5} atm, a pressure higher than those usually encountered during sintering of oxide and similar phases. Vapor-phase transfer plays an important part in the changes occurring during treatment of halides such as sodium chloride and is important for the changes in configuration observed in snow and ice technology.

Solid-State Processes. The difference in free energy or chemical potential between the neck area and the surface of the particle provides a driving force which causes the transfer of material by the fastest means available. If the vapor pressure is low, material transfer may occur more readily by solid-state processes, several of which can be imagined. As shown in Fig. 10.21 and Table 10.1, in addition to vapor transport (process 3), matter can move from the particle surface, from the particle bulk, or from the grain boundary between particles by surface, lattice, or grain-boundary diffusion. Which one or more of these processes actually contributes significantly to the sintering process in a particular system depends on their relative rates, since each is a parallel method of lowering the free energy of the system (parallel reaction paths have been discussed in Chapter 9). There is a most significant difference between these paths for matter transport: the transfer of material from the surface to the neck by surface or lattice diffusion, like vapor transport, does not lead to any decrease in the distance between particle centers. That is, these processes do not result in shrinkage of the compact and a decrease in porosity. Only



Fig. 10.21.
Courtesy M.

Table 10.1. Alternate Paths for Matter Transport During the Initial Stages of Sintering^a

Mechanism Number	Transport Path	Source of Matter	Sink of Matter
1	Surface diffusion	Surface	Neck
2	Lattice diffusion	Surface	Neck
3	Vapor transport	Surface	Neck
4	Boundary diffusion	Grain boundary	Neck
5	Lattice diffusion	Grain boundary	Neck
6	Lattice diffusion	Dislocations	Neck

^aSee Fig. 10.21.

transfer of
between p
Let us c
to the nec
is exactly
vapor-pa
surface ar
The geom

The proce

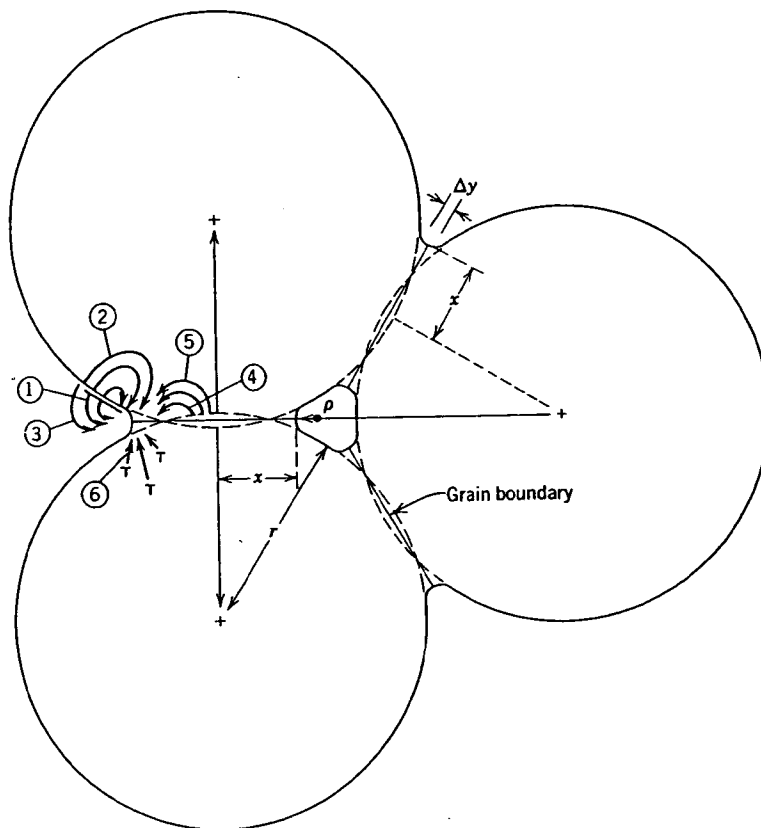


Fig. 10.21. Alternate paths for matter transport during the initial stages of sintering. Courtesy M. A. Ashby. (See Table 10.1.)

transfer of matter from the particle volume or from the grain boundary between particles causes shrinkage and pore elimination.

Let us consider mechanism 5, matter transport from the grain boundary to the neck by lattice diffusion. Calculation of the kinetics of this process is exactly analogous to determination of the rate of sintering by a vapor-phase process. The rate at which material is discharged at the surface area is equated to the increase in volume of material transferred. The geometry is slightly different:

$$\rho = \frac{x^2}{4r}; \quad A = \frac{\pi^2 x^3}{2r}; \quad V = \frac{\pi x^4}{4r} \quad (10.20)$$

The process can be visualized most easily by considering the rate of

migration of vacancies. In the same way that there are differences in vapor pressure between the surface of high negative curvature and the nearly flat surfaces, there is a difference in vacancy concentration. If c is the concentration of vacancies and Δc is the excess concentration over the concentration on a plane surface c_0 , then, equivalent to Eq. 10.15,

$$\Delta c = \frac{\gamma a^3 c_0}{kT\rho} \quad (10.21)$$

where a^3 is the atomic volume of the diffusing vacancy and k is the Boltzmann constant. The flux of vacancies diffusing away from the neck area per second per centimeter of circumferential length under this concentration gradient can be determined graphically and is given by

$$J = 4D_v \Delta c \quad (10.22)$$

Where D_v is the diffusion coefficient for vacancies, D_v equals $D^*/a^3 c_0$ if D^* is the self-diffusion coefficient. Combining Eqs. 10.22 and 10.21 with the continuity equation similar to Eq. 10.17, we obtain the result

$$\frac{x}{r} = \left(\frac{40\gamma a^3 D^*}{kT} \right)^{1/5} r^{-3/5} t^{1/5} \quad (10.23)$$

With diffusion, in addition to the increase in contact area between particles, there is an approach of particles centers. The rate of this approach is given by $d(x^2/2r)/dt$. Substituting from Eq. 10.23, we obtain

$$\frac{\Delta V}{V_0} = \frac{3 \Delta L}{L_0} = 3 \left(\frac{20\gamma a^3 D^*}{\sqrt{2}kT} \right)^{2/5} r^{-6/5} t^{2/5} \quad (10.24)$$

These results indicate that the growth of bond formation between particles increases as a one-fifth power of time (a result which has been experimentally observed for a number of metal and ceramic systems) and that the shrinkage of a compact densified by this process should be proportional to the two-fifths power of time. The decrease in densification rate with time gives rise to an apparent end-point density if experiments are carried out for similar time periods. However, when plotted on a log-log basis, the change in properties is seen to occur as expected from Eq. 10.24. Experimental data for sodium fluoride and aluminum oxide are shown in Fig. 10.22.

The relationships derived in Eqs. 10.23 and 10.24 and similar relationships for the alternate matter transport processes, which we shall not derive, are important mainly for the insight that they provide on the variables which must be controlled in order to obtain reproducible processing and densification. It is seen that the sintering rate steadily decreases with time, so that merely sintering for longer periods to obtain

GF

 $\frac{\Delta L}{L_0}$ $\frac{\Delta L}{L_0}$

0

0

Fig. 10.22. (Aluminum oxide compact)

improved
critical var
Control
roughly pr
diameter a
illustrated
even these
size is dec

differences in
ature and the
tration. If c is
centration over
to Eq. 10.15,

(10.21)

and k is the
from the neck
h under this
is given by

(10.22)

als D^*/a^3c_0 if
nd 10.21 with
result

(10.23)

area between
rate of this
, we obtain

(10.24)

tion between
ich has been
systems) and
ss should be
densification
experiments
plotted on a
pected from
um oxide are

ilar relation-
we shall not
vide on the
reproducible
rate steadily
ods to obtain

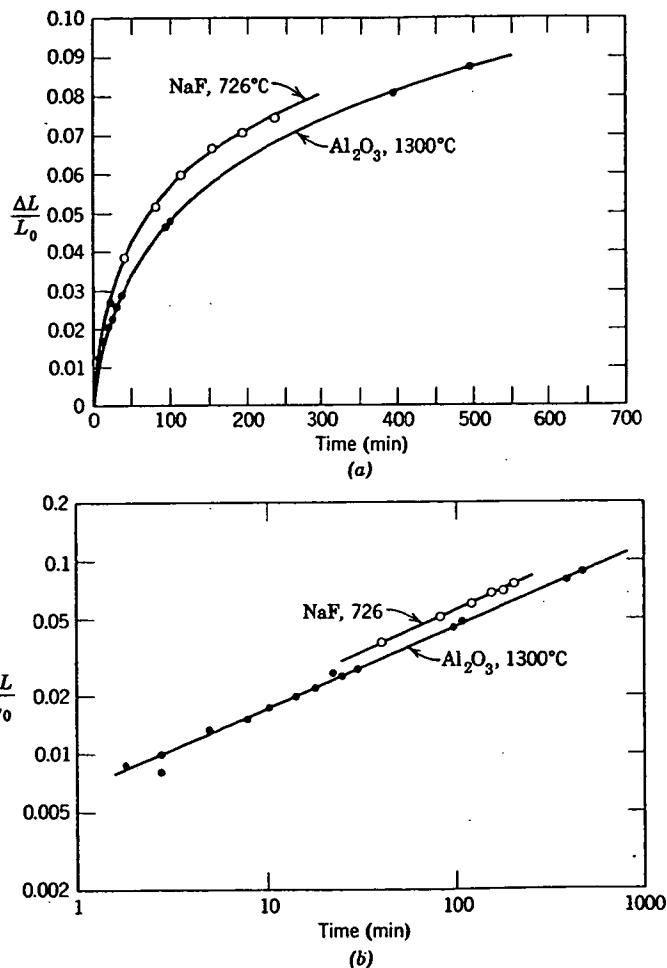


Fig. 10.22. (a) Linear and (b) log-log plots of shrinkage of sodium fluoride and aluminum oxide compacts. From J. E. Burke and R. L. Coble.

improved properties is impracticable. Therefore, time is not a major or critical variable for process control.

Control of particle size is very important, since the sintering rate is roughly proportional to the inverse of the particle size. The interface diameter achieved after sintering for a period of 100 hr at 1600°C is illustrated in Fig. 10.23 as a function of particle size. For large particles even these long periods do not cause extensive sintering; as the particle size is decreased, the rate of sintering is raised.

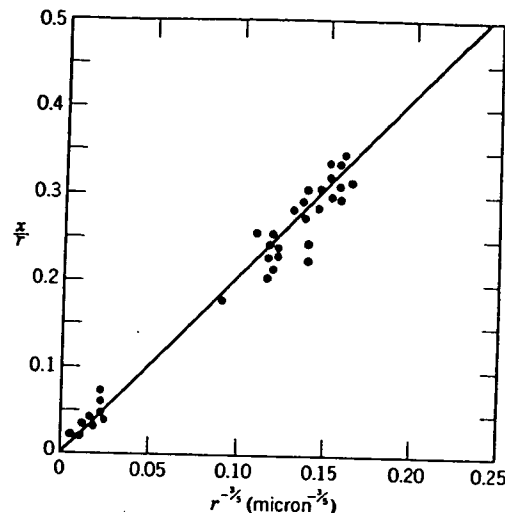


Fig. 10.23. Effect of particle size on the contact area growth in Al_2O_3 , heated 100 hr at 1600°C . From R. L. Coble.

The other variable appearing in Eqs. 10.22 and 10.24 that is subject to analysis and some control is the diffusion coefficient; it is affected by composition and by temperature; the relative effectiveness of surfaces, boundaries, and volume as diffusion paths is affected by the microstructure. A number of relationships similar to Eqs. 10.23 and 10.24 have been derived, and it has been shown that surface diffusion is most important during early stages of sintering (these affect the neck diameter between particles but not the shrinkage or porosity); grain-boundary diffusion and volume diffusion subsequently become more important. In ionic ceramics, as discussed in Chapter 9, both the anion and the cation diffusion coefficients must be considered. In Al_2O_3 , the best studied material, oxygen diffuses rapidly along the grain boundaries, and the more slowly moving aluminum ion at the boundary or in the bulk controls the overall sintering rate. As discussed in Chapter 5, the grain-boundary structure, composition, and electrostatic charge are influenced strongly by temperature and by impurity solutes; as discussed in Chapter 6, the exact mechanism of grain-boundary diffusion remains controversial. Estimates of the grain-boundary-diffusion width from sintering data range from 50 to 600 Å. These complications require us to be careful not to overanalyze data in terms of specific numerical results, since the time or temperature dependence of sintering may be in accordance with several plausible models. In general the presence of solutes which enhance either

boundary or sintering. As coefficients sintering rate

In order to solid-state particle size temperature

As an example effect of titanium in a region processes as ally as Ti^{+3}

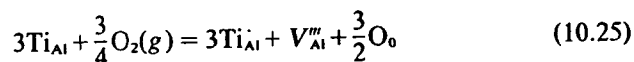
from which



boundary or volume diffusion coefficients enhance the rate of solid-state sintering. As discussed in Chapter 6, both boundary and volume diffusion coefficients are strongly temperature-dependent, which means that the sintering rate is strongly dependent on the temperature level.

In order to effectively control sintering processes which take place by solid-state processes, it is essential to maintain close control of the initial particle size and particle-size distribution of the material, the sintering temperature, the composition and frequently the sintering atmosphere.

As an example of the influence of solutes, Fig. 10.24 illustrates the effect of titania additions on the sintering rate of a relatively pure alumina in a region of volume diffusion. (Both volume and boundary diffusion processes are enhanced.) It is believed that Ti enters Al_2O_3 substitutionally as Ti^{3+} and Ti^{4+} (Ti_{Al} and Ti_{Al}'). At equilibrium



from which

$$K_1 = \frac{[\text{Ti}_{\text{Al}}]^3 [V_{\text{Al}}''']}{[\text{Ti}_{\text{Al}}]^3 [P_{\text{O}_2}]^{3/4}} \quad (10.26)$$

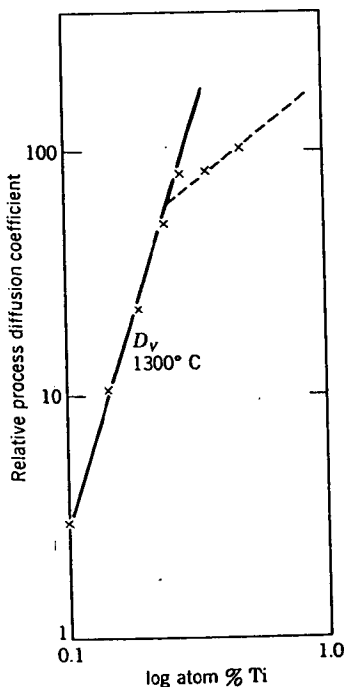


Fig. 10.24. Data for the relative sintering process diffusion coefficient with Ti additions to Al_2O_3 . $D_v[\text{Ti}]^3$. From R. D. Bagley, I. B. Cutler, and D. L. Johnson, *J. Am. Ceram. Soc.*, 53, 136 (1970); R. J. Brook, *J. Am. Ceram. Soc.*, 55, 114 (1972).

In the powders used, divalent impurities such as magnesium exceed in concentrations the intrinsic defect levels, so that overall charge neutrality at moderate titania levels is achieved by

$$[\text{Ti}_{\text{Al}}'] = [\text{Mg}_{\text{Al}}'] \quad (10.27)$$

and at constant impurity and oxygen pressure levels, combining Eqs. 10.26 and 10.27 gives

$$[V_{\text{Al}}'''] = K_2[\text{Ti}_{\text{Al}}']^3 \quad (10.28)$$

Since the total Ti addition ($\text{Ti}_{\text{Al}} + \text{Ti}_{\text{Al}}'$) is much greater than the impurity levels, $[\text{Ti}]_{\text{Total}} \approx [\text{Ti}_{\text{Al}}']$ and $[V_{\text{Al}}'''] \approx K_2[\text{Ti}]_{\text{Total}}^3$. The dependence of lattice defect concentrations on titania concentration is shown in Fig. 10.25 for the proposed model. As discussed in Chapter 6, the diffusion coefficient is proportional to the vacancy concentration; as a result the effect of this model is to anticipate an increase in the sintering rate proportional to the third power of titania concentration as experimentally observed (Fig. 10.24). At higher concentrations the dependence on titania concentration should become less steep, which is suggested by the sintering data.

Thus far our discussion of the variables influencing the sintering process has been based on the initial stages of the process, in which models are based on solid particles in contact. As the process continues, an intermediate microstructure forms in which the pores and solid are both continuous, followed by a later stage in which isolated pores are separated from one another. A number of analytical expressions have

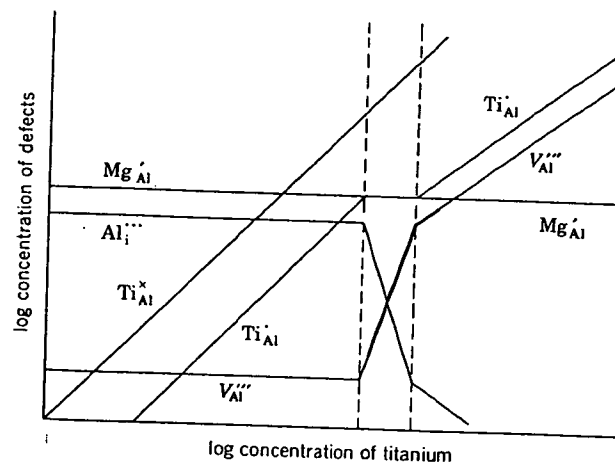


Fig. 10.25. Model for the dependence of defect concentrations on the Ti concentration in Al_2O_3 . From R. J. Brook, *J. Am. Ceram. Soc.*, 55, 114 (1972).

been deriv
processes li
mechanism
boundary a
spherical p

where D_v
concentrati
material-so
sort of anal

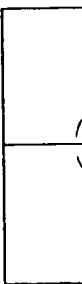


Fig. 10.26. more of the

with a large
diffusion
elimination
porosity. T
volume or
solute con
the geome
variety of

With fir
increase i
treatment
results fr
sinter rap
rapid grai
the bound

been derived from specific microstructural models for the transport processes listed in Table 10.1. In the later stages of the process only two mechanisms are important: boundary diffusion from sources on the boundary and lattice diffusion from sources on the boundary. For a nearly spherical pore the flux of material to a pore can be approximated as

$$J = 4\pi D_v \Delta c \left(\frac{rR}{R-r} \right) \quad (10.29)$$

where D_v is the volume diffusion coefficient, Δc is the excess vacancy concentration (Eq. 10.21), r is the pore radius, and R is the effective-material-source radius. The importance of microstructure in applying this sort of analysis to specific systems is illustrated in Fig. 10.26. For a sample

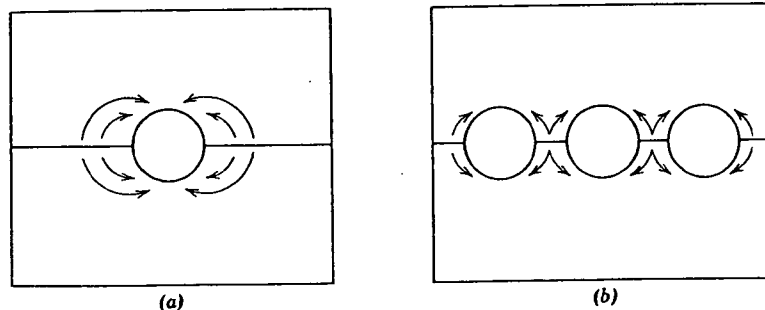


Fig. 10.26. The mean diffusion distance for material transport is smaller when there are more of the same size of pores in a boundary.

with a larger number of pores, all the same size, on a boundary the mean diffusion distance is smaller when there are more pores, and pore elimination is accomplished more quickly for the sample with the higher porosity. Thus, although the terms which influence the rate of sintering—volume or boundary diffusion coefficient (and therefore temperature and solute concentration) surface energy and pore size—are well established, the geometrical relationship of grain boundaries to the pores may have a variety of forms and is critical in determining what actually occurs.

With fine-grained materials such as oxides, it is usual to observe an increase in both grain size and pore size during the early stages of heat treatment, as illustrated for Lucalox alumina in Fig. 10.27. This partially results from the presence of agglomerates of the fine particles which sinter rapidly, leaving interagglomerate pores, and is partly due to the rapid grain growth during which pores are agglomerated by moving with the boundaries, as illustrated in Fig. 10.9. In cases in which agglomeration



Fig. 10.27. Progressive development of microstructure in Lucalox alumina. Scanning electron micrographs of (a) initial particles in the compact (5000 \times), (b) after 1 min at 1700°C (5000 \times).

Fig. 10.27 (c
and (d) after
variations in

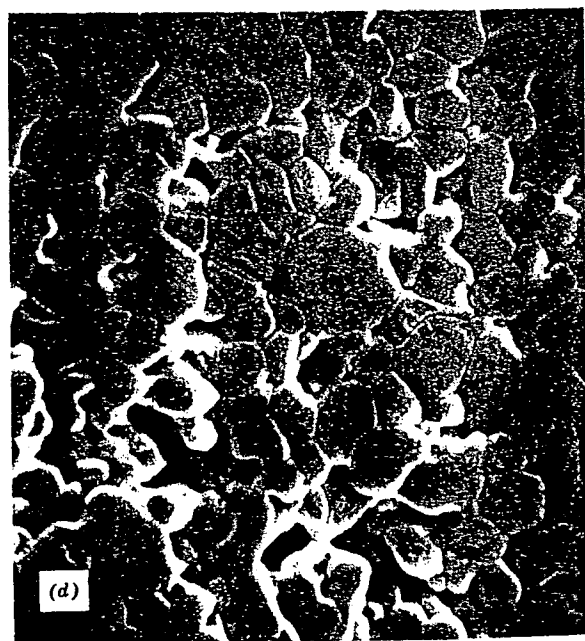
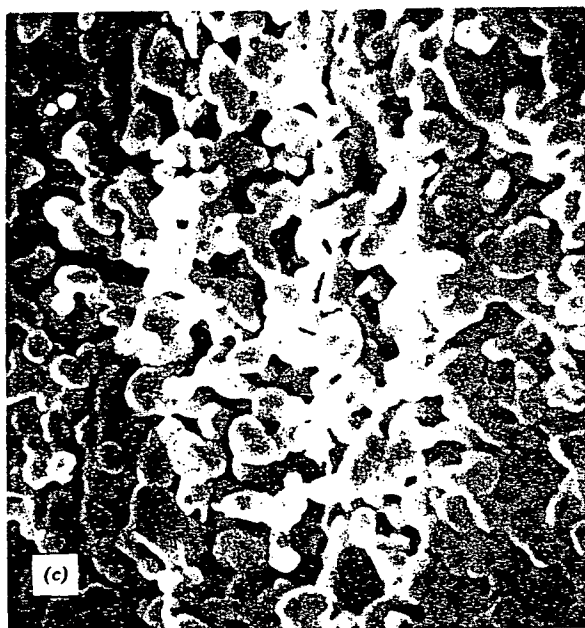


Fig. 10.27 (Continued) (c) Scanning electron micrographs after $2\frac{1}{2}$ min at 1700°C (5000 \times), and (d) after 6 min at 1700°C (5000 \times). Note that pores and grains increase in size, that there are variations in packing and in pore size, and that pores remain located between dense grains.

nina. Scanning
1-min at 1700°C

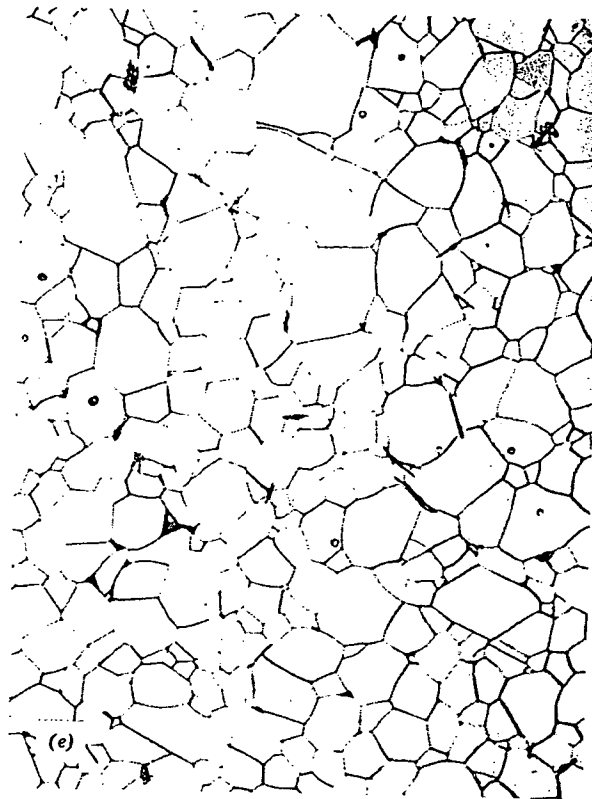


Fig. 10.27 (Continued) (e) The final microstructure is nearly porefree, with only a few pores located within grains (500 \times). Courtesy C. Greskovich and K. W. Lay.

of fine precipitated particles into clumps is severe, ball milling to break up the agglomerates leads to a remarkable increase in the sintering rate. Even minor variations in the original particle packing are exaggerated during the pore growth process; in addition, spaces between agglomerates and occasional larger voids resulting from the bridging of particles or agglomerates are present. As a result, during intermediate stages of the sintering process there is a range of pore sizes present, and the slower elimination of the larger pores leads to variations in pore concentration in the later stages of the sintering process, as illustrated in Fig. 10.28c.

In addition to local agglomerates and packing differences, pore-concentration variations in the later stages of sintering can result from particle-size variations in the starting material, from green density varia-

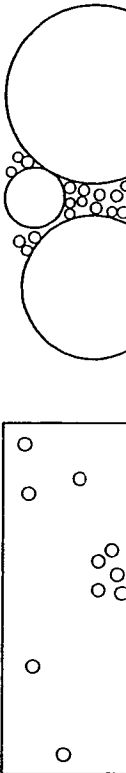


Fig. 10.28. Po
die friction, (c
elimination ne

tions caused
elimination
during heati
in pore con
containing p
That is, the
adjacent gr
orders of n
sintered oxi

Not only
residual po
thermodyna

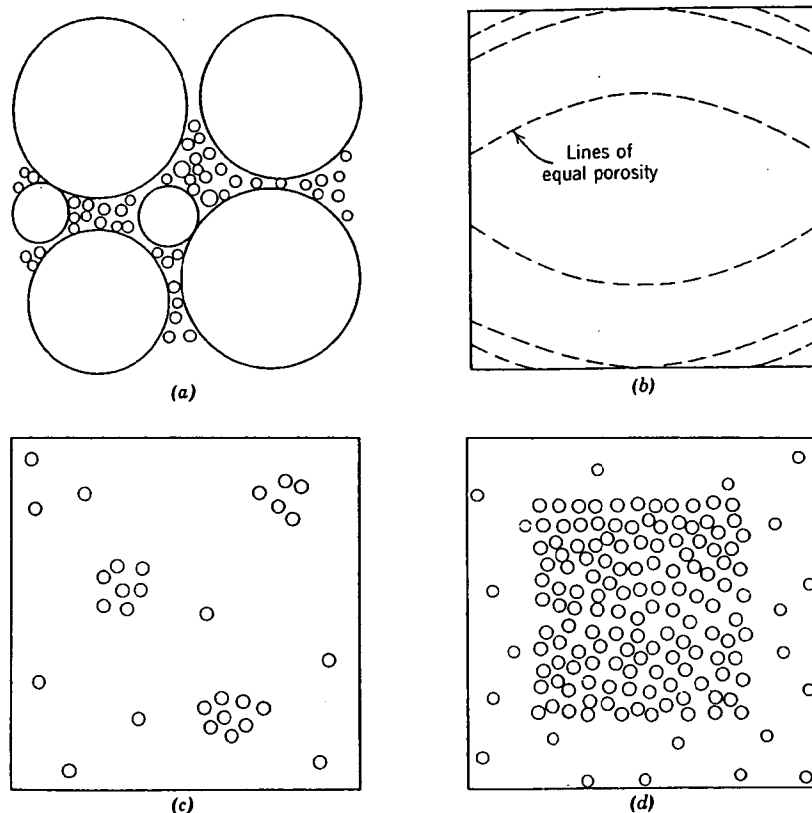


Fig. 10.28. Pore-concentration variations resulting from (a) a variation in grain sizes, (b) die friction, (c) local packing and agglomeration differences, and (d) more rapid pore elimination near surfaces.

tions caused by die-wall friction during pressing, and from the more rapid elimination of porosity near surfaces caused by temperature gradients during heating, as shown in Fig. 10.28. The importance of local variations in pore concentration results from the fact that the part of the sample containing pores tends to shrink but is restrained by other porefree parts. That is, the effective diffusion distance is no longer from the pore to an adjacent grain boundary but a pore-pore or pore-surface distance many orders of magnitude larger. An example of residual pore clusters in a sintered oxide is shown in Fig. 10.29.

Not only the kinetics of pore elimination can lead to "stable" and residual porosity, but it is also possible in some cases to have a thermodynamically metastable equilibrium pore configuration. In Fig.

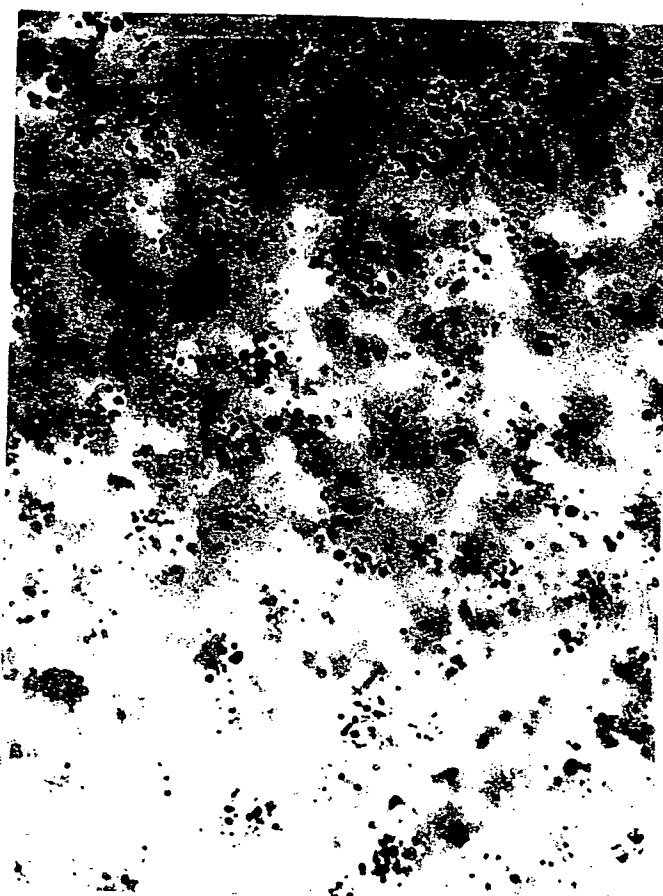


Fig. 10.29. Residual pore clusters resulting from improper powder processing in a sample of 90 mole % Y_2O_3 -10 mole % ThO_2 . Transmitted light, 137 \times . Courtesy C. Greskovich and K. N. Woods.

10.26 we have drawn spherical pores located on a grain boundary, the usual model description, but we know from our discussion of interface energies in Chapter 5 that there is a dihedral angle ϕ at the pore-boundary intersection determined by the relative interface energies;

$$\cos \frac{\phi}{2} = \frac{\gamma_{gb}}{2\gamma_s} \quad (10.30)$$

In most cases the dihedral angle for pure oxides is about 150° , and the spherical pore approximation is quite good; but for $Al_2O_3 + 0.1\%$ MgO the

value
carbide
nonsp

As c
and 10
on the
grains
polyhe
of the
angle
When

Ratio of circumscribed sphere radius to pore curvature (r/p)

Fig. 10
numbe

value is 130° , for $\text{UO}_2 + 30 \text{ ppm C}$ the value is 88° , and for impure boron carbide the value is about 60° . For these materials the consequences of nonspherical pores have to be considered.

As discussed for discontinuous grain growth and illustrated in Figs. 10.4 and 10.11, the boundary curvature between grains or phases depends both on the value of the dihedral angle and on the number of surrounding grains. If we take r as the radius of a circumscribed sphere around a polyhedral pore surrounded by grains, the ratio of the radius of curvature of the pore surfaces ρ to the spherical radius depends both on the dihedral angle and on the number of surrounding grains, as shown in Fig. 10.30a. When r/ρ decreases to zero, the interfaces are flat and have no tendency

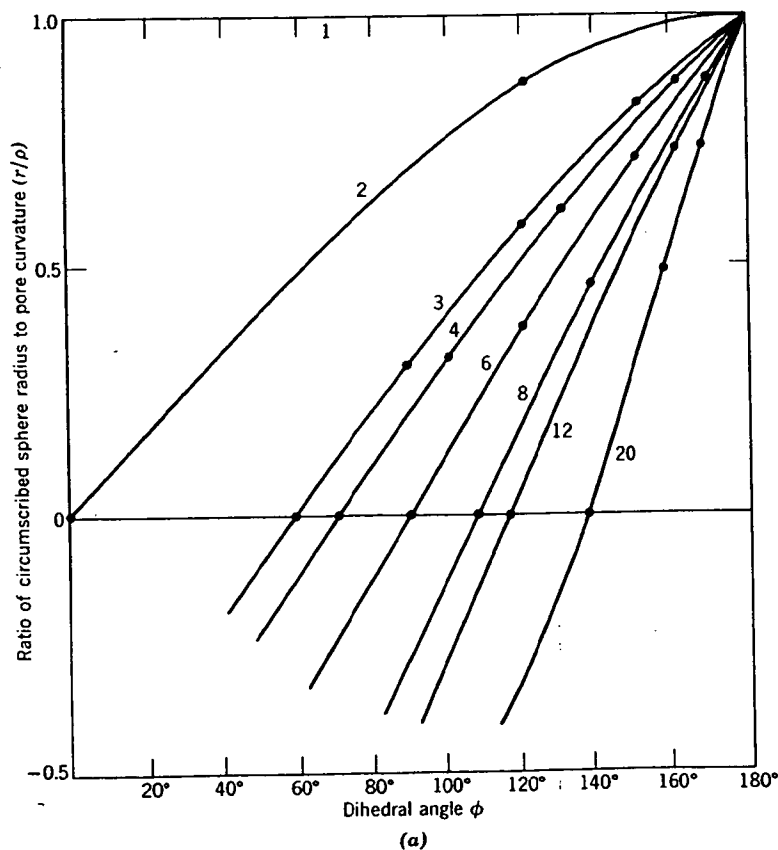


Fig. 10.30. (a) Change in the ratio (r/ρ) with dihedral angle for pores surrounded by different numbers of grains as indicated on individual curves.

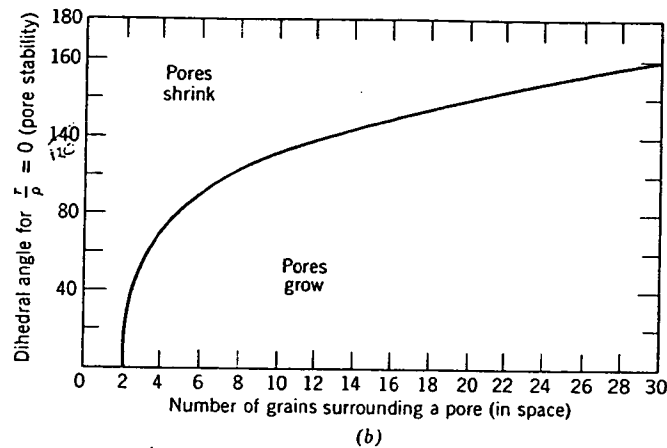


Fig. 10.30 (Continued). (b) Conditions for pore stability.

for shrinkage; when r/p is negative, the pore tends to grow. This is illustrated in Fig. 10.30b. For a uniform grain size the space-filling form is a tetrakaidecahedron with 14 surrounding grains. From an approximate relationship between the number of surrounding grains and the pore-diameter to grain-diameter ratio we can derive a relationship for pore stability as a function of dihedral angle and the ratio of pore size to grain size, as shown in Fig. 10.31. From this figure we can see why large pores present in poorly compacted powder such as shown in Fig. 10.32 not only remain stable but grow. It is also seen that an enormous disparity between

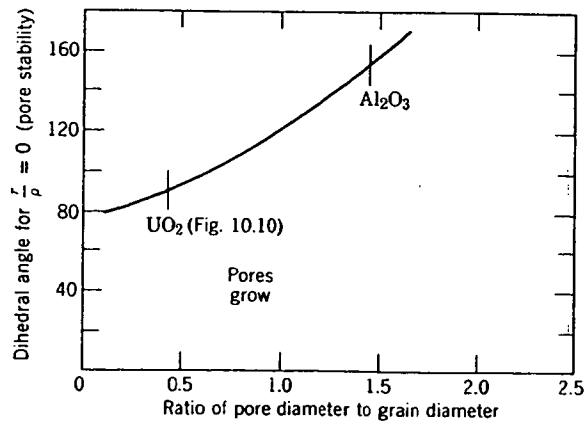


Fig. 10.31. Conditions for pore stability.

Fig. 10.32. L with scanning

grain size and size of and affects the process.

The inter two-way sintering, grain growth can occur once the pore growth can temperature from grain grain bound illustrated has occurred reduction in oxide show discontinuous grain bound



Fig. 10.32. Large voids formed by bridging of agglomerates in fine Al_2O_3 powder viewed with scanning electron microscope at 2000 \times . Courtesy C. Greskovich.

grain size and pore size is not necessary for pore stability. That is, the site and size of the porosity relative to the grain-boundary network not only affects the necessary distance for diffusion but also the driving force for the process.

The interaction of grain boundaries and porosity is, of course, a two-way street. When many pores are present during the initial stages of sintering, grain growth is inhibited. However, as discussed in Section 10.1, once the porosity has decreased to a value such that secondary grain growth can occur, extensive grain growth may result at high sintering temperatures. When grain growth occurs, many pores become isolated from grain boundaries, and the diffusion distance between pores and a grain boundary becomes large, and the rate of sintering decreases. This is illustrated in Fig. 10.16b, in which extensive secondary recrystallization has occurred, with the isolation of pores in the interior of grains and a reduction in the densification rate. Similarly, the sample of aluminum oxide shown in Fig. 10.33 has been sintered at a high temperature at which discontinuous grain growth occurred. Porosity is only removed near the grain boundaries, which act as the vacancy sink. The importance of

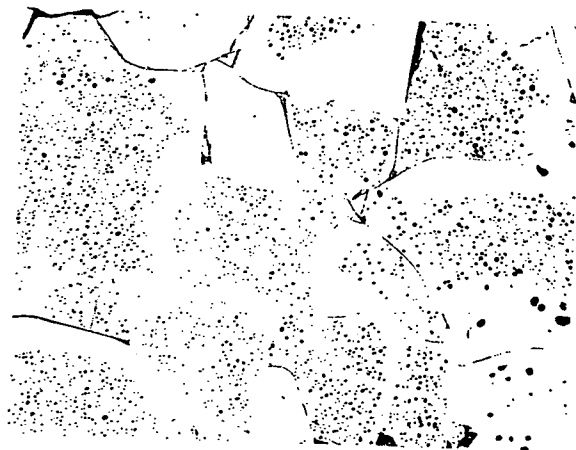


Fig. 10.33. Sintered Al_2O_3 illustrating elimination of porosity adjacent to grain boundaries with residual porosity remaining at grain centers. Courtesy J. E. Burke.

controlling grain growth as an integral part of controlling sintering phenomena cannot be overestimated. Consequently, the grain-growth processes discussed in Section 10.1 must be actively prevented in order to obtain complete densification. Usually densification continues by a diffusion process until about 10% porosity is reached; at this point rapid grain growth occurs by secondary recrystallization, and the rate of densification is sharply reduced. In order to obtain densification much beyond this level, prevention of secondary recrystallization is essential. The most satisfactory way of doing this is with additives which prevent or slow down boundary migration to a point at which it is possible to obtain pore elimination. Additions of MgO to Al_2O_3 , ThO_2 to Y_2O_3 , and CaO to ThO_2 , among others, have been found to slow boundary migration and allow complete pore elimination by solid-state sintering in these systems. The porefree microstructure of a polycrystalline ceramic having optical transparency suitable for use as a laser material is shown in Fig. 10.34.

10.3 Vitrification

To vitrify is to make glasslike and the vitrification process—densification with the aid of a viscous liquid phase—is the major firing process for the great majority of silicate systems. (In some current glossaries vitrification is defined as being identical to densification on firing, but the more specific usage is preferred.) A viscous liquid silicate is formed at the firing temperature and serves as a bond for the body. For

Fig. 10.34. Pol
Courtesy C. Gr

satisfactory
such that de
slumping or
rates of the
large extent
firing.

Process Ki
10.21), there

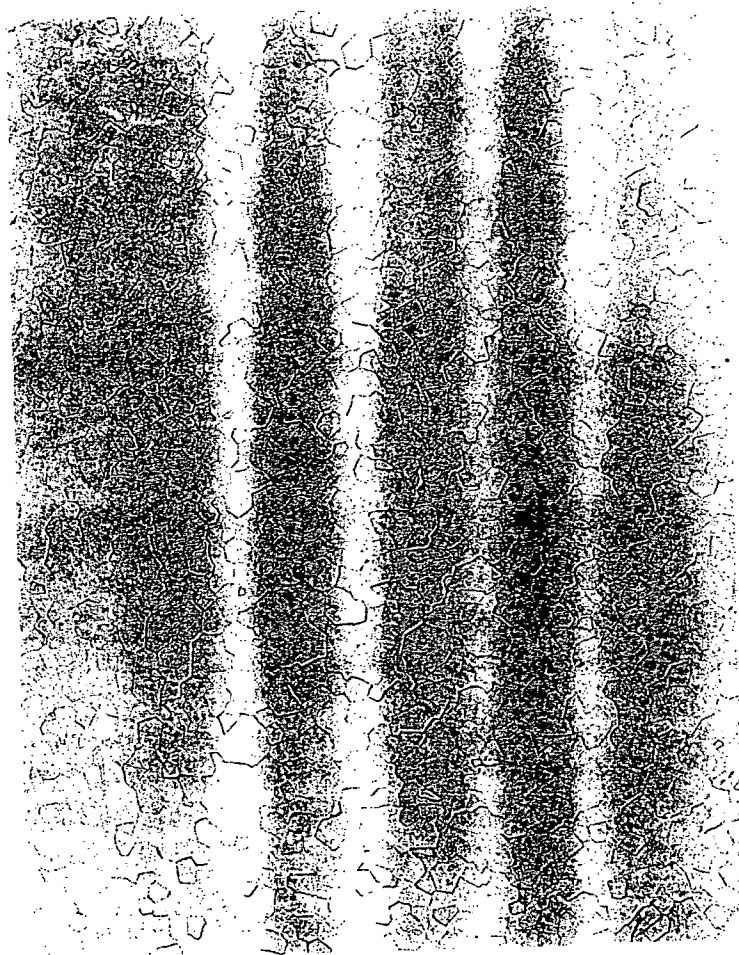


Fig. 10.34. Polished section of $Y_2O_3 + 10$ mole % ThO_2 sintered to porefree state. 100 \times . Courtesy C. Greskovich and K. N. Woods.

satisfactory firing the amount and viscosity of the liquid phase must be such that densification occurs in a reasonable time without the ware slumping or warping under the force of gravity. The relative and absolute rates of these two processes (shrinkage and deformation) determine to a large extent the temperature and compositions suitable for satisfactory firing.

Process Kinetics. If we consider two particles initially in contact (Fig. 10.21), there is a negative pressure at the small negative radius of

curvature ρ compared with the surface of the particles. This causes a viscous flow of material into the pore region. By an analysis similar to that derived for the diffusion process, the rate of initial neck growth is given as*

$$\frac{x}{r} = \left(\frac{3\gamma}{2\eta\rho} \right)^{1/2} t^{1/2} \quad (10.31)$$

The increase in contact diameter is proportional to $t^{1/2}$; the increase in area between particles is directly proportional to time. Factors of most importance in determining the rate of this process are the surface tension, viscosity, and particle size. The shrinkage which takes place is determined by the approach between particle centers and is

$$\frac{\Delta V}{V_0} = \frac{3 \Delta L}{L_0} = \frac{9\gamma}{4\eta r} t \quad (10.32)$$

That is, the initial rate of shrinkage is directly proportional to the surface tension, inversely proportional to the viscosity, and inversely proportional to the particle size.

The situation after long periods of time can best be represented as small spherical pores in a large body (Fig. 10.35). At the interior of each pore

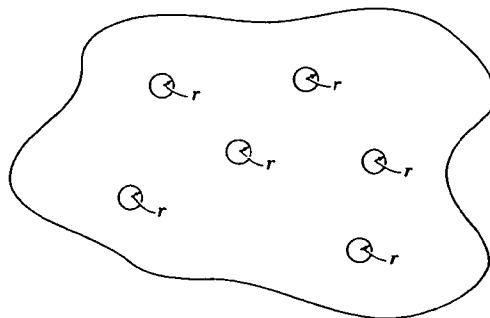


Fig. 10.35. Compact with isolated spherical pores near the end of the sintering process.

there is a negative pressure equal to $2\gamma/r$; this is equivalent to an equal positive pressure on the exterior of the compact tending to consolidate it. J. K. Mackenzie and R. Shuttleworth† have derived a relation for the rate of shrinkage resulting from the presence of isolated equal-size pores in a viscous body. The effect of surface tension is equivalent to a pressure of $-2\gamma/r$ inside all pores or, for an incompressible material, to the applica-

*J. Frenkel, *J. Phys (USSR)*, 9, 385 (1945).

†*Proc. Phys. Soc. (London)*, B62, 833 (1949).

tion of a hyc
is to deduce
viscosity of
an equation

where ρ' is
density or t
the number
pores depe

By combin

where r_0 is

The gene
plot of rel
10.36 follo
reach a rel
of the sir

Fig. 10.36.
material. Fr
(1949).

This causes a similar to that growth is given

(10.31)

the increase in factors of most surface tension, rate is deter-

(10.32)

on the surface solely propor-

is noted as small of each pore

ring process.

to an equal consolidate it. for the rate of pores in a pressure of the applica-

tion of a hydrostatic pressure of $+2\gamma/r$ to the compact. The real problem is to deduce the properties of the porous material from the porosity and viscosity of the dense material. The method of approximation used gives an equation of the form

$$\frac{d\rho'}{dt} = \frac{2}{3} \left(\frac{4\pi}{3} \right)^{1/3} n^{1/3} \frac{\gamma}{\eta} (1 - \rho')^{2/3} \rho'^{1/3} \quad (10.33)$$

where ρ' is the relative density (the bulk density divided by the true density or the fraction of true density which has been reached) and n is the number of pores per unit volume of real material. The number of pores depends on the pore size and relative density and is given by

$$n \frac{4\pi}{3} r^3 = \frac{\text{Pore volume}}{\text{Solid volume}} = \frac{1 - \rho'}{\rho'} \quad (10.34)$$

$$n^{1/3} = \left(\frac{1 - \rho'}{\rho'} \right)^{1/3} \left(\frac{3}{4\pi} \right)^{1/3} \frac{1}{r} \quad (10.35)$$

By combining with Eq. 10.33,

$$\frac{d\rho'}{dt} = \frac{3\gamma}{2r_0\eta} (1 - \rho') \quad (10.36)$$

where r_0 is the initial radius of the particles.

The general course of the densification process is best represented by a plot of relative density versus nondimensional time, illustrated in Fig. 10.36 following Eq. 10.33. Spherical pores are formed very quickly to reach a relative density of about 0.6. From this point until the completion of the sintering process about one unit of nondimensional time is

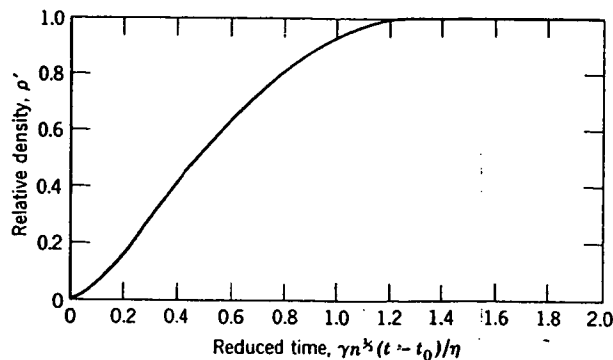


Fig. 10.36. Increase in relative density of compact with reduced time for a viscous material. From J. K. Mackenzie and R. Shuttleworth, *Proc. Phys. Soc. (London)*, B62, 833 (1949).

required. For complete densification

$$t_{\text{sec}} \sim \frac{1.5r_0\eta}{\gamma} \quad (10.37)$$

Some experimental data for the densification of a viscous body are shown in Fig. 10.37, in which the strong effect of temperature, that is, the viscosity of the material, is illustrated by the rapid change in sintering rates. The solid lines in Fig. 10.37 are calculated from Eq. 10.33. The

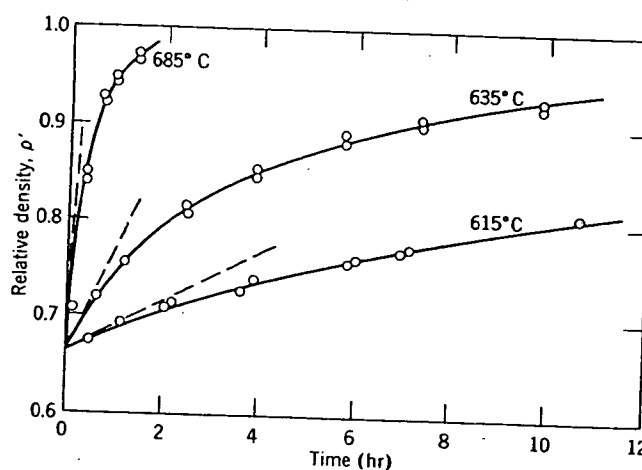


Fig. 10.37. Densification of a soda-lime-silica glass.

initial rates of sintering indicated by the dashed curves are calculated from Eq. 10.32. The good agreement of these relationships with the experimental results gives us confidence in applying them to vitrification processes in general.

Important Variables. The particular importance of Eqs. 10.31 to 10.37 is the dependence of the rate of densification on three major variables—the particle size, viscosity, and surface tension. For silicate materials the surface tension is not changed much by composition, although there are some systems for which surface energy is particularly low, as illustrated in Chapter 5. However, surface tension is not a variable that normally causes difficulty during the design of compositions or the control of processing. The particle size has a strong effect on the sintering rate and must be closely controlled if the densification process is going to be controlled. In changing from a 10-micron to 1-micron particle, the rate of sintering is increased by a factor of 10. Even more important for control

purposes typical sintering rates over an interval of 100°C may be closely controlled by changing the temperature. The relative viscosity of the material under the stresses due to grain growth supported by the grain boundaries is a factor in naturally occurring vitrification.

Silicate Systems. The fact that the rate of sintering and the pressure required for densification are much lower for silicate systems than for other systems is due to the fact that silicate systems are in the eutectic region between 75SiO₂ and 12SiO₂, and the composition is such that the viscosity is high relative to other systems, especially those of a

purposes is the viscosity and its rapid change with temperature. For a typical soda-lime-silica glass the viscosity changes by a factor of 1000 over an interval of 100°C; the rate of densification changes by an equal factor over the temperature range. This means that the temperature must be closely controlled. Viscosity is also much changed by composition, as discussed in Chapter 3. The rate of densification, then, can be increased by changing the composition to lower the viscosity of the glassy material. The relative values of viscosity and particle size are also important; the viscosity must not be so low that appreciable deformation takes place under the forces of gravity during the time required for densification. This makes it necessary for the particle size to be in such a range that the stresses due to surface tension are substantially larger than the stresses due to gravitational forces. Materials sintered in a fluid state must be supported so that deformation does not occur. The best means of obtaining densification without excessive deformation is to use very fine-grained materials and uniform distribution of materials. This requirement is one of the reasons why successful compositions in silicate systems are composed of substantial parts of talc and clays that are naturally fine-grained and provide a sufficient driving force for the vitrification process.

Silicate Systems. The importance of the vitrification process lies in the fact that most silicate systems form a viscous glass at the firing temperature and that a major part of densification results from viscous flow under the pressure caused by fine pores. Questions that naturally arise are how much liquid is present and what are its properties. Let us consider Fig. 7.26, which shows an isothermal cut at 1200°C in the $K_2O-Al_2O_3-SiO_2$ system; this is the lower range of firing temperatures used for semivitreous porcelain bodies composed of about 50% kaolin (45% Al_2O_3 , 55% SiO_2), 25% potash-feldspar, and 25% silica. This and similar compositions are in the primary field of mullite, and at 1200°C there is an equilibrium between mullite crystals and a liquid having a composition approximately 75 SiO_2 , 12.5 K_2O , 12.5 Al_2O_3 , not much different in composition from the eutectic liquid in the feldspar-silica system (Fig. 7.14). In actual practice only a small part of the silica present as flint enters into the liquid phase, and the composition of the liquid depends on the fineness of the grinding as well as on the overall chemical composition. However, the amount of silica which dissolves does not have a large effect on the amount and composition of the liquid phase present. The liquid is siliceous and has a high viscosity; the major effect of compositional changes is to alter the relative amounts of mullite and liquid phases present. Since mullite is very fine-grained, the fluid flow properties of the body correspond to those of a liquid having a viscosity greater than the pure liquid phase. For

some systems the overall flow process corresponds to plastic flow with a yield point rather than to true viscous flow. This changes the kinetics of the vitrification process by introducing an additional term in Eqs. 10.33 and 10.36 but does not change the relative effects of different variables.

Although phase diagrams are useful, they do not show all the effects of small changes in composition. For example, a kaolinite composition should show equilibrium between mullite and tridymite at 1400°C with no glassy material. However, it is observed experimentally that even after 24 hr about 60 vol% of the original starting material is amorphous and deforms as a liquid. The addition of a small amount of lithium oxide as Li_2CO_3 has been observed to give a larger content of glass than additions of the same composition as the fluoride. Similar small amounts of other mineralizers can also have a profound effect in the firing properties of particular compositions. That fine grinding and intimate mixing reduce the vitrification temperature follows from the analysis in Eqs. 10.31 to 10.37. S. C. Sane and R. L. Cook* found that ball milling for 100 hr reduced the final porosity of a clay-feldspar-flint composition from 17.1 to 0.3% with the same firing conditions. This change is caused in part by increased tendencies toward fusion equilibrium and uniform mixing of constituents and in part by the smaller initial particle and pore size. In contrast to triaxial (flint-feldspar-clay) porcelains, which frequently do not reach fusion equilibrium, many steatite bodies and similar compositions which are prepared with fine-particle, intimately mixed material and form a less siliceous liquid reach phase equilibrium early in the firing process.

The time-temperature relationship and the great dependence of vitrification processes on temperature can perhaps be seen best in the experimental measurements illustrated in Fig. 10.38. As shown there, the time required for a porcelain body to reach an equivalent maturity changes by almost an order of magnitude with a 50° temperature change. There are changes in both the amount and viscosity of the glassy phase during firing, so that it is difficult to elucidate a specific activation energy for the process with which to compare the activation energy for viscous flow. However, the temperature dependence of the vitrification rate of a composition such as this (a mixture of clay, feldspar, and flint) is greater than the temperature dependence of viscosity alone. This is to be expected from the increased liquid content at the higher firing temperatures.

In summary, the factors determining the vitrification rate are the pore size, viscosity of the overall composition (which depends on amount of liquid phase present and its viscosity), and the surface tension. Equivalent

*J. Am. Ceram. Soc., 34, 145 (1951).

Fig. 10.38. E
from F. H. N

densificatio
In controll
of the incre
tures. Chai
vitrification

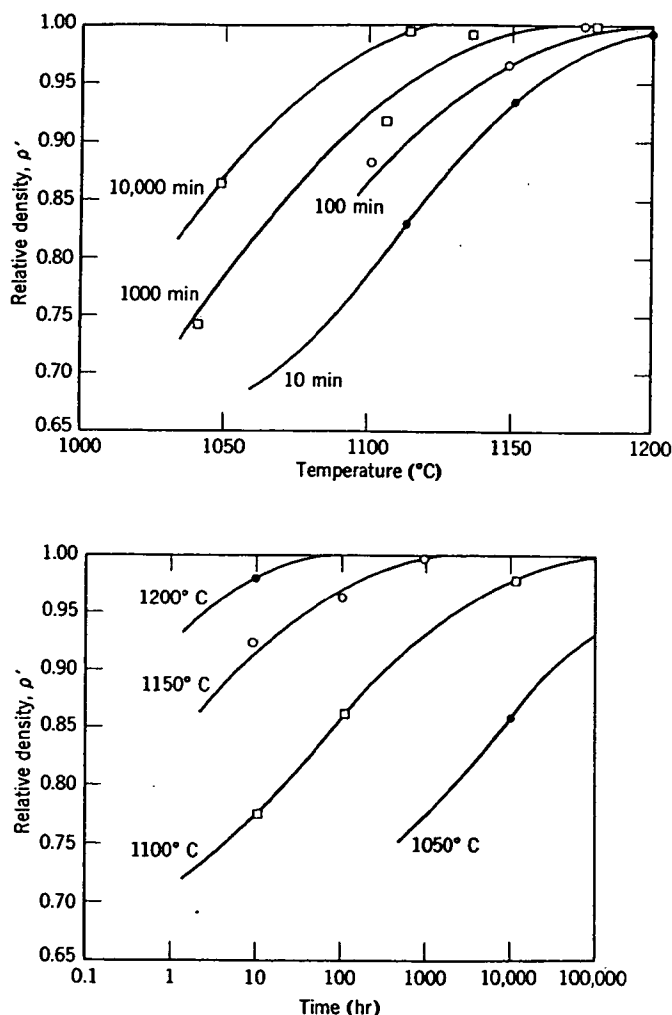


Fig. 10.38. Effect of time and temperature on the vitrification of a porcelain body. Data from F. H. Norton and F. B. Hodgdon, *J. Am. Ceram. Soc.*, 14, 177 (1931).

densification results from longer periods of time at the same temperature. In controlling the process, the temperature dependence is great because of the increase in liquid content and lowered viscosity at higher temperatures. Changes in processing and changes in composition affect the vitrification process as they affect these parameters.

10.4 Sintering with a Reactive Liquid

Another quite different process which leads to densification is sintering in the presence of a reactive liquid. Here we are referring to systems in which the solid phase shows a certain limited solubility in the liquid at the sintering temperature; the essential part of the sintering process is the solution and reprecipitation of solids to give increased grain size and density. This kind of process occurs in cermet systems such as bonded carbides and also in oxide systems when the liquid phase is fluid and reactive, such as magnesium oxide with a small amount of liquid phase present (Fig. 10.39), UO_2 with the addition of a small amount of TiO_2 (Fig. 7.11), and high-alumina bodies which have an alkaline earth silicate as a bonding material.

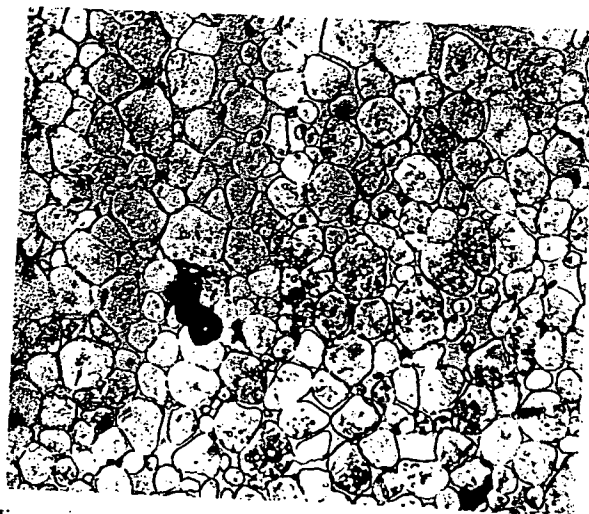


Fig. 10.39. Microstructure of magnesium—2% kaolin body resulting from reactive-liquid sintering (245 \times).

Studies of a large number of systems indicate that for densification to take place rapidly it is essential to have (1) an appreciable amount of liquid phase, (2) an appreciable solubility of the solid in the liquid, and (3) wetting of the solid by the liquid. The driving force for densification is derived from the capillary pressure of the liquid phase located between the fine solid particles, as illustrated in Fig. 10.40. When the liquid phase wets the solid particles, each interparticle space becomes a capillary in which a substantial capillary pressure is developed. For submicron particle sizes, capillaries with diameters in the range of 0.1 to 1 micron

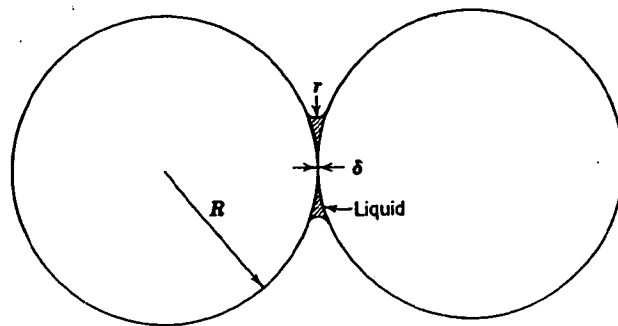


Fig. 10.40. (a) S
Drop of liquid bet
of forsterite cera

interfering
stems in
id at the
s is the
ize and
bonded
uid and
d phase
O₂ (Fig.
ate as a



(a)



(b)



(c)

Fig. 10.40. (a) Surface of solid-liquid composite with varying amounts of liquid phase. (b) Drop of liquid between two solid spheres exerts pressure to pull them together. (c) Surface of forsterite ceramic showing liquid capillary depression between crystals.

ve-liquid

ition to
unt of
and (3)
ition is
etween
l phase
lary in
micron
micron

develop pressures in the range of 175 to 1750 psi for silicate liquids and in the range of 975 to 9750 psi for a metal such as liquid cobalt (see discussion in Chapter 5 and Table 5.2).

The capillary pressure results in densification by different processes which occur coincidentally. First, on formation of a liquid phase there is a rearrangement of particles to give a more effective packing. This process can lead to complete densification if the volume of liquid present is sufficient to fill in the interstices completely. Second, at contact points where there are bridges between particles high local stresses lead to plastic deformation and creep, which allow a further rearrangement. Third, there is during the sintering process a solution of smaller particles and growth of larger particles by material transfer through the liquid phase. The kinetics of this solution-precipitation process have already been discussed in Chapter 9. Because there is a constantly imposed capillary pressure, additional particle rearrangement can occur during grain-growth and grain-shape changes and give further densification. (As discussed for vapor transport and surface diffusion in solid-state sintering, mere solution-precipitation material transfer without the imposed capillary pressure would not give rise to densification). Fourth, in cases in which liquid penetrates between particles the increased pressure at the contact points leads to an increased solubility such that there is material transfer away from the contact areas so that the particle centers approach one another and shrinkage results; the increase in solubility resulting from the contact pressure has been discussed in Chapter 5. Finally, unless there is complete wetting, recrystallization and grain growth sufficient to form a solid skeleton occur, and the densification process is slowed and stopped.

Perhaps even more than for the solid-state process, sintering in the presence of a liquid phase is a complex process in which a number of phenomena occur simultaneously. Each has been shown to occur, but experimental systems in which a single process had been isolated and analysed during sintering have not been convincingly demonstrated. Clearly, the process requires a fine-particle solid phase to develop the necessary capillary pressures which are proportional to the inverse capillary diameter. Clearly, the liquid concentration relative to the solid particle packing must be in a range appropriate for developing the necessary capillary pressure. Clearly, if and when a solid skeleton develops by particle coalescence, the process stops.

A critical and still controversial question is the degree of wetting required for the process to proceed. In some important systems such as tungsten carbide-cobalt and titanium carbide-nickel-molybdenum the dihedral angle is zero. In other systems such as iron-copper and magnesia-silicate liquids this is not the case at equilibrium; but the dihedral angle is

low, and the necessary capillary pressure for the liquid phase process, as essential for effective as

Fig. 10.41. G
compositions
Trans. Brit. C

10.5 Press

The sintering pressures required for densification at elevated temperatures are also removable at advantage temperatures.

*R. L. Cob

low, and the solid is wetted by the liquid phase, as required to develop the necessary capillary pressure. For grain growth of periclase particles in a silicate liquid, the dihedral angle has a large effect on the grain-growth process, as illustrated in Fig. 10.41. Although zero dihedral angle is not essential for liquid-phase sintering to occur, the process becomes more effective as this ideal is approached.

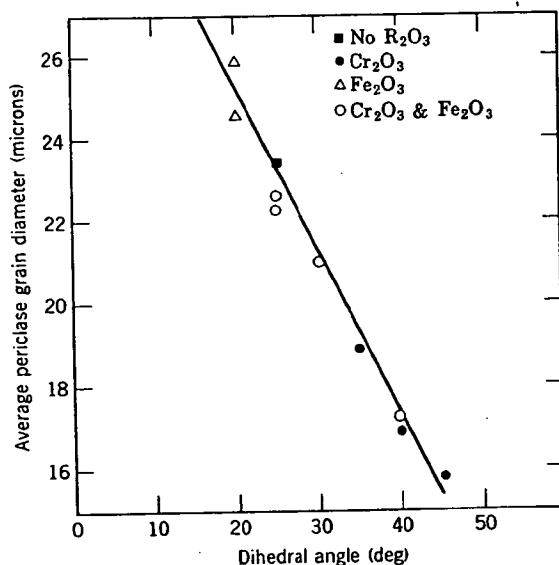


Fig. 10.41. Grain growth of periclase particles in liquid-phase-sintered periclase-silicate compositions as a function of dihedral angle. From B. Jackson, W. F. Ford, and J. White, *Trans. Brit. Ceram. Soc.*, 62, 577 (1963).

10.5 Pressure Sintering and Hot Pressing

The sintering processes thus far discussed depend on the capillary pressures resulting from surface energy to provide the driving force for densification. Another method is to apply an external pressure, usually at elevated temperature, rather than relying entirely on capillarity.* This is desirable in that it eliminates the need for very fine-particle materials and also removes large pores caused by nonuniform mixing. An additional advantage is that in some cases densification can be obtained at a temperature at which extensive grain growth or secondary recrystalliza-

*R. L. Coble, *J. Appl. Phys.* 41, 4798 (1970).

tion does not occur. Since the mechanical properties of many ceramic systems are maximized with high density and small grain size, optimum properties can be obtained by hot-pressing techniques. The effect of added pressure on the densification of a beryllium oxide body is illustrated in Fig. 10.42. The main disadvantages of hot pressing for oxide

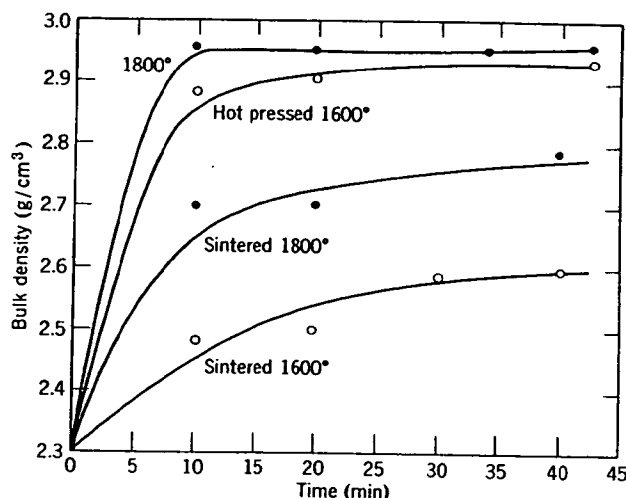


Fig. 10.42. Densification of beryllia by sintering and by hot pressing at 2000 psi.

bodies are the unavailability of inexpensive and long-life dies for high temperatures and the difficulty in making the process into an automatic one to achieve high-speed production. Both factors make the hot-pressing process an expensive one. For oxide materials which have to be pressed at temperature above 1200 or 1300°C (often at 1800 to 2000°C) graphite is the most satisfactory die material available; the maximum stress is limited to a few thousand pounds per square inch, and the life of dies is usually limited to seven or eight pieces. The entire die must be heated and cooled with the formation of each piece. Techniques for using high temperatures in a process in which the die is maintained cool with the material heated have shown some promise in laboratory tests but have not been developed for production.

For lower-temperature materials, such as glasses or glass-bonded compositions which can be pressed in metal dies at temperatures below 800 to 900°C, the hot-pressing process can be developed as an automatic and inexpensive forming method. This is similar to the normal pressing of

glass as
shape 1

Dens
which
liquid-
when h
materi
densifi
pressur
erature
optimu
nearly
carbide
It is of
MgO,
induce

10.6

The
connec
growth
these
occur
chemi
closed
pressu
genera
major
them
possib

Oxi
which
as bin
oxidiz
organi
tempe
tempe
this p
carbon
before
tempe

glass as a glass-forming method in which it is used to obtain the desired shape rather than as a means of eliminating porosity.

Densification during pressure sintering can occur by all the mechanisms which have been discussed for solid-state sintering, vitrification, and liquid-phase sintering. In addition, particularly during the early stages, when high stresses are present at the particle contact points, and for soft materials, such as the alkali halides, plastic deformation is an important densification mode. Since the grain-growth process is insensitive to pressure, pressure-sintering oxides at high pressures and moderate temperatures allows the fabrication of high-density-small-grain samples with optimum mechanical properties and with sufficiently low porosity to be nearly transparent. Covalent materials such as boron carbide, silicon carbide, and silicon nitride can be hot-pressed to nearly complete density. It is often advantageous to add a small fraction of liquid phase (i.e., LiF to MgO, B to silicon carbide, MgO to silicon nitride) to allow pressure-induced liquid phase, or liquid-film, sintering to occur.

10.6 Secondary Phenomena

The primary processes which occur on heating and are important in connection with the firing behavior of all ceramic compositions are grain growth and densification, as discussed in previous sections. In addition to these changes, there are a large number of other possible effects which occur during the firing of some particular compositions. These include chemical reactions, oxidation, phase transitions, effects of gas trapped in closed pores, effects of nonuniform mixing, and the application of pressure during heating. Although they are not processes of the most general importance, they frequently cause the main problems and the major phenomena observed during firing. Although we cannot discuss them in great detail, we should at least be familiar with some of the possibilities.

Oxidation. Many natural clays contain a few percent organic matter which must be oxidized during firing. In addition, varnishes or resins used as binders, as well as starches and other organic plasticizers, must be oxidized during firing, or difficulties result. Under normal conditions organic materials char at temperatures above 150°C and burn out at temperatures ranging from 300 to 400°C. Particularly with low-firing-temperature compositions, it is necessary to heat at a slow enough rate for this process to be completed before shrinkage becomes substantial. If the carbonaceous material is sealed off from the air by vitrification occurring before oxidation is completed, it acts as a reducing agent at higher temperatures. Sometimes this may merely affect the color, giving rise to

black coring of brick and heavy clay products whose interiors are in a reduced state, black in color. A typical example of a stoneware heated too rapidly for oxidation to be completed is illustrated in Fig. 10.43, which shows the central black core. Very often impurities present, particularly sulfides, may cause difficulties unless oxidized before vitrification. Sulfides in general react with oxygen in the temperature range of 350 to 800°C, forming SO_2 gas which escapes through open pores.

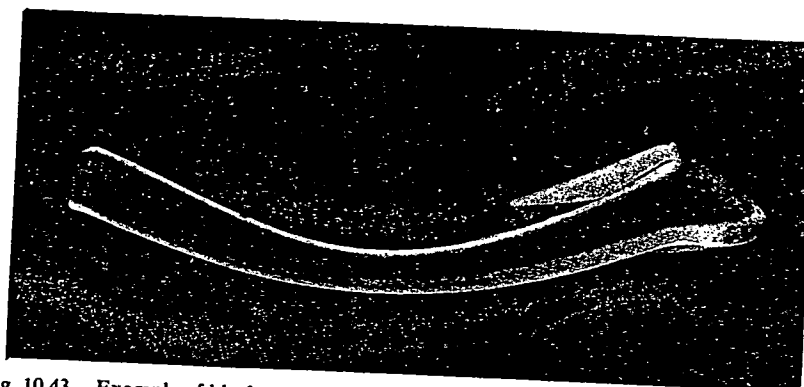


Fig. 10.43. Example of black core produced when time allowed for oxidation reactions was insufficient for completion of the reaction.

In ferrite and titania compositions control of oxidation reactions during firing is particularly important. As illustrated for the Ti-TiO_2 and Fe-O_2 systems (Chapter 7), the phases present depend on the oxygen pressure. In addition, as discussed in Chapter 4, the composition of these phases covers a substantial range of stoichiometry and depends on the oxygen pressure. It is common practice in the manufacture of ferrites to control the oxygen pressure during firing so that the composition of each phase present, and the overall phase composition of the body, is maintained to give the best magnetic properties.

Decomposition Reactions. Many of the constituents used in ceramic bodies are in the form of carbonates or hydrated compounds; these decompose during firing to form the oxide plus a gaseous product (CO_2 , H_2O). Many impurities are also incorporated as carbonates, hydrates, and sulfates and decompose during firing (see Section 9.4).

Hydrates decompose over a wide temperature range between 100 and 1000°C, depending on the particular composition. Carbonates decompose over a temperature range from 400 to 1000°C, also depending on the particular composition. For each temperature there is, of course, an

equilibrium further decomposition encountered at higher temperatures. Large pores, to form cell off before a phase that is particularly a temperature gradient and are the two firing.

Sulfates decompose they remain bodies. In a high sulfur burned brick salts to the barium calcium sulf

Decomposition. A particular of kyanite, to 1450°C. mullite and than kyanite composition other constituents Al_2O_3 to form magnesia a high-temperature heating car

Phase Transformations. Possible and anticipated transformations cannot since the time such a large

equilibrium pressure of the gaseous product; if this pressure is exceeded, further decomposition does not take place, leading to the major problem encountered, the sealing of pores before complete dissociation. As the temperature is raised, the decomposition pressure increases and forms large pores, blistering, and bloating. (This is, of course, the method used to form cellular glass products in which the surface is intentionally sealed off before chemical reaction or decomposition takes place to form a gas phase that expands and produces a foamed product.) This kind of defect is particularly common when high heating rates are used, for then there is a temperature gradient between the surface and interior of the ware, and the surface layer vitrifies, sealing off the interior. This temperature gradient and the time required for oxidation of constituents or impurities are the two most important reasons for limiting the rate of heating during firing.

Sulfates create a particular problem in firing because they do not decompose until a temperature of 1200 to 1300°C is reached. Therefore they remain stable during the firing process used for burning many clay bodies. In particular, CaSO_4 is stable but slightly soluble in water, so that a high sulfate content leads to a high concentration of soluble salts in the burned brick. This causes efflorescence—the transport of slightly soluble salts to the surface, forming an undesirable white deposit. Addition of barium carbonate prevents the deposit from forming by reacting with calcium sulfate to precipitate insoluble barium sulfate.

Decomposition also occurs in some materials to form new solid phases. A particular example used in refractory technology is the decomposition of kyanite, $\text{Al}_2\text{O}_3 \cdot \text{SiO}_2$, to form mullite and silica at a temperature of 1300 to 1450°C. This reaction proceeds with an increase in volume, since both mullite and the silica glass or cristobalite formed have lower densities than kyanite. The reaction is useful, since the addition of kyanite to a composition can counteract a substantial part of the firing shrinkage if the other constituents are carefully selected. Similarly, reaction of MgO with Al_2O_3 to form spinel occurs with a decrease in volume. By incorporating magnesia and alumina in a refractory mix, or more commonly in a high-temperature ramming mix or cement, the shrinkage taking place on heating can be decreased.

Phase Transformations. Polymorphic transformations may be desirable or undesirable, depending on the particular composition and the anticipated use. If a large volume change accompanies the polymorphic transformation, difficulties result; owing to the induced stresses. Refractories cannot be made containing pure zirconium oxide, for example, since the tetragonal monoclinic transformation at about 1000° involves such a large volume change that the ware is disrupted. The source of these

stresses has been discussed in Chapter 5 in connection with boundary stresses caused by differential thermal expansion or contraction of different grains. The expansion or contraction of a crystal in a matrix leads to the same sort of stresses that may give rise to actual cracking, illustrated for quartz grains in a porcelain body in Fig. 10.44. The stresses in individual grains can be reduced if the grain size is reduced; properties of porcelains are improved if fine-grained flint is used rather than coarse material.

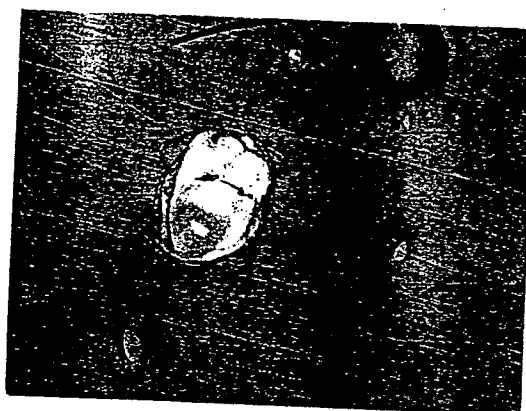


Fig. 10.44. Cracked quartz grain and surrounding matrix in a porcelain body. Differential expansion due mainly to the α - β quartz transition leads to cracking of larger grains but leaves small grains intact (500 \times).

Sometimes desirable phase transformations only occur sluggishly. This is what happens, for example, with the firing of refractory silica brick. The transition from quartz, the starting material, to tridymite and cristobalite, the desired end constituents, occurs only slowly. In order to increase the rate of transformation, calcium oxide is added as a mineralizer. The calcium oxide forms a liquid in which silica is soluble. Consequently the quartz dissolves and precipitates as tridymite, which is the more stable phase (Chapter 7). Some of the quartz transforms directly to cristobalite during the process as well. In general, mineralizers help in achieving equilibrium conditions by providing a mechanism of material transfer—solution or vaporization—that circumvents energy barriers to direct transformations. In silicate systems the addition of fluorides or hydroxyl ions is particularly helpful in this regard, since they greatly increase the fluidity of the liquid phase present.

Trapped Gases. In addition to the bloating occasioned by decomposition reactions, trapping of gases within closed pores imposes a limitation

on the ultimate water vapor pressure from close carbon monoxide solubility spherical of 0.8 atm. when the limited. A negative negative to $1/r$; this factor required, translucent

Nonuniform sintering. short of imperfections present. common. (that is, introduction of these porosity forming

Overfiring. variety of a reduced titanates higher temperature there is optimum common cause of gases

10.7 Firing

As for amount of material removed

on the ultimate density that can be reached during firing. Gases such as water vapor, hydrogen, and oxygen (to a lesser extent) are able to escape from closed pores by solution and diffusion. In contrast, gases such as carbon monoxide, carbon dioxide, and particularly nitrogen have a lower solubility and do not normally escape from closed pores. If, for example, spherical pores are closed at a total porosity of 10% and a partial pressure of 0.8 atm nitrogen, the pressure has increased to 8 atm (about 110 psi) when they have shrunk to a total porosity of 1%, and further shrinkage is limited. At the same time that the gas pressure is increasing, however, the negative radius of curvature of the pore becomes small so that the negative pressure produced by surface tension is increased proportional to $1/r$; the gas pressure builds up proportional to $1/r^3$. For sintering in air this factor usually limits densification; where very high densities are required, as for optical materials or dental porcelains requiring high translucency, vacuum or hydrogen atmosphere is preferred.

Nonuniform Mixing. Although not mentioned in most discussions of sintering, the most important reason why densification and shrinkage stop short of complete elimination of pores is that gross defects caused by imperfect mixing and compact consolidation prior to firing are usually present. Examination of typical production ceramics shows that they commonly contain upward of 10% porosity in the millimeter size range (that is, pores much larger than the particle size of the raw materials introduced in the composition). These pores are caused by local variations induced during forming, and there is no tendency for elimination of these pores during firing. Corrective treatment must be taken in the forming method.

Overfiring. Ware is commonly referred to as overfired if for any of a variety of reasons a higher firing temperature leads to poorer properties or a reduced shrinkage. For solid-state sintering, such as ferrites and titanates, a common cause is secondary recrystallization occurring at the higher temperature before the elimination of porosity. Consequently, there is some maximum temperature at which the greatest density or optimum properties are obtained. For vitreous ceramics the most common cause of overfiring is the trapping of gases in pores or the evolution of gases which cause bloating or blistering.

10.7 Firing Shrinkage

As formed, green ware contains between 25 and 50 vol% porosity. The amount depends on the particle size, particle-size distribution, and forming method (Chapter 1). During the firing process this porosity is removed; the volume firing shrinkage is equal to the pore volume

eliminated. This firing shrinkage can be substantially decreased by addition of nonshrinking material to the mix; fire-clay brick is commonly manufactured with grog (prefired clay) additions which serve to decrease firing shrinkage. Similarly, this is one of the functions of the flint in the porcelain body; it provides a nonshrinking structure which reduces the shrinkage during firing. Terra-cotta compositions, composed of mixtures of fired grog and clay, can be made in large shapes because a large part of the raw material has been prefired and the firing shrinkage is low.

If firing is carried to complete densification, the fractional porosity originally present is equal to the shrinkage taking place during firing. This commonly amounts to as much as 35% volume shrinkage or 12 to 15% linear shrinkage and causes difficulty in maintaining close tolerances. However, the main difficulties are warping or distortion caused by different amounts of firing shrinkage at different parts of the ware. Nonuniform shrinking can sometimes even cause cracks to open.

Warping. A major cause of warping during firing is density variations in the green ware. There are many reasons for differences in porosity in the green ware. The density after firing is nearly uniform, and there is higher shrinkage for the parts that had a low density than for the parts that had a high density in the green ware. In pressed ware, pressure variations in the die (Chapter 1) cause different amounts of compaction at different parts of a pressed piece; usually the shrinkage at the center is larger than the shrinkage at the ends, and an hourglass shape results from an initially cylindrical sample (Fig. 10.45a).

Another source of warping during firing is the presence of temperature gradients. If ware is laid on a flat plate and heated from above, there is a temperature difference between the top and bottom of the ware that may cause greater shrinkage at the top than at the bottom and a corresponding warping. In some cases the gravitational stresses may be sufficient to make the ware lie flat, even though shrinkage is nonuniform. The relationship between temperature distribution, warpage, and deformation under the stresses developed is complicated and difficult to analyze quantitatively. Another source of warpage in firing is preferred orientation of the platy clay particles during the forming process. This causes the drying and firing shrinkage to have directional properties.

Vitreous ware is also warped by flow under forces of gravity. This is especially true for large heavy pieces in which substantial stresses are developed. In the forming of vitreous sanitary ware, the upper surface of a closet bowl (Fig. 10.45c) or a lavatory (Fig. 10.45d) must be designed with a greater curvature than is desired in the end product so that the settling which occurs on firing produces a final shape that is satisfactory. A final contributor to warpage during firing is the frictional force or *drag*

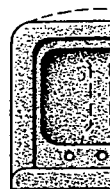


Fig. 10.45. Firing shrinkage with different density variations and frictional forces.

of the ware shrink less so that the top of the ware is wider than the bottom.

Difficulties in firing and warping can be avoided by using a method to fire the ware in a way that causes uniform shrinkage. This is done by firing the ware in a furnace that is designed to fire the ware uniformly. The other source of length to mixtures that cause a deformation. During an unsymmetrical firing, the ware can be overfired, as shown in Fig. 10.4

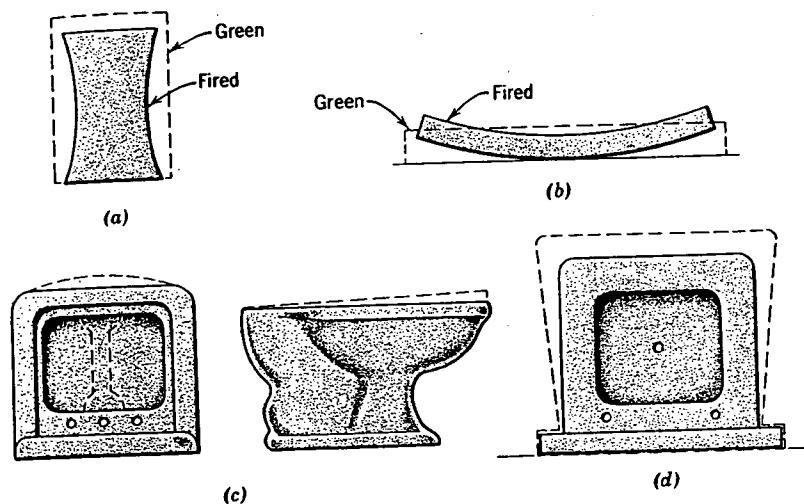


Fig. 10.45. Firing shrinkage of (a) pressed crucible with differential shrinkage due to green density variations, (b) tile with differential shrinkage due to temperature gradients, (c) ware with differential shrinkage due to gravity settling, and (d) differential shrinkage due to frictional force of setting.

of the ware against the setter. This means that the bottom surface tends to shrink less than the upper surface (Fig. 10.45d). Ware must be designed so that the final shape, including shrinkage, comes out to be rectangular.

Difficulties caused by differential firing shrinkage, resulting distortion, and warping can be eliminated in three ways: first, altering the forming method to minimize the causes of warping; second, designing shapes in a way that compensates for warping; and third, using setting methods in firing that minimize the effects of warping. One obvious improvement in forming methods is to obtain uniformity of the structure during initial forming. This requires elimination of pressure gradients, segregation, and other sources of porosity variation. Pressing samples that have long ratios of length to die diameter cause density variations. Extruded and pressed mixes that have low plasticity are particularly prone to large pressure variations and green density differences. Slip casting and extrusion both cause a degree of segregation and density differences during firing. Some settling may occur during the casting process, causing structural variations. During extrusion pressure differences at various parts of the die or an unsymmetrical setting for the die can cause variations.

Sometimes variations in firing shrinkage and difficulties from warping can be overcome by compensating the shapes. This is true, for example, in Fig. 10.45, in which the closet bowl and lavatory are designed in such a

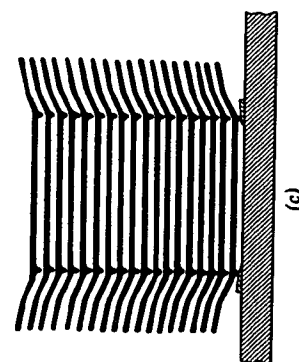
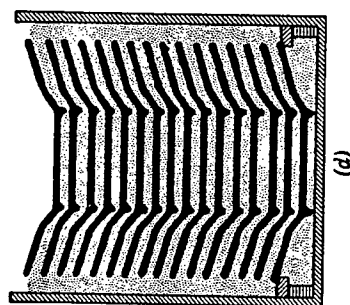
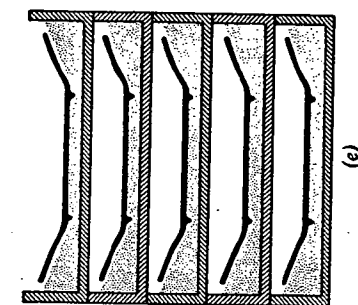
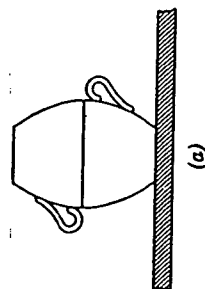
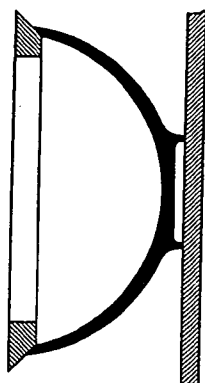
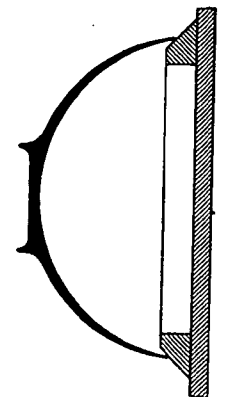
ally decreased by
brick is commonly
serve to decrease
of the flint in the
which reduces the
posed of mixtures
use a large part of
kage is low.

rational porosity
during firing. This
age or 12 to 15%
close tolerances.
ortion caused by
rts of the ware.
ks to open.

density variations
ces in porosity in
orm, and there is
for the parts that
ressure variations
action at different
ter is larger than
s from an initially

of temperature
above, there is a
he ware that may
a corresponding
be sufficient to
nonuniform. The
and deformation
difficult to analyze
referred orienta-
ness. This causes
erties.

gravity. This is
tial stresses are
upper surface of
must be designed
duct so that the
t is satisfactory.
ial force or drag





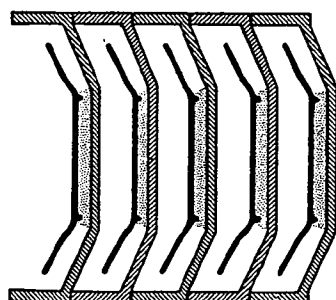
(e)



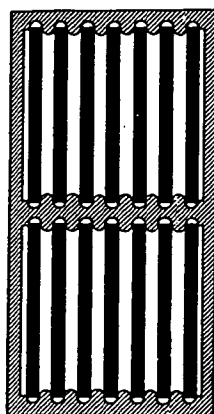
(d)



(c)



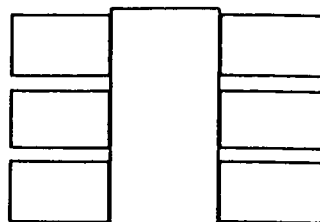
(b)



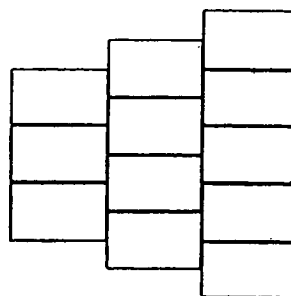
(h)



(g)



(i)



(j)

Fig. 10.46. Setting methods for (a) cups and bowls, (b) large bowls, (c) earthenware, (d) hotel china plates, (e) bone china plates, (f) frit porcelain plates, (g) hard porcelain plates, (h) tile, (i) brick checkerwork, (j) brick bench setting. From F. H. Norton.

way that the final shape is satisfactory. In the same way, when plates are fired in the horizontal position there is a tendency for the rims to settle; this can be compensated for by adjusting the shape of the initial piece.

Correct setting methods are important in eliminating difficulties caused by firing-shrinkage variations. These have been most extensively developed for porcelain compositions in which complete vitrification is desired and high shrinkages result. Some of the standard setting methods are illustrated in Fig. 10.46. Cups and bowls are commonly boxed as indicated in Fig. 10.46a. This keeps the rim circular, since warpage of one restricts warpage of the other; in addition, it prevents the thin rims from being too rapidly heated. For larger pieces, unfired setters are necessary as a means of controlling shrinkage and maintaining circular rims. A variety of methods is used for setting different kinds of plate compositions, depending on the amount of shrinkage expected. For ware fired to complete vitrification individual setting and support are essential. For ware fired to partial densification, plates can be stacked with no ill effects. In general, large tiles and brick do not cause much difficulty.

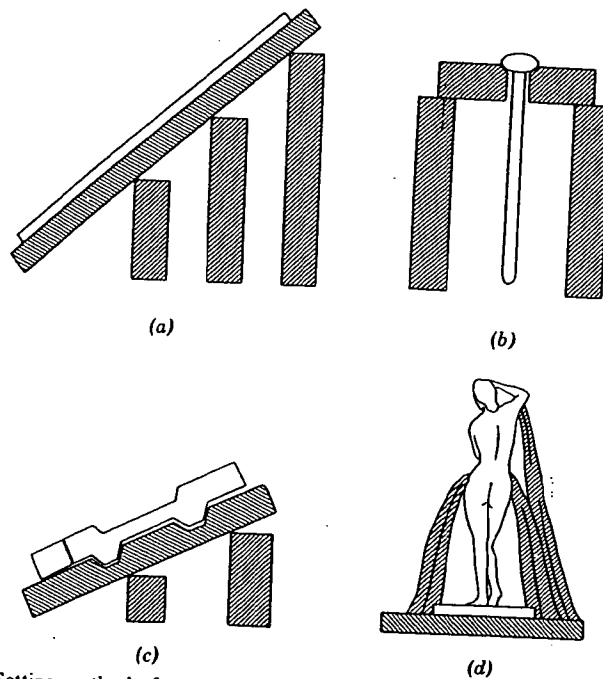


Fig. 10.47. Setting methods for special shapes. (a) Large tiles set at an angle of repose; (b) slender rod supported by collar; (c) special shape; (d) sculptured piece. From F. H. Norton.

G

Special sl
verse effect
angle of rep
shrink with
an inclined
10.47b). Gr
several feet
designed fo
handle uniq
are particul
from unfire

1. G. C. Ku
Phenomen
2. G. C. Ku
Research,
3. R. L. Co
Burke, E
4. W. D. Ki
Cambridg
5. W. D. Ki
ogy Press
6. J. E. Burl
Prog. Me
7. E. Schra
Bodies,"
8. For addi
(1970); D.

- 10.1. Disting
tallizat
import
- 10.2. Explai
approx
gradien
- 10.3. Can g
grain g

Special shapes may require special setting methods to eliminate adverse effects of firing shrinkage. Large refractory tile can be set at an angle of repose on a flat surface (Fig. 10.47a). This allows the tile to shrink without much stress. In the same way rods or tubes may be set in an inclined V groove or supported by a collar from the upper end (Fig. 10.47b). Gravitational forces keep the tubes straight up to lengths of several feet. Unique shapes can always be supported on special setters designed for the particular sample. Some experience is necessary to handle unique shapes efficiently. Small pieces of sculptured vitrified ware are particularly difficult. The safest setting provides complete support from unfired struts (Fig. 10.47d).

Suggested Reading

1. G. C. Kuczyuski, N. A. Hooton, and C. F. Gibson, Eds., *Sintering and Related Phenomena*, Gordon and Breach, New York, 1967.
2. G. C. Kuczyuski, Ed., "Sintering and Related Phenomena", *Materials Science Research*, Vol. 6, Plenum Press, New York, 1973.
3. R. L. Coble and J. E. Burke, *Progress in Ceramic Science*, Vol. III, J. E. Burke, Ed., Pergamon Press, 1963.
4. W. D. Kingery, Ed., *Ceramic Fabrication Process*, Part IV, Technology Press, Cambridge, Mass., and John Wiley & Sons, New York, 1958.
5. W. D. Kingery, Ed., *Kinetics of High-Temperature Process*, Part IV, Technology Press, Cambridge, Mass., and John Wiley & Sons, New York, 1959.
6. J. E. Burke and D. Turnbull, "Recrystallization and Grain Growth in Metals," *Prog. Met. Phys.*, 3, 220 (1952).
7. E. Schramm and F. P. Hall, "The Fluxing Effect of Feldspar in Whiteware Bodies," *J. Am. Ceram. Soc.*, 15, 159 (1936).
8. For additional papers on sintering see: R. L. Coble, *J. Appl. Phys.*, 41, 4798 (1970); D. L. Johnson and I. B. Cutler, *J. Am. Ceram. Soc.* 46, 541 (1963).

Problems

- 10.1. Distinguish between primary recrystallization, grain growth, and secondary recrystallization as to (a) source of driving force, (b) magnitude of driving force, and (c) importance in ceramic systems.
- 10.2. Explain why the activation energy for grain-boundary migration corresponds approximately with that for boundary diffusion, even though no concentration gradient exists in the former case.
- 10.3. Can grain growth during sintering cause compaction of ceramics? Explain. Can grain growth affect the sintering rate? Explain.

BRIEF ATTACHMENT C

IN THE UNITED STATES PATENT AND TRADEMARK OFFICE

In re Patent Application of

Applicants: Bednorz et al.

Serial No.: 08/479,810

Filed: June 7, 1995

For: **NEW SUPERCONDUCTIVE COMPOUNDS HAVING HIGH TRANSITION
TEMPERATURE, METHODS FOR THEIR USE AND PREPARATION**

Date: March 1, 2005

Docket: YO987-074BZ

Group Art Unit: 1751

Examiner: M. Kopec

Commissioner for Patents
P.O. Box 1450
Alexandria, VA 22313-1450

FIRST SUPPLEMENTAL AMENDMENT

Sir:

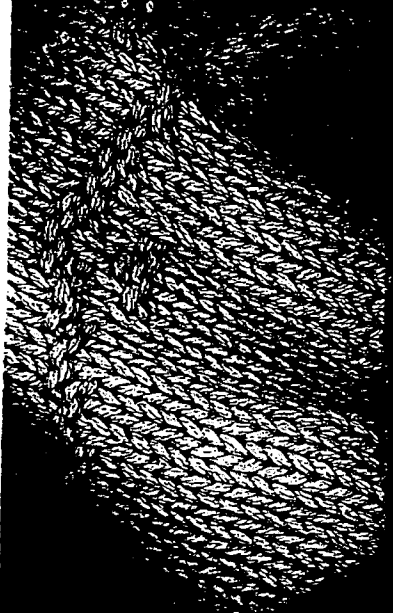
In response to the Office Action dated July 28, 2004, please consider the
following:

ATTACHMENT C

POLAR DIELECTRICS AND THEIR APPLICATIONS

JACK C. BURFOOT and GEORGE W. TAYLOR

University of California Press
Berkeley and Los Angeles



University of California Press
Berkeley and Los Angeles, California

ISBN: 0-520-03749-9

Library of Congress Catalog Card Number: 78-62835

Copyright © 1979 by Jack C. Burfoot and George W. Taylor

Printed in Great Britain

2

Preparation of Polar Materials

This chapter summarises the techniques used for fabricating polar materials in single crystal, ceramic, thin film and glass forms. It then goes on to discuss the various post-fabrication procedures such as annealing, poling, cutting, thinning, polishing and electroding which are usually needed before the polar materials can be used for either experiments or applications.

For basic studies, where the polar material should be as near perfect as possible, it is desirable to use single crystals. For applications, where dimensions, reproducibility and cost are crucial factors then the polar material is usually fabricated in ceramic, thin film or glass form. This division is not precise. For example, some materials have not yet been grown as single crystals and hence basic studies must be made in the ceramic form. In other cases, the larger dielectric, piezoelectric, pyroelectric, electro-optic, etc., coefficients obtainable with particular single crystal materials can make this fabrication form mandatory for certain applications. And yet again thin films offer an important advantage for studying surface layer physics.

The two major problems in fabricating large samples of high quality polar materials are the maintenance of the correct stoichiometry and the avoidance of strains. Chemical, thermal and optical methods, as well as sophisticated

techniques such as X-ray, electron, neutron and proton diffraction scattering are used to determine the quality of the fabricated material. By comparison, the fabrication techniques themselves are still much of an art, as evidenced by the variety of 'recipes' reported for particular materials. This however may be changing. For example, it is now customary to make a careful determination of the phase diagram of the material so as to choose the optimum fabrication conditions. These diagrams can be quite complex, as can be seen from figures 2.1 and 2.2, the phase diagrams for BaTiO_3 and $\text{Pb}(\text{ZrSnTiNb})\text{O}_3$. Note that in figure 2.2 because of the ternary nature of the material, (a) the material is best considered a Nb doped PbZrO_3 - PbSnO_3 - PbTiO_3 solid solution, (b) a different phase diagram is needed for each temperature. Another example of the scientific approach is the use of fluid dynamic principles to try to understand circulation currents in the melt during growth³.

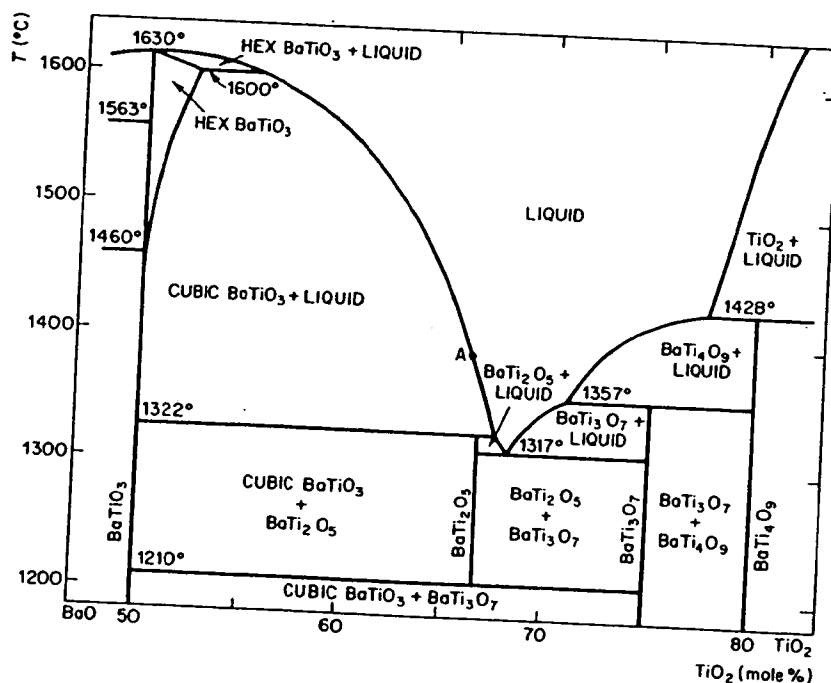


Figure 2.1 Barium titanate. Phase diagram (Rase and Roy¹)

Many measurements can be made to determine the degree to which a ceramic, thin film or glass material approaches the properties of its single crystal counterpart. The hysteresis loop is a simple yet powerful criterion for making this determination. The squarer the loop and the larger its polarisation, then the better the orientation of the crystallites and the smaller the

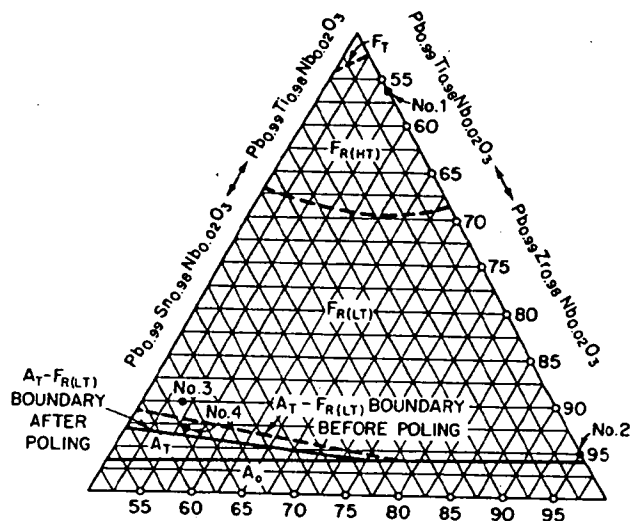


Figure 2.2 Part of the phase diagram of $\text{Pb}_{0.99}(\text{ZrSnTi})_{0.98}\text{Nb}_{0.02}\text{O}_3$ at 25°C (poled at 25°) F = Ferroelectric, A = antiferroelectric, T = tetragonal, R = rhombohedral, LT = low temperature phase, HT = high temperature phase (Raider and Cook²)

percentage of non-polar material and voids present. In general, doctor-bladed ceramics and epitaxial thin films are the fabrication techniques producing materials closest to the single crystal form, whilst the glasses and conventionally sintered ceramics are the furthest away.

2.1 Growth of Single Crystals

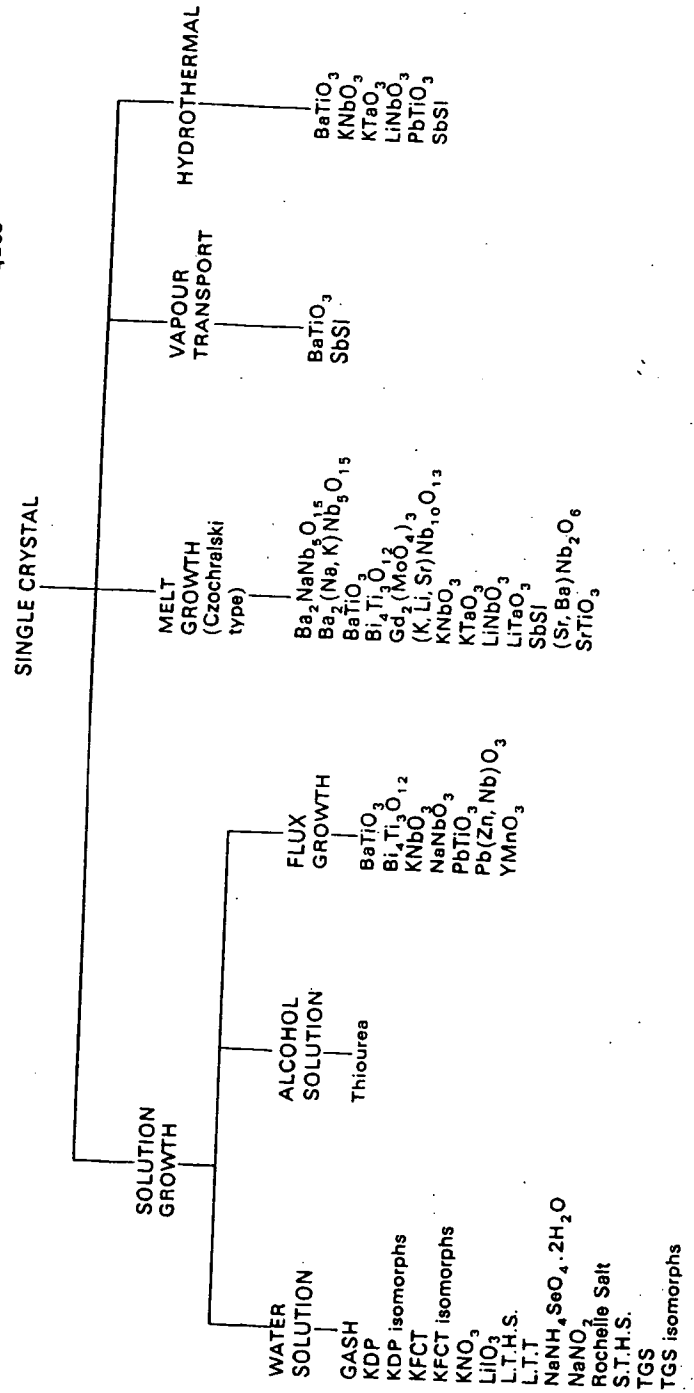
The two major methods that have been used to date for fabricating single crystals have been the solution (or flux) growth technique and the melt growth technique.

2.1a Solution Grown Crystals

This method has been successfully used for both water soluble materials and those that are soluble in other liquids or fluxes.

The first stage in growing a water soluble crystal is to prepare an aqueous saturated solution of the polar material. Crystals can be grown by either keeping the solution at a constant temperature and allowing a gradual evaporation of the solvent or by slowly lowering the temperature while keeping the solution saturated. Slow growth, taking a thousand hours or more, usually produces the best and largest crystals. Other factors which affect the crystal

Table 2.1 Single crystal polar materials that have been grown by various techniques



growth are the purity of the materials, the solubility-temperature characteristics of the solution, the fineness of the temperature control, the use of stirring to prevent temperature and concentration gradients from developing in the solution, and the use of seed crystals suspended in the solution to enhance growth.

Table 2.1 contains a fairly comprehensive listing of the polar materials which have been successfully grown from aqueous solution. Figure 2.3 shows a large solution-grown crystal of triglycine sulphate, TGS. The original seed crystal is visible in the centre of the photograph. The organic polar material thiourea can be grown from an aqueous solution; however, better results are obtained from an alcoholic solution.

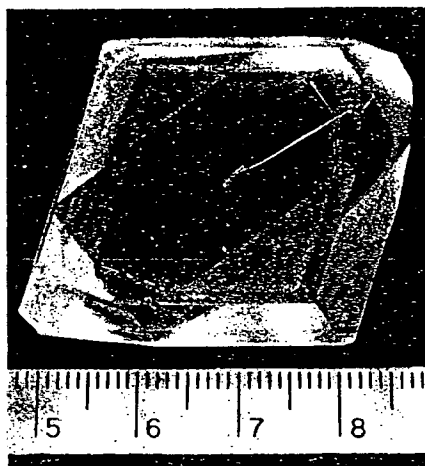


Figure 2.3 Photograph of a TGS crystal (Linz⁴)

Polar materials that are not soluble in water or alcohol can often be dissolved at high temperature in other materials, usually referred to as fluxes. For example, 26 different fluxes have been reported⁵ for barium titanate, BaTiO_3 . In some cases, an excess of one of the constituents can act as a flux. For example, additional Bi_2O_3 will serve as a flux in growing crystals of bismuth titanate, $\text{Bi}_4\text{Ti}_3\text{O}_{12}$.⁶

Besides the particular flux used there are many other variables in flux growth. They include the purity and particle size of the component materials, the time-temperature cycle used for forming the molten flux solution, the crucible material and its shape and size, the method of heating (both resistive and r.f. induction heating are used), the time-temperature cycle used for cooling, the thermal gradients established in the furnace (both vertical and

horizontal gradients have been used), and the atmosphere maintained in the furnace.

Some of the crystals that have been grown by flux techniques are shown in table 2.1. Space does not permit detailing the growth conditions used for each material. To give some idea, however, it is worth summarising the successful technique developed by Remeika⁷ for the flux growth of BaTiO_3 crystals. A platinum crucible containing 30% BaTiO_3 powder, 70% KF (the flux) and a small trace of Fe_2O_3 is heated for 8 h at 1175°C . The Fe_2O_3 compensates for the loss of oxygen at high temperature. The crucible is then cooled slowly to 875°C , at which stage the excess liquid flux is poured off. The crystals thus formed are then cooled slowly to room temperature. Any residual flux is removed by acid etching. The crystals have a plate-like morphology and some typical examples are shown in figure 2.4a.

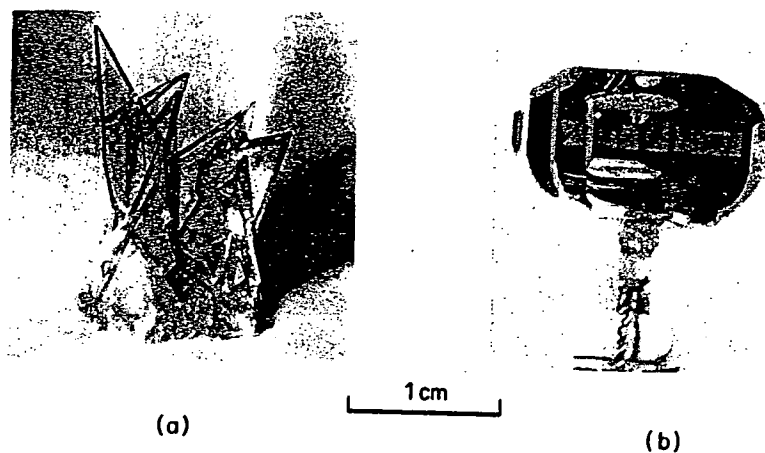


Figure 2.4 Photograph of barium titanate crystals.
(a) Crystals grown by flux method (Epstein⁸).
(b) Crystals grown by Czochralski method (Belruss *et al.*¹¹)

2.1b Melt Growth

If a polar material melts congruently, that is, if stoichiometry is maintained, then the crystal can be grown directly from the melt. As the crystal grows, either by spontaneous nucleation on to a chemically inert platinum or iridium wire or onto a seed crystal, it is gradually withdrawn from the molten liquid. In the Stockbarger method, this is done by withdrawal of the crucible containing the melt. In the Czochralski method (figure 2.5), the crystal is gradually 'pulled' out of the melt, and it is usual to rotate the crystal while pulling, to minimise thermal and stress gradients. Also suitable optics are provided for

viewin
growe
desigr
metho
and le
are pc
and a
used.
at 70
atmos
Bel
times
gradu
grown
crysta
132°C
figure

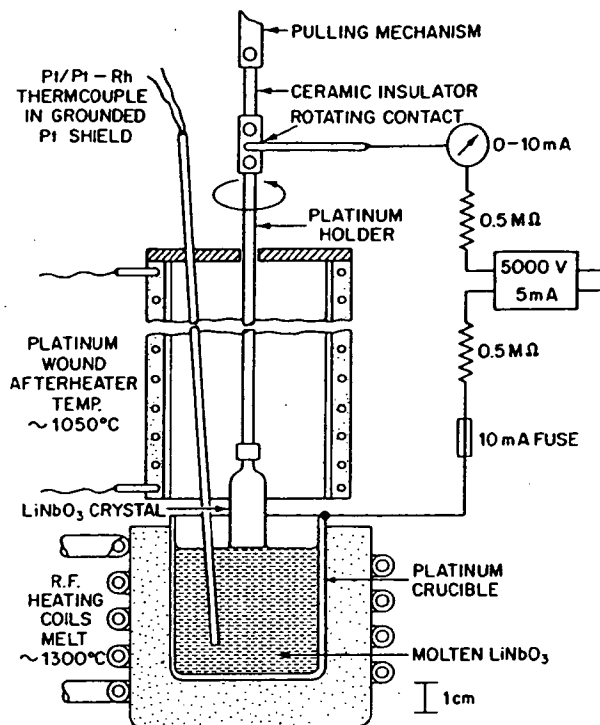


Figure 2.5 Czochralski crystal grower for lithium niobate (Nassau⁹)

viewing the crystal during growth. Figure 2.5 shows a Czochralski crystal grower used for growing lithium niobate, LiNbO_3 . The apparatus is also designed to pole the crystal during the growth process. The Czochralski method is usually the best for polar materials, in that it produces less strains and less twinning in the crystal. A large number of variations in the technique are possible including variation of the pulling and rotation rates, the method and amount of after-heating used as the crystal emerges, and the atmosphere used. Figure 2.6 is a photograph of a $\text{Gd}_2(\text{MoO}_4)_3$ crystal pulled by Kumada at 70 mm/h using a rotational speed of 100 rev/min in an oxygen rich atmosphere¹⁰. Most Czochralski grown crystals have the form of figure 2.6.

Belruss *et al.*¹¹ have developed a modified Czochralski technique, sometimes referred to as 'top seeding', in which the temperature of the melt is gradually dropped ($0.2^\circ\text{C}/\text{h}$) as pulling proceeds. The crystal of figure 2.4b was grown by this technique, using a pulling rate of 0.7 mm/h. Pulled BaTiO_3 crystals have a polyhedral morphology and a transition temperature, T_c of 132°C . By comparison, the Remeika⁷ flux grown BaTiO_3 crystals, shown in figure 2.4a have a plate-like structure and a T_c of 120°C . The lower T_c is due to

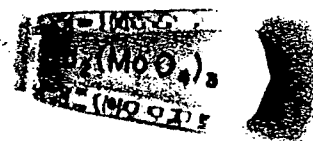


Figure 2.6 Single crystal of gadolinium molybdate (Kumada¹⁰)

the substitution of K atoms at some Ba sites and Fe at some Ti sites in the BaTiO_3 crystal lattice; the K and Fe impurities originate from the flux used.

The polar material single crystals that have been successfully grown from the melt by Czochralski type techniques are listed in table 2.1.

2.1c Other Techniques

Single crystals of both BaTiO_3 and antimony sulpho-iodide, SbSI , have been grown by vapour transport¹². Hydrothermal methods, which involve a combination of high pressure and temperature have been used to grow single crystals of several types of polar materials¹³⁻¹⁵—see also table 2.1.

2.2 Ceramic Fabrication

The classical technique for forming ceramics is sintering at atmospheric pressure. Recent variations on this process are doctor-blading and hot pressing.

2.2a Sintering

The constituents (or their oxides) of the polar material are mixed in the correct proportions with an organic binder and then pressed at room temperature into a structure having the desired shape and dimensions. In most cases this is a cylinder, although for some applications, for example sonar, more complex shapes are used. The pressed structure is sintered or fired at an appropriate temperature in an appropriate atmosphere. This causes the organic binder to be burnt out and the pressed materials to react chemically and form the desired polar material. Table 2.2 contains a list of some of the polar materials which have been fabricated as sintered ceramics.

Table 2.2 Ceramic polar materials that have been fabricated by various techniques

CERAMICS			
SINTERED	DOCTOR BLADED	HOT PRESSED	
AgNbO ₃	Pb(Fe, Nb)O ₆	BaTiO ₃	(Na, K)NbO ₃
AgTaO ₃	PbHfO ₃	PbNb(Zr, Sn, Ti)O ₃	Pb(Zr, Ti)O ₃
AgVO ₃	Pb ₃ (Mg, Nb ₂)O ₉	Pb(Zr, Ti)O ₃	PbBi(Zr, Ti)O ₃
Ba ₂ NaNb ₅ O ₁₅	PbNb ₂ O ₆		PbLa(Zr, Ti)O ₃
BaTiO ₃	PbTiO ₃		PbNb(Zr, Ti)O ₃
Bi ₄ Ti ₃ O ₁₂	PbZrO ₃		Pb(Sn, Zr, Ti)O ₃
Cd ₂ Nb ₂ O ₇	PbBi(Zr, Sn, Ti)O ₃		
CdTiO ₃	PbNb(Zr, Sn, Ti)O ₃		
(K, Li, Sr)Nb ₁₀ O ₁₃	PbBi(Zr, Ti)O ₃		
KNbO ₃	PbLa(Zr, Ti)O ₃		
KTaO ₃	PbNb(Zr, Ti)O ₃		
K(Nb, Ta)O ₃	RbTaO ₃		
LiNbO ₃	SrBaNb ₂ O ₆		
LiTaO ₃	SrTiO ₃		
(Na, K)NbO ₃	WO ₃		
NaNbO ₃			
NaTaO ₃			
Na(NbTa)O ₃			

2.2b Doctor-Blading

Doctor-Blading¹⁶ is particularly suited for forming large area, thin sheets of ceramic. The constituents of the polar materials are mixed in a liquid together with a suitable plasticiser and the resultant slurry is poured onto flat glass. A stainless steel blade, accurately positioned a small distance, S , above the substrate is then drawn through the slurry. The resulting sheet is allowed to dry after which it can be peeled off the glass. At this stage the material is termed 'green' because it can be easily cut or punched into any two dimensional shape. The sintering is done in a two step process, viz. a lower temperature firing to burn out the plasticiser and then a higher temperature firing in a controlled atmosphere to form the polar material.

Whenever a ceramic is sintered there is a large amount of shrinkage. For a doctor-bladed material, the shrinkage is particularly evident as a decrease in thickness. Figure 2.7 shows the relationship between the thickness of 'green' and fired materials for a PbNb(Zr, Sn, Ti)O₃ ceramic. A fired and electroded doctor-bladed ceramic strip is shown in figure 2.14.

2.2c Hot Pressing

In the hot-pressing process the ceramic is sintered under pressure, typically developed in a hydraulic press. Hot pressing can result in ceramic densities

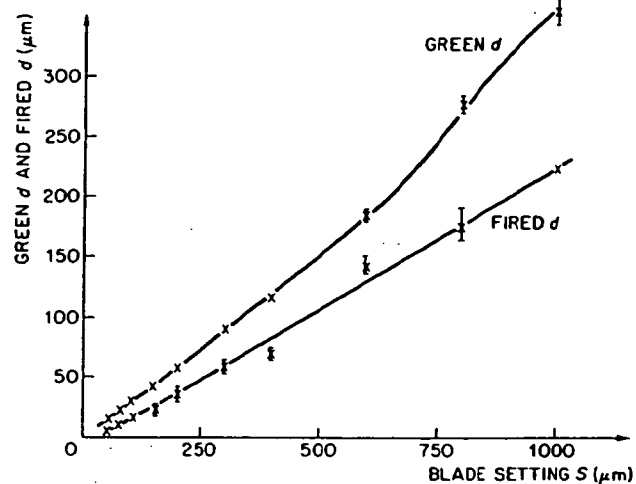


Figure 2.7 Thickness of 'green' and fired materials as a function of blade setting, S , for a doctor-bladed $\text{Pb}(\text{ZrSnTiNb})\text{O}_3$ ceramic (Wentworth and Taylor¹⁶)

even higher than 99.9% of the theoretical maximum. As a result, such materials have properties approaching those of a single crystal. For example, the hot-pressed ceramic can have a high value of remanent polarisation, a low value of coercive field and, as shown in figure 2.8, can be transparent.

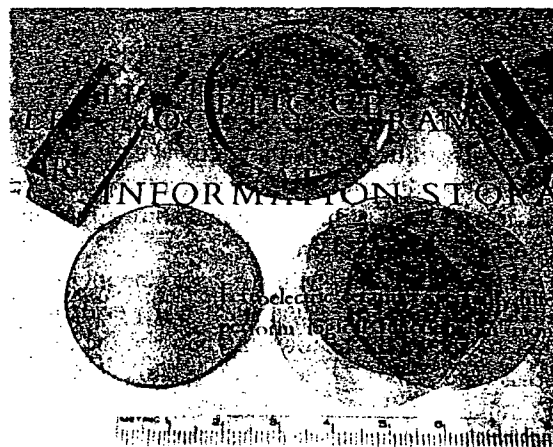


Figure 2.8 Photograph of polished transparent $\text{Pb}(\text{ZrTiLa})\text{O}_3$ hot-pressed ceramic samples. (Haertling and Land¹⁸)

Haertling^{17, 18} has extensively studied how the parameters of time, pressure, temperature, chemical purity and firing atmosphere affect the properties of hot-pressed Nb, Sn, Bi and La doped and Sn, Ba, and La modified^{*} $\text{Pb}(\text{Zr}, \text{Ti})\text{O}_3$ ceramics. Figure 2.9 is typical of such results. In this case the effects of time, pressure, and temperature, on grain size of a $\text{PbNb}(\text{Zr}, \text{Sn}, \text{Ti})\text{O}_3$ ceramic are shown. As discussed in section 15.2a the grain size is important in determining the electro-optic properties of certain ceramic compositions. It also affects many other properties of the ceramic including the permittivity. Other ceramics that have been hot pressed are listed in table 2.2.

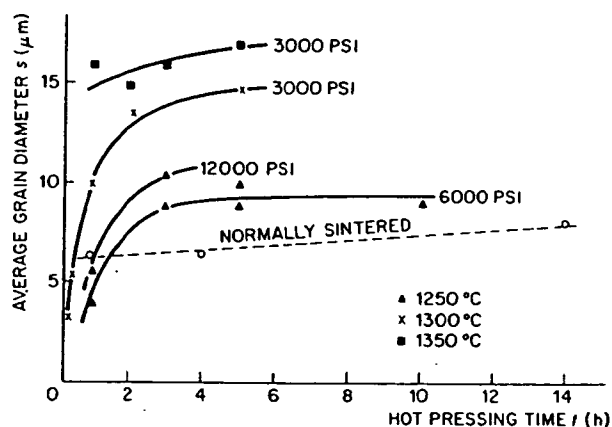


Figure 2.9 Effect of hot pressing time, temperature and pressure on average grain diameter of a hot pressed $\text{PbNb}(\text{ZrSnTi})\text{O}_3$ ceramic (Haertling¹⁷)

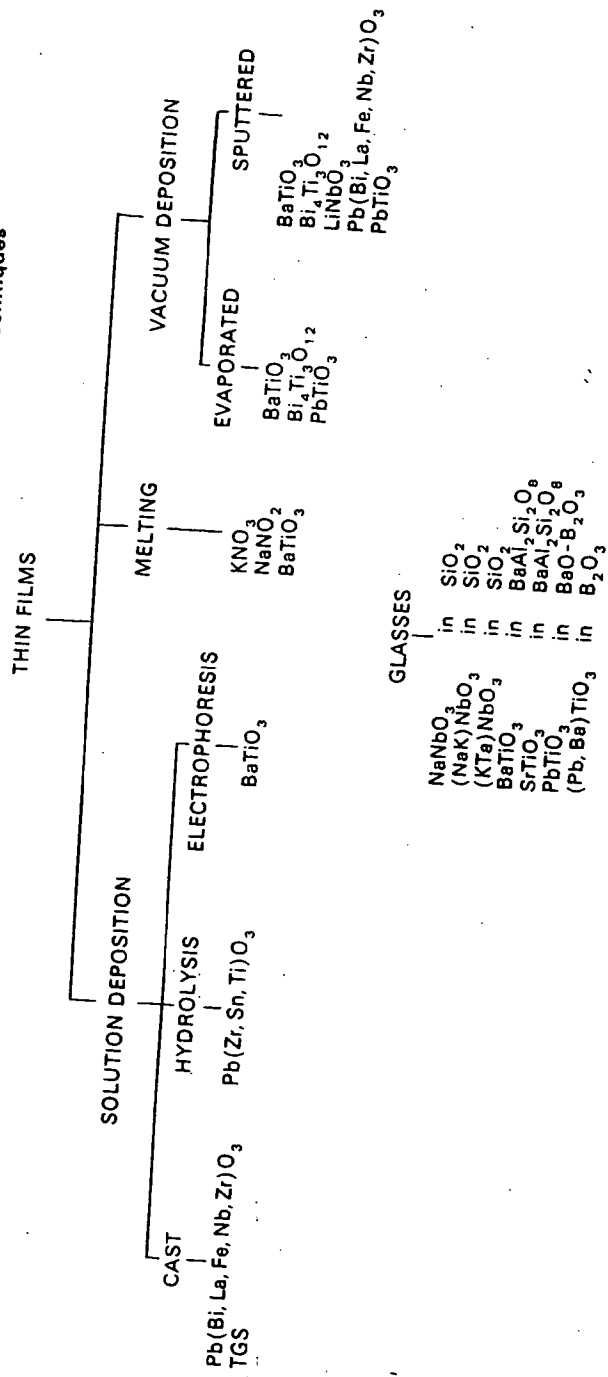
2.3 Thin Film Fabrication

There has recently been much general interest in thin films of polar materials (i.e. less than about $10 \mu\text{m}$ thick). In particular, for device applications, thin films have important advantages which include (a) formation of large capacitances, (b) low switching voltages, (c) the possibility of forming the film directly on the integrated semiconductor 'driving' circuits.

The various techniques used for making thin films are described below. The materials that have been made by these techniques are summarised in table 2.3. With the exception of r.f. sputtering, the fabrication techniques generally

* As described in sections 15.2 and 17.4, the properties of the $\text{Pb}(\text{Zr}, \text{Ti})\text{O}_3$ ceramics vary greatly depending on whether the amount of additive is less or greater than about 5 atom per cent. As a result it is convenient to use the term *doped* $\text{Pb}(\text{ZrTi})\text{O}_3$ when the additive is less than 5 atom per cent and the term *modified* $\text{Pb}(\text{ZrTi})\text{O}_3$ when the additive is greater than 5 atom per cent.

Table 2.3 Thin film polar materials that have been formed by various techniques



produce polycrystalline films, which have properties more similar to ceramics than to single crystals.

2.3a Solution Deposition

Three types of solution deposition have been used for forming thin films. They are casting, hydrolysis and electrophoresis.

Casting

Beerman¹⁹ has made thin films of TGS (a water soluble polar material) by spraying an aqueous solution of TGS onto a suitable substrate. Chapman²⁰ has formed thin films of the complex ferroelectric $\text{Pb}(\text{BiLaFeNbZr})\text{O}_3$ by first making a colloidal suspension, or slurry, of the basic oxides of the composition. The suspension was then centrifuged onto a metallic substrate and sintered at 900°C to form the ferroelectric thin film.

Hydrolysis

Lure *et al.*²¹ have deposited a mixture of Pb, Zr, Sn and Ti oxides on a metallic substrate by hydrolysing a solution of Pb, Zr, Sn and Ti tetrachlorides. The oxides were then sintered to form a ferroelectric film of $\text{Pb}(\text{ZrSnTi})\text{O}_3$.

Electrophoresis

Lamb *et al.*²² placed two noble metal electrodes into a suspension of BaTiO_3 particles in ether. The application of about 200 V cm^{-1} between the electrodes caused a film to be formed on the anode. Subsequent sintering in an atmosphere of 98% helium and 2% oxygen at 1350°C created a stable BaTiO_3 film.

2.3b Melting

Nolta *et al.*²³ have shown that a thin layer of potassium nitrate, KNO_3 , can be easily formed by melting KNO_3 powder onto a metal substrate. However, KNO_3 has the disadvantage that it is only ferroelectric at room temperature and atmospheric pressure for a short time, before reverting to a non-ferroelectric phase²⁴. Sodium nitrite, NaNO_2 , and barium titanate, BaTiO_3 films have also been prepared by melting.

2.3c Vacuum Deposition

Evaporation and sputtering techniques have been used for the vacuum deposition of thin films.

Evaporation

In his early work Feldman²⁵ evaporated BaTiO_3 from a coated tungsten

filament onto a metallic substrate in a vacuum of less than 5×10^{-5} mm Hg. Due to the difference in volatility of the constituent oxides, the resultant film consisted of separated layers of BaO and TiO₂. To combine the oxides the film had to be subsequently heated in air at 1100°C.

Flash evaporation onto a heated substrate is a technique developed by Müller *et al.*²⁶ and Burfoot *et al.*²⁷ which overcomes the dissociation problem. The polar material is evaporated in small-thickness increments, typically corresponding to a few crystal lattice spacings, by dropping the source material, a grain at a time, onto a filament heated to a temperature of about 2000°C. One variation which has proved successful in improving the quality of the evaporated films has been to leak a small amount of oxygen into the vacuum chamber. This improved stoichiometry by overcoming oxygen deficiencies. Another successful technique has been the use of multiple evaporation sources. For example, in forming BaTiO₃, a source of BaO and a source of TiO₂ are used. The multiple sources can reduce the amount of filament material in the film.

In addition to BaTiO₃, thin films of lead titanate, PbTiO₃, and bismuth titanate, Bi₄Ti₃O₁₂, have been evaporated. Films evaporated onto metal substrates such as platinum are polycrystalline in nature. An epitaxial film of BaTiO₃ with its *c*-axis uniformly aligned perpendicular to the substrate can be evaporated if the substrate is a freshly cleaved alkali halide crystal such as LiF or NaF. Burfoot²⁷ has developed a technique for removing the film from the insulating substrate, so that an electrode can be placed on the thin film for electrical measurements.

Sputtering

Francombe²⁸ has suggested that sputtering offers several advantages over evaporation, namely (a) better control of stoichiometry, especially for the more complex oxide materials, (b) better thickness control and (c) freedom from material contamination. Most sputtering has been r.f. sputtering from ceramic targets. However, diode, triode and tetrode sputtering has also been used. The polar materials which have been sputtered are listed in table 2.3. Two of these materials, BaTiO₃ and Bi₄Ti₃O₁₂, have also been sputtered epitaxially.

It is instructive to summarise the sputtering technique developed for monoclinic Bi₄Ti₃O₁₂, since the problems which occur are rather typical, and the results obtained have been the most impressive. Takei *et al.*²⁹ used a 10 cm² ceramic target of bismuth titanate mounted on a water-cooled metallic base and positioned 4 cm from a heated substrate. Using a 4 mm atmosphere of O₂ and Ar they were able to sputter Bi₄Ti₃O₁₂ films at a rate of about 1 Å s⁻¹ using a power level of 1 W cm⁻² and a self bias of 700 V.

The problem in vacuum deposition, as with single crystal and ceramic fabrication, is to develop the correct stoichiometry so that only the required phase is formed. In the case of sputtering Bi₄Ti₃O₁₂, this is done by using a

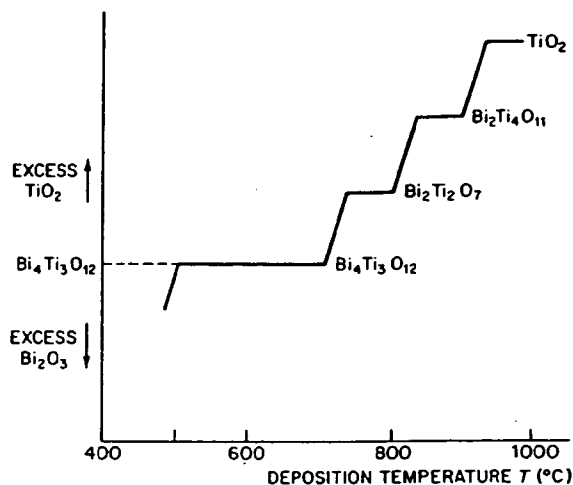


Figure 2.10 Dependence of composition on substrate temperature for films r.f. sputtered from a target of composition 80% $\text{Bi}_4\text{Ti}_3\text{O}_{12}$, 20% $\text{Bi}_{12}\text{TiO}_{20}$. (Francombe²⁸)

ceramic target of 0.8 $\text{Bi}_4\text{Ti}_3\text{O}_{12}$, 0.2 $\text{Bi}_{12}\text{TiO}_{20}$ and a substrate temperature of 650°C. The bismuth enriched target compensates for the high volatility of that oxide, while as can be seen from figure 2.10, the chosen substrate temperature favours $\text{Bi}_4\text{Ti}_3\text{O}_{12}$ over the other phases.

The $\text{Bi}_4\text{Ti}_3\text{O}_{12}$ film can be sputtered epitaxially and aligned along any preferred direction by choosing a substrate having a suitable crystal lattice. Substrates which have been used are Pt, single crystal $\text{Bi}_4\text{Ti}_3\text{O}_{12}$ and MgO and MgAl_2O_4 . Except for a higher coercive field, the electrical and optical properties of the epitaxial films closely match those of the bulk (single crystal) material; see, for example, figure 2.11. The most dramatic evidence of the quality of the sputtered films of $\text{Bi}_4\text{Ti}_3\text{O}_{12}$ is their ability, as shown in figure 2.12, to duplicate the complex electro-optic light valve switching properties of the single crystal material described in section 15.2a.

2.4 Fabrication of Polar Glasses

Borrelli, Herczog and colleagues^{31, 32} at Corning have succeeded in crystallising NaNbO_3 and $(\text{NaK})\text{NbO}_3$ in glass matrices of SiO_2 , and BaTiO_3 and SrTiO_3 in a matrix of $\text{BaAl}_2\text{Si}_2\text{O}_8$. Also, Isard and his colleagues^{33, 34} at Sheffield have made glasses of PbTiO_3 and $(\text{PbBa})\text{TiO}_3$ in B_2O_3 matrices and $(\text{K Ta})\text{NbO}_3$ in a SiO_2 matrix. These polar glasses are made by the rapid quench cooling of the appropriate molten oxides, followed by suitable annealing treatment to crystallise the polar material in the low permittivity,

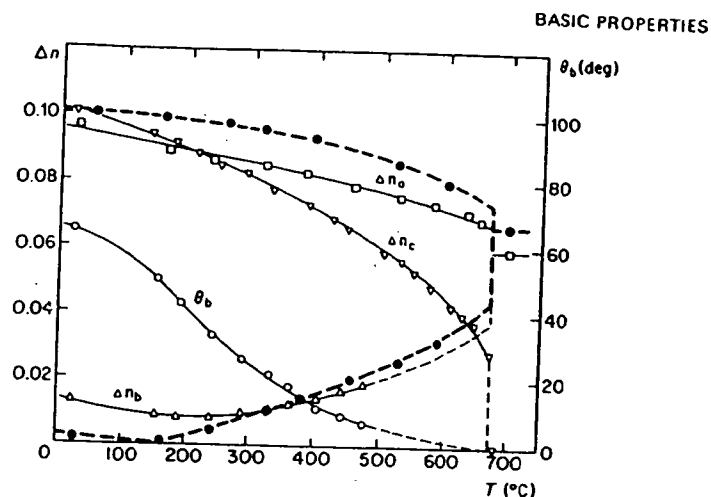
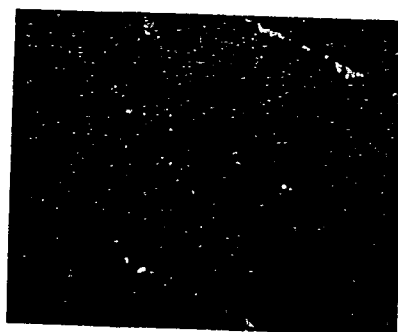
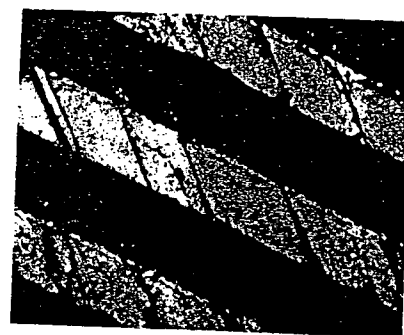


Figure 2.11 Birefringence values and extinction angle of bismuth titanate as a function of temperature measured at wavelength 5890 Å. The solid lines are from single crystal, and the dashed lines from film. The subscripts a, b, and c indicate the monoclinic axis along which light was directed for each measurement. (Wu *et al.*³⁰)



(a)



(b)

Figure 2.12 A sputtered bismuth titanate film viewed between crossed polarisers in (a) 'off' condition (b) 'on' condition (Wu *et al.*³⁰). Microphotographs of an interdigital electrode array.

high resistivity glass matrix. The volume per cent of glass matrix present should be kept as small as possible: 20% is an achievable amount. The electrical properties of the glasses are enhanced by a large crystallite grain size for the polar material portion, while the optical properties are favoured by a small grain size. For electro-optic applications, 0.5 μm is a typical compromise grain size.

The polar glass materials have the characteristic advantages associated with glass, namely an absence of pores and hence a high dielectric breakdown and mechanical strength. Also, they can be conveniently fabricated in thin uniform sheets. On the other hand, the presence of the glass matrix with its relatively low dielectric permittivity as compared to the polar materials means that the electrical and optical coefficients are smaller than those of the corresponding ceramic or single crystal material. The properties are, however, still sufficiently significant for some electro-optic applications and for some cryogenic temperature, capacitor applications.³²

2.5 Post-Fabrication Procedures

2.5a Annealing

Crystals grown from the melt often develop strains which lead to undesirable domain structures (twinning) and mechanical cracking. The strains are mainly caused by the mechanical constraints imposed during the growth process. The easiest way to remove these strains is by thermal annealing. This can be done by cooling the crystal through its transition temperature at a prescribed rate in a suitable temperature gradient. For example, Hopkins and Miller³⁵ have found that the strains due to domain structures in $\text{Bi}_4\text{Ti}_3\text{O}_{12}$ can be successfully annealed out by placing the crystals on an alumina surface in a tube furnace with a temperature gradient of 5°C cm^{-1} and cooling at the rate of 2°C min^{-1} . Annealing is also used to remove strains which can develop in thin film materials and ceramics while they are being fabricated.

2.5b Poling

In a newly fabricated ceramic, the crystallites, and hence the polar axis, can lie in a large number of directions. This will cause the material to have only a quasi-isotropic response in its electrical, optical, piezoelectric and other characteristics. A lack of orientation can also exist in certain freshly prepared single crystal and thin film materials due to there being more than one possible orientation for the polar axis. For example in BaTiO_3 there are three possible orientations for the polar axis and each orientation has two possible directions.

Before such unaligned materials can be used for measurements and applications, it is necessary to orient the polar axis in a common direction usually normal to the major surfaces. (However, in the case of the electro-optic PLZT ceramics it is necessary, for some modes of operation (see section 15.2), to pole parallel to the surface.)

Polar axis orientation is done by a poling technique which consists of applying a D.C. voltage for a sufficient time to suitable electrodes on the material. The amplitude and duration of the voltage required for poling vary substantially between materials. Some materials will pole easily and if used in



Figure 2.13 Single crystal bismuth titanate poled in central region, as viewed between crossed polarisers (Hopkins and Miller³⁵): scale has 1 mm divisions.

large-signal switching applications may not even require a preliminary poling cycle. Others can only be poled near their Curie point where the coercive field of the material is small. Sometimes the poling is done during the crystal growth—see figure 2.5. The maximum poling voltage that can be applied is limited by breakdown and arcing in the material. Hence poling is often done in an oil bath. Figure 2.13 shows a $\text{Bi}_4\text{Ti}_3\text{O}_{12}$ crystal which has been poled in its central section. The crystal is viewed between crossed polars and hence only the poled region is uniformly extinguished.

2.5c Cutting, Thinning and Polishing

Depending on the intended usage, it is often necessary to cut and thin the 'as grown' single crystal or the 'as sintered' ceramic slug or disc to smaller dimensions. If the material is water soluble then the cutting can be done with a water soaked string. Other materials may require cutting with a high speed diamond coated wire. The thinning can be done by slicing, mechanical grinding or etching. In the latter process, depending on the material, the etch solution can vary from water to aqua regia. Some materials will, with a suitably applied high impulse pressure, naturally cleave into thin platelets. Desputtering, where-in the polar material is made the sputtering source, is a technique that permits very carefully controlled thinning of a material.³⁸

For optical use it is almost mandatory to have a finely polished surface to minimise light scattering. Several methods are used for polishing. One of the most common is a series of polishes with alumina powder of progressively smaller particle size.

2.5d Electroding

Many measurements and most devices require the application of electric fields to the material. This is done by applying a voltage between electrodes placed on the surfaces of the polar material. Because of the high ϵ of polar materials, the electrodes must be in intimate contact with the surfaces. Virtually any airgap will cause an intolerable reduction in the voltage developed in the polar material.

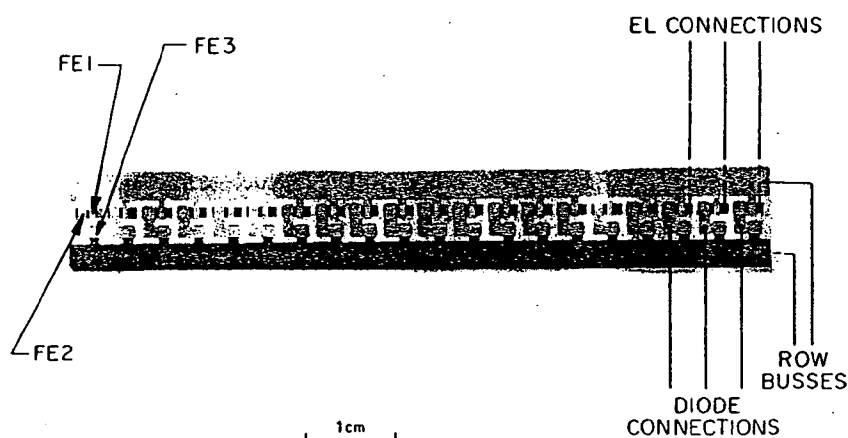


Figure 2.14 An evaporated gold electrode pattern on a doctor bladed ceramic strip (Taylor³⁶).

For quick measurements, air drying silver paste is often used as an electrode. For applications which require accurately defined electrodes, it is usual to evaporate metal through photomechanically formed masks. Figure 2.14 shows such an electrode pattern formed with evaporated gold on a doctor-bladed PZT-type ceramic. Silk screening and sputtering are two other techniques which have been used for forming electrodes. For electro-optic applications, it is often necessary to have transparent electrodes. Very thin (less than 500 Å thick) evaporated metal electrodes can sometimes be used. However, r.f. sputtered indium and/or tin oxide has proved to be a more satisfactory transparent electrode. Such electrodes can have a resistance of less than 10 Ω per square and an optical transmission of greater than 90% in the visible spectrum.

At first sight, electroding would seem to be no more than a technical process. However, as discussed in detail in section 3.2c, electrodes can have a significant effect on the ageing phenomena in polar materials. For example, if metal electrodes are used, single crystal BaTiO₃ ages after repeated polarisation reversals. With conducting liquid electrodes (e.g. an aqueous lithium chloride

solution) no ageing occurs¹⁷. These and other results indicate that the surface physics involved is complicated and not well understood. The large electric field gradients which exist near the surfaces of polar materials undoubtedly contribute to the effects that the electrodes can have on the switching properties of polar materials.

References

1. D. E. Rase and R. Roy, *J. Am. ceram. Soc.*, **38**, 110 (1965)
2. M. E. Raider and W. R. Cook, *J. appl. Phys.*, **38**, 1977 (1967)
3. J. R. Carruthers and K. Nassau, *J. appl. Phys.*, **39**, 5205 (1968)
4. A. Linz, private communication
5. M. L. Sholokhovitch and I. N. Belyaev, *Zhur. Obschehei. Khim.*, **24**, 218 (1954); *ibid.*, 1118 (1954)
6. A. D. Morrison, F. A. Lewis and A. Miller, *Ferroelectrics*, **1**, 75 (1970)
7. J. P. Remeika, *J. Am. chem. Soc.*, **76**, 940 (1954)
8. D. J. Epstein, U. S. Air Force Contract Report AFAL-TR-70-172
9. K. Nassau, *Ferroelectricity* (ed. E. F. Weller), Elsevier, Amsterdam, p. 266 (1967)
10. A. Kumada, *Ferroelectrics*, **3**, 115 (1972)
11. V. Belruss, J. Kalnajs, A. Linz and R. Folweiler, *Materials Research Bulletin*, **6**, 899 (1971)
12. T. Mori, H. Tamura and E. Sawaguchi, *J. phys. Soc. Japan*, **20**, 1294 (1965)
13. V. I. Popolitov and B. N. Litvin, *Sov. Phys. Crystall.*, **13**, 483 (1968)
14. V. G. Hill and K. G. Zimmerman, *J. electrochem. Soc.*, **115**, 978 (1968)
15. A. A. Shternberg and V. A. Kuznetsov, *Sov. Phys. Crystall.*, **13**, 647 (1968)
16. C. Wentworth and G. W. Taylor, *Am. ceram. Soc. Bull.*, **46**, 1186 (1967)
17. G. H. Haertling, *J. Am. ceramic Soc.*, **42**, 679 (1963); *ibid.*, **49**, 113 (1966)
18. G. H. Haertling and C. E. Land, *J. Am. ceram. Soc.*, **54**, 1 (1971)
19. G. H. Haertling and C. E. Land, *Ferroelectrics*, **3**, 269 (1972)
19. H. P. Beerman, *Ferroelectrics*, **2**, 123 (1971)
20. D. W. Chapman, *J. appl. Phys.*, **40**, 2381 (1969)
21. M. S. Luré, E. I. Vasil'eva and I. V. Ignat'eva, *Bull. Acad. Sci. USSR*, **24**, 1372 (1960)
22. V. A. Lamb and H. I. Salmon, *Bull. Am. ceramic Soc.*, **41**, 781 (1962)
23. J. P. Nolte and N. W. Schubring, *Phys. Rev. Letters*, **9**, 285 (1962)
23. R. A. Dork, N. W. Schubring and J. P. Nolte, *J. appl. Phys.*, **35**, 1984 (1964)
23. N. W. Schubring, R. A. Dork and J. P. Nolte, *J. appl. Phys.*, **38**, 1671 (1967)
24. G. W. Taylor and B. J. Lechner, *J. appl. Phys.*, **39**, 2372 (1968)
25. C. Feldman, *Phys. Rev.*, **96**, 819 (1954)
25. C. Feldman, *Rev. scient. Instrum.*, **26**, 463 (1955)
26. E. K. Müller, B. J. Nicholson and M. H. Francombe, *Electrochem. Technology*, **1**, 158 (1963)

27. J. C. Burfoot and J. R. Slack, *Proc. European Meeting*, Saarbrücken (1969)
J. C. Burfoot and J. R. Slack, *J. phys. Soc. Japan*, **28**, Supplement, 417 (1970)
28. M. H. Francombe, *Ferroelectrics*, **3**, 199 (1972)
29. W. J. Takei, N. P. Formigoni and M. H. Francombe, *Appl. Phys. Letters*, **15**, 256 (1969)
W. J. Takei, N. P. Formigoni and M. H. Francombe, *J. Vacuum Sci. Tech.*, **7**, 442 (1970)
30. S. Y. Wu, W. J. Takei and M. H. Francombe, *Ferroelectrics*, **10**, 209 (1976)
31. N. F. Borrelli, A. Herczog and R. D. Mauer, *Appl. Phys. Letters*, **7**, 117 (1965)
N. F. Borrelli, *J. appl. Phys.*, **38**, 4243 (1967)
N. F. Borrelli and M. M. Layton, *IEEE Trans. Electron Devices*, **ED-16**, 511 (1969)
32. W. N. Lawless, *Ferroelectrics*, **3**, 287 (1972); *ibid.*, **7**, 379 (1974)
33. D. G. Grossman and J. O. Isard, *J. Phys. D. appl. Phys.*, **3**, 1058 (1970)
34. D. V. Keight and J. O. Isard, paper given at British Ceramic Society Meeting (Dec. 1972)
35. M. M. Hopkins and A. Miller, *Ferroelectrics*, **1**, 37 (1970)
36. G. W. Taylor, *IEEE Trans. Electron Devices*, **ED16**, 565 (1969)
37. G. W. Taylor, Ph.D. Thesis, University of London (1961)
38. J. Vossen, private communication